

Copyright

by

Andrew Charles Brown

2013

**The Dissertation Committee for Andrew Charles Brown Certifies that this is the approved version of the following dissertation:**

**The Behavior of Drilled Shaft Retaining Walls in Expansive Clay Soils**

**Committee:**

---

Robert B. Gilbert, Supervisor

---

Jorge G. Zornberg

---

Chadi S. El Mohtar

---

Sharon L. Wood

---

Bridget R. Scanlon

**The Behavior of Drilled Shaft Retaining Walls in Expansive Clay Soils**

**by**

**Andrew Charles Brown, B.S.C.E., M.S.C.E.E.**

**Dissertation**

Presented to the Faculty of the Graduate School of

The University of Texas at Austin

in Partial Fulfillment

of the Requirements

for the Degree of

**Doctor of Philosophy**

**The University of Texas at Austin**

**August 2013**

## **Dedication**

For my wife and family.

## **Acknowledgements**

The author would like to thank his supervisor, Dr. Robert B. Gilbert, for his assistance throughout his undergraduate and graduate education. Many thanks are extended to the Texas Department of Transportation, whose funding made this research possible. The author would also like to thank Drs. Jorge G. Zornberg, Chadi S. El Mohtar, Sharon L. Wood, Bridget R. Scanlon, and Richard E. Klingner for their contributions to the development and review of this research. The author is indebted to Roy Lee, for donating the use of his property to this research, and the staff at Lymon C. Reese and Associates, Fugro Consultants, Inc., McKinney Drilling Company, and HVJ and Associates for their assistance at the testing site. In particular, the author would like to thank Dr. Shin-Tower Wang, Jose Arrellaga, Dr. Gonzalo Vasquez, Dr. Bill Isenhower, Rebecca Russo, and Russell Sieg for their personal assistance with research and testing activities. The author thanks his colleagues Greg Dellinger, Trent Ellis, Iraklis Koutrouvelis, and Ali Helwa, who provided tremendous assistance during the research process and whose presence made the many hours of field work much more entertaining. Finally, the author wishes to thank his friends, family, and especially his wife Jennifer, for their support during his doctoral studies.

# **The Behavior of Drilled Shaft Retaining Walls in Expansive Clay Soils**

Andrew Charles Brown, Ph.D.

The University of Texas at Austin, 2013

Supervisor: Robert B. Gilbert

Drilled shaft retaining walls are common earth retaining structures, well suited to urban environments where noise, space, and damage to adjacent structures are major considerations. The design of drilled shaft retaining walls in non-expansive soils is well established. In expansive soils, however, there is no consensus on the correct way to account for the influence of soil expansion on wall behavior. Based on the range of design assumptions currently in practice, existing walls could be substantially over- or under-designed.

The goal of this research is to advance the understanding of the effects of expansive clay on drilled shaft retaining walls. The main objectives of this study are to identify the processes responsible for wall loading and deformation in expansive clay, to evaluate how these processes change with time, and to provide guidance for design practice to account for these processes and ensure adequate wall performance.

The primary source of information for this research is performance data from a four-year monitoring program at the Lymon C. Reese research wall, a full-scale instrumented drilled shaft retaining wall constructed through expansive clay in Manor, Texas. The test wall was instrumented with inclinometers and fiber optic strain gauges, and performance data was recorded during construction, excavation, during natural moisture fluctuations, and during controlled inundation tests that provided the retained soil

with unlimited access to water. In addition to the test wall study, a field assessment of existing TxDOT drilled shaft retaining walls was conducted.

The main process influencing short-term wall deformation was found to be global response to stress relief during excavation, which causes the wall and soil to move together without the development of large earth pressures or bending stresses. Long-term wall deformations were governed by the development of drained conditions in both the retained soil and the foundation soil after approximately eight months of controlled inundation testing. To ensure adequate wall performance, the deformations and structural loads associated with short- and long-term conditions should be combined and checked against allowable values.

## Table of Contents

List of Tables .....	xv
List of Figures .....	xvi
<b>CHAPTER 1: OVERVIEW OF RESEARCH STUDY .....</b>	<b>1</b>
1.1: Introduction.....	1
1.2: Objectives .....	1
1.3: Methodology.....	2
1.4: Organization.....	2
<b>CHAPTER 2: BACKGROUND INFORMATION AND SIGNIFICANCE OF WORK .....</b>	<b>4</b>
2.1: Overview.....	4
2.2: The Design and Use of Drilled Shaft Retaining Walls in Texas .....	4
2.2.1: Drilled Shaft Walls in Texas.....	4
2.2.2: Estimation of Lateral Earth Pressures.....	4
2.2.3: Summary of Current TxDOT Design Procedure for Stiff Clays (after TxDOT, 2009).....	5
2.3: The Effects of Expansive Clay on Retaining Structures.....	9
2.3.1: Swell Pressures, Overconsolidation, and Other Concerns.....	9
2.3.2: Recent Failures in Overconsolidated, Expansive Clay .....	10
2.4: Field Performance of Existing TxDOT Walls .....	11
2.4.1: Expansive Clay Concerns versus Real-World Mitigating Factors .....	11
2.4.2: Assessment of Existing TxDOT Walls.....	12
2.5: Proposed Models for Lateral Earth Pressure and Foundation Soil Response.....	13
2.5.1: Proposed Models of Long-Term Earth Pressure Loading .....	13
2.5.2: Proposed p-y Models of Foundation Soil Response .....	14
2.5.2.a: Stiff Clay Without Free Water .....	15
2.5.2.b: Stiff Clay With Free Water .....	15



2.5.2.c: Drained p-y Curves for Cohesionless Soil.....	15
2.5.2.d: Summary of Proposed p-y Curves for Comparison.....	19
2.6: Previous Reports on Lymon C. Reese Research Wall.....	20
2.6.1: Ellis (2011): A Subsurface Investigation in Taylor Clay .....	20
2.6.2: Dellinger (2011): The Use of Time Domain Reflectometry Probes for the Moisture Monitoring of a Drilled Shaft Retaining Wall in Expansive Clay .....	21
2.6.3: Koutrouvelis (2012): Earth Pressures Applied on Drilled Shaft Retaining Walls in Expansive Clay during Natural Cycles of Moisture Fluctuation .....	22
<b>CHAPTER 3: DESIGN AND CONSTRUCTION OF FULL-SCALE     INSTRUMENTED TEST WALL.....</b>	<b>24</b>
3.1: Location of Test Wall .....	24
3.2: Site Conditions.....	25
3.2.1: Overview.....	25
3.2.2: Preliminary Geotechnical Investigation (January 2010) .....	26
3.3: Design of Test Wall.....	27
3.4: Design of Instrumentation Program.....	30
3.4.1: Overview.....	30
3.4.2: Strain Gauges.....	31
3.4.3: Inclinometers .....	32
3.4.4: Additional Instrumentation .....	32
3.5: Construction of Full-Scale Instrumented Test Wall .....	34
3.6: Monitoring Plan.....	36
3.7: Data Reduction and Analysis.....	36
3.7.2: Strain Gauge Data Reduction .....	37
3.7.3: Inclinometer Data Reduction.....	39
3.7.3.a: Rotation Profiles Recorded in the Field.....	39
3.7.3.b: Combining and Smoothing Rotation Profiles.....	40

3.7.3.c: Obtaining Bending Moment Profiles from Rotation Data .....	48
3.7.3.d: Obtaining Net Earth Pressures from Bending Moment Profiles	52
3.7.3.e: Generating p-y Curves from Inclinometer Data .....	55
3.7.3.e.1: Discussion of “Net” Soil Resistance .....	55
3.7.3.e.2: Correcting Soil Resistance for Excavation Location ..	55
3.7.3.e.3: Correcting Horizontal Deflections for Center of Rotation .....	56
3.7.3.e.4: Example p-y Curves Developed from Inclinometer Data .....	58
3.8: Summary and Conclusions .....	59
<b>CHAPTER 4: TEST WALL PERFORMANCE BEFORE EXCAVATION (APRIL 2010 – AUGUST 2010) .....</b>	<b>61</b>
4.1: Overview .....	61
4.2: Climatic Information .....	61
4.3: Summary of Field Instrumentation Data .....	62
4.3.1: Strain Gauge Data .....	62
4.3.2: Stand Pipe Piezometer .....	71
4.4: Data Interpretation .....	71
4.4.1: Concrete Curing .....	71
4.4.2: Shrinkage Cracking in Concrete .....	72
4.4.3: Expansive Soil Movement .....	74
4.4.4: Development of Residual Stresses and Strains .....	75
4.5: Summary and Conclusions .....	77
<b>CHAPTER 5: TEST WALL PERFORMANCE DURING EXCAVATION (AUGUST 2010 – SEPTEMBER 2010) .....</b>	<b>78</b>
5.1: Overview .....	78
5.1.1: Summary of Excavation Progress .....	78
5.1.2: Climatic Information .....	79

5.2: Summary of Field Instrumentation Data .....	81
5.2.1: Inclinometer Data .....	81
5.2.2: Linear Potentiometer Data .....	85
5.2.3: Strain Gauge Data .....	85
5.3: Data Interpretation .....	93
5.3.1: Immediate Response to Stress Relief.....	93
5.3.2: Strain Gauge Behavior.....	95
5.3.2.a: Thermal Strains .....	95
5.3.2.b: Gauges Above Excavation Line (1-13 feet below ground surface)	
.....	96
5.3.2.c: Gauges Below Excavation Line (15-29 feet below ground surface)	
.....	97
5.3.3: Design Predictions versus Observed Behavior .....	97
5.3.4: Finite Element Model .....	102
5.3.5: Modified LPILE Analysis.....	107
5.3.5.a: Selection of Loading Conditions and p-y Curves .....	107
5.3.5.b: Results of Modified LPILE Analysis.....	113
5.4: Summary and Conclusions .....	117
<b>CHAPTER 6: TEST WALL BEHAVIOR DURING NATURAL MOISTURE</b>	
<b>CYCLES (OCTOBER 2010 – APRIL 2012) .....</b>	<b>120</b>
6.1: Overview.....	120
6.2: Important Events and Qualitative Observations .....	120
6.2.1: Installation of Shotcrete Facing .....	120
6.2.2: Installation of Time-Domain Reflectometry Probes.....	121
6.2.3: Excavation Slope Repair and Erosion Control .....	122
6.2.4: Climatic Information.....	123
6.3: Summary of Field Instrumentation Data .....	125
6.3.1: Inclinometer Data .....	125
6.3.2: Time Domain Reflectometry (TDR) Probe Data.....	126

6.3.3: Strain Gauge Data.....	129
6.4: Data Interpretation .....	138
6.4.1: Phases of Wall Motion.....	138
6.4.1.a: Drying Cycle 1: October 8, 2010 – January 6, 2011 (3 months) .....	138
6.4.1.b: Wetting Cycle 1: January 6, 2011 – March 11, 2011 (2 months) .....	139
6.4.1.c: Drying Cycle 2: March 11, 2011 – November 16, 2011 (8 months) .....	140
6.4.1.d: Wetting Cycle 2: November 16, 2011 – April 10, 2012 (5 months) .....	142
6.4.2: Deflected Shapes at Key Dates .....	143
6.4.3: Earth Pressure Reductions from Soil Shrinkage.....	146
6.4.4: Thermal Strains and Bending Curvatures .....	149
6.4.4.b: Daily Variation in Temperature and Bending Strains .....	151
6.4.4.c: Analysis of Thermal Deformations on March 11, 2011 and November 16, 2011.....	154
6.4.5: Earth Pressure Increases from Soil Expansion .....	158
6.5: Summary and Conclusions .....	158
 <b>CHAPTER 7: TEST WALL BEHAVIOR DURING CONTROLLED INUNDATION TESTING (MAY 2012 – JULY 2013) .....</b>	<b>161</b>
7.1: Overview.....	161
7.2: Summary of Key Events .....	161
7.2.1: Site Investigation and Installation of Inundation Berm and Piezometers .....	161
7.2.2: Summary of Inundation Cycles .....	164
7.2.2.a: First Inundation Cycle (May 2012 – July 2012).....	164
7.2.2.b: First Drying Cycle (July 2012 – February 2013).....	164
7.2.2.c: Second Inundation Cycle (February 2013 – June 2013).....	164
7.2.2.d: Second Drying Cycle (June 2013 – July 2013) .....	165
7.2.3: Climatic Information.....	166

7.3: Summary of Field Instrumentation Data .....	168
7.3.1: Inclinometer Data .....	168
7.3.2: Soil Moisture Content Data .....	171
7.3.3: Stand Pipe Piezometer Data.....	172
7.3.4: Time Domain Reflectometry (TDR) Probe Data.....	176
7.3.5: Strain Gauge Data.....	179
7.4: Data Interpretation .....	188
7.4.1: Immediate Response to Water .....	188
7.4.2: Development and Characterization of Drained, Fully Softened Strengths .....	193
7.4.3: LPILE Analysis.....	194
7.5: Summary and Conclusions .....	203
<b>CHAPTER 8: DEVELOPMENT OF DESIGN GUIDELINES.....</b>	<b>205</b>
8.1: Long-Term Design Guidelines .....	205
8.1.1: Summary of Long-Term Guidelines.....	205
8.1.2: Design Predictions vs. Observed Behavior.....	210
8.1.3: Hypothetical Test Wall Redesign Using Fully Softened Strengths and Hydrostatic Pressures from Natural Water Table .....	215
8.2: Short-Term Design Guidelines .....	218
8.3: Summary and Conclusions .....	220
<b>CHAPTER 9: CONCLUSIONS AND RECOMMENDATIONS.....</b>	<b>223</b>
9.1: Overview.....	223
9.2: Summary of Research Study.....	223
9.2.1: Instrumentation Program .....	223
9.2.1.a: Structural Performance of Drilled Shafts.....	223
9.2.1.b: Soil Moisture Monitoring .....	224
9.2.2: Behavior Before Excavation.....	224
9.2.3: Behavior During Excavation .....	225

9.2.4: Behavior During Natural Moisture Cycles .....	225
9.2.4.a: Response to Moisture Fluctuations .....	225
9.2.4.b: Thermal Strains and Bending Curvatures .....	226
9.2.5: Behavior During Controlled Inundation Testing .....	226
9.2.6: Development of Design Guidelines .....	227
9.2.6.a: Long Term Behavior After Cycles of Wetting and Drying ..	227
9.2.6.b: Short-Term Behavior During Excavation .....	228
9.3: Conclusions of Research Study .....	228
9.4: Recommendations for Future Work .....	230
References .....	232
Vita	235

## **List of Tables**

Table 3.1: Baseline assumptions and design parameters for test wall. ....	28
Table 3.2: Summary of wall construction activities and measured concrete strengths. .....	35
Table 5.1: Baseline assumptions and design parameters for short-term LPILE analysis.....	98
Table 5.2: Baseline assumptions and design parameters for modified LPILE analysis. .....	113
Table 6.1: Baseline assumptions and design parameters for initial soil shrinkage LPILE analysis.....	147
Table 7.1: Baseline assumptions and design parameters for long-term LPILE analysis of inundation conditions. ....	201
Table 8.1: Baseline assumptions and design parameters for LPILE analysis using proposed long-term design guidelines. ....	210

## List of Figures

Figure 2.1: Initial estimation of maximum moment using TxDOT design procedure. .....	7
Figure 2.2: Ultimate load ratio vs. clear spacing / drilled shaft diameter (after TxDOT, 2012).....	8
Figure 2.3: Examples of proposed long-term earth pressure envelopes for expansive clay (pressures are acting on a 2.5-foot shaft width). ....	14
Figure 2.4: Typical $k_{py}$ values for clays (after Dodds and Martin, 2007).....	17
Figure 2.5: Typical $k_{py}$ values for sands (after Dodds and Martin, 2007). ....	18
Figure 2.6: Illustration of strength reductions due to passive failure wedge interaction of closely spaced piles in sand (after Wang and Reese, 1986). ....	19
Figure 2.7: Summary of proposed p-y curves, calculated for the test wall at a depth of 16 feet below the original ground surface (1 foot below excavation line). .....	20
Figure 3.1: Location of full-scale test wall (Google, Inc.).....	24
Figure 3.2: Detailed site plan with location of test wall. ....	25
Figure 3.3: Taylor Clay from the project site in Manor, Texas. ....	26
Figure 3.4: Results of Atterberg Limit and UU testing from January, 2010 (three months before shaft construction; seven months before excavation).27	
Figure 3.5: Cross-section of wall and excavation at center shaft, facing east (not to scale). ....	29
Figure 3.6: Plan view of wall and excavation.....	29
Figure 3.7: Plan view of instrumented rebar cage before concrete placement. ....	30
Figure 3.8: Distribution of sensors within an instrumented shaft.....	31



Figure 3.9: Instrumentation on the project site. Clockwise from top left: temperature resistant datalogger and enclosure for continuous strain readings; signal conditioner for individual strain readings; linear potentiometer; TDR probe installed through facing. ....	33
Figure 3.10: Construction of test wall, April 2010. ....	34
Figure 3.11: Lifting an instrumented cage with two cranes. ....	35
Figure 3.12: Mathematical relationship between deflection (y), slope (S), bending moment (M), shear force (V), and soil reaction force (p) for a laterally loaded pile (after Reese and Van Impe, 2001). ....	37
Figure 3.13: Strain gauge data reduction (after Koutrouvelis 2012). ....	38
Figure 3.14: Sample rotation data from May 28, 2013. Reference survey is July 27, 2010, immediately before excavation. ....	40
Figure 3.15: Tukey's method of end value smoothing (after Tukey 1977). ....	44
Figure 3.16: Illustration of the 3RH smooth with re-roughing applied to the center shaft rotation data between 0 and 14 feet. ....	45
Figure 3.17: Comparison of original and smoothed rotation data from the center shaft on 5/28/2013. ....	46
Figure 3.18: Comparison of raw rotation data from the three instrumented shafts with the final smoothed rotation profile for differentiation. ....	47
Figure 3.19: Illustration of piecewise third-order polynomial fitting to a moving window of five points at a depth of 14 feet. First derivative at 14 feet is estimated numerically using a central difference approximation between polynomial values at 13.5 and 14.5 feet. ....	49
Figure 3.20: Relationship between bending curvature and bending moment (M- $\Phi$ relationship) used for LPILE and field instrumentation data analysis. ....	51

Figure 3.21: Bending moment profile generated from piecewise polynomial fitting of smoothed rotation profile and M- $\Phi$ relationship from LPILE.....	52
Figure 3.22: Soil resistance profiles generated using piecewise polynomial differentiation of averaged rotation profiles (with and without data smoothing applied during the differentiation process). .....	54
Figure 3.23: Using a third-order polynomial to adjust values of net soil resistance for p-y curves.....	56
Figure 3.25: Example p-y curves generated from inclinometer data at the test wall. Reference survey is October 8, 2010. ....	59
Figure 4.1: Monthly rainfall totals for Austin, Texas (Jan. 2009 - Jul. 2010; data from www.wunderground.com). Drilled shafts were installed in early April, 2010.....	62
Figure 4.2: Pre-Excavation Strain Data for Gauges 1 Foot Below Ground Surface. ....	63
Figure 4.3: Pre-Excavation Strain Data for Gauges 3 Feet Below Ground Surface.	64
Figure 4.4: Pre-Excavation Strain Data for Gauges 5 Feet Below Ground Surface.	64
Figure 4.5: Pre-Excavation Strain Data for Gauges 7 Feet Below Ground Surface.	65
Figure 4.6: Pre-Excavation Strain Data for Gauges 9 Feet Below Ground Surface.	65
Figure 4.7: Pre-Excavation Strain Data for Gauges 11 Feet Below Ground Surface. ....	66
Figure 4.8: Pre-Excavation Strain Data for Gauges 13 Feet Below Ground Surface. ....	66
Figure 4.9: Pre-Excavation Strain Data for Gauges 15 Feet Below Ground Surface. ....	67

Figure 4.10: Pre-Excavation Strain Data for Gauges 17 Feet Below Ground Surface. .....	67
Figure 4.11: Pre-Excavation Strain Data for Gauges 19 Feet Below Ground Surface. .....	68
Figure 4.12: Pre-Excavation Strain Data for Gauges 21 Feet Below Ground Surface. .....	68
Figure 4.13: Pre-Excavation Strain Data for Gauges 23 Feet Below Ground Surface. .....	69
Figure 4.14: Pre-Excavation Strain Data for Gauges 25 Feet Below Ground Surface. .....	69
Figure 4.15: Pre-Excavation Strain Data for Gauges 27 Feet Below Ground Surface. .....	70
Figure 4.16: Pre-Excavation Strain Data for Gauges 29 Feet Below Ground Surface. .....	70
Figure 4.17: Three weeks of strain measurements during concrete curing. Concrete placed on April 1; concrete in adjacent shafts placed on April 6. Positive strain indicates tension. ....	72
Figure 4.18: Illustration of tension crack formation in concrete near gauge. ....	73
Figure 4.19: Strains occurring between concrete curing and excavation. The gauge at a depth of 7 feet may be experiencing changes in side shear due to moisture fluctuations in the active zone (e.g., Kim & O'Neill, 1998). ....	75
Figure 4.20: Development of residual strains at a depth of 9 feet between shaft construction and excavation (after Koutrouvelis, 2012). ....	76
Figure 5.1: Photos of initial excavation progress (7/29/2010 – 8/5/2010). ....	78
Figure 5.2: Photos of later excavation progress (8/23/2010 - 10/1/2010). ....	79

Figure 5.3: Monthly rainfall totals for Austin, Texas (Jul. 2010 – Oct. 2010; data from <a href="http://www.wunderground.com">www.wunderground.com</a> ).....	80
Figure 5.4: Daily precipitation for Manor, Texas (Jul. 2010 – Oct. 2010; data from <a href="http://www.wunderground.com">www.wunderground.com</a> ). .....	80
Figure 5.5: Daily temperature data for Manor, Texas (Jul. 2010 – Oct. 2010; data from <a href="http://www.wunderground.com">www.wunderground.com</a> ).....	81
Figure 5.6: Progression of lateral deflections and key events during excavation.	82
Figure 5.7: Deflected shape of east instrumented shaft at various dates during excavation. ....	83
Figure 5.8: Cumulative deflections recorded in inclinometer installed through the soil 5.5 feet behind the center instrumented shaft. ....	84
Figure 5.9: Deflection measured at top of wall during excavation. Excavation began on July 29 and continued through August 27. ....	85
Figure 5.10: Strain Data 1 Foot Below Ground Surface During Excavation. ....	86
Figure 5.11: Strain Data 3 Feet Below Ground Surface During Excavation. ....	86
Figure 5.12: Strain Data 5 Feet Below Ground Surface During Excavation. ....	87
Figure 5.13: Strain Data 7 Feet Below Ground Surface During Excavation. ....	87
Figure 5.14: Strain Data 9 Feet Below Ground Surface During Excavation. ....	88
Figure 5.15: Strain Data 11 Feet Below Ground Surface During Excavation. ....	88
Figure 5.16: Strain Data 13 Feet Below Ground Surface During Excavation. ....	89
Figure 5.17: Strain Data 15 Feet Below Ground Surface During Excavation. ....	89
Figure 5.18: Strain Data 17 Feet Below Ground Surface During Excavation. ....	90
Figure 5.19: Strain Data 19 Feet Below Ground Surface During Excavation. ....	90
Figure 5.20: Strain Data 21 Feet Below Ground Surface During Excavation. ....	91
Figure 5.21: Strain Data 23 Feet Below Ground Surface During Excavation. ....	91

Figure 5.22: Strain Data 25 Feet Below Ground Surface During Excavation.....	92
Figure 5.23: Strain Data 27 Feet Below Ground Surface During Excavation.....	92
Figure 5.24: Strain Data 29 Feet Below Ground Surface During Excavation.....	93
Figure 5.25: Progression of excavation depth along wall face. ....	94
Figure 5.26: Contour plot of final surveyed excavation dimensions (all units in feet). .....	94
Figure 5.27: Development of bending strains in a pair of strain gauges located 23 feet below ground surface in the center shaft. ....	95
Figure 5.28: Strains related to temperature changes in exposed concrete. Gauge located 1 foot below ground surface on exposed side of wall. Soil at gauge location was excavated on July 29-31.....	96
Figure 5.29: Comparison of p-y prediction with measured field data. P-y analysis used a triangular earth pressure distribution of 40 psf/ft. ....	99
Figure 5.30: Comparison of predicted and measured shaft rotation profiles induced by removal of soil during excavation.....	100
Figure 5.31: Comparison of predicted and measured bending moment profiles induced by removal of soil during excavation. ....	101
Figure 5.32: Global response to removal of soil in linear elastic FEM. ....	103
Figure 5.33: Global shear strains in response to removal of soil in linear elastic FEM. .....	103
Figure 5.34: Comparison of linear elastic finite element model predictions with measured field data. ....	104
Figure 5.35: SASW testing at the test wall prior to excavation, June 2010. ....	105
Figure 5.36: Comparison of measured shear modulus profiles from SASW testing with finite element model prediction (after Ellis, 2011).....	106

Figure 5.37: Calculated values of bending moment and net soil resistance during excavation, based on measured rotation profiles from inclinometer data. .....	108
Figure 5.38: Comparison of calculated p-y curves during excavation with proposed p-y curves at a depth of 16 feet below original ground surface. ....	109
Figure 5.39: Comparison of calculated p-y curves during excavation with proposed p-y curves at a depth of 18 feet below original ground surface. ....	110
Figure 5.40: Comparison of calculated p-y curves during excavation with proposed p-y curves at a depth of 20 feet below original ground surface. ....	111
Figure 5.41: Comparison of calculated p-y curves during excavation with proposed p-y curves at a depth of 22 feet below original ground surface. ....	112
Figure 5.42: Comparison of measured and calculated profiles of deflection and bending moment in advanced LPILE analysis.....	115
Figure 5.43: Comparison of measured and calculated profiles of soil resistance in advanced LPILE analysis.....	116
Figure 5.44: Estimated horizontal deflection due to global movements of the soil-shaft system during excavation.....	117
Figure 6.1: Installation of Shotcrete Facing on October 1, 2010.....	120
Figure 6.2: Installation of TDR Moisture Probes Behind Wall Facing. ....	121
Figure 6.3: Installation of TDR Moisture Probes Through Ground Surface. ....	121
Figure 6.4: Approximate Locations of TDR Moisture Probes. ....	122
Figure 6.5: Excavation slopes are reshaped on August 17, 2011. ....	123
Figure 6.6: Erosion control material is installed on October 18, 2011. ....	123
Figure 6.7: Monthly Rainfall Totals for Austin, Texas (Oct. 2010 – Apr. 2012; data from <a href="http://www.wunderground.com">www.wunderground.com</a> ).....	124

Figure 6.8: Daily Temperature Data for Manor, Texas (Oct. 2010 – Apr. 2012; data from www.wunderground.com).....	125
Figure 6.9: Variation of top-of-wall deflection with natural moisture cycles. Deflections are referenced to installation of facing on October 8, 2010. .....	126
Figure 6.10: Electrical conductivity data from a TDR probe located 1.5 feet below ground surface (Oct. 2010 – Apr. 2012). ....	128
Figure 6.11 Electrical conductivity data from a TDR probe located 1.5 feet below ground surface, presented on a logarithmic scale (Oct. 2010 – Apr. 2012). ....	128
Figure 6.12: Strain Data 1 Foot Below Ground Surface (Oct. 2010 – Apr. 2012).	130
Figure 6.13: Strain Data 3 Feet Below Ground Surface (Oct. 2010 – Apr. 2012).	131
Figure 6.14: Strain Data 5 Feet Below Ground Surface (Oct. 2010 – Apr. 2012).	131
Figure 6.15: Strain Data 7 Feet Below Ground Surface (Oct. 2010 – Apr. 2012).	132
Figure 6.16: Strain Data 9 Feet Below Ground Surface (Oct. 2010 – Apr. 2012).	132
Figure 6.17: Strain Data 11 Feet Below Ground Surface (Oct. 2010 – Apr. 2012).	133
Figure 6.18: Strain Data 13 Feet Below Ground Surface (Oct. 2010 – Apr. 2012).	133
Figure 6.19: Strain Data 15 Feet Below Ground Surface (Oct. 2010 – Apr. 2012).	134
Figure 6.20: Strain Data 17 Feet Below Ground Surface (Oct. 2010 – Apr. 2012).	134
Figure 6.21: Strain Data 19 Feet Below Ground Surface (Oct. 2010 – Apr. 2012).	135
Figure 6.22: Strain Data 21 Feet Below Ground Surface (Oct. 2010 – Apr. 2012).	135
Figure 6.23: Strain Data 23 Feet Below Ground Surface (Oct. 2010 – Apr. 2012).	136
Figure 6.24: Strain Data 25 Feet Below Ground Surface (Oct. 2010 – Apr. 2012).	136
Figure 6.25: Strain Data 27 Feet Below Ground Surface (Oct. 2010 – Apr. 2012).	137
Figure 6.26: Strain Data 29 Feet Below Ground Surface (Oct. 2010 – Apr. 2012).	137

Figure 6.27: Inclinator Data from January 6, 2011.....	139
Figure 6.28: Inclinator Data from March 11, 2011.....	140
Figure 6.29: The use of a deep inclinometer casing and concrete pad as a qualitative indicator of soil shrinkage near the test wall (not to scale).....	141
Figure 6.30: Inclinator Data from November 16, 2011. ....	142
Figure 6.31: Inclinator Data from April 10, 2012.....	143
Figure 6.32: Deflected shapes of test wall at key dates, referenced to the installation of facing on October 8, 2010, compared with the initial p-y design analysis.....	145
Figure 6.33: Profiles of shaft rotation and estimated reduction in net earth pressures in response to soil shrinkage between March 11 and November 16, 2011. ....	148
Figure 6.34: Comparison of LPILE prediction with horizontal deflections and bending moments between March 11 and November 16, 2011.....	149
Figure 6.35: Air temperature in Manor, Texas on March 11 and November 16, 2011 (data from <a href="http://www.wunderground.com">www.wunderground.com</a> ).....	151
Figure 6.36: Comparison of air temperature in Manor, Texas and strain data at a depth of 3 feet in the center instrumented shaft (October 22 – October 27, 2011; weather data from <a href="http://www.wunderground.com">www.wunderground.com</a> ). ....	152
Figure 6.37: Comparison of air temperature in Manor, Texas and measured bending curvature in the test wall at various depths in the center shaft (temperature data from <a href="http://www.wunderground.com">www.wunderground.com</a> ). ....	153



Figure 6.38: Comparison of LPILE prediction with horizontal deflections and bending moments between March 11 and November 16, 2011. A bending moment of 150 in-kip was applied at the top of the shaft to simulate thermal effects. ....	156
Figure 6.39: Comparison of measured and calculated soil reaction forces due to expansive soil shrinkage. ....	157
Figure 7.1: Location of inundation zone and stand pipe piezometers. Piezometers A and C are screened from 5 to 15 feet; piezometer B is screened between 3.4 and 4.6 feet; piezometer D is screened between 3.6 and 4.8 feet. ....	162
Figure 7.2: Schematic of inundation berm. ....	163
Figure 7.3: Inundation berm and stand pipe piezometers (April 26, 2012). ....	163
Figure 7.4: Flooding in response to a large storm before the May 6, 2013 data surveys. Water level in the excavation reached ground surface. ....	165
Figure 7.5: Inundation zone on June 17, 2013, two weeks into second drying cycle. Stand pipe piezometer casing is 4" across. ....	166
Figure 7.6: Monthly rainfall totals for Austin, Texas (May 2012 - Jun. 2013; data from <a href="http://www.wunderground.com">www.wunderground.com</a> ). ....	167
Figure 7.7: Daily average temperature data for Manor, Texas (May 2012 - Jul. 2013; data from <a href="http://www.wunderground.com">www.wunderground.com</a> ). ....	168
Figure 7.8: Average deflected shapes at key dates during inundation testing. Data is referenced to installation of facing in October, 2010. ....	169
Figure 7.9: Top-of-wall deflections during inundation testing (key dates indicated by vertical dashed lines). Reference survey is facing installation in October, 2010. ....	170

Figure 7.10: Rate of deflection at ground surface during inundation testing (key dates indicated by vertical dashed lines).....	170
Figure 7.11: Summary of measured soil moisture contents during controlled inundation testing.....	172
Figure 7.12: Water level in Piezometer B-3 (outside inundation zone) during inundation testing.....	174
Figure 7.13: Data from shallow-screened stand pipe piezometers during second inundation cycle.....	175
Figure 7.14: Data from deeper-screened stand pipe piezometers during second inundation cycle.....	175
Figure 7.15: Electrical conductivity data from a TDR probe located 1.5 feet below ground surface (May 2012 – Jul. 2013).....	177
Figure 7.16: Electrical conductivity data from a TDR probe located 1.5 feet below ground surface during first inundation cycle (May – Jul. 2012).....	177
Figure 7.17: Electrical conductivity data from a TDR probe located 1.5 feet below ground surface during first drying cycle (Jul. 2012 – Feb. 2013).....	178
Figure 7.18: Electrical conductivity data from a TDR probe located 1.5 feet below ground surface during second inundation cycle (Feb. – Jun. 2013).....	178
Figure 7.19: Electrical conductivity data from a TDR probe located 1.5 feet below ground surface during second drying cycle (Jun. – Jul. 2013).....	179
Figure 7.20: Strain Data 1 Foot Below Ground Surface (May 2012 – July 2013).....	181
Figure 7.21: Strain Data 3 Feet Below Ground Surface (May 2012 – July 2013).....	181
Figure 7.22: Strain Data 5 Feet Below Ground Surface (May 2012 – July 2013).....	182
Figure 7.23: Strain Data 7 Feet Below Ground Surface (May 2012 – July 2013).....	182
Figure 7.24: Strain Data 9 Feet Below Ground Surface (May 2012 – July 2013).....	183

Figure 7.25: Strain Data 11 Feet Below Ground Surface (May 2012 – July 2013).	183
Figure 7.26: Strain Data 13 Feet Below Ground Surface (May 2012 – July 2013).	184
Figure 7.27: Strain Data 15 Feet Below Ground Surface (May 2012 – July 2013).	184
Figure 7.28: Strain Data 17 Feet Below Ground Surface (May 2012 – July 2013).	185
Figure 7.29: Strain Data 19 Feet Below Ground Surface (May 2012 – July 2013).	185
Figure 7.30: Strain Data 21 Feet Below Ground Surface (May 2012 – July 2013).	186
Figure 7.31: Strain Data 23 Feet Below Ground Surface (May 2012 – July 2013).	186
Figure 7.32: Strain Data 25 Feet Below Ground Surface (May 2012 – July 2013).	187
Figure 7.33: Strain Data 27 Feet Below Ground Surface (May 2012 – July 2013).	187
Figure 7.34: Strain Data 29 Feet Below Ground Surface (May 2012 – July 2013).	188
Figure 7.35: The inundation zone is filled on May 3, 2012.....	189
Figure 7.36: Electrical conductivity data from one TDR probe shows a response within minutes of beginning the inundation test. Probe is located 1.5 feet below ground surface.....	190
Figure 7.37: Water infiltration into the excavation was first observed 90 minutes from the start of inundation.....	190
Figure 7.38: Moisture content profiles immediately before and after first inundation cycle. Natural water table is located at a depth of approximately 8 feet. .....	192
Figure 7.39: Comparison of measured fully softened strength test data from the project site with data from Ellis (2011) and established correlations.	194
Figure 7.40: Comparison of calculated long-term p-y curves during inundation testing with proposed p-y curves at a depth of 16 feet below original ground surface.....	196

Figure 7.41: Comparison of calculated long-term p-y curves during inundation testing with proposed p-y curves at a depth of 18 feet below original ground surface.....	197
Figure 7.42: Comparison of calculated long-term p-y curves during inundation testing with proposed p-y curves at a depth of 20 feet below original ground surface.....	198
Figure 7.43: Comparison of calculated long-term p-y curves during inundation testing with proposed p-y curves at a depth of 22 feet below original ground surface.....	199
Figure 7.44: Comparison of calculated long-term p-y curves during inundation testing with proposed p-y curves at a depth of 24 feet below original ground surface.....	200
Figure 7.45: Comparison of long-term LPILE Prediction and calculated soil reaction forces.....	202
Figure 8.1: Summary of long-term design guidelines. ....	206
Figure 8.2: Typical $k_{py}$ values for clays (after Dodds and Martin 2007).....	208
Figure 8.3: Typical $k_{py}$ values for sands (after Dodds and Martin 2007). ....	209
Figure 8.4: Summary of measured and predicted values of deflected shapes using long-term design guidelines.....	212
Figure 8.5: Summary of measured and predicted bending moments using long-term design guidelines.....	213
Figure 8.6: Comparison of Long-Term Modified LPILE Prediction and Calculated Soil Reaction Forces. ....	214

Figure 8.7: Comparison of long-term p-y curves predicted by modified LPILE analysis with p-y curves estimated from field data (reference survey is after installation of shotcrete facing on October 8, 2010). .....215

Figure 8.8: Input earth pressure envelope for wettest test wall conditions prior to inundation testing (natural groundwater table at 8 feet below ground surface).....217

Figure 8.9: Comparison of deflected shapes and bending moments for hypothetical test wall redesign using proposed long-term conditions.....218

Figure 8.10: Comparison of measured data with predictions from linear elastic finite element model including anisotropy and stiffness reductions. ....220

# **CHAPTER 1: OVERVIEW OF RESEARCH STUDY**

## **1.1: Introduction**

The design of drilled shaft retaining walls in non-expansive soils is well established. In expansive soils, however, there is no consensus on the correct way to model the effects of soil expansion on wall behavior during cycles of wetting and drying. Based on the range of design assumptions currently in practice, existing walls could be substantially over- or under-designed. The purpose of this research is to advance the understanding of the behavior of drilled shaft retaining walls installed through expansive clay. The primary source of information for this study will be data from a full-scale instrumented test wall, which was installed through highly overconsolidated, expansive clay in Manor, Texas, and monitored for a period of four years. This study includes a summary of existing research, technical information on the design and construction of the instrumented test wall, an examination of the relationship between soil behavior and wall deformation during the three year monitoring period, and recommendations on how to account for the effects of expansive soil in design. The analysis of test wall response includes summaries of behavior before excavation, during excavation, during long-term moisture fluctuations which included an extreme drought, and during controlled inundation testing which provided the retained soil unlimited access to water until the wall deflections reached equilibrium.

## **1.2: Objectives**

The goal of this research is to advance our understanding of the long-term behavior of retaining structures in expansive clays. The observed performance and instrumentation data from our test wall will be used to address the following objectives:

1. Identify and analyze the processes responsible for wall loading and deformation.

2. Evaluate how these processes change with time and moisture cycles.
3. Provide guidance for design practice to account for these processes and ensure adequate wall performance.

### **1.3: Methodology**

The objectives of this research study will be accomplished according to the following methodology:

1. Design and construct a full-scale instrumented test wall through expansive clay.
2. Monitor the performance of the test wall during construction, excavation, natural seasonal moisture fluctuations, and controlled inundation testing which provides the expansive clay with unlimited access to water.
3. Analyze test wall performance data using standard of practice design methods.
4. Develop guidance for design practice based on results of analyses.

This study is primarily based on data from the Lymon C. Reese research wall in Manor, Texas. While the Taylor clay at the research site is typical of an overconsolidated, high plasticity, stiff-fissured clay in Texas, the behavior of other expansive soil deposits may deviate from the behavior presented in this dissertation. Unless otherwise noted, the conclusions presented in this study are not intended to be applied to walls or sites beyond the Lymon C. Reese research wall.

### **1.4: Organization**

Because data from the Lymon C. Reese research wall provides the primary basis for this research, this dissertation will address the design, construction, performance monitoring, and data analysis for the test wall. A background on the design and use of

drilled shaft retaining walls in expansive clays, along with a summary of existing research on the Lymon C. Reese research wall, is presented in Chapter 2. The design, construction, and data reduction procedures for the test wall and instrumentation program are covered in Chapter 3. Analyses of test wall behavior before excavation, during excavation, during long-term moisture fluctuations which included an extreme drought, and during controlled inundation testing which provided the retained soil unlimited access to water are respectively presented in Chapters 4 - 7. The development of design guidelines, including a discussion of how to represent earth pressures in the retained soil and p-y curves in the foundation soil, is covered in Chapter 8. The conclusions of the research study are presented in Chapter 9.



## **CHAPTER 2: BACKGROUND INFORMATION AND SIGNIFICANCE OF WORK**

*Note: Portions of this section have been previously submitted by the author in Report No. FHWA/TX-11/0-6603-1 (Brown et al., CTR 2011).*

### **2.1: Overview**

This section presents background information on the topic of drilled shaft retaining walls in expansive clay soils and a summary of published research on the Lymon C. Reese research wall. Additional discussion of existing research, where applicable, is included in subsequent chapters.

### **2.2: The Design and Use of Drilled Shaft Retaining Walls in Texas**

#### **2.2.1: DRILLED SHAFT WALLS IN TEXAS**

Cantilever drilled shaft retaining walls are common earth-retaining structures in Texas. They are well suited to use in urban environments where noise, space, and damage to adjacent structures are major considerations (Wang and Reese 1986). Additionally, because of the prevalence of drilled shaft foundations in Texas, experienced contractors are readily available. The design of drilled shaft retaining walls has changed over time. While initial design methods were based on limit equilibrium calculations, more refined p-y analyses based on soil-structure interaction have been developed and are currently in use by TxDOT (Wang and Reese 1986; TxDOT 2009).

#### **2.2.2: ESTIMATION OF LATERAL EARTH PRESSURES**

There is uncertainty in how to account for lateral earth pressures acting on drilled shaft walls installed through expansive clay. In Texas, some of the most problematic expansive clay deposits are also highly overconsolidated. For this reason, an examination

of retaining wall design procedures for stiff, overconsolidated clay can provide a reference point for the design of walls in expansive clay deposits.

Commonly, the earth pressure on walls in stiff, overconsolidated clay is estimated using Coulomb active earth pressures with drained properties (Wang and Reese 1986). The TxDOT Design Procedure for Cantilever Drilled Shaft Walls employs this method with a recommended friction angle of 30 degrees for “medium to stiff clays” (TxDOT 2009). For clays common in Texas, this approach results in earth pressures that correspond to an equivalent fluid unit weight of approximately 35 to 40 pounds per cubic foot (pcf).

### **2.2.3: SUMMARY OF CURRENT TxDOT DESIGN PROCEDURE FOR STIFF CLAYS (AFTER TxDOT, 2009)**

In the current TxDOT design procedure, drilled shaft size and spacing is based on moment capacity. The following section presents a shortened version of the procedure that appears in TxDOT (2009). More detailed design information can be found in TxDOT (2012).

1. Determine earth pressures to be applied as loads using a Coulomb analysis with cohesion equal to zero.
  - a. For stiff clays, use a friction angle of 30 degrees. Assume angle of wall friction is equal to two-thirds the soil friction angle.
  - b. Assume no water behind the wall.
  - c. Include soil or traffic surcharge loads where appropriate.
2. Estimate maximum moment in shaft.
  - a. Compute groundline moment from earth pressure distribution.
  - b. Increase groundline moment by 50% to estimate the maximum earth pressure below the excavation line, i.e.  $M_{\max} = 1.5 \cdot M_{GL}$  (Figure 2.1).
3. Choose trial drilled shaft size and spacing based on moment capacity.

- a. Use load factor of 1.7 for earth pressure to compute ultimate moment ( $M_u$ )
  - b. Use nominal moment ( $M_n$ ) from shaft properties, then check that the factored moment capacity ( $\phi \cdot M_n$ ) exceeds  $M_u$  with  $\phi = 0.9$ .
4. Determine properties of the soil below the finished groundline.
    - a. Use ultimate soil strengths for p-y curves.
    - b. Reduce soil strengths from 0 to 5 feet below the excavation line by 50% to account for loss of strength after excavation.
  5. Run p-y analysis using COM624 or LPILE.
    - a. Reduce soil strengths to account for close shaft spacing based on Figure 2.2.
    - b. Use uncracked section properties for the shaft.
    - c. Ensure bending moments and deflections are within allowable values.  
Limit deflections to 1% of the cantilever height.
  6. Determine depth of shaft fixity based on several embedment values.
    - a. Determine depth of fixity where top-of-wall deflection is no longer affected by embedment depth.
    - b. Determine final embedment depth by multiplying depth of fixity by 1.33.

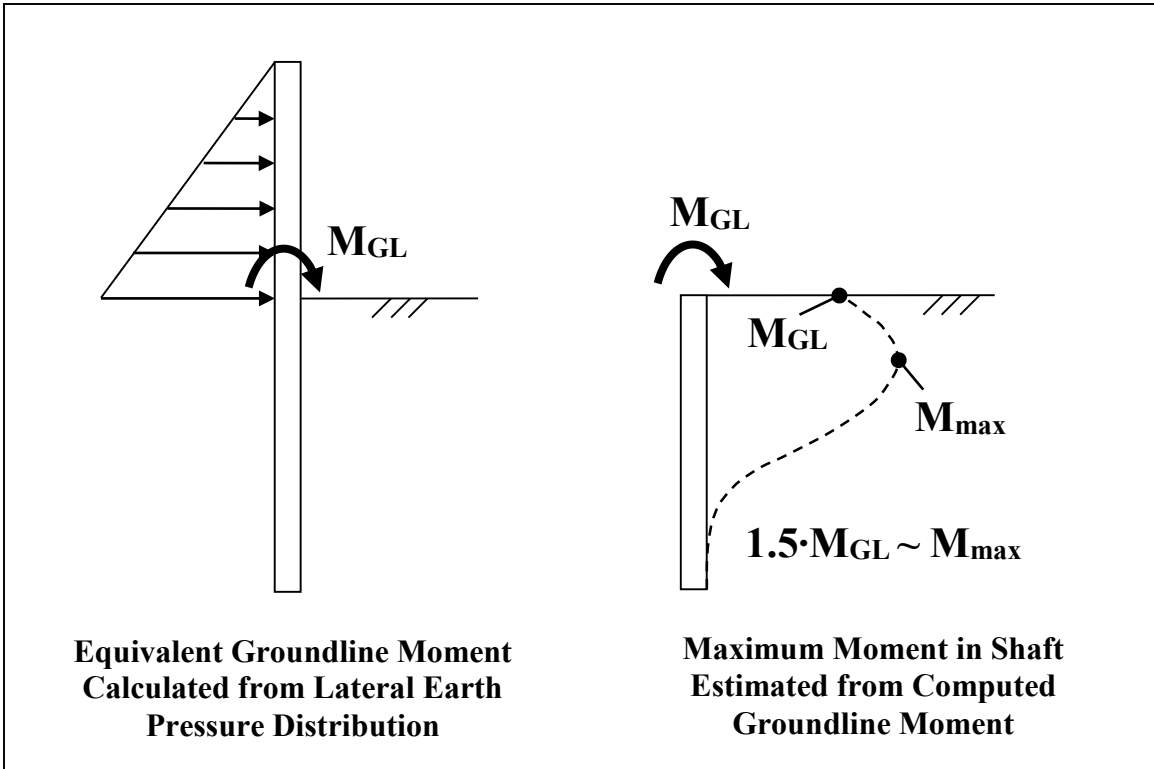


Figure 2.1: Initial estimation of maximum moment using TxDOT design procedure.

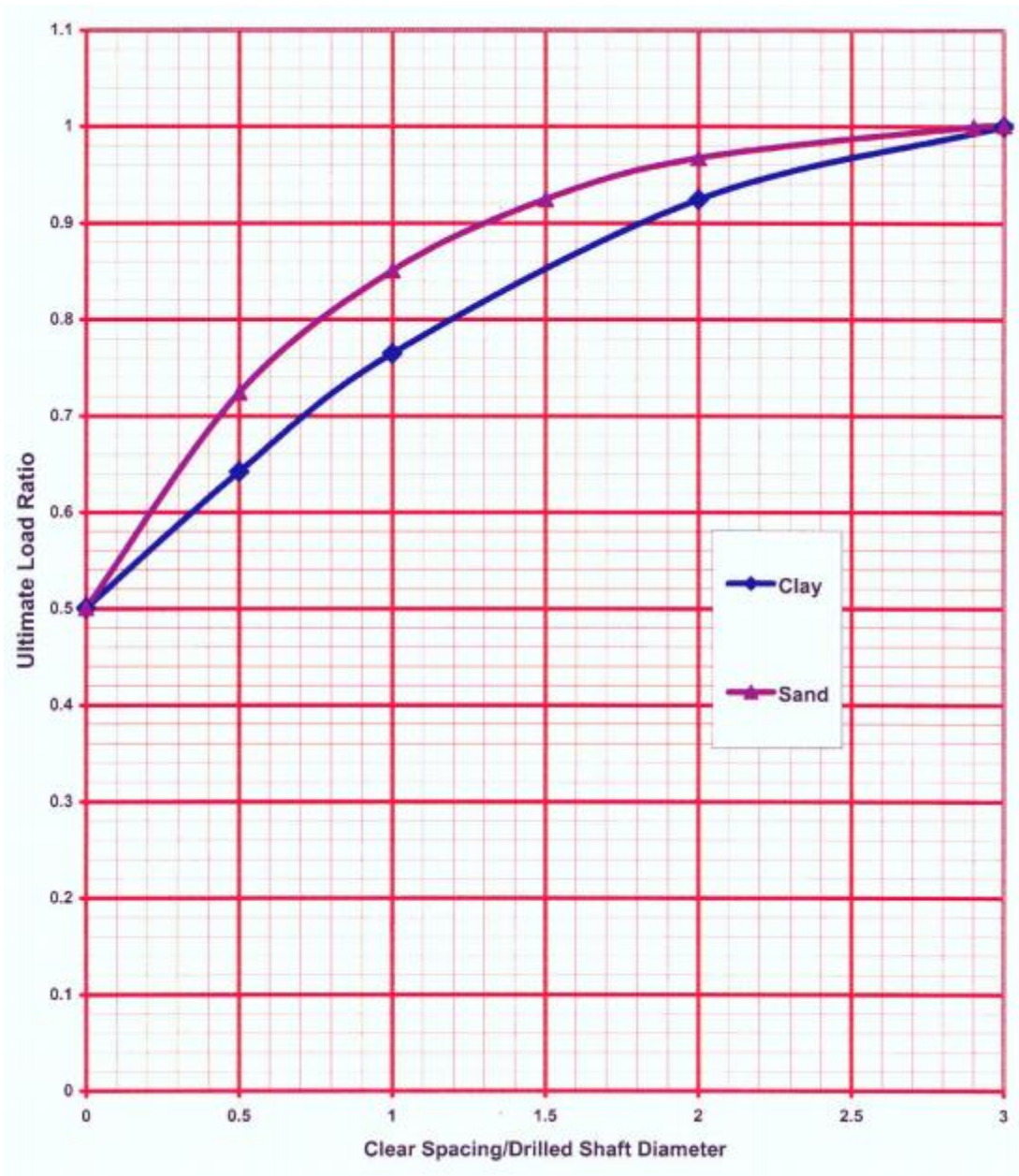


Figure 2.2: Ultimate load ratio vs. clear spacing / drilled shaft diameter (after TxDOT, 2012).

## **2.3: The Effects of Expansive Clay on Retaining Structures**

### **2.3.1: SWELL PRESSURES, OVERCONSOLIDATION, AND OTHER CONCERNS**

There have been concerns raised over the potential effects of expansive soils on retaining structures. The most common of these concerns is the magnitude of horizontal swelling pressures exerted on the wall by the expansive soil. Lytton (2007) summarizes some relevant studies that seek to quantify this effect. Various, the potential lateral pressures acting on a wall in expansive clay have been estimated to be four times the overburden pressure, 6000 psf at three feet of depth in a lab study, 8000 psf at three feet of depth in another lab study, and 1700 psf at three feet of depth in a field study – any of these scenarios are significantly higher than the currently accepted values used for retaining wall design. These studies are described in more detail in Lytton (2007). In general, the expansive soil pressure exerted on a wall is considered to be limited by the passive resistance of the retained soil (Pufahl et al. 1983 and Hong 2008).

In addition to the potential for high lateral pressures, other potential concerns have been identified for retaining walls in expansive clay. Pufahl et al. (1983) describe a hypothetical structure “ratcheting” out with wetting and drying cycles. During dry seasons, the soil could pull back from the wall, incompressible debris could fill the gap, and soil expansion could push the wall and debris further out with each new rewetting cycle. Puppala et al. (2011) describe that cracks near drilled shafts could create zones for moisture infiltration, increasing the depth of the active zone near the shafts.

In Texas, many expansive soil deposits are also heavily overconsolidated. In overconsolidated clay, in-situ horizontal stresses can be very large. When the unloading associated with retaining wall excavation takes place, these large horizontal stresses can impact wall performance. Furthermore, the residual strength of overconsolidated clay can be very low – residual friction angles of 18 degrees or less have been widely reported. The

transition from peak-drained strength to residual-drained strength could influence the increase in lateral earth pressures with time (Wang and Reese 1986). The lateral swell pressures from moisture changes in overconsolidated clay have been reported to be higher than those in normally consolidated clay (Ellis 2011).

### **2.3.2: RECENT FAILURES IN OVERCONSOLIDATED, EXPANSIVE CLAY**

Because the potential for expansion and a high degree of overconsolidation coexist in expansive clays in Texas, it is difficult to separate the effects of swelling from the effects of overconsolidation when considering wall failures. Smith et al. (2009) examine the failure of a bridge deck completed using top down construction in the overconsolidated, expansive Eagle Ford shale near Dallas, TX. In this case, the bridge deck was installed before complete excavation of the underpass and installation of tiebacks. Ultimately, an estimated four inches of inward movement caused the failure of the bridge deck. The authors concluded that the major issue was the use of a design at-rest earth pressure coefficient ( $K_o$ ) value of approximately 0.7; actual values of  $K_o$  for the Eagle Ford shale and other overconsolidated clays are often reported to be between 2 and 3. Expansive soil movement was cited as a “likely” contributing factor (Smith et al. 2009).

Another wall failure in the Eagle Ford shale, this time of a Vertically Earth Reinforced Technology (VERT) wall system, is detailed by Adil Haque and Bryant (2011). This paper indicates that the high  $K_o$  values and low residual strengths of overconsolidated clay, as well as expansion from moisture changes, should have been considered in design. The paper also states that “the swell pressure due to unloading could also exert a significant pressure on the wall, much greater than the swell pressure on the walls from moisture changes” (Adil Haque and Bryant 2011).

## **2.4: Field Performance of Existing TxDOT Walls**

### **2.4.1: EXPANSIVE CLAY CONCERNS VERSUS REAL-WORLD MITIGATING FACTORS**

Despite the numerous problems potentially associated with the expansive soils in Texas, relatively few failures of drilled shaft retaining walls have been observed. There are several possible explanations for the general lack of problems associated with drilled shaft retaining walls in expansive clays in Texas.

First, the load factors and deflection requirements used by the TxDOT design procedure will result in drilled shafts that can withstand higher pressures than the nominal values used in design. After calculating the maximum moment in the shaft, a load factor of 1.7 is applied to estimate the design moment. If the differences in active Coulomb earth pressures induced by residual soil strength and/or soil swell are within the range encompassed by this load factor, it is possible that the potential increases in soil pressures are not causing visible distress on walls (for reference, a Coulomb analysis using a residual friction angle of 18 degrees results in an equivalent fluid pressure of approximately 60 psf/ft, about 50% higher than the nominal value of 40 psf/ft). While the top-of-shaft deflections might exceed one percent of the wall height, the structural integrity of the shafts may be preserved. Furthermore, the final as-built drilled shafts may have greater capacity than the minimum allowed by design due to other factors such as constructability (although the risk for lower-than-design capacities due to poor construction exists as well).

Additionally, pavement and drainage systems behind drilled shaft walls may limit the severity of moisture changes causing shrinking and swelling. In pavements with expansive subgrades, moisture contents tend to increase from their natural moisture content to a “steady state” value after the installation of pavement (Snethen et al. 1975, Wise et al. 1971). While the subgrade is still subject to moisture changes, the magnitude of these changes may be smaller than those of exposed soil. The presence of pavement near the



shaft can also prevent the problems associated with water and/or debris entering the gap between the shaft and the soil (Puppala et al. 2011).

Finally, despite the potential to generate very large swell pressures under confinement, swell pressures can be reduced by allowing relatively small wall deformations to take place (Thomas et al. 2009). For projects as large as the typical TxDOT drilled shaft retaining wall, it is possible that expansive soil pressures are being accommodated by small wall deformations that would not be noticed without careful instrumentation.

#### **2.4.2: ASSESSMENT OF EXISTING TxDOT WALLS**

In 2011, our research team completed an assessment of existing TxDOT walls. The report provides assessment information and analysis for three drilled shaft walls constructed through expansive clay in Houston, Texas. The walls assessed in this study are generally representative of typical drilled shaft walls in Texas. The three walls have cantilevered heights ranging from 5 to 23 feet, and at the time of the study, the walls had been in service for 14, 9, and 2 years. Over this time period, Houston experienced a range of climate related soil moisture fluctuations that could potentially lead to expansive soil movement. A field inspection of each wall revealed no obvious signs of distress. Based on LPILE analyses of these walls, earth pressures greater than a linear increase of 80 psf/ft would likely be required to produce significant distress that could be readily observed (Brown et. al. 2011).

## **2.5: Proposed Models for Lateral Earth Pressure and Foundation Soil Response**

### **2.5.1: PROPOSED MODELS OF LONG-TERM EARTH PRESSURE LOADING**

Long-term conditions generally govern retaining wall design in high plasticity clays. Often, for embankments and retaining walls, the development of drained, fully softened strengths is a suitable ultimate condition for design (Wright 2005). A variety of models have been proposed for representing the long-term earth pressures induced by expansive soil. For clays in the Taylor formation, where the Lymon C. Reese research wall is constructed, peak drained friction angles are approximately 37 degrees (Long 1983 and Ellis 2011), and average fully softened friction angles in the upper 15 feet are estimated to be approximately 24 degrees based on liquid limit relationships (e.g. Wright 2007) and laboratory test data discussed in Chapter 7. The resulting earth pressure envelopes using the fully softened strengths of the Taylor clay, assuming both no water behind the wall and hydrostatic conditions behind the wall, are pictured in Figure 2.3, along with TxDOT's typical design earth pressure envelope and a hypothetical model of expansive soil swelling pressures similar to that presented in Hong (2008).

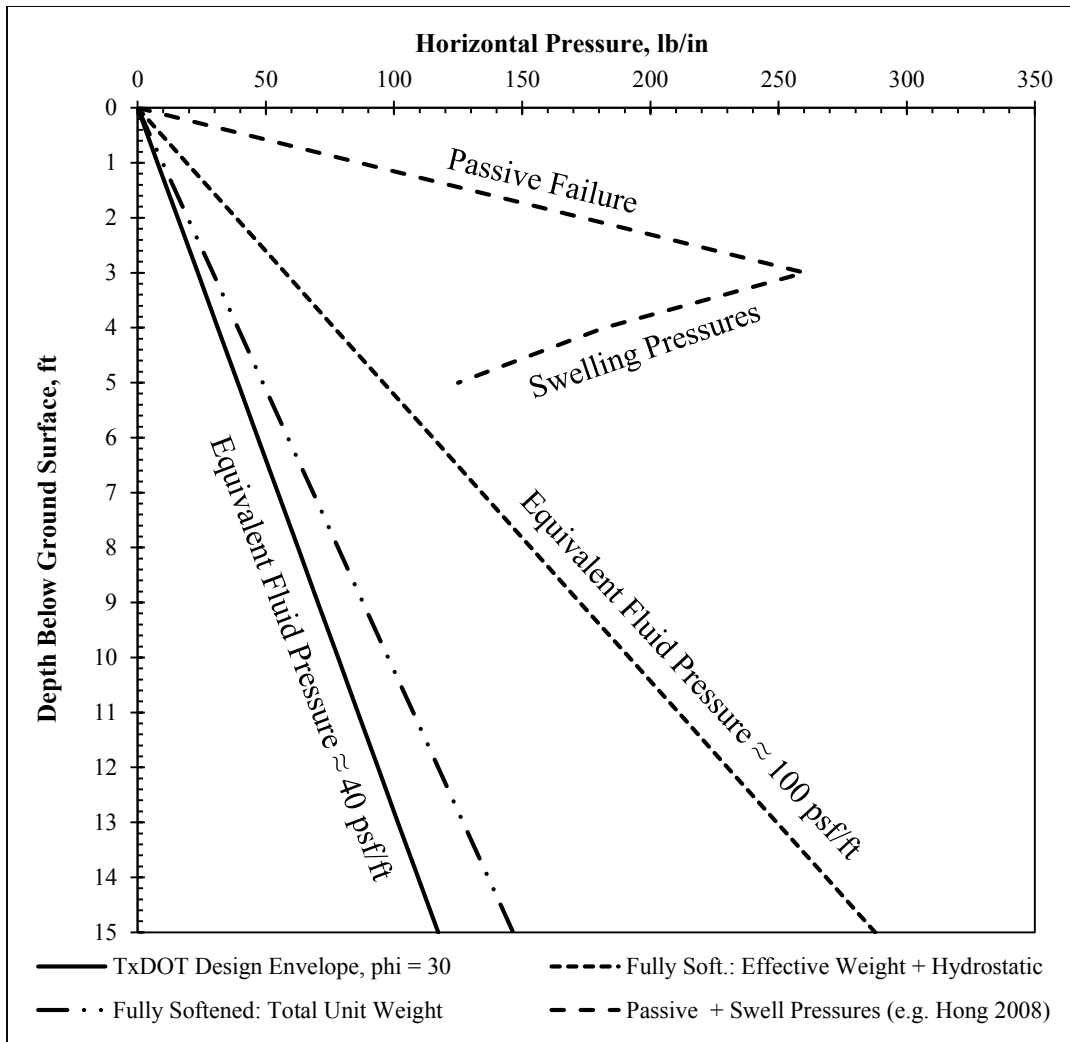


Figure 2.3: Examples of proposed long-term earth pressure envelopes for expansive clay (pressures are acting on a 2.5-foot shaft width).

### 2.5.2: PROPOSED P-Y MODELS OF FOUNDATION SOIL RESPONSE

In addition to the uncertainty associated with the behavior of the retained soil, several p-y models have been proposed to model the response of the foundation soil in expansive clay. Some of these curves are briefly explained below; illustrations of the calculated curves at a depth of 16 feet below the original ground surface (1 foot below the

design excavation base) for the Lymon C. Reese research wall are provided for comparison in Figure 2.7.

#### **2.5.2.a: Stiff Clay Without Free Water**

Typically, the TxDOT design procedure for stiff clays uses p-y curves for “stiff clay without free water,” developed from tests in Houston, Texas (TxDOT 2009, Reese et. al. 2006, Reese and Welch 1972). To account for strength reductions due to the removal of overburden pressures during excavation, a common procedure for excavations in stiff-fissured clay is to translate the profile of undrained strengths from the original ground surface down to the excavation line. Additionally, soil strengths are reduced to account for the effect of close pile spacing as shown in Figure 2.2 (TxDOT 2012; Wang and Reese 1986). For the Lymon C. Reese wall, average undrained strengths used for the development of representative p-y curves shown in Figure 2.7 were approximately 1600 to 2000 psf (before strength reductions). Total soil unit weights are used for these curves.

#### **2.5.2.b: Stiff Clay With Free Water**

It is possible that if water stays in the excavation base, the use of curves developed for “stiff clay in the presence of free water” may be appropriate. These curves were developed from load tests in the Taylor formation in Manor, Texas (Reese et. al. 1975). Strength reductions to account for the removal of overburden pressures and close pile spacing are applied before calculating the curves as shown in Reese et. al. 2006. Curves developed for clays in the presence of free water use effective unit weights.

#### **2.5.2.c: Drained p-y Curves for Cohesionless Soil**

If the long-term conditions of drilled shaft walls in expansive clays are governed by the development of drained conditions, the use of drained p-y curves developed for cohesionless soils may be appropriate. Because the initial stiffness of the clay in response

to loading at small strains is governed by undrained behavior, the initial stiffness value  $k_{py}$  for the p-y curves is selected according to the undrained properties of the clay as shown in Figure 2.4. The use of default  $k_{py}$  values for modeling curves at low friction angles associated with expansive clay soils results in unrealistically low values of initial stiffness (Figure 2.5). The selection of unit weight is based on the expected hydrostatic conditions on the project site.

The selection of drained friction angle and appropriate strength reductions due to pile spacing is less straightforward for long-term, drained conditions in clay. Drained friction angles for the Taylor clay can range from 37 degrees at peak, to approximately 24 degrees under fully softened conditions, to as low as 15 – 18 degrees under residual conditions. For short-term drained loading in sand, at low values of clear spacing, the passive soil resistance wedges from each shaft interact with each other, and a “shadowing” effect is present as shown in Figure 2.6. For short-term drained loading in sands, ultimate soil loads are reduced in accordance with Figure 2.2. For long-term loading in clay, however, the mechanism of pile interaction at close spacing is less clear. For the curves shown in Figure 2.7, no reductions are applied for close pile spacing (test wall data will be compared with the proposed curves to evaluate this condition).

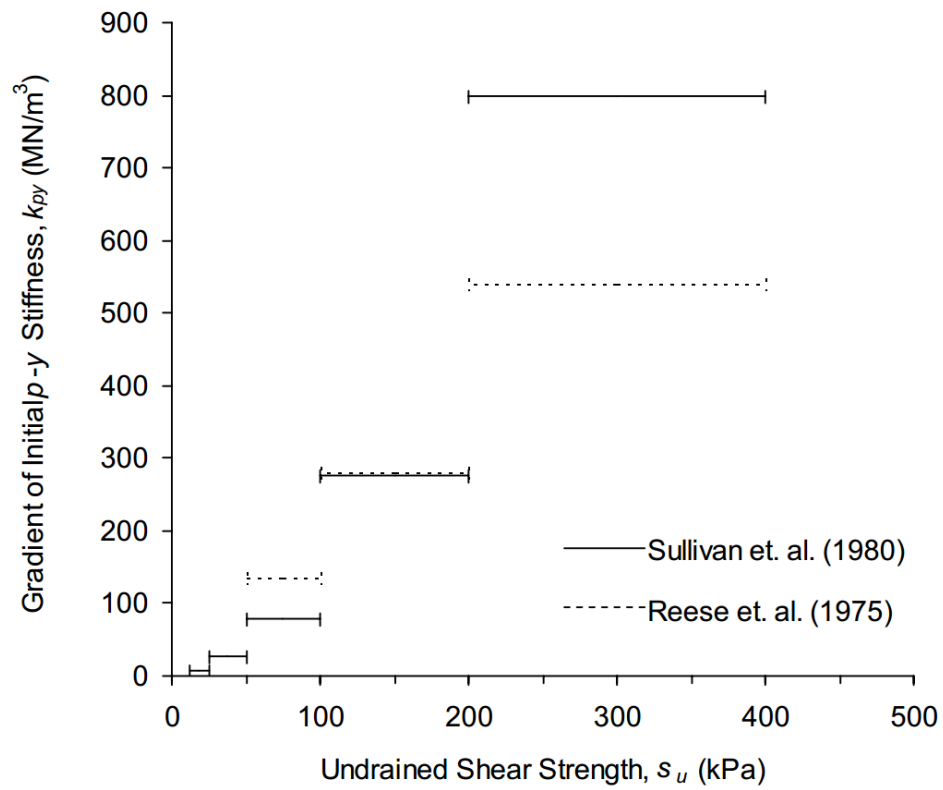


Figure 2.4: Typical  $k_{py}$  values for clays (after Dodds and Martin 2007).

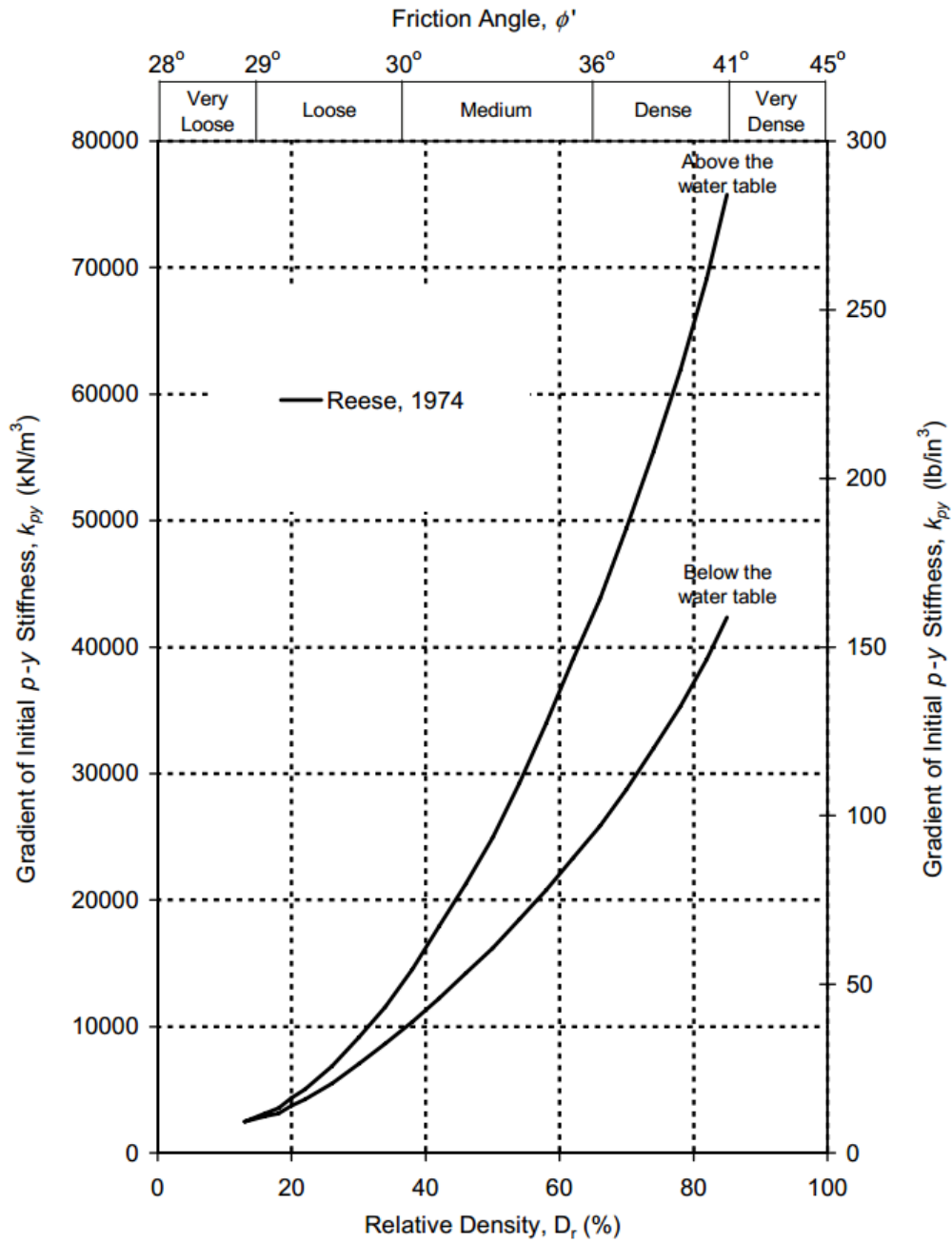


Figure 2.5: Typical  $k_{py}$  values for sands (after Dodds and Martin 2007).

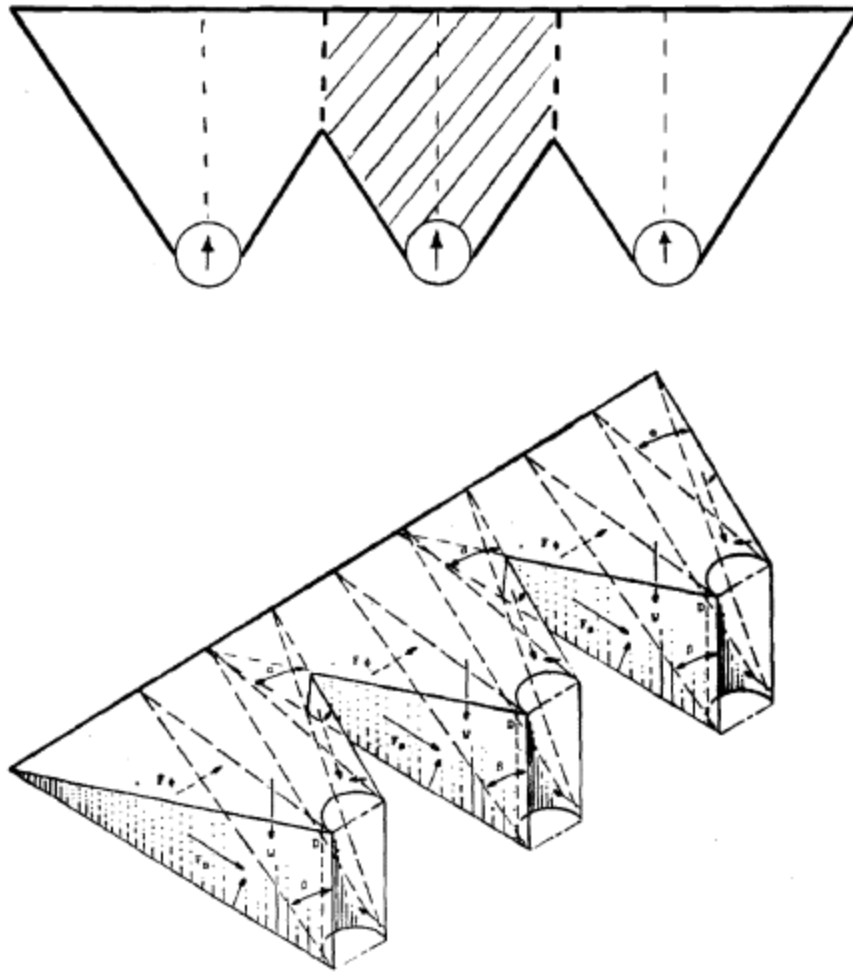


Figure 2.6: Illustration of strength reductions due to passive failure wedge interaction of closely spaced piles in sand (after Wang and Reese 1986).

#### 2.5.2.d: Summary of Proposed p-y Curves for Comparison

A summary of the proposed p-y curves discussed in the previous sections, calculated for the test wall at a depth of 16 feet below the original ground surface (1 foot below the excavation line) is shown in Figure 2.7 for comparison. For this research study, p-y curves estimated from test wall data will be compared with the family of curves discussed in this section.



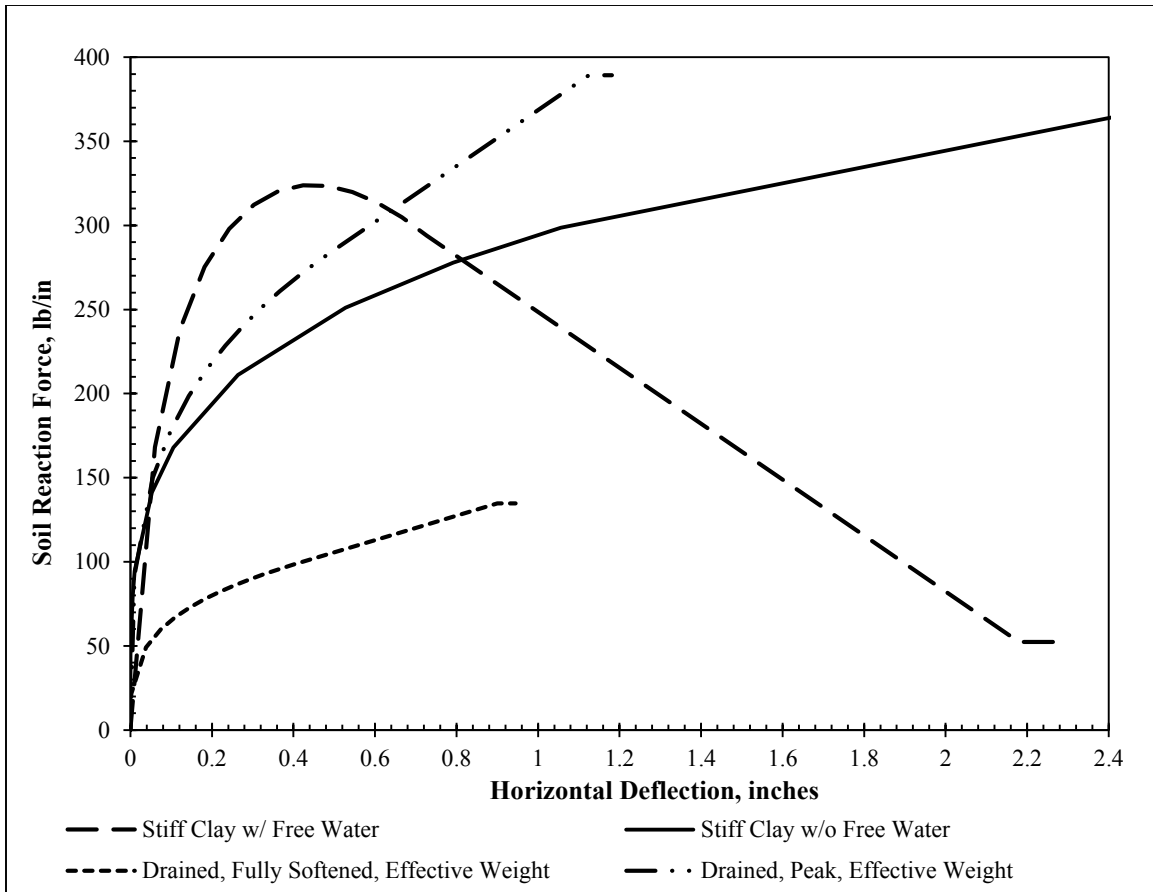


Figure 2.7: Summary of proposed p-y curves, calculated for the test wall at a depth of 16 feet below the original ground surface (1 foot below excavation line).

## 2.6: Previous Reports on Lymon C. Reese Research Wall

Three graduate research assistants at the University of Texas at Austin have used the Lymon C. Reese research wall as the subject of their Master’s thesis. Their findings are summarized in this section.

### 2.6.1: ELLIS (2011): A SUBSURFACE INVESTIGATION IN TAYLOR CLAY

Ellis (2011) presents “a comprehensive field and laboratory investigation at the location of the Lymon C. Reese Research Wall.” Geological information for the project

site is presented, along with the measured properties of the Taylor clay from field and laboratory investigations. In addition to standard tests for index properties, consolidation parameters, and undrained shear strength, several advanced tests were performed, including cyclic lateral shrink-swell testing.

Relatively high undrained shear strengths were measured on the project site, and a secondary structure in the soil often resulted in sample disturbance that made precise laboratory testing difficult. The soil's swelling strain from in-situ moisture conditions was estimated to be approximately 0.8 – 1.0 percent; repeated cycles of wetting and drying with large changes in moisture content resulted in a higher swell potential. The active zone was estimated to extend to a depth of approximately 10 feet. Estimates of laboratory and field values of hydraulic conductivity were “drastically different,” with field estimates being up to 10 orders of magnitude higher than laboratory estimates due to the presence of preferential moisture pathways created by fissures in the secondary soil structure. These results are generally consistent with the behavior of heavily overconsolidated, stiff-fissured clays (Ellis 2011).

#### **2.6.2: DELLINGER (2011): THE USE OF TIME DOMAIN REFLECTOMETRY PROBES FOR THE MOISTURE MONITORING OF A DRILLED SHAFT RETAINING WALL IN EXPANSIVE CLAY**

Dellinger (2011) summarizes the use of Time Domain Reflectometry (TDR) probes for moisture monitoring at the Lymon C. Reese research wall. The theory governing the application of TDR probes is presented, along with a summary of previous research using TDR probes in expansive clay. The calibration and installation of TDR probes at the research site is presented, along with a summary of field performance data.

In general, TDR probes installed at the project site were unable to produce reliable measurements of moisture content due to signal attenuation from the high electrical

conductivity of the soil. These results are consistent with other studies in highly conductive soils. Additionally, because TDR probes require a consistent contact surface with the soil, loss of probe rod contact during drying cycles is an inherent problem for expansive soils which shrink and swell with moisture changes.

While moisture contents could not be directly measured with TDR probes in the highly conductive, expansive soil on the project site, the use of electrical conductivity data from the probes to qualitatively describe moisture conditions is possible. Electrical conductivity measurements, combined with periodic physical sampling using a hand auger, can provide reasonable insight on moisture conditions at the project site (Dellinger 2011).

### **2.6.3: KOUTROUVELIS (2012): EARTH PRESSURES APPLIED ON DRILLED SHAFT RETAINING WALLS IN EXPANSIVE CLAY DURING NATURAL CYCLES OF MOISTURE FLUCTUATION**

Koutrouvelis (2012) summarizes the behavior of the Lymon C. Reese research wall during natural cycles of moisture fluctuation. A summary of the different types of analysis used for drilled shaft retaining walls is presented, including methods for estimating the p-y relationship for stiff-fissured clays. Data reduction and analysis procedures for the test wall instrumentation are summarized, along with an analysis of the various microscale effects that can introduce errors into the strain gauge data, including the development of residual stresses and strains prior to excavation. Various methods of obtaining moment-curvature relationships for the test wall are explored. Profiles of deflection, bending moment, and earth pressures are presented for various dates, and the influence of side shear and thermal effects on wall behavior is estimated.

The research concluded that residual stresses and strains developed prior to excavation were “significant” and caused by a combination of concrete curing and local site conditions, including the soil moisture content at the time of construction. Based on

analysis of the inclinometer data, the base of the wall was not fixed and experienced rotation during the excavation process. Moisture fluctuations in the soil influenced the deflected shapes, along with (to a much lesser degree) temperature fluctuations in the concrete. Additionally, the presence of a tension crack behind the wall was exacerbated by low moisture contents causing soil shrinkage.

The results of the strain gauges were highly variable due to a combination of “various microscale and environmental factors (tension cracks and temperature effects).” In order to directly use the strain data for calculations of bending moments and curvatures, data processing to eliminate these effects was deemed to be necessary. After data processing, results generated from strain gauge data were comparable to those generated from inclinometer data. A p-y analysis of the research wall indicated that the lateral response of the wall is strongly affected by the selection of the value of  $\epsilon_{50}$ , which is developed from the stress-strain response of the soil and influences the shape of the p-y curves. The use of an initial “global” displacement profile was introduced to provide consistency between field inclinometer measurements and p-y predictions. The influence of thermal effects and side shear on lateral wall movements was found to be small; however, the potential influence of thermal effects and side shear on bending moments is more significant and may need to be accounted for. When natural soil moisture content is high, the predicted bending moments due to side shear were positive (Koutrouvelis 2012).

## CHAPTER 3: DESIGN AND CONSTRUCTION OF FULL-SCALE INSTRUMENTED TEST WALL

*Note: Portions of this section have been previously published by the author (Brown et al., Geo-Frontiers 2011).*

### 3.1: Location of Test Wall

To allow for complete control of project scheduling and access to the test site, a full-scale test wall was constructed specifically for this project. The Lyman C. Reese research wall is located in Manor, Texas on the property of R&L Transfer & Storage Co., Inc. (Figure 3.1). A site plan, showing the location of the test wall, is shown in Figure 3.2.

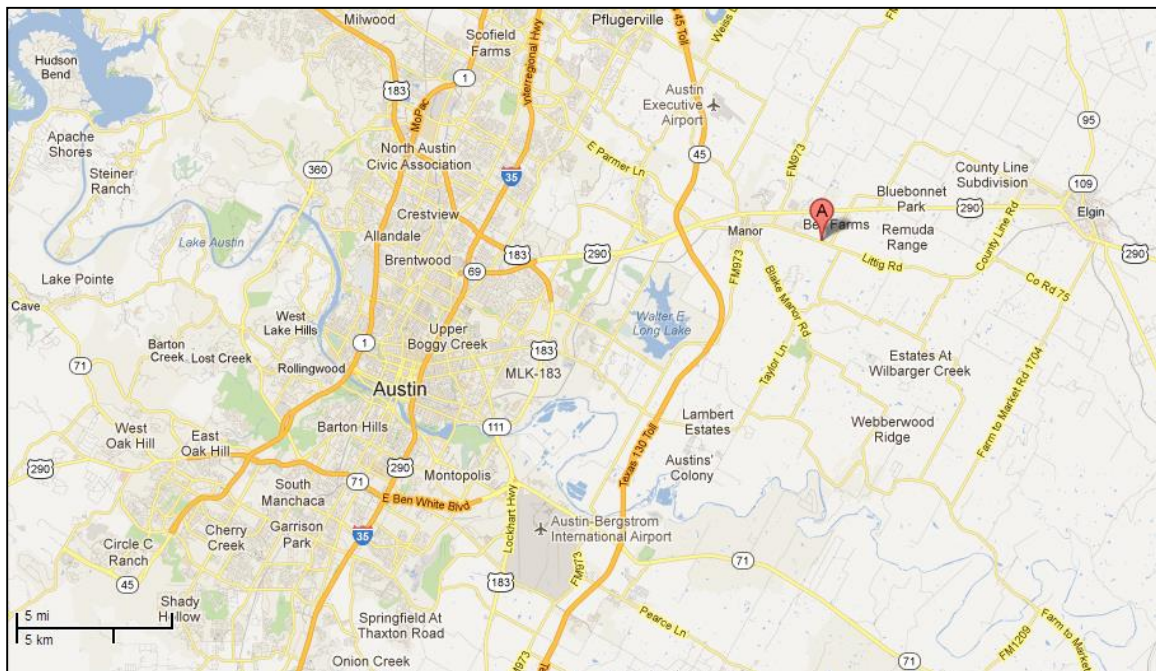


Figure 3.1: Location of full-scale test wall (Google, Inc.).

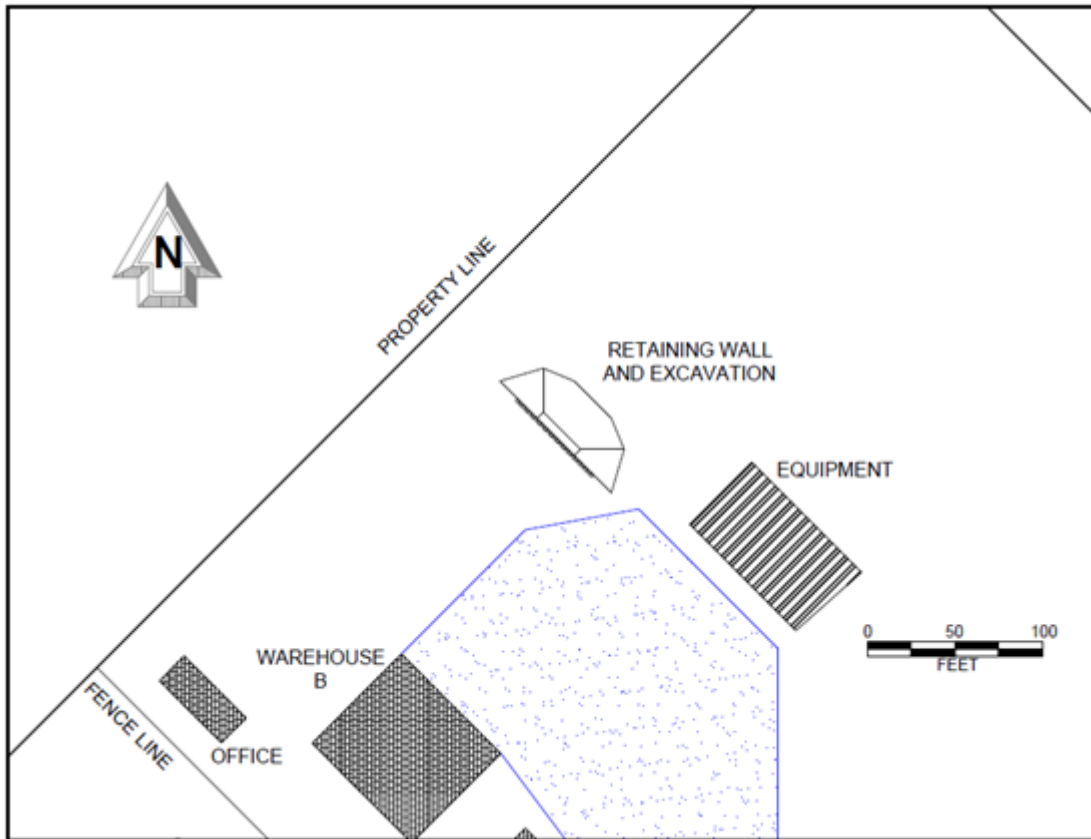


Figure 3.2: Detailed site plan with location of test wall.

## 3.2: Site Conditions

### 3.2.1: OVERVIEW

The test wall is underlain by approximately 50 feet of the Taylor Formation, a highly expansive and problematic clay. A sample of the Taylor Formation from the project site is pictured in Figure 3.3.



Figure 3.3: Taylor Clay from the project site in Manor, Texas.

### **3.2.2: PRELIMINARY GEOTECHNICAL INVESTIGATION (JANUARY 2010)**

Three 50-foot deep soil borings were drilled in January 2010, a relatively wet season. Both Texas Cone Penetrometer (TCP) testing and Standard Penetration Testing (SPT) were performed to provide information consistent with the standard of practice in Texas. An inclinometer was installed in one boring and a piezometer in another. The liquid limit ranges from about 80 to 100 percent and the plastic limit ranges from about 20 to 30 percent. Natural water contents at the time of investigation averaged 38 percent. The profiles of natural water content and undrained shear strength from UU testing are shown in Figure 3.4. The water table has remained about 8 feet below the ground surface during construction and excavation.

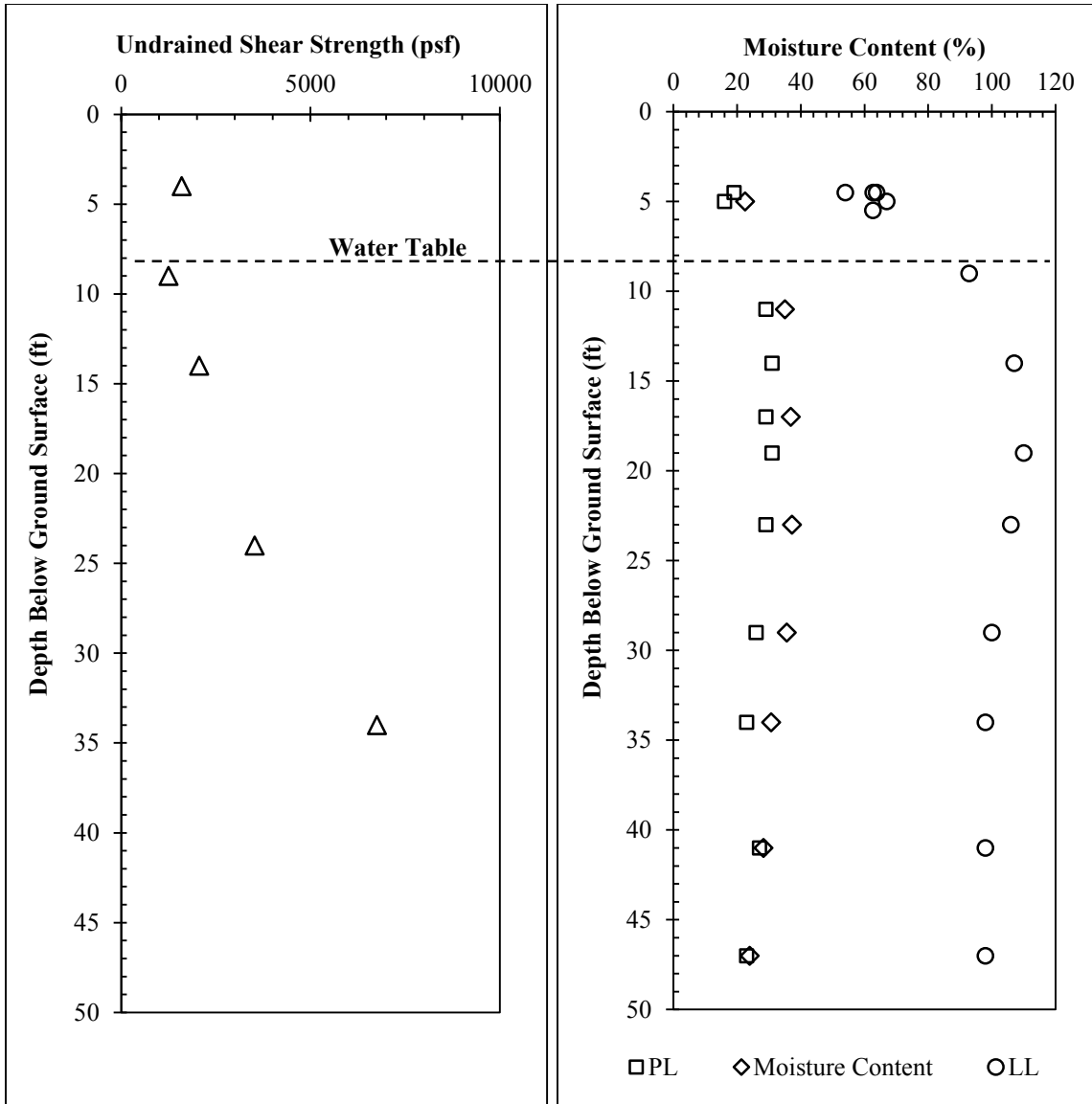


Figure 3.4: Results of Atterberg Limit and UU testing from January, 2010 (three months before shaft construction; seven months before excavation).

### 3.3: Design of Test Wall

The design for the test wall was developed using a procedure similar to the existing TxDOT design procedure for cantilever drilled shaft walls (TxDOT 2009). The goal was to create a structure which would be structurally sound and consistent with typical TxDOT



walls, but would produce enough deformations to infer the earth pressures acting on the wall. A summary of design assumptions and shaft geometry for the test wall is provided in Table 3.1. The test wall consists of 25 drilled shafts embedded to depths from 18 to 35 feet below ground surface (Figure 3.5). The shafts have a diameter of 24 inches and a center to center spacing of 30 inches. The reinforcing bar cage consists of 12 #7 bars. The cantilevered height is 15 feet, the penetration depth is 20 feet, and the shafts end four feet above ground surface. The shaft stickup allows the project team to run a lateral load test if desired; it also allows the site owner to use the wall as a loading dock upon completion of the project. The final wall design is pictured in Figure 3.5 and Figure 3.6.

Table 3.1: Baseline assumptions and design parameters for test wall.

<b>Parameter</b>	<b>Value</b>
Total Unit Weight of Soil, $\gamma_t$	130 pcf
Equivalent Fluid Pressure Loading, $\gamma_{EF}$	40 psf/ft
Coefficient of Active Earth Pressure, $k_a$	0.31 (from $\gamma_{EF} / \gamma_t$ )
Undrained Shear Strength, $S_U$	4,000 psf
Foundation Soil p-y Curves	Stiff Clay Without Free Water
Cracking Moment, $M_{Cr}$	680 k-in.
Yielding Moment, $M_y$	3,200 k-in.
Uncracked Bending Stiffness, $EI_{uc}$	$67 \times 10^6$ k-in.
Cracked Bending Stiffness, $EI_{cr}$	$18 \times 10^6$ k-in.
c-c Spacing Between Shafts, B	30 in.
Shaft Diameter	24 in.
Height of Retained Soil, H	180 in.
Reinforcement	12 #7 bars (1.6% of gross area)

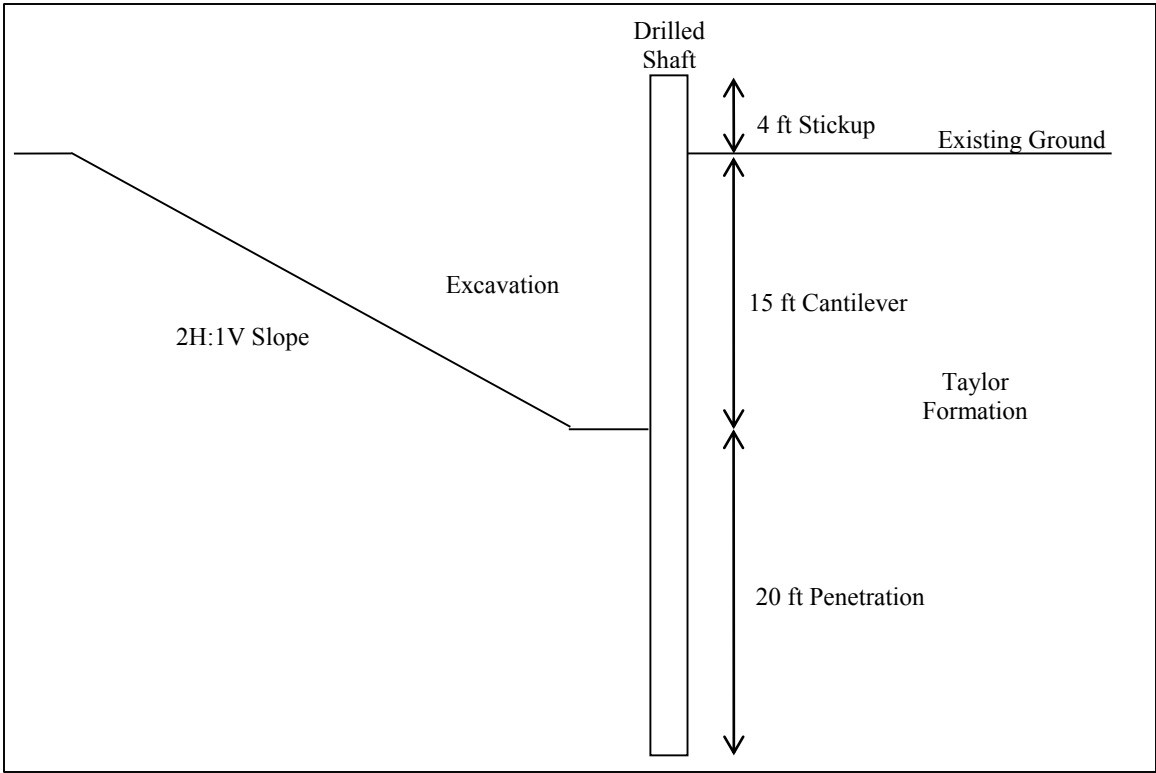


Figure 3.5: Cross-section of wall and excavation at center shaft, facing east (not to scale).

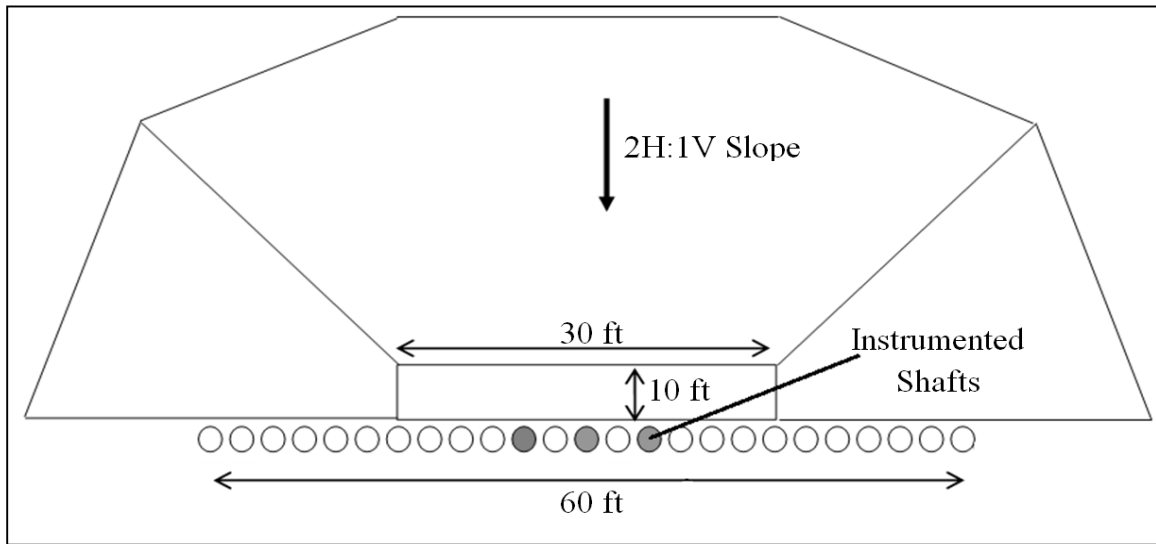


Figure 3.6: Plan view of wall and excavation.

### 3.4: Design of Instrumentation Program

#### 3.4.1: OVERVIEW

The primary objectives of the instrumentation program are to accurately monitor deformations in the test wall, and to estimate the lateral earth pressures applied to the shaft over a period of three years. Three shafts in the test wall are instrumented (shaded in Figure 3.6). In each of these shafts, there are 30 fiber optic strain gauges and one inclinometer casing. Additionally, one inclinometer casing was installed 5.5 feet behind the wall, and thermocouples were installed in the center shaft at depths of 3, 15, and 29 feet below ground surface for temperature monitoring. In the soil surrounding the wall, 20 Time Domain Reflectometry (TDR) moisture sensors were installed after excavation. Figure 3.7 shows an instrumented cage as it is lowered into the ground, and Figure 3.8 shows the distribution of sensors within each instrumented shaft.

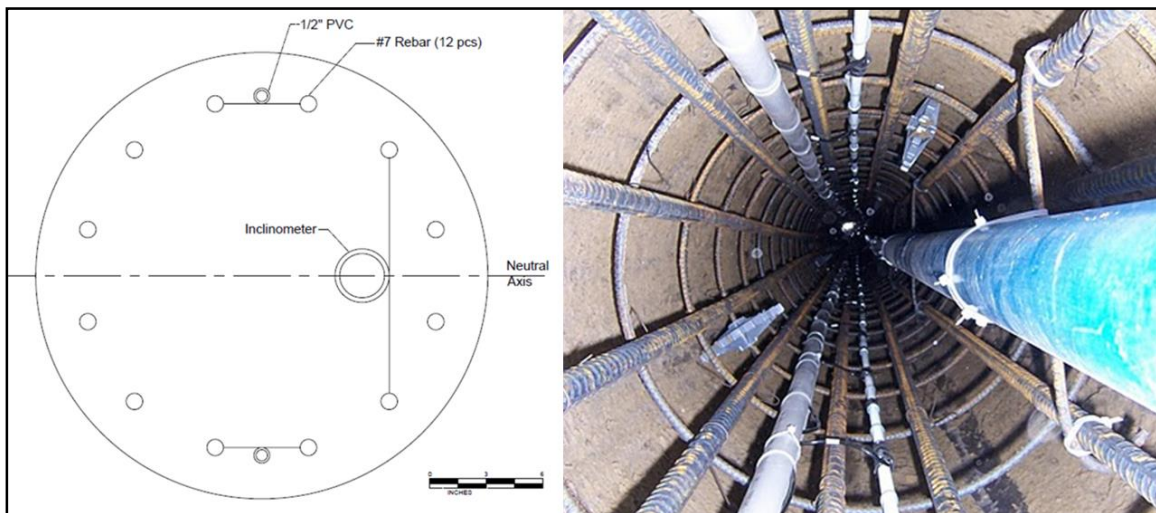


Figure 3.7: Plan view of instrumented rebar cage before concrete placement.

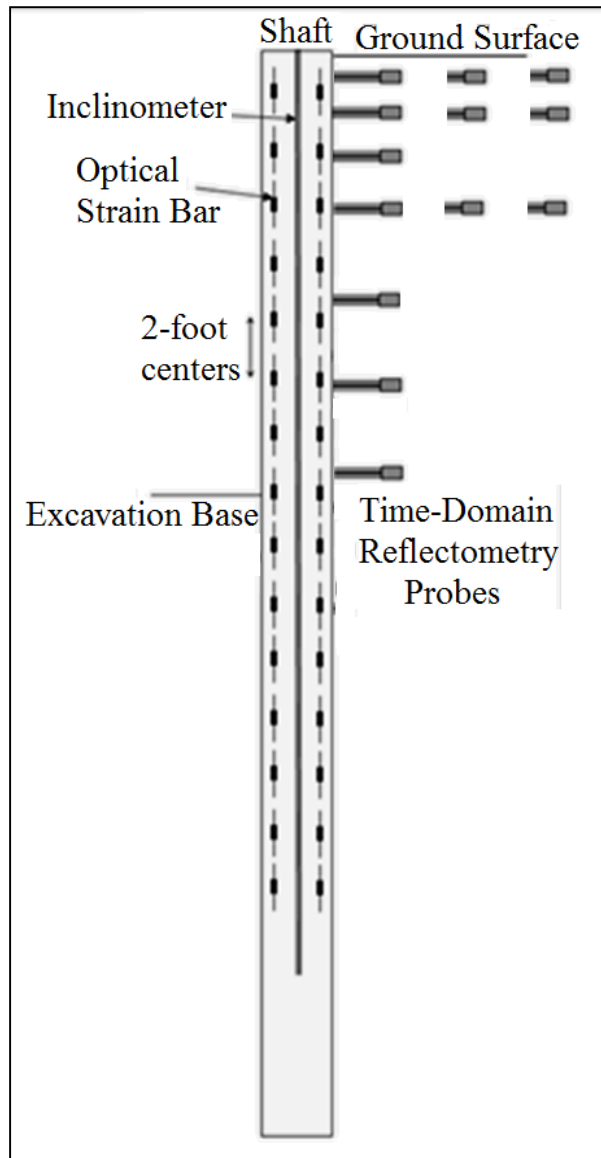


Figure 3.8: Distribution of sensors within an instrumented shaft.

### 3.4.2: STRAIN GAUGES

Because of their reputation for stability with time and relative insensitivity to moisture and temperature changes, optical strain gauges (Fabry-Perot type) were selected for strain monitoring. Optical gauges provide higher resolution than conventional electrical resistance or vibrating wire gauges, and are less susceptible to zero-drift over

time. Additionally, because their strain measurements are generated using a light source, optical strain gauges are less affected by moisture and temperature changes than conventional gauges. The optical strain gauges were purchased from OPSSENS in Canada, and the sister bars were fabricated by Lymon C. Reese and Associates of Austin, Texas. Prior to installation, each sister bar was calibrated to ensure linearity in the readings within the operating strain range of 1,000 microstrains and to establish a response curve. There are a total of 90 optical strain gauges installed in the test wall; in each instrumented shaft, there are 15 gauges on either side of the neutral axis (Figure 3.8).

Large temperature fluctuations occurred at the project site, and thermal expansion of the shafts produced significant strains. Additionally, the potential for errors in measurements due to rapid changes in temperature of the optical light source and datalogger was a design consideration. To minimize these errors, temperature resistant dataloggers were designed and installed in enclosures that limit rapid temperature change (Figure 3.9).

### **3.4.3: INCLINOMETERS**

The rotation profile along the length of the drilled shaft is measured directly with an inclinometer, and integrated to yield a profile of deflected shape. Three inclinometer casings were attached to the reinforcing bar cage and cast into the shaft during construction. Readings are taken every 2 feet over the length of the shaft using a readout unit manufactured by Slope Indicator.

### **3.4.4: ADDITIONAL INSTRUMENTATION**

To provide redundancy in top-of-wall deflections measured by the inclinometers, a linear potentiometer was installed on the project site prior to excavation and anchored to the wall near the ground surface. It was attached to shaft #16, adjacent to the west

instrumented shaft (shaft #15). The linear potentiometer provides continuous data on top-of-wall deflection and redundancy with the inclinometer data. To provide information on the moisture conditions in the retained soil, a total of 20 Time Domain Reflectometry (TDR) moisture probes were installed in behind the wall. Because of the high spatial variability of rainfall across the region, an electronic tipping bucket rain gauge was installed at the test wall to augment measurements from nearby weather stations. The linear potentiometer, TDR moisture probes, and rain gauge are monitored continuously. Figure 3.9 shows some of the instrumentation installed on the project site.



Figure 3.9: Instrumentation on the project site. Clockwise from top left: temperature resistant datalogger and enclosure for continuous strain readings; signal conditioner for individual strain readings; linear potentiometer; TDR probe installed through facing.

### 3.5: Construction of Full-Scale Instrumented Test Wall

The drilled shafts and instrumentation were installed in early April, 2010 by McKinney Drilling Company (Figure 3.10). In order to prevent excessive bending of the rebar cage and damage to the instrumentation, the instrumented cages were lifted with two cranes (Figure 3.11). To prevent sensor damage during concrete placement, cables were protected within slotted PVC pipes and concrete was directed down the center of the rebar cage with shovels. Initial sensor survivability was excellent, with 88 of 90 strain gauges and all inclinometer casings functional after rebar cage placement and concrete installation. A summary of wall construction activities and concrete strength data is provided in Table 3.2.



Figure 3.10: Construction of test wall, April 2010.



Figure 3.11: Lifting an instrumented cage with two cranes.

Table 3.2: Summary of wall construction activities and measured concrete strengths.

<b>Date</b>	<b>Notes (* = Instrumented Shaft)</b>	<b>7-Day Concrete Strength (psi)</b>	<b>28-Day Concrete Strength (psi)</b>
March 30, 2010	Mobilize Equipment, Assembled Instrument Cages, Constructed Shafts 1 and 4	6055	7955
March 31, 2010	Constructed Shafts 7, 10, 13*, 22, and 25	4970	7000
April 1, 2010	Constructed Shafts 2, 5, 8, 11*, 15*, and 17	4480	6065
April 2, 2010	Constructed Shafts 3, 6, 9, 16, 19, and 23	4410	5875
Apr. 3 - 4, 2010	Weekend	N/A	N/A
April 5, 2010	Constructed Shafts 18, 21, and 24	4000	5950
April 6, 2010	Constructed Shafts 12, 16, and 14	4400	6800
April 7, 2010	Demobilize Equipment	N/A	N/A



### **3.6: Monitoring Plan**

Since installation of instrumentation, the activity of the test wall has been closely monitored. An automated datalogger records strain readings from the center shaft at 6-minute intervals. The linear potentiometer, rain gauge, thermocouples, and TDR moisture probes are measured by another datalogger at 15-minute intervals. Inclinator profiles, piezometer water levels, and strain readings from the east and west shafts are recorded, on average, once per week. The frequency of these measurements has changed according to the amount of activity at the wall site, ranging from several readings per day to once per month. Additionally, meteorological data from nearby weather stations and observational information from the test wall supplement our instrumentation data.

### **3.7: Data Reduction and Analysis**

Because the magnitude and distribution of earth pressures acting on the test wall is a primary goal of this research, methods of using strain gauge and inclinometer data from the test wall to estimate earth pressures must be developed. A summary of the mathematical relationship between deflection, slope, bending moment, shear, and earth pressures for a typical pile is shown in Figure 3.12. The methods described in the following section are applicable to data from the Manor, Texas test wall only, and should not be used for other projects or data sets without careful validation.

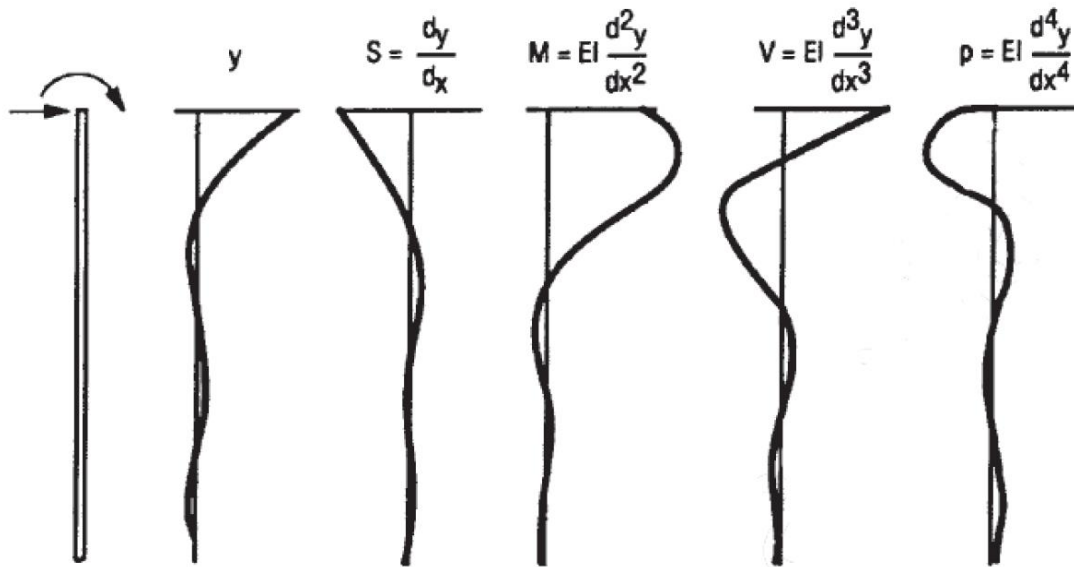


Figure 3.12: Mathematical relationship between deflection ( $y$ ), slope ( $S$ ), bending moment ( $M$ ), shear force ( $V$ ), and soil reaction force ( $p$ ) for a laterally loaded pile (after Reese and Van Impe, 2001).

### 3.7.2: STRAIN GAUGE DATA REDUCTION

The strain gauges placed on either side of the shaft's neutral axis measure axial strains in the tensile and compressive direction ( $\epsilon_t$  and  $\epsilon_c$ , respectively). The difference in tensile and compressive strains on either side of the neutral axis is divided by the horizontal distance between the gauges to obtain a value of bending curvature at a given depth. The calculated value of bending curvature is converted to a value of bending moment according to the moment-curvature relationship defined by the structural properties of the shaft. Following this procedure at each depth where strain gauges are installed yields a profile of bending moment in the shaft versus depth, which can be differentiated once to obtain a profile of shear force versus depth, or differentiated twice to obtain a profile of soil resistance versus depth. This process is summarized in Figure 3.13. A more detailed

explanation of strain gauge data reduction for the Lymon C. Reese research wall can be found in Koutrouvelis (2012).

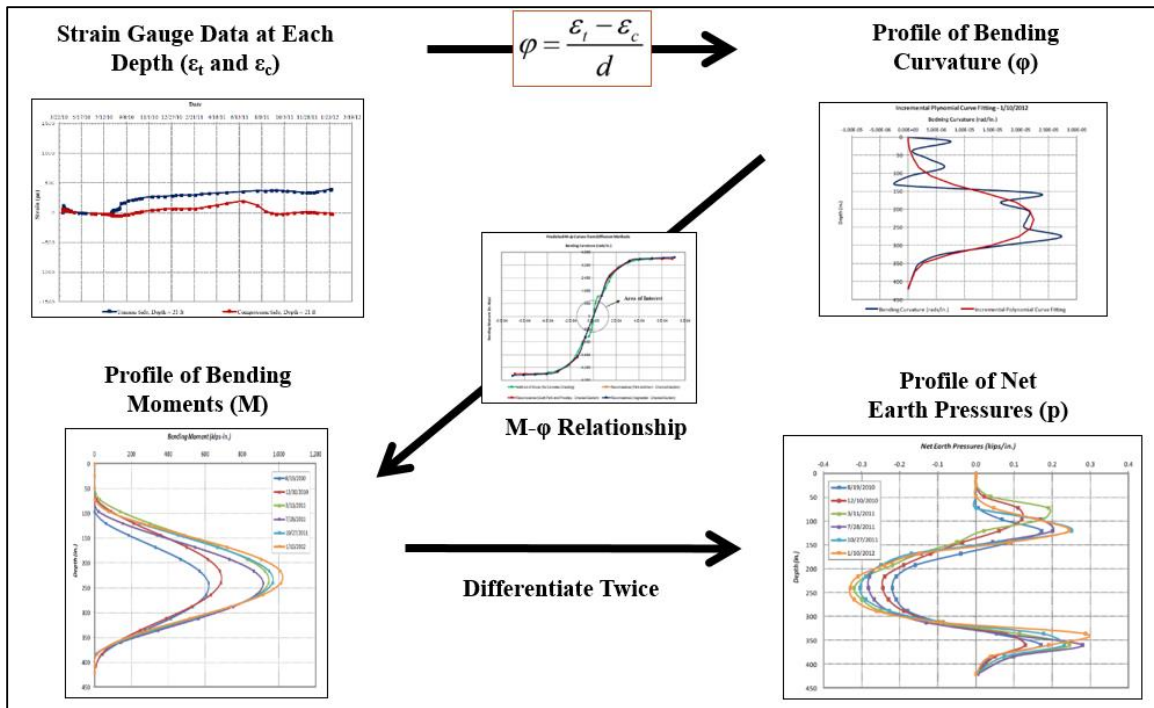


Figure 3.13: Strain gauge data reduction (after Koutrouvelis 2012).

For this research study, strain gauge nomenclature indicates which instrumented shaft the gauge is installed in (East, Center, or West), the depth of the strain gauge below original ground surface (1 – 29 feet), and which side of the neutral axis the gauge is installed on (Tension or Compression; tensile strains are positive). Using this nomenclature, gauge E.17.T is located in the east instrumented shaft, 17 feet below ground surface, on the tensile side of the neutral axis.

### 3.7.3: INCLINOMETER DATA REDUCTION

#### 3.7.3.a: Rotation Profiles Recorded in the Field

While inclinometer data is most commonly presented as a displacement profile, the instrument itself records rotation data; these data are then integrated to calculate displacement. By extracting the raw rotation data from the instrument, a profile of bending curvature can be obtained with just one derivative. Sample rotation data from the three instrumented shafts on May 28, 2013, when the wall was near its maximum deflection, is presented in Figure 3.14. It is important to note that the last data point is at a depth of 32 feet for the center and west shafts, and 30 feet for the east shaft (shaft base is at 35 feet).

The inclinometer probe measures the shaft rotation in two directions; the A-axis (in the direction of the wheels) and the B-axis (in the direction perpendicular to the wheels). This allows for the lateral deflection to be determined in any direction. For the purposes of this analysis, all deflections are assumed to be perpendicular to the wall, and the cumulative deflection is calculated by combining the rotation profiles from the A-axis and B-axis using the distance formula:

$$y_{total} = \sqrt{y_A^2 + y_B^2}$$

This method of estimating deflections can slightly overestimate deflections in the case of very noisy data set, since it interprets any small amount of instrument error to be a positive deflection perpendicular to the wall. However, the method is reliable, slightly conservative, and is much more straightforward to apply to the data set than more advanced correction methods.

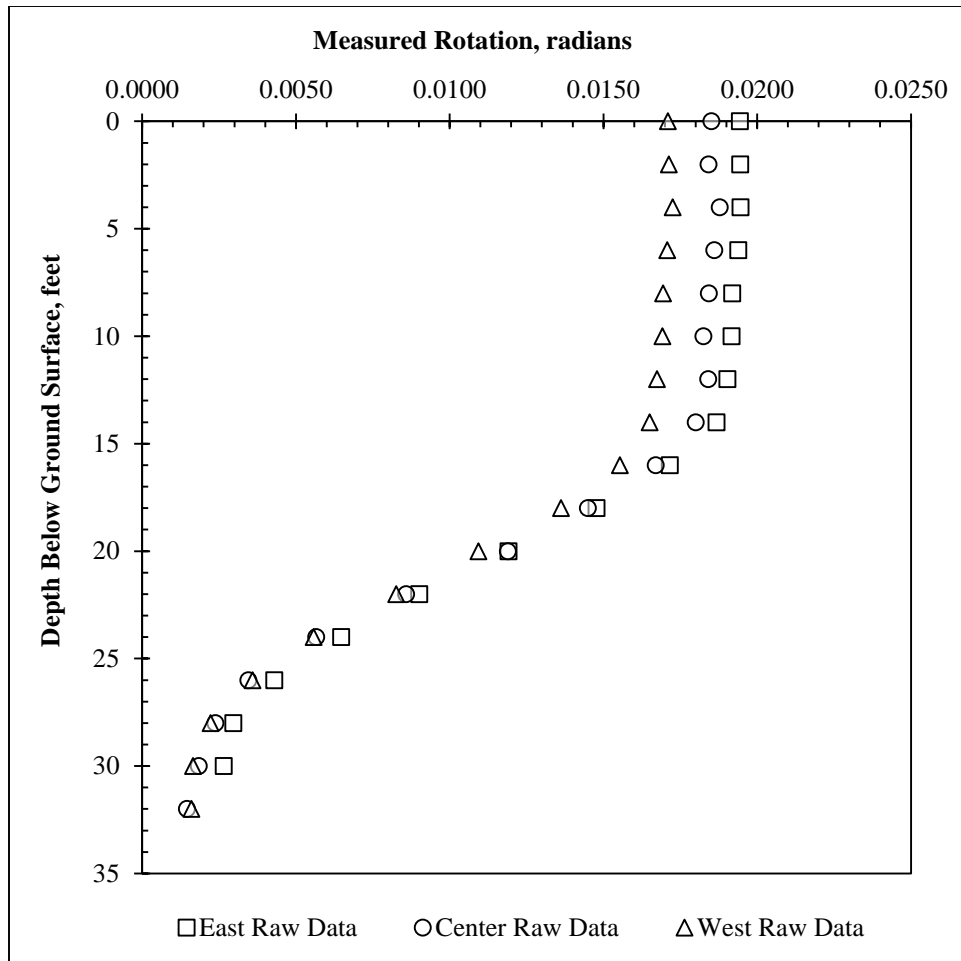


Figure 3.14: Sample rotation data from May 28, 2013. Reference survey is July 27, 2010, immediately before excavation.

### 3.7.3.b: Combining and Smoothing Rotation Profiles

While there are small differences in the behavior of the instrumented shafts, combining the three slope profiles into an average slope profile results in values that are similar to those obtained from the center instrumented shaft, and provides a much smoother curve for differentiation. To account for the presence of base rotation, the final rotation measurement is extended vertically down from the last measurement to the shaft base. In a typical analysis, the shaft base is assumed to be a fixed point – zero deflection, zero

rotation. However, based on the instrumentation data from the test wall, it is clear that some base rotation occurred (rotation measurements near the shaft base were consistently above zero throughout the life of the test wall; unrealistic loads would need to be present to return the shaft base rotation to zero in the remaining few feet). Mathematically, extending the final slope measurement to the shaft base indicates that the shaft base has rotated, but is not experiencing a bending moment.

A smoothing algorithm was applied to the data from each shaft before averaging the three profiles. The final averaged profile was smoothed again, although after averaging, the effects of smoothing are minimal. The smoothing algorithms are summarized in Tukey (1977), and are adapted for use in Excel by Quantdec (2004). To smooth each shaft's rotation profile, a "3RH" smooth with re-roughing is applied to the original data set. The process is summarized below; more detailed explanations of the individual smoothing processes are explained in the subsequent paragraphs, Figure 3.15 to Figure 3.18, and in Tukey (1977).

1. Apply a repeated medians-of-three smooth (3R) to each rotation profile.
  - a. Each point in the data set is replaced by the median of the original point and the two adjacent data points:

$$\theta_{i,3 \text{ smoothed}} = \text{median}(\theta_{i-1}, \theta_i, \theta_{i+1})$$

- b. Repeat the process until there are no further changes in the data:

$$\theta_{i,3R \text{ smoothed}} = \theta_{i,3 \text{ smoothed}} = \text{median}(\theta_{i-1}, \theta_i, \theta_{i+1})$$

2. Hann the 3R smoothed data to create a 3RH smooth (end values are not Hanned):

$$\theta_{i,hann \text{ smoothed}} = 0.25\theta_{i-1} + 0.50\theta_i + 0.25\theta_{i+1}$$

3. "Re-rough" the smooth.
  - a. Calculate a profile of residuals:

$$\theta_{i,residual} = \theta_{i,original} - \theta_{i,smoothed}$$

- b. Smooth the profile of residuals using a 3RH smooth as described above.
- c. Add the profile of smoothed residuals to the original smoothed data set:

$$\theta_{i,smoothed,re-roughed} = \theta_{i,smoothed} + \theta_{i,residual}$$

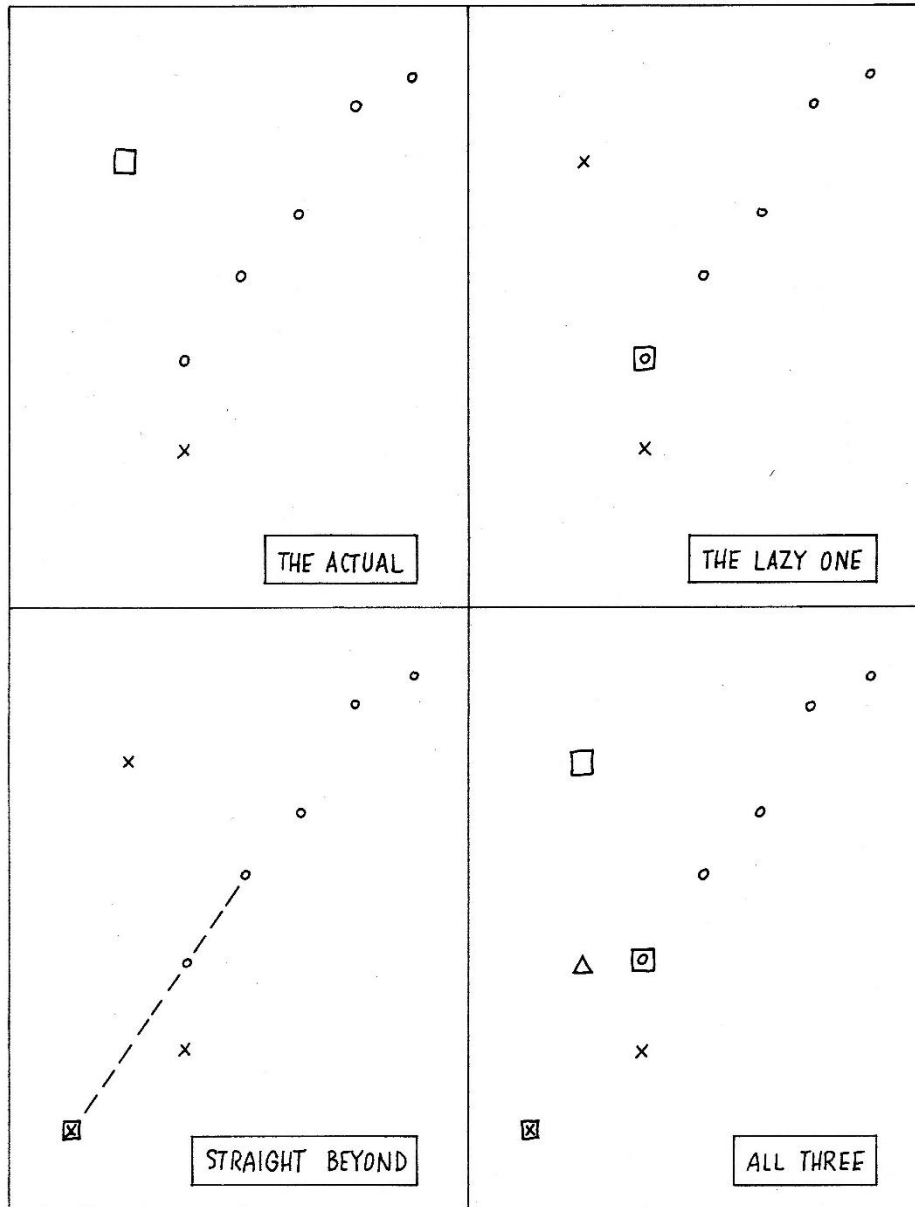
End values are smoothed after the application of the 3R smooth (before Hanning) by calculating the median of the previous two points on the smoothed curve and a point extrapolated one unit beyond the end of the smoothed curve (e.g.  $(\theta_{32}')$  is the median of  $(\theta_{28}')$ ,  $(\theta_{30}')$ , and  $(3 \cdot \theta_{28}' - 2 \cdot \theta_{30}')$ , after Quantdec (2004)). In the author's opinion, while the method developed by Quantdec (2004) is simple and easy to apply to a large data set, it is less accurate than the original method described by Tukey (1977), which also incorporates the original raw data into the final end value (Figure 3.15). For this research study, however, because the most important conclusions are drawn from the middle portions of the data set, the method of end value smoothing does not greatly affect the final results and the simple method developed by Quantdec (2004) is adequate.

To “re-rough” the smooth, a profile of residuals is calculated as the difference between the original raw data and the smoothed data. A 3RH smooth is then applied to the profile of residuals, and the smoothed residuals are added to the original smoothed data set. An illustration of the 3RH smooth with re-roughing is provided in Figure 3.16 for depths of 0 to 14 feet in the center shaft, with the entire profile shown in Figure 3.17. Re-roughing ensures that the smoothed data points remain reasonably close to the original values. This smoothing method kept the maximum bending moments and top-of-wall deflections consistent with the original raw data values, but provided a curve more suitable for piecewise differentiation. Other combinations of smoothing methods (e.g. medians-of-three smoothing only, 3RH smoothing without re-roughing, etc.) provide similar results when applied to the measured rotation data, but change the final data points slightly more

than the re-roughed 3RH smooth which was selected for subsequent analysis. A comparison of the original raw data from the three instrumented shafts with the final smoothed slope profile for differentiation is provided in Figure 3.18.



### End-value smoothing: parts and result



x = end input values      □ = the actual      Δ = the smooth end value  
 o = medians of 3          ◻ = the lazy one      = the median of ⊠, ◻,  
    ⊠ = straight beyond      and □

Figure 3.15: Tukey's method of end value smoothing (after Tukey 1977).

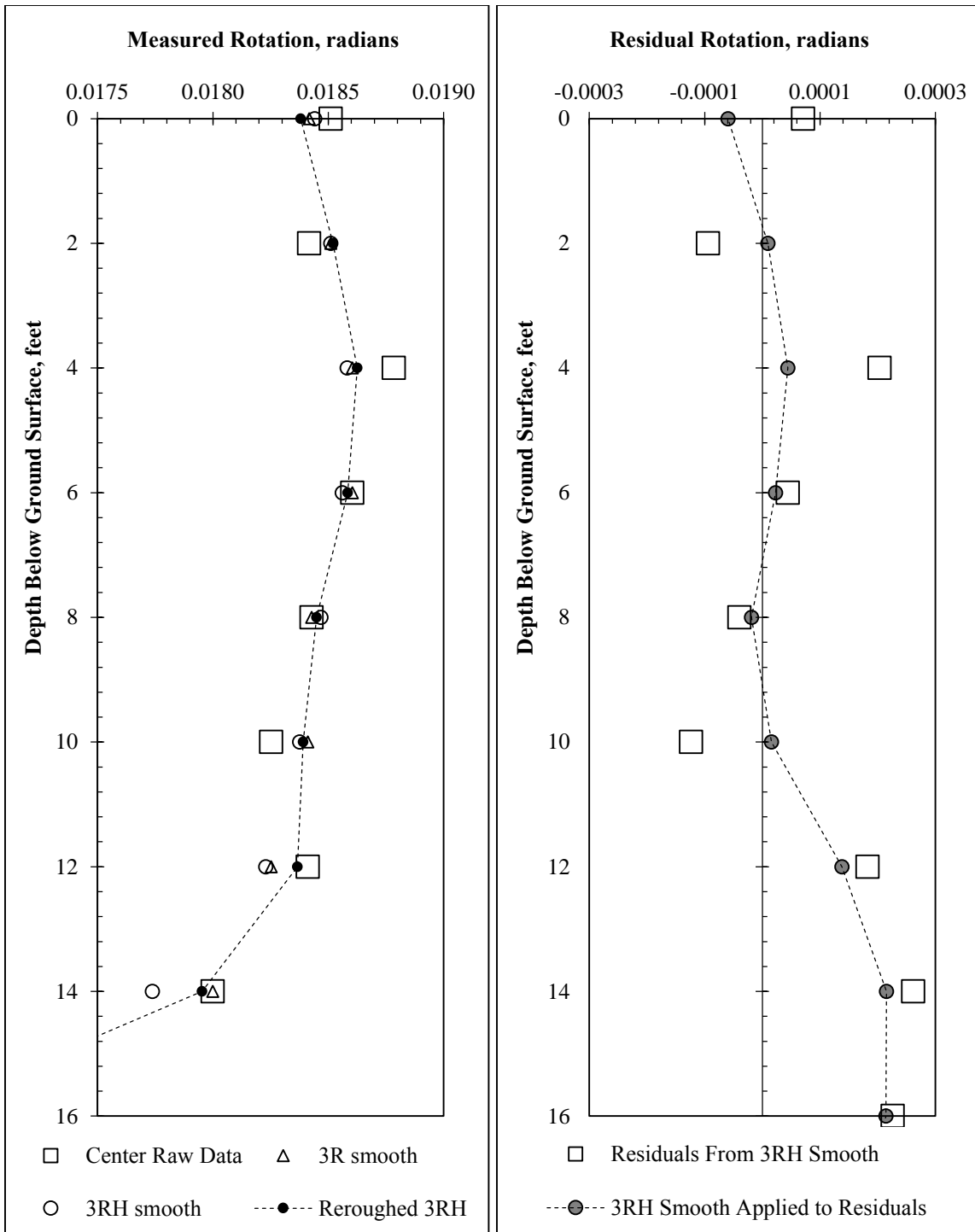


Figure 3.16: Illustration of the 3RH smooth with re-roughing applied to the center shaft rotation data between 0 and 14 feet.

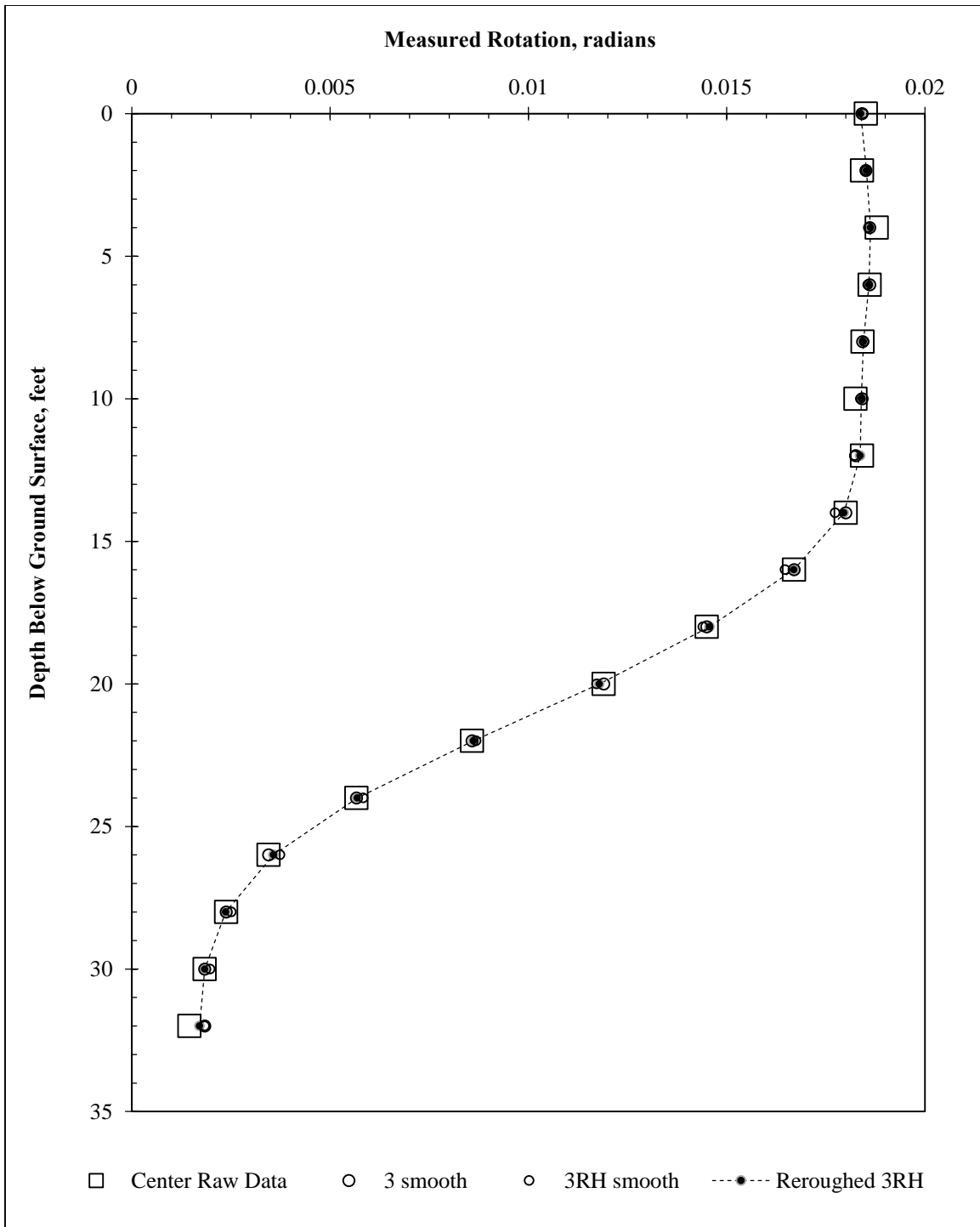


Figure 3.17: Comparison of original and smoothed rotation data from the center shaft on 5/28/2013.

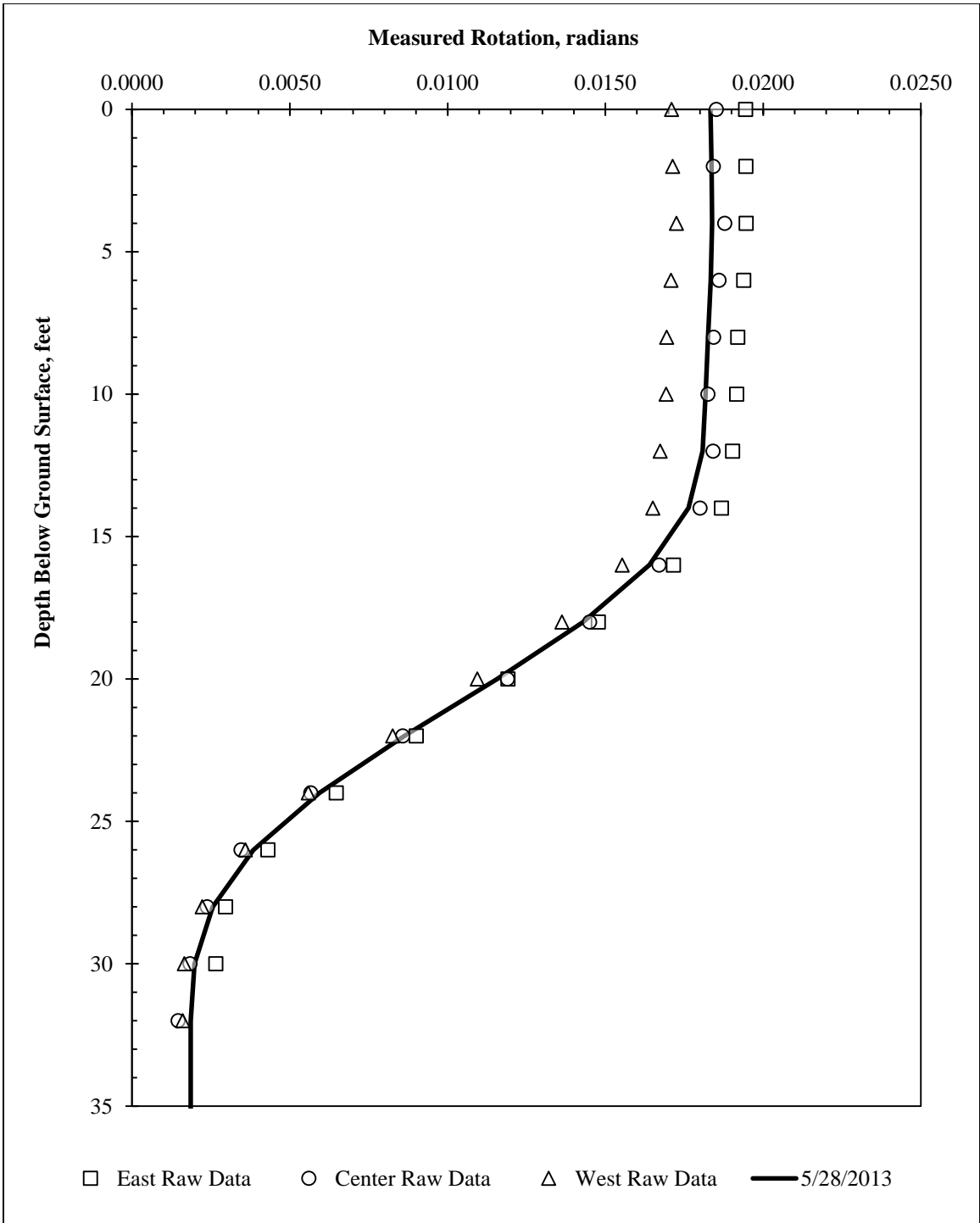


Figure 3.18: Comparison of raw rotation data from the three instrumented shafts with the final smoothed rotation profile for differentiation.

### **3.7.3.c: Obtaining Bending Moment Profiles from Rotation Data**

Ooi and Ramsey (2003) detail a variety of methods for obtaining bending moments and curvatures from inclinometer data. Of the methods surveyed, the most favorable was found to be fitting a third-order polynomial to a moving window of five points along the deflection profile, then analytically taking the second derivative of this curve to obtain a profile of bending curvature. For inclinometer data recorded at the test wall, a third-order polynomial was fit to a moving window of five points along the smoothed rotation profile, and the first derivative was taken numerically at the center point (using a central difference approximation at depths  $\pm 0.5$  feet from the center point). This process is illustrated in Figure 3.19 at a depth of 14 feet.

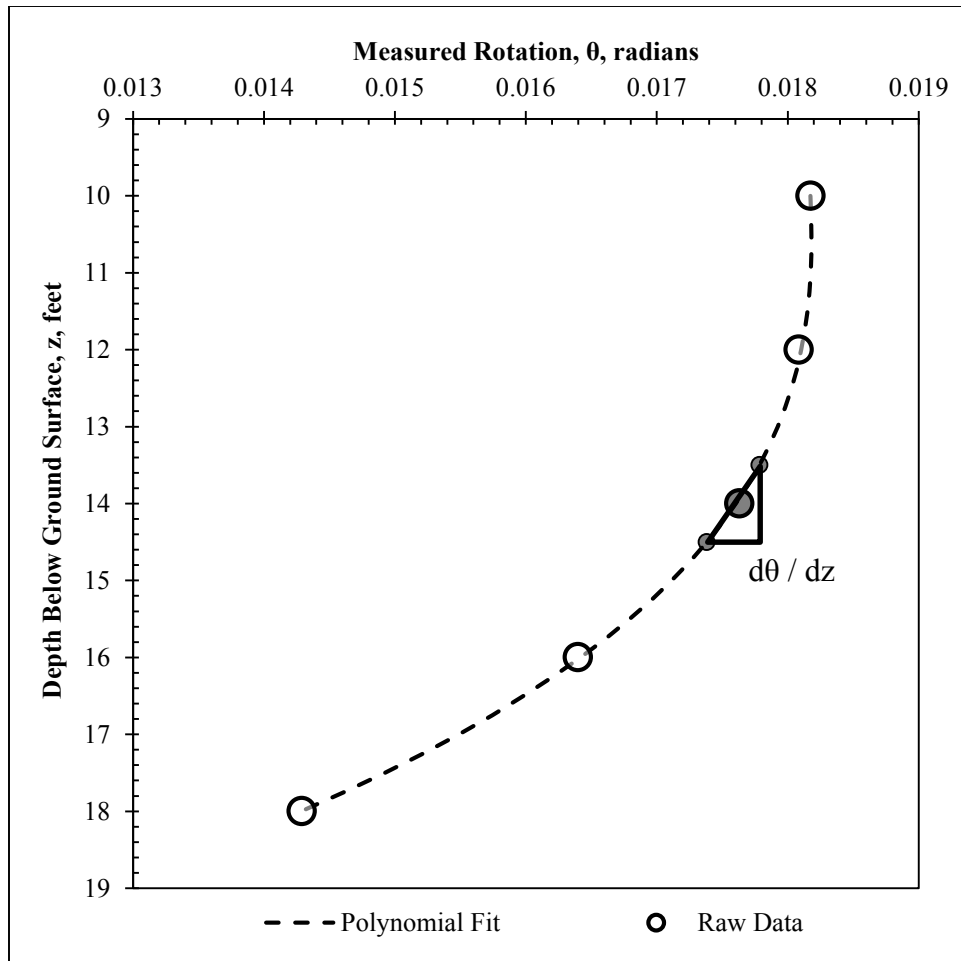


Figure 3.19: Illustration of piecewise third-order polynomial fitting to a moving window of five points at a depth of 14 feet. First derivative at 14 feet is estimated numerically using a central difference approximation between polynomial values at 13.5 and 14.5 feet.

Repeating the piecewise polynomial fitting process for each depth yields a profile of bending curvature. The profile of bending curvature is smoothed using a 3RH smooth with reroughing. To provide consistency with standard of practice methods, the values of bending curvature are converted into bending moments using the  $M-\Phi$  relationship generated by the computer program LPILE (Figure 3.20). The resulting bending moment profile, calculated by converting values of bending curvature to the corresponding values

of bending moment as shown in Figure 3.20, is shown in Figure 3.21. Using cracked section properties in the  $M-\Phi$  relationship generates a smoother profile of bending moment versus depth (there is no “hitch” near the cracking moment), but analysis of the test wall data for this project indicates that the earth pressures estimated at locations with small bending curvatures are unrealistically small when using cracked section properties. This may be a function of the heterogeneous nature of the concrete itself, which inherently produces variations in local stress-strain behavior at different locations within the shaft. If structural stresses are concentrated in the stiff (i.e. uncracked) sections of the shaft, and deformations are primarily located in the more flexible (i.e. cracked) sections, some difficulty in data interpretation can be encountered in the range of small strains. Despite this difficulty, because bending moments in the range of interest are larger than the cracking moment, the interpretation of maximum bending moment in the shaft is relatively unaffected by the choice of cracked or uncracked properties. The influence of concrete cracking on data interpretation is discussed in more detail in subsequent chapters.

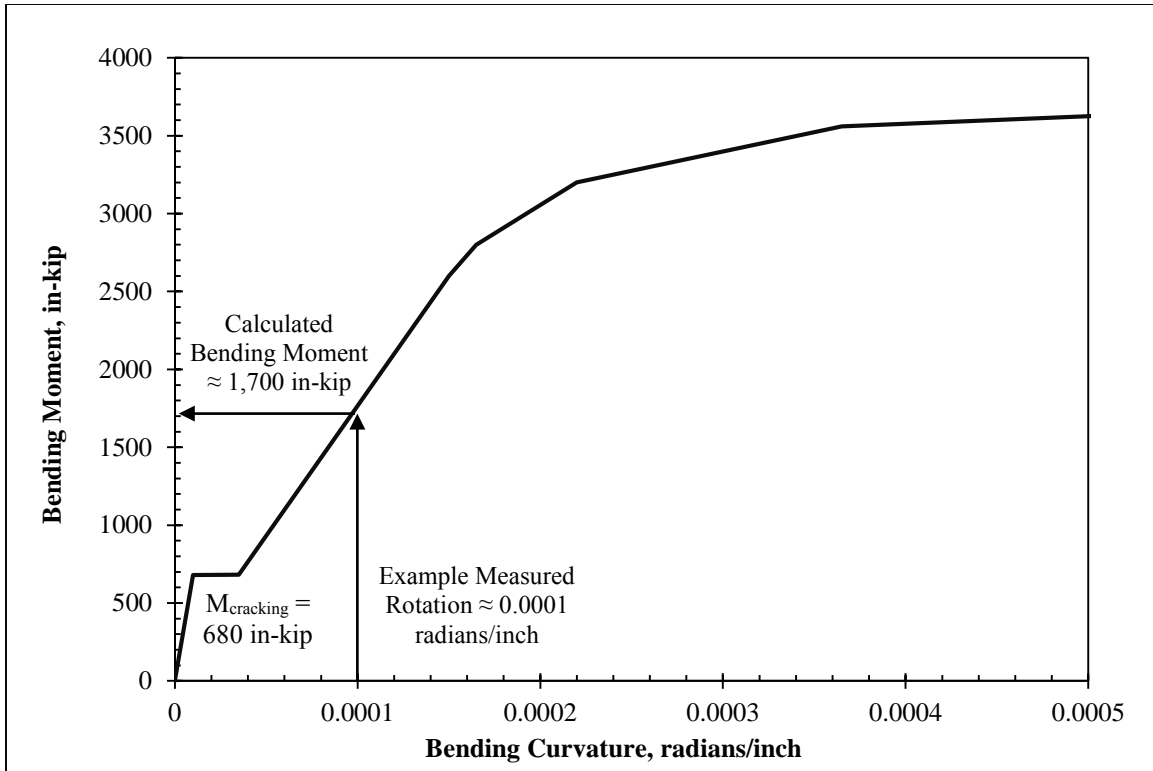


Figure 3.20: Relationship between bending curvature and bending moment ( $M-\Phi$  relationship) used for LPILE and field instrumentation data analysis.



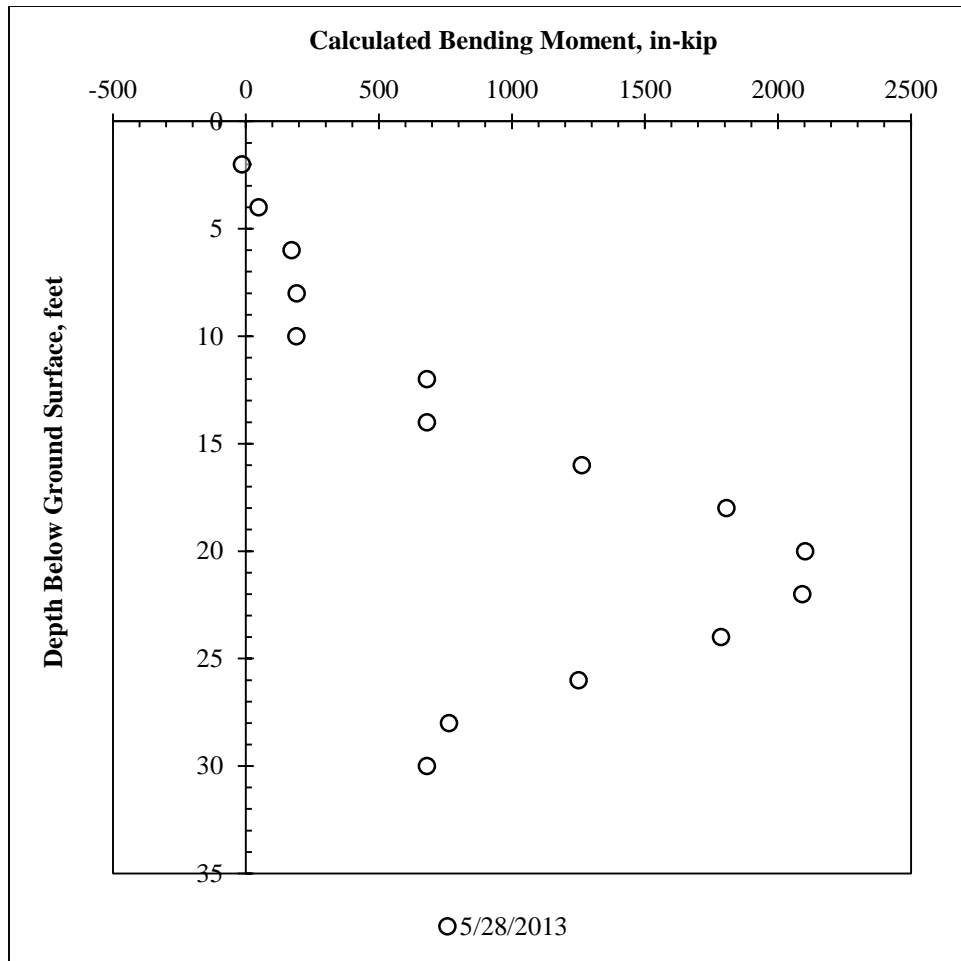


Figure 3.21: Bending moment profile generated from piecewise polynomial fitting of smoothed rotation profile and M- $\Phi$  relationship from LPILE.

### 3.7.3.d: Obtaining Net Earth Pressures from Bending Moment Profiles

To generate profiles of shear forces in the shaft, the same procedure used to differentiate the smoothed rotation profile is applied to the bending moment profile. Because the bending moment profile was generated from a smoothed profile of bending curvature, and to preserve the nonlinear moment-curvature behavior displayed in Figure 3.20, no smoothing is applied to the bending moment profile. To differentiate the profile of bending moment, piecewise third-order polynomials are fit to a window of five points

along the depth of the shaft. The resulting shear force profile is smoothed using a 3RH smooth with re-roughing, then differentiated using piecewise polynomials to obtain a profile of soil resistance, which is smoothed again with a re-roughed 3RH smooth. The resulting soil resistance values for the 5/28/13 profile are shown in Figure 3.22, along with comparison values calculated using only the averaged rotation profile with piecewise polynomial differentiation (no smoothing used). In Figure 3.22, the large values of soil resistance in the non-smoothed data above the excavation line are the result of small errors in the original raw rotation data. Small jumps in the original data set become larger with each successive differentiation; after three differentiations, small errors can become large, unrealistic spikes. The judicious use of data smoothing during differentiation can minimize the effects of random errors on the final result.

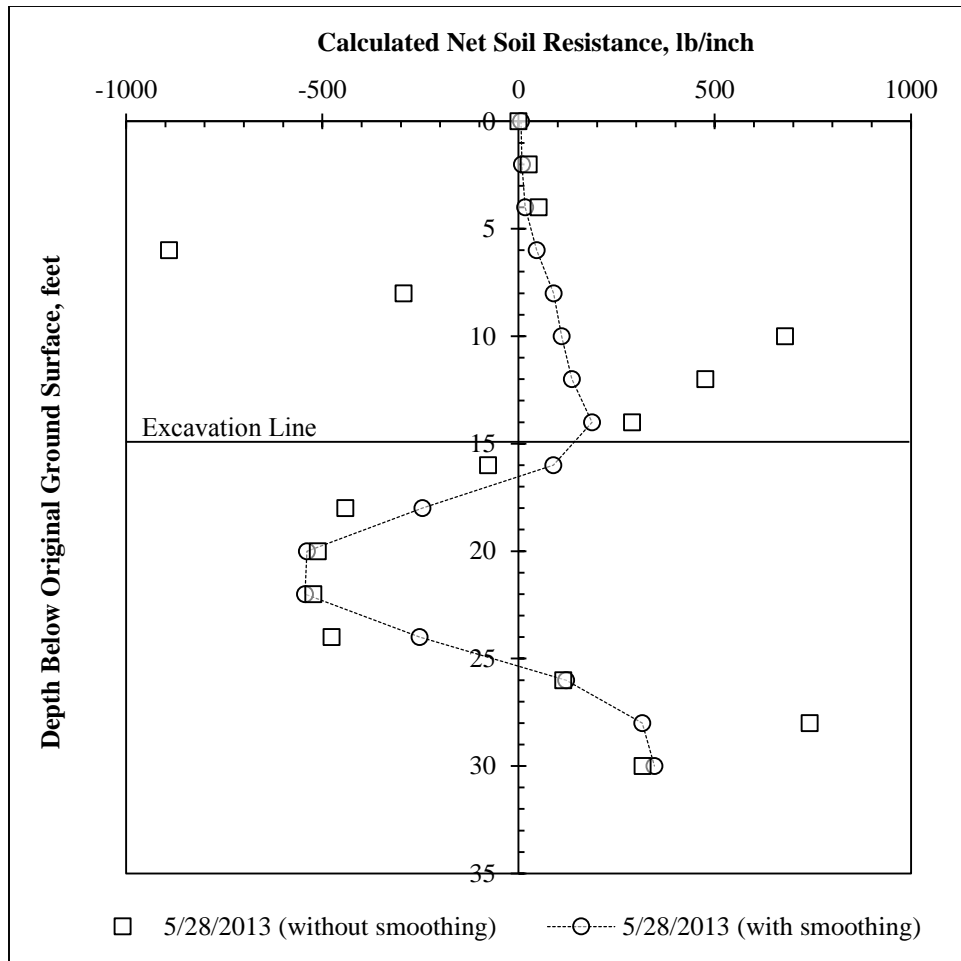


Figure 3.22: Soil resistance profiles generated using piecewise polynomial differentiation of averaged rotation profiles (with and without data smoothing applied during the differentiation process).

On inspection, the differentiation process produces reasonable results when the data smoothing algorithm is used throughout the differentiation process. The profile of net soil resistance reaches zero value close to the excavation depth of 15 feet, and reaches zero again near the shaft's center of rotation at approximately 27 feet. While the soil pressures between 30 and 35 feet must be inferred due to the lack of inclinometer data at those depths, the earth pressures above 30 feet are consistent with those obtained from LPILE results.

### **3.7.3.e: Generating p-y Curves from Inclinometer Data**

With the procedure described above, values of soil resistance ( $p$ ) and horizontal deflection ( $y$ ) are obtained for each depth. With readings for a variety of dates, corresponding to a variety of deflections,  $p$  and  $y$  can be plotted against each other at each depth to create a family of  $p$ - $y$  curves.

#### ***3.7.3.e.1: Discussion of “Net” Soil Resistance***

In the following sections, it should be noted that the driving earth pressures acting toward the excavation are defined as ( $w$ ), and the earth pressures resisting this motion are defined as ( $p$ ). The profile of net soil resistance generated using the differentiation process is actually a profile of ( $w - p$ ). Above the excavation line,  $p$  is zero and  $(w - p) = w$ . At large depths below the excavation line,  $w$  is generally assumed to be negligible relative to  $p$ , and  $(w - p) = p$ . However, near the excavation line, both  $w$  and  $p$  are acting on the shaft, and their effects can be difficult to separate from one another. For the purposes of this analysis,  $w$  is assumed to reach zero at the excavation line.

#### ***3.7.3.e.2: Correcting Soil Resistance for Excavation Location***

Because the soil resistance values near the excavation line are influenced by points above the excavation line, and the influence of driving earth pressures extending slightly beyond the shaft base, the soil resistance at the excavation line obtained from point-by-point differentiation is often a negative value. Because this is not physically possible with a positive deflection, polynomial curve fitting is applied to ensure net soil resistance values are not negative at the excavation line. To provide consistency with design practice, which often assumes a value of zero soil resistance at the excavation line, a third-order polynomial fit using least-squares regression was used to represent the profile of soil resistance versus

depth. This maintains the general magnitude and shape of the soil resistance profile, but allows every profile to reach zero at the excavation line (Figure 3.23).

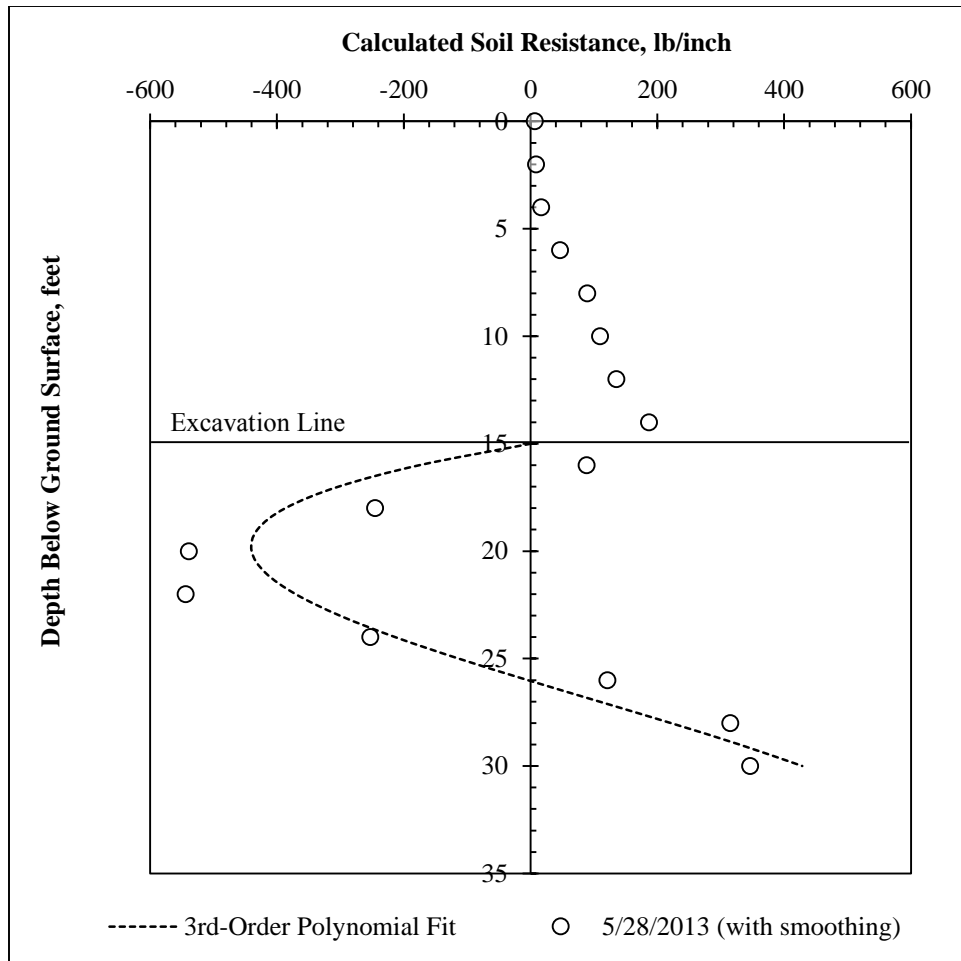


Figure 3.23: Using a third-order polynomial to adjust values of net soil resistance for p-y curves.

### 3.7.3.e.3: Correcting Horizontal Deflections for Center of Rotation

In limit equilibrium and numerical models such as LPILE, the shaft rotates about a center of rotation (at approximately 26 feet in Figure 3.1). Above the center of rotation, deflections are positive, and below, the deflections are negative. In a standard deflected

shape generated from inclinometer data, however, the shaft base is assumed to be fixed, and all deflections appear to be positive. This can provide misleading results for p-y curves; if the raw inclinometer deflections are used, at the center of rotation, the shaft appears to have moved without any corresponding increase in earth pressure. Similarly, without corrections to deflection data, at the shaft base, nonzero soil forces appear to be present without any shaft deflections. To prevent unrealistic results such as these in data interpretation, and to allow for pile conditions closer to force equilibrium, the inclinometer data is adjusted to allow the shaft to rotate about the center of rotation (defined for the purposes of this analysis as the depth at which the soil resistance below the excavation is equal to zero) as shown in Figure 3.24.

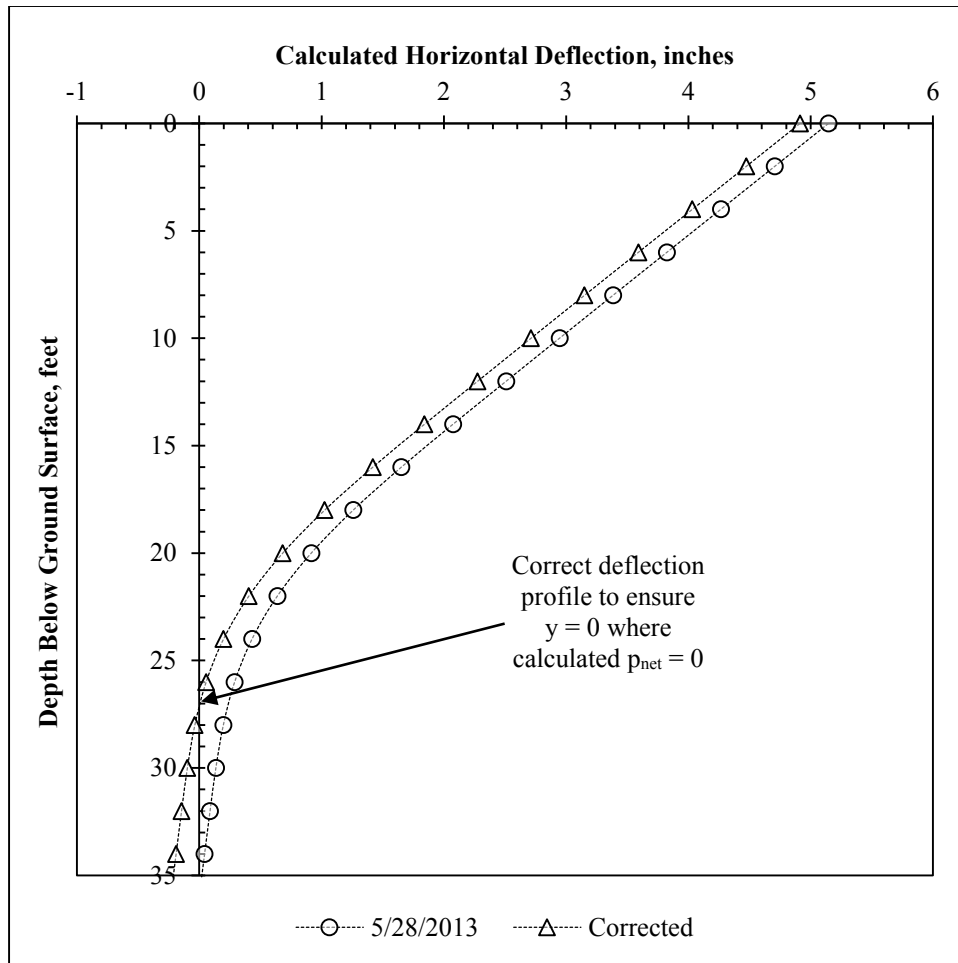


Figure 3.24: Correction of deflected shape about center of rotation for p-y curves

#### 3.7.3.e.4: Example p-y Curves Developed from Inclinometer Data

By plotting corrected values of soil resistance ( $p$ ) against corrected values of deflection ( $y$ ), p-y curves comparable to those used for analysis in programs such as LPILE can be generated. An example family of curves for depths between 16 and 24 feet below the original ground surface, zeroed on October 8, 2010, and consisting of all measurements through May 28, 2013, is shown in Figure 3.25.

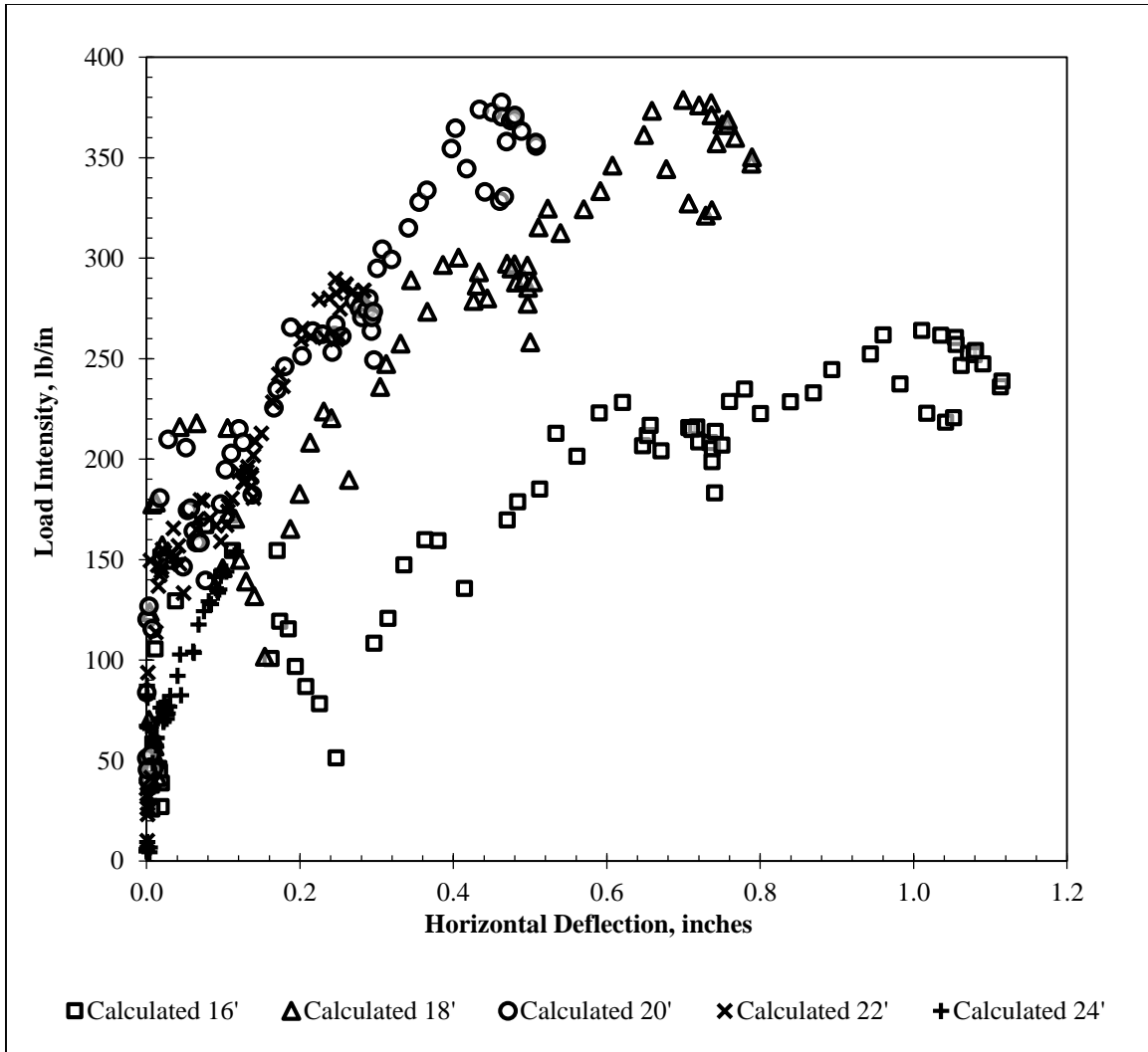


Figure 3.25: Example p-y curves generated from inclinometer data at the test wall. Reference survey is October 8, 2010.

### 3.8: Summary and Conclusions

The Lymon C. Reese research wall is constructed through expansive clay in Manor, Texas. The wall was designed according to standard of practice methods, and is instrumented with inclinometers, strain gauges, and Time Domain Reflectometry (TDR) moisture probes. Conclusions include:



- The drilled shafts and instrumentation were installed during early April, 2010. The design goal was to provide a wall which was structurally sound and consistent with design practice, but would produce enough deformations to infer the earth pressures acting on the wall.
- Strain gauges record values of axial strain on either side of the shaft's neutral axis. By dividing the difference in axial strain at a given depth by the horizontal distance between gauges, axial strains can be converted to values of bending curvature. Values of bending curvature can be converted to values of bending moment using standard nonlinear moment-curvature relationships for reinforced concrete.
- Inclinerometers record values of rotation along the length of the shaft. The rotation profile can be integrated to calculate a profile of lateral deflections, or differentiated to calculate a profile of bending curvature.
- A method of developing p-y curves from inclinometer data is presented. Rotation profiles from the three instrumented shafts are combined and differentiated using a combination of piecewise polynomial differentiation and numerical smoothing techniques. To achieve force equilibrium conditions consistent with existing design practice, corrections are applied to the calculated values of soil resistance to ensure soil resistance reaches zero at the excavation line, and to ensure the shaft deflection is zero where the net soil resistance reaches zero at depth. The resulting values of net soil resistance ( $p_{net}$ ) are compared with calculated horizontal deflections ( $y$ ) to develop a model of nonlinear soil response at each depth below the excavation line.

## **CHAPTER 4: TEST WALL PERFORMANCE BEFORE EXCAVATION (APRIL 2010 – AUGUST 2010)**

*Note: Portions of this section have been previously published by the author (Brown et. al., Geo-Frontiers 2011).*

### **4.1: Overview**

Between installation of the drilled shafts and instrumentation in early April, 2010, and test wall excavation in August, 2010, strain measurements shed light on the processes that take place within the concrete of a drilled shaft retaining wall prior to excavation. In order to fully understand these measurements, excavation was delayed until early August 2010. This section explains the deformations observed in the wall prior to excavation.

### **4.2: Climatic Information**

Monthly rainfall totals for Austin, Texas between January, 2009 and July, 2010 are presented in Figure 4.1. For approximately eight months prior to shaft construction in early April, 2010, the test wall site experienced average to above average rainfall. Rainfall totals were significant enough that surface water was frequently present at the test wall site beginning in November, 2009, softening the surface soils and delaying initial site investigation until January, 2010. After shaft construction, the wall site experienced two months of below average rainfall in April and May, followed by two months of above average rainfall in June and July.

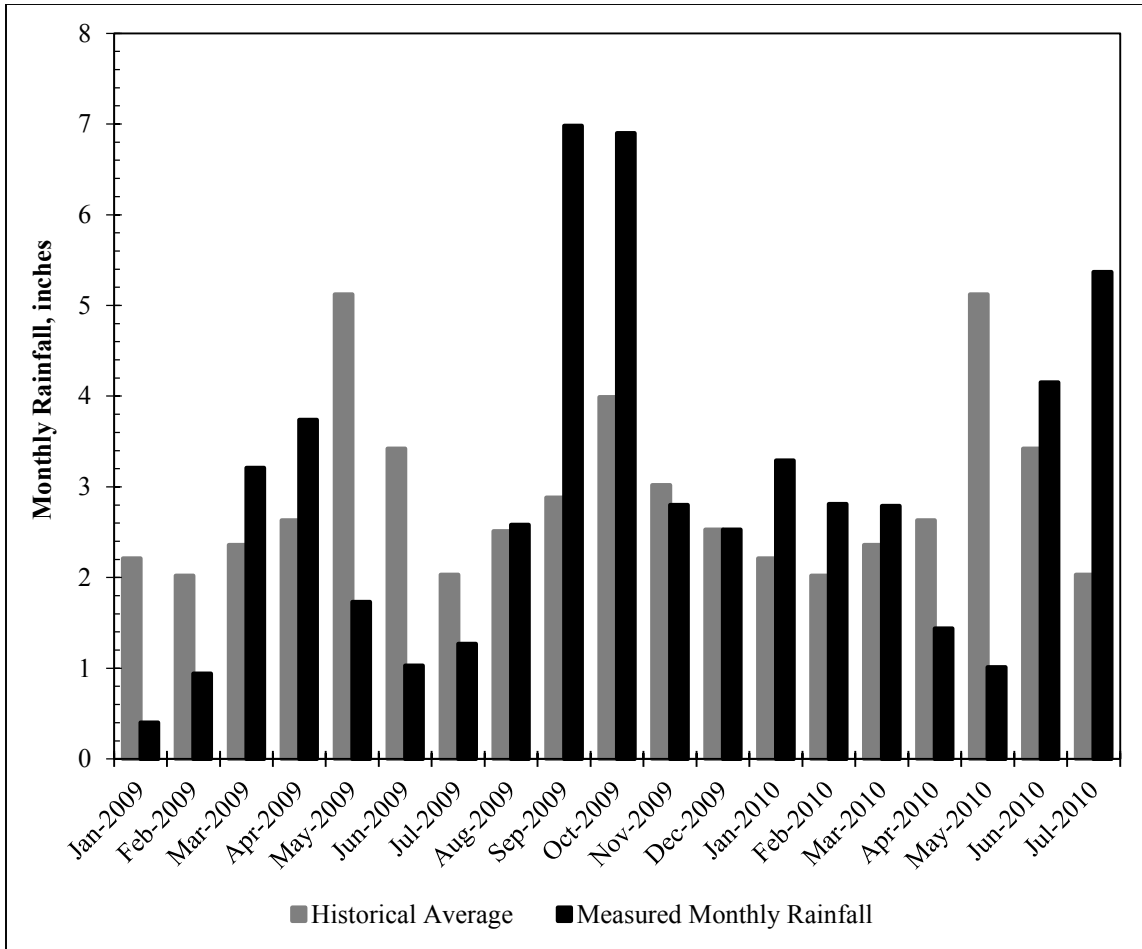


Figure 4.1: Monthly rainfall totals for Austin, Texas (Jan. 2009 - Jul. 2010; data from [www.wunderground.com](http://www.wunderground.com)). Drilled shafts were installed in early April, 2010.

### 4.3: Summary of Field Instrumentation Data

#### 4.3.1: STRAIN GAUGE DATA

After test wall construction was completed, strain gauge data were recorded at least once per week until excavation occurred. Early in the concrete curing process, the measurement interval was approximately once per day; as the concrete curing activity slowed down, the frequency of measurements decreased to approximately once per week

until excavation began. The pre-excavation strain data is presented in Figure 4.2 - Figure 4.16.

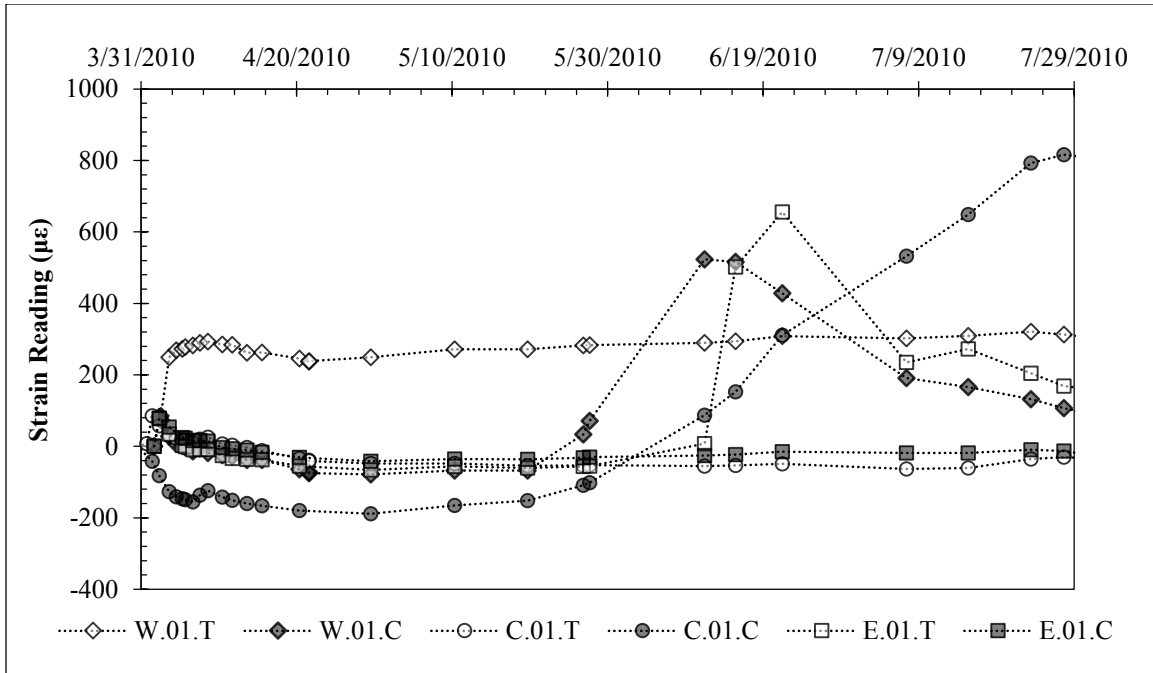


Figure 4.2: Pre-Excavation Strain Data for Gauges 1 Foot Below Ground Surface.

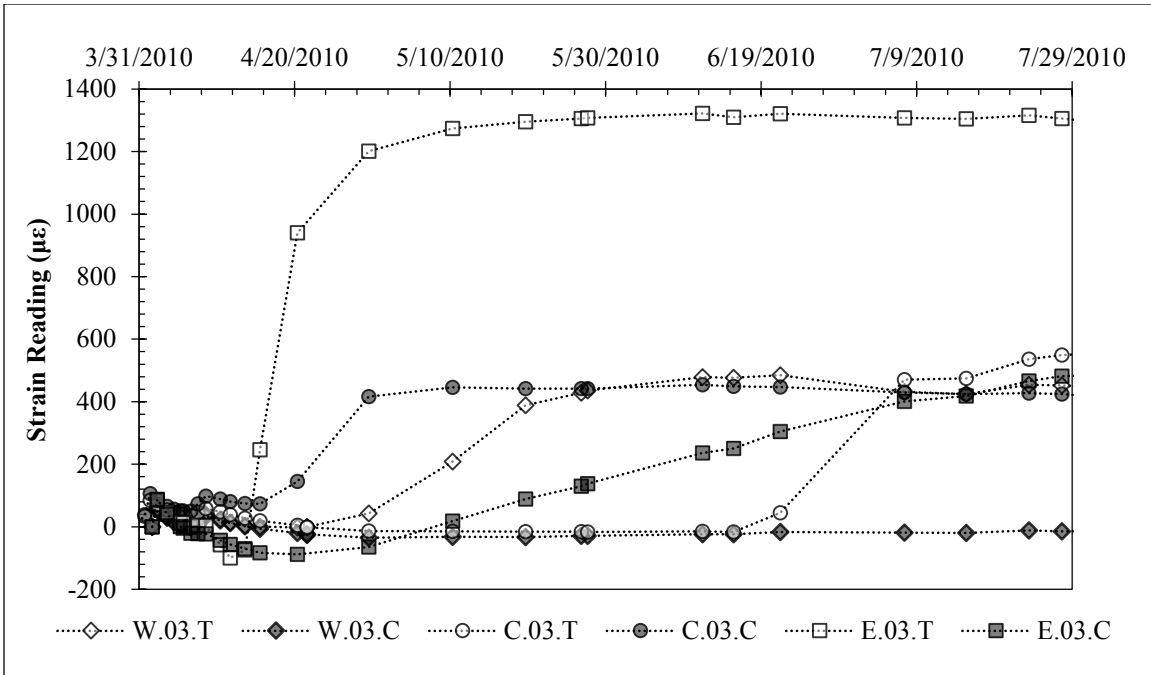


Figure 4.3: Pre-Excavation Strain Data for Gauges 3 Feet Below Ground Surface.

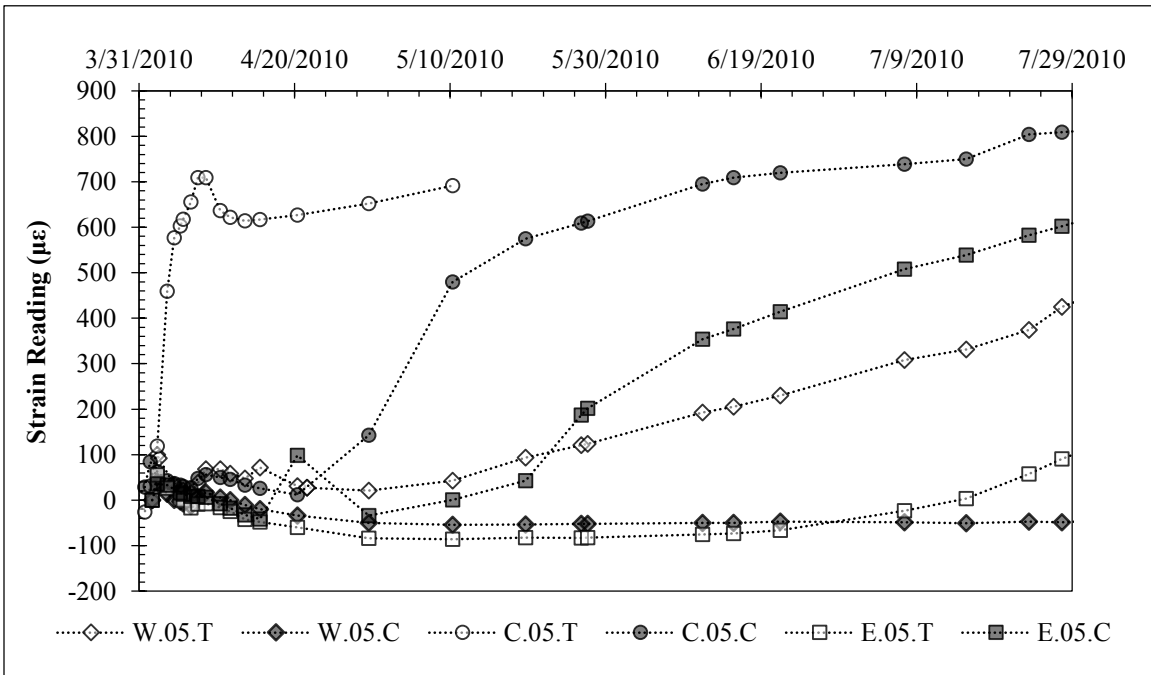


Figure 4.4: Pre-Excavation Strain Data for Gauges 5 Feet Below Ground Surface.

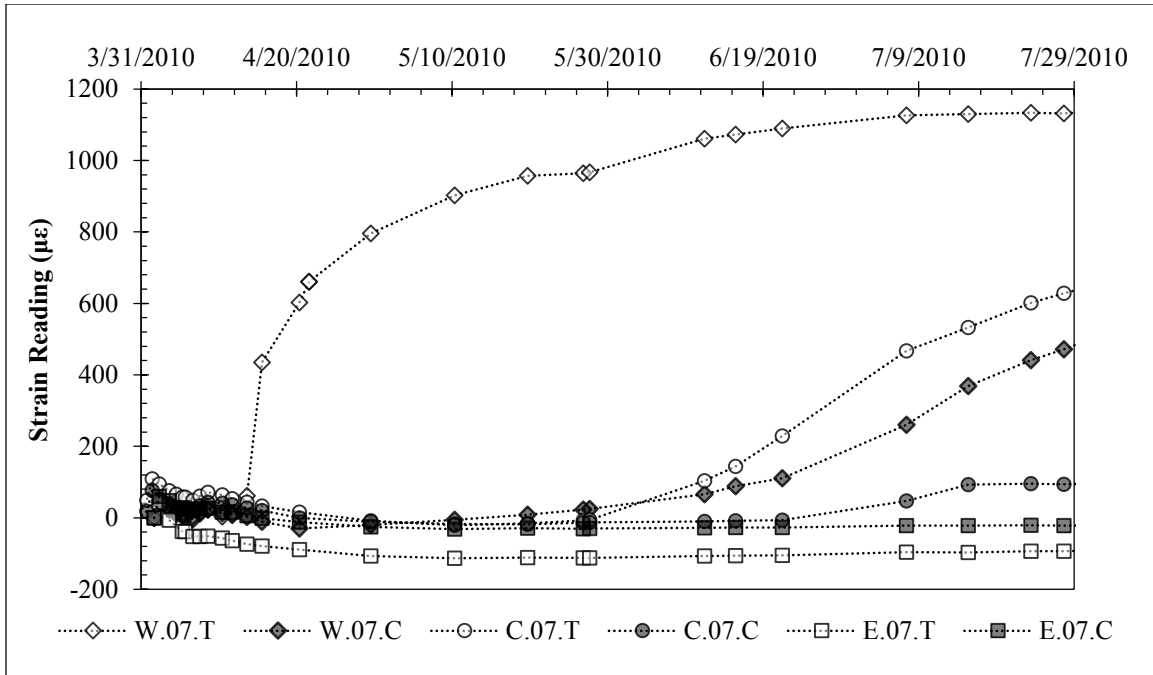


Figure 4.5: Pre-Excavation Strain Data for Gauges 7 Feet Below Ground Surface.

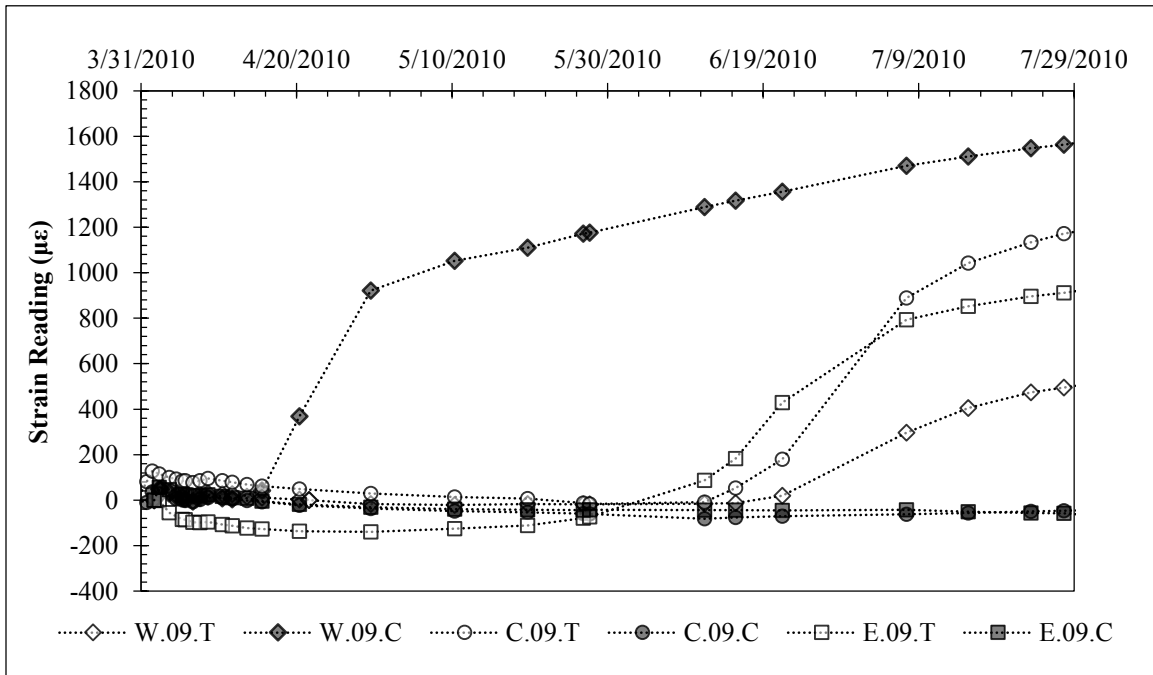


Figure 4.6: Pre-Excavation Strain Data for Gauges 9 Feet Below Ground Surface.

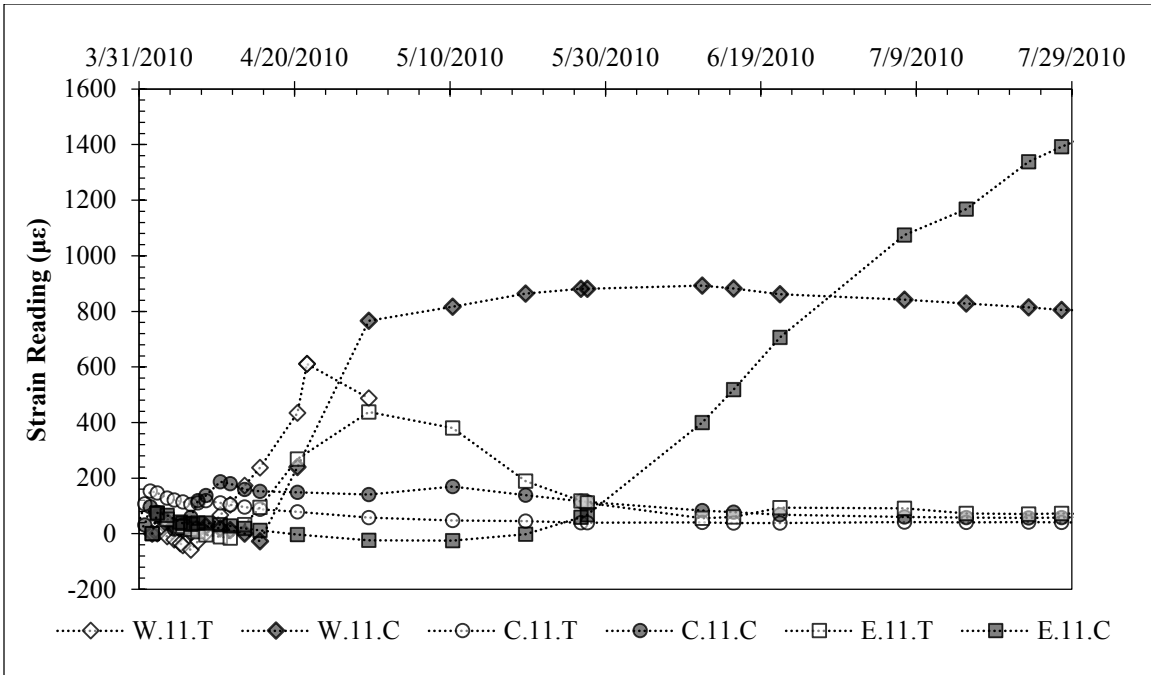


Figure 4.7: Pre-Excavation Strain Data for Gauges 11 Feet Below Ground Surface.

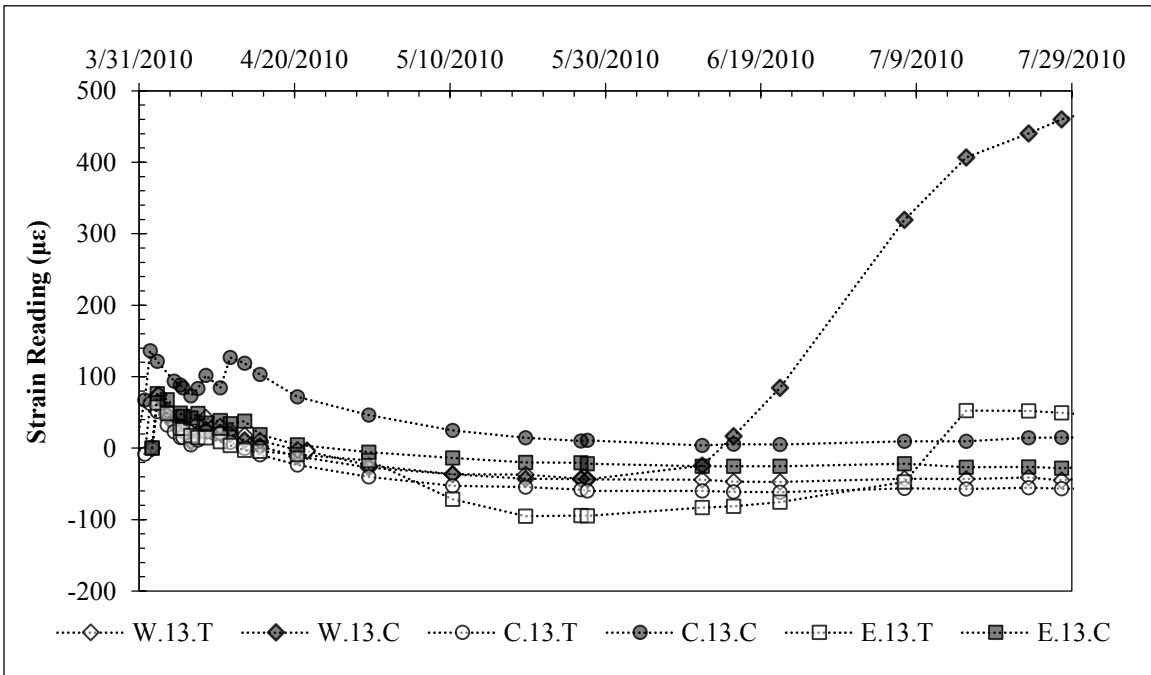


Figure 4.8: Pre-Excavation Strain Data for Gauges 13 Feet Below Ground Surface.

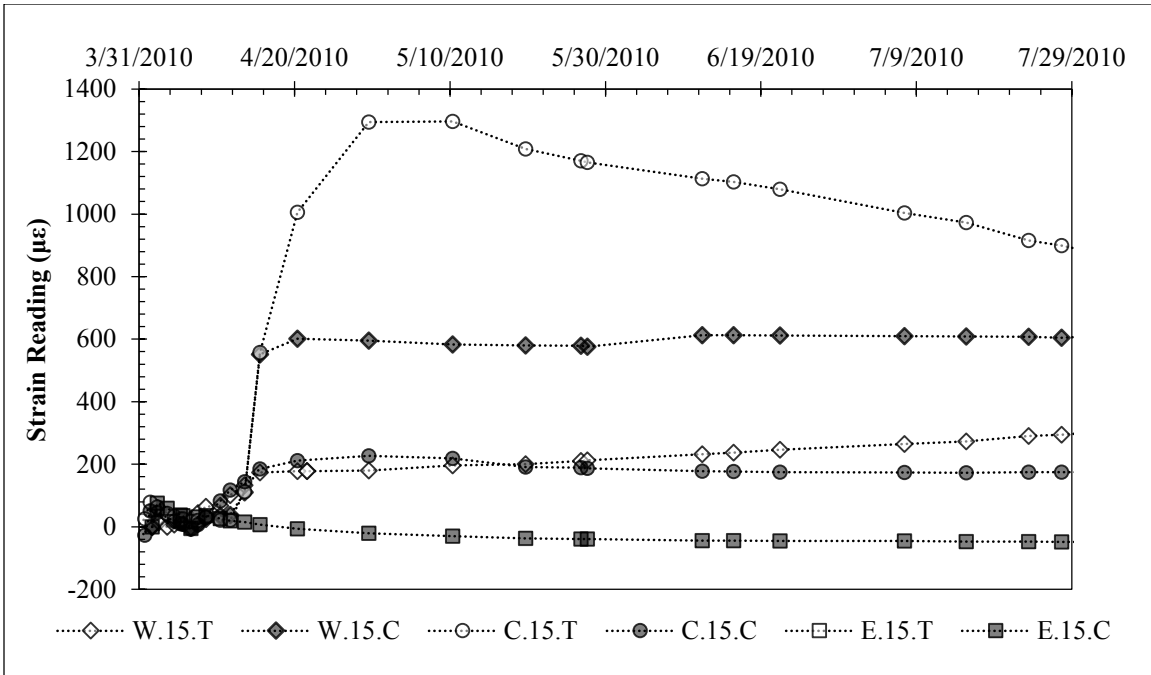


Figure 4.9: Pre-Excavation Strain Data for Gauges 15 Feet Below Ground Surface.

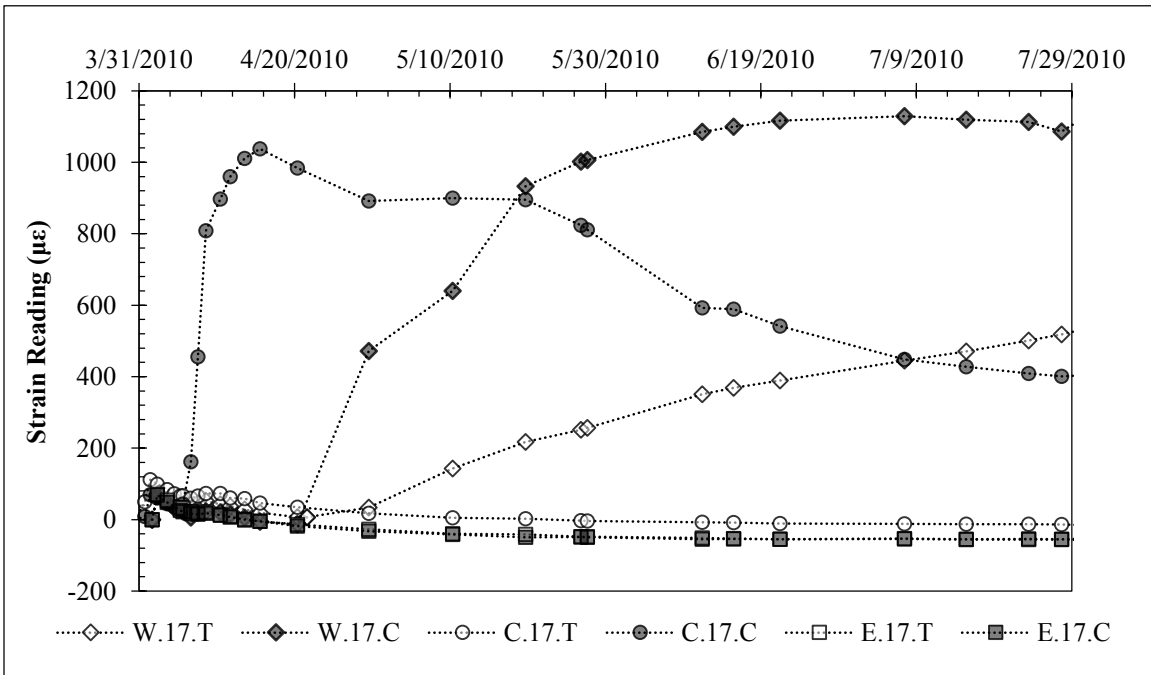


Figure 4.10: Pre-Excavation Strain Data for Gauges 17 Feet Below Ground Surface.



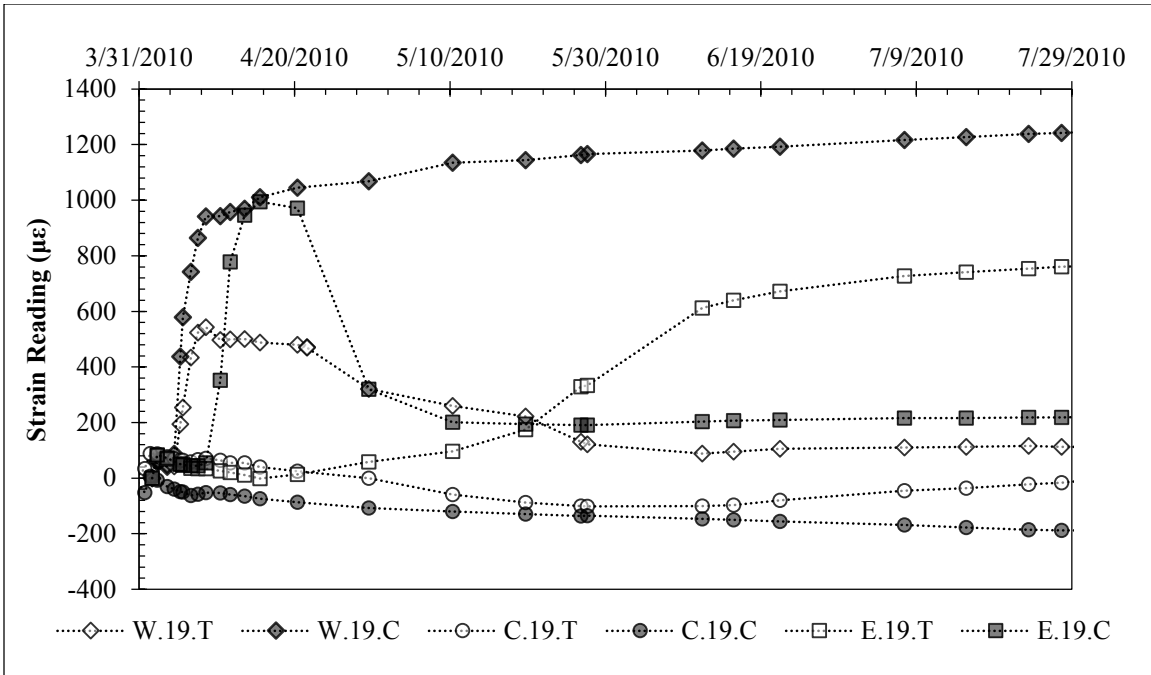


Figure 4.11: Pre-Excavation Strain Data for Gauges 19 Feet Below Ground Surface.

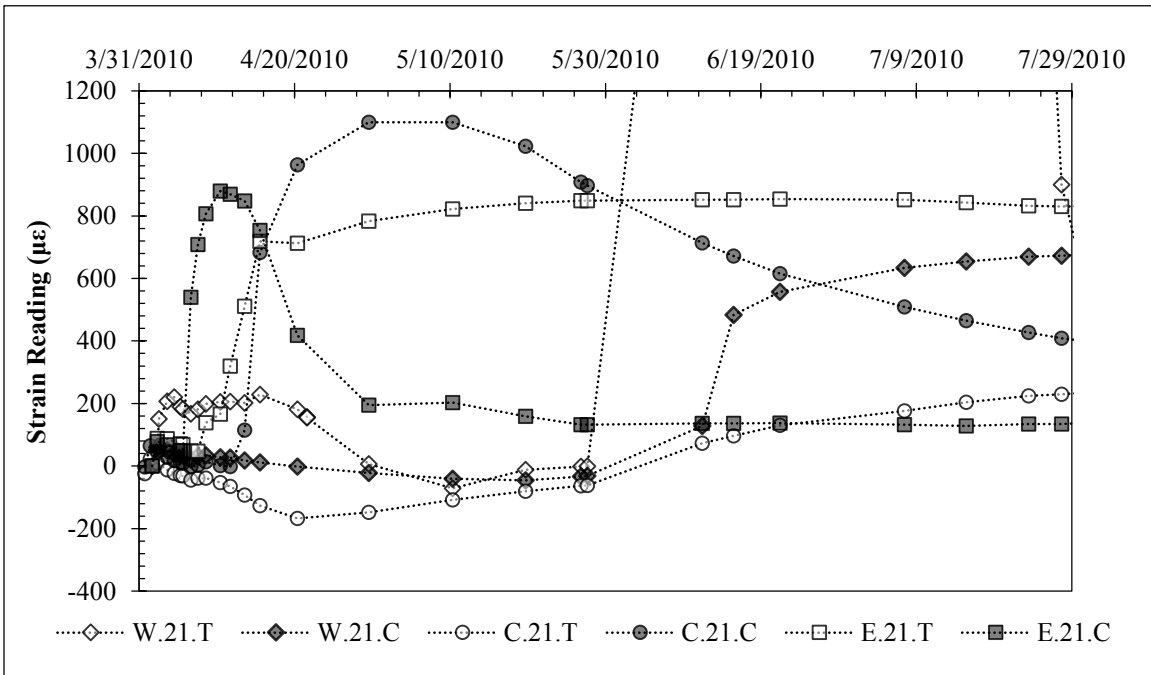


Figure 4.12: Pre-Excavation Strain Data for Gauges 21 Feet Below Ground Surface.

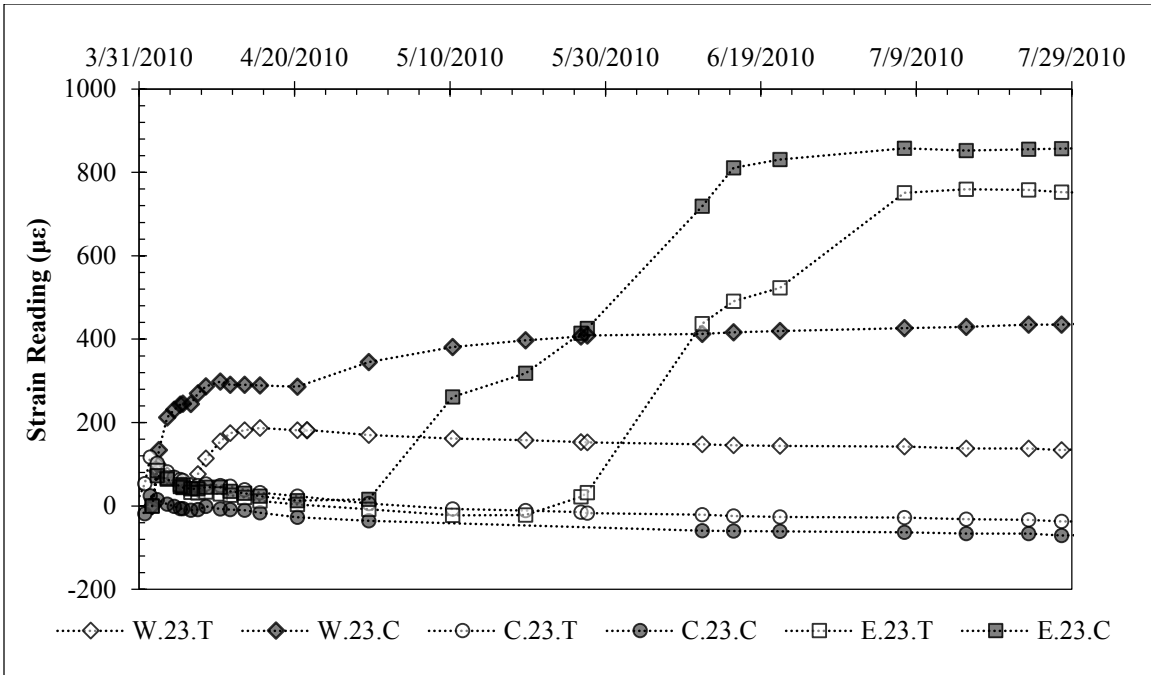


Figure 4.13: Pre-Excavation Strain Data for Gauges 23 Feet Below Ground Surface.

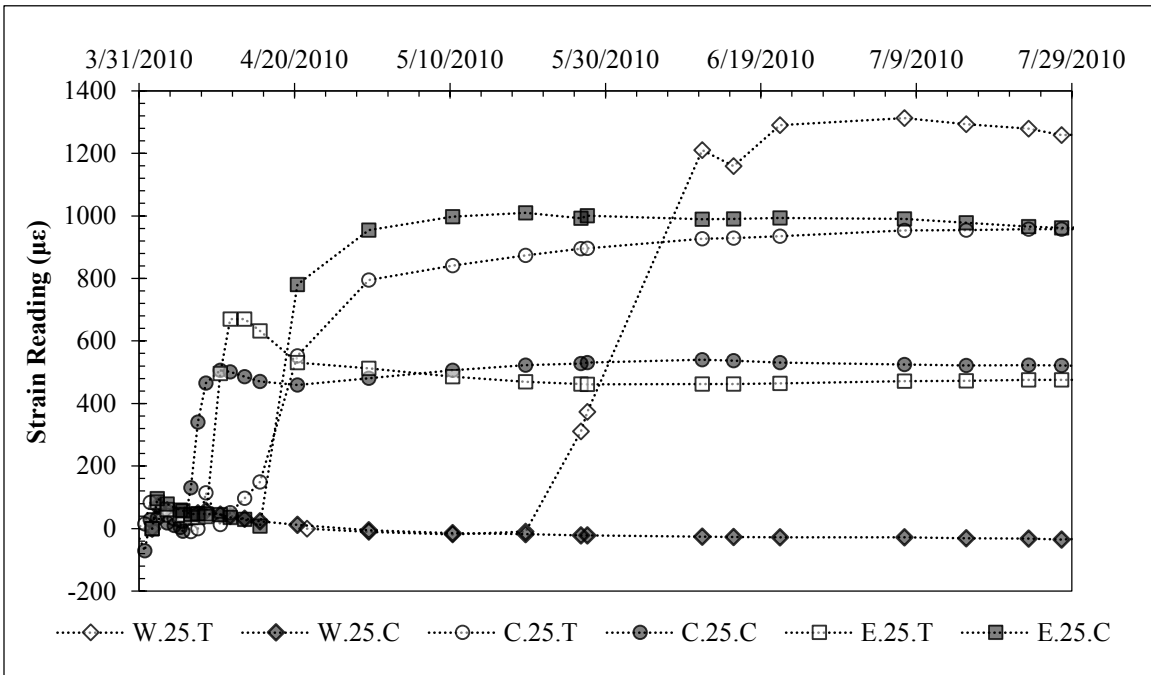


Figure 4.14: Pre-Excavation Strain Data for Gauges 25 Feet Below Ground Surface.

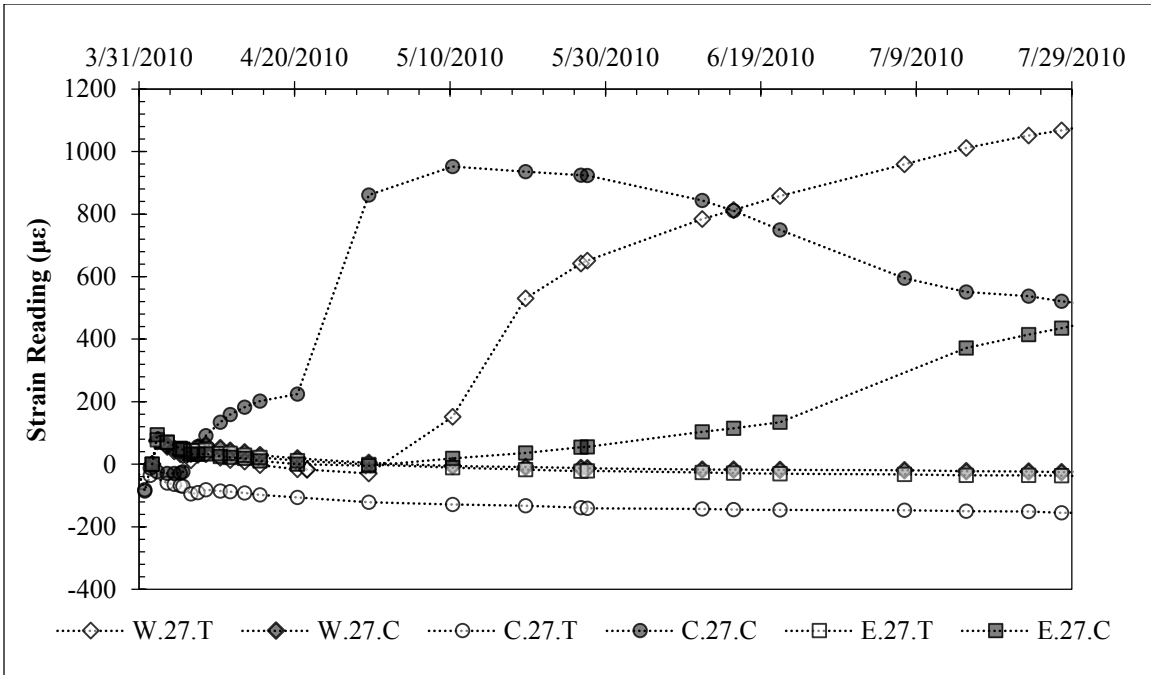


Figure 4.15: Pre-Excavation Strain Data for Gauges 27 Feet Below Ground Surface.

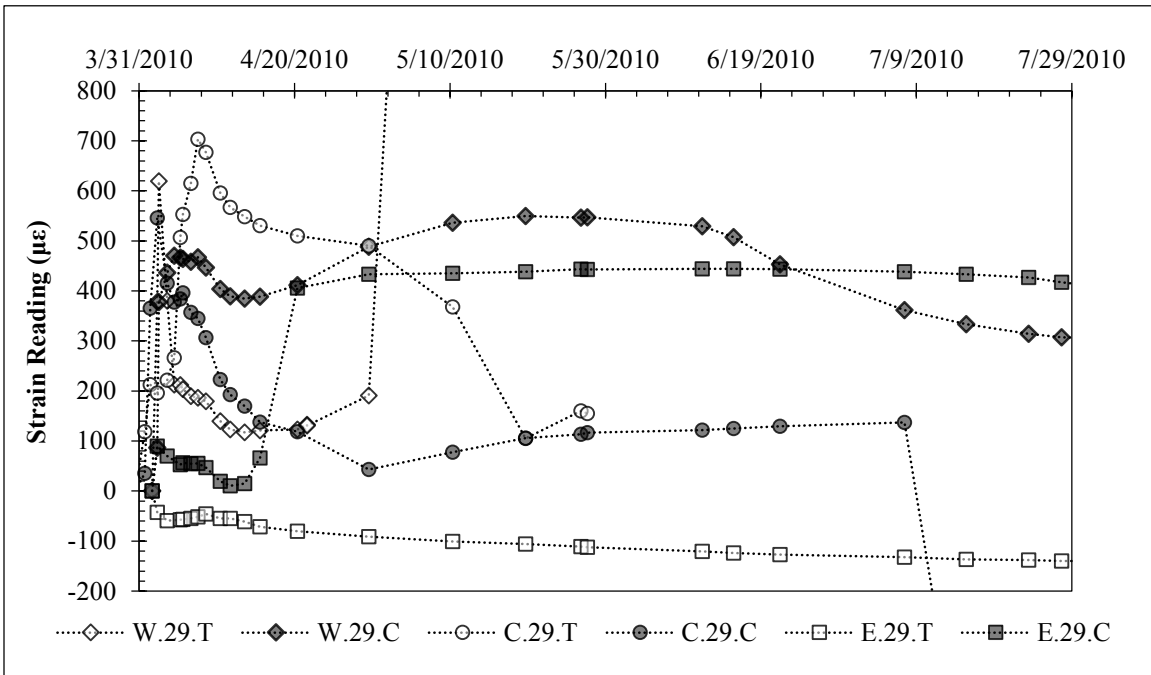


Figure 4.16: Pre-Excavation Strain Data for Gauges 29 Feet Below Ground Surface.

### **4.3.2: STAND PIPE PIEZOMETER**

The groundwater level was measured prior to excavation, and the piezometer was developed by removing water from the piezometer casing with a hand bailer and allowing the water level to return to its natural value over time. If the resulting values of water level versus time are analyzed as a rising head test, the hydraulic conductivity is approximately  $3 \times 10^{-5}$  ft/day (approximately  $10^{-8}$  cm/s) below the water table. While this was far from a formal test, the results are consistent with other published data for the Taylor formation (e.g. Ellis, 2011) and with general values for high plasticity, fine-grained clays. Final groundwater level at excavation was approximately 8 feet below ground surface.

## **4.4: Data Interpretation**

### **4.4.1: CONCRETE CURING**

After successful installation of the strain gauges and field enclosure, strain measurements were taken at least once per day for several weeks. Initial strain measurements behaved similarly as other published data from concrete curing (e.g., Fellenius et al 2009). As the concrete heated after placement, tensile strains tended to rise sharply and then decrease gradually as the concrete cooled (Figure 4.17). Heating from adjacent shafts also caused less pronounced spikes in tension (Figure 4.17). Because the gauges were zeroed in the lab to a value of zero force and no drift has been observed, nonzero initial strains are assumed to represent forces picked up during installation and concrete placement prior to the first reading.

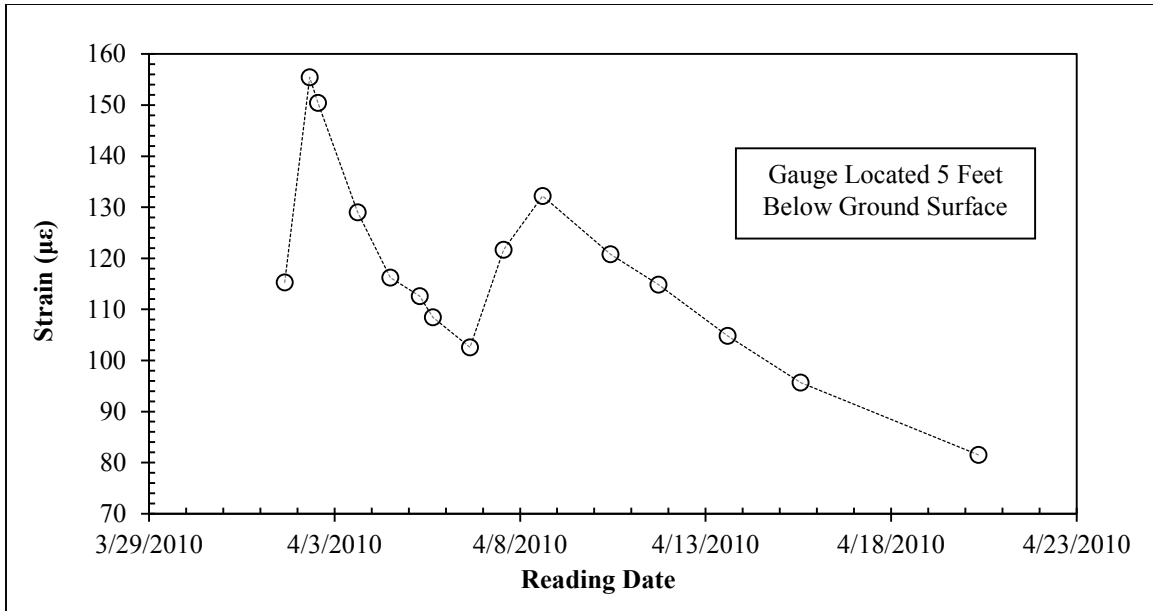


Figure 4.17: Three weeks of strain measurements during concrete curing. Concrete placed on April 1; concrete in adjacent shafts placed on April 6. Positive strain indicates tension.

#### 4.4.2: SHRINKAGE CRACKING IN CONCRETE

Beginning approximately one week after concrete placement, and continuing over the next several weeks, about 20 percent of the strain gauges exhibited large and sudden jumps into tension. These jumps occurred between one and four weeks after concrete placement, were most frequent in the second and third weeks, and have no clear relationship with depth. Figure 4.18 shows measurements recorded for one gauge as an example.

These jumps are likely the result of small tension cracks forming in the concrete due to shrinkage. For example, at seven days, the concrete compressive strength was approximately 4 kips/in<sup>2</sup>, giving an average tensile strength of about 0.4 kips/in<sup>2</sup>. Distributed throughout the shaft, this represents a tensile load of about 180 kips. If this tensile load is released as a crack extends across the shaft, the load will be redistributed to

the 12 #7 bars. A tensile force of 180 kips corresponds to a strain of about 900 microstrains in the bars, which is consistent with the magnitude of tensile strains associated with these jumps (Figure 4.18).

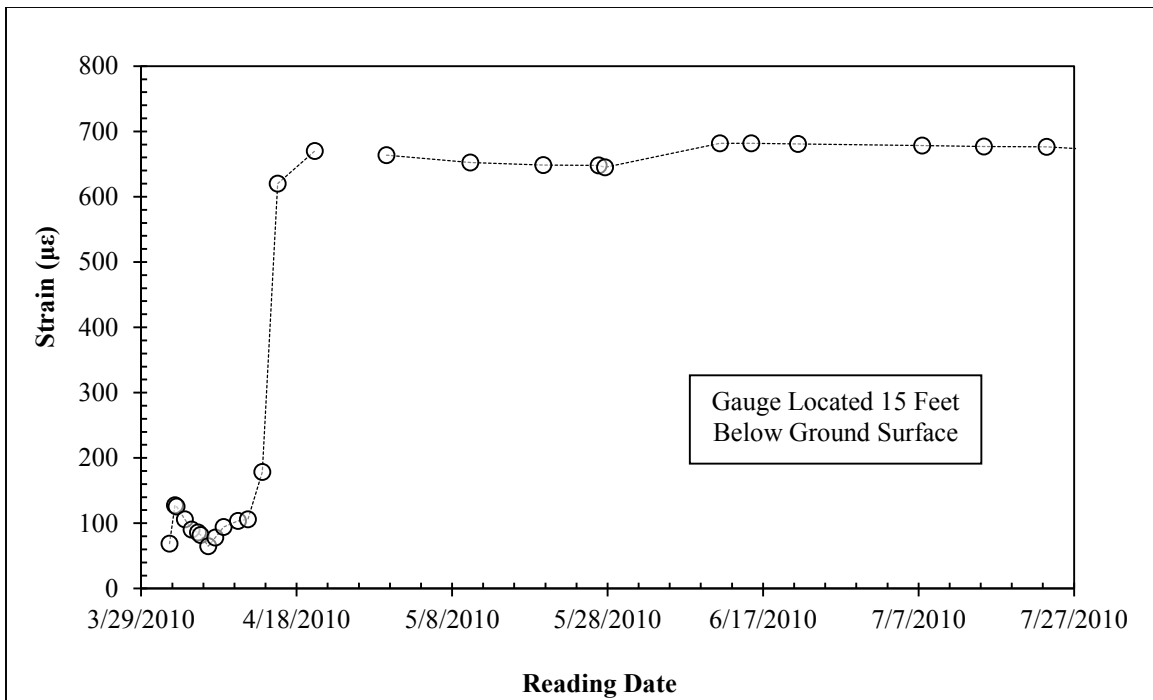


Figure 4.18: Illustration of tension crack formation in concrete near gauge.

Another issue with concrete cracking is the risk of breaking the strain gauge. If a tension crack forms very close to the exposed optical fiber, the fiber can be damaged and the gauge can be lost (Fuhr et al., 1993). Soon after cracking in the concrete began, two gauges jumped to over 3,000 microstrains, which was outside their range of measurement and likely indicated damage to the gauge. Over the course of the project, gauges which suddenly register measurements in this range have usually malfunctioned shortly thereafter.

#### **4.4.3: EXPANSIVE SOIL MOVEMENT**

After the influence of concrete curing and tension cracks diminished, approximately 10 percent of gauges showed steady increases in tension over the remaining three months between concrete placement and excavation. The increases in tension occurred most commonly in gauges located between 0 and 10 feet below the ground surface. Figure 4.19 shows a gauge, located seven feet below ground surface, exhibiting this behavior. A gauge at 23 feet showed similar strain behavior early on, but did not exhibit the same increase in tension with time. Qualitatively, the increase in tension begins at a similar time as the transition from below average rainfall in April and May to above average rainfall in June and July. A pre-excavation strain value of approximately 700 microstrains also suggests that a tension crack may also be present near the gauge. The shaft may be experiencing changes in side shear stresses due to moisture content changes in high plasticity clay (e.g., Kim and O'Neill, 1998), along with the effects of tension cracking in the concrete. This behavior is most pronounced in gauges located between 5 and 9 feet below ground surface, above the water table where the natural moisture content fluctuates in response to weather patterns.

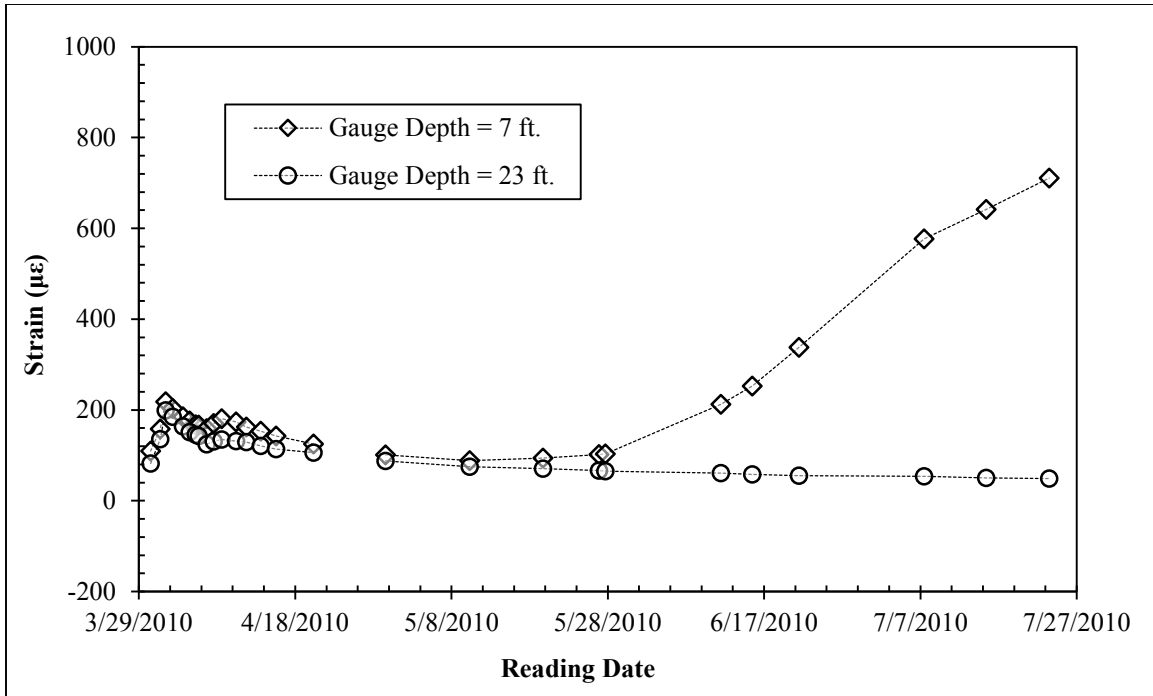


Figure 4.19: Strains occurring between concrete curing and excavation. The gauge at a depth of 7 feet may be experiencing changes in side shear due to moisture fluctuations in the active zone (e.g., Kim & O'Neill, 1998).

#### 4.4.4: DEVELOPMENT OF RESIDUAL STRESSES AND STRAINS

Koutrovelis (2012) attempted to idealize the residual stresses that existed in the concrete of the Manor test wall prior to excavation by interpreting data from the optical strain gauges. The analysis suggested that, on average, our test wall experienced an initial increase in tension followed by a period of compression (Figure 4.20).



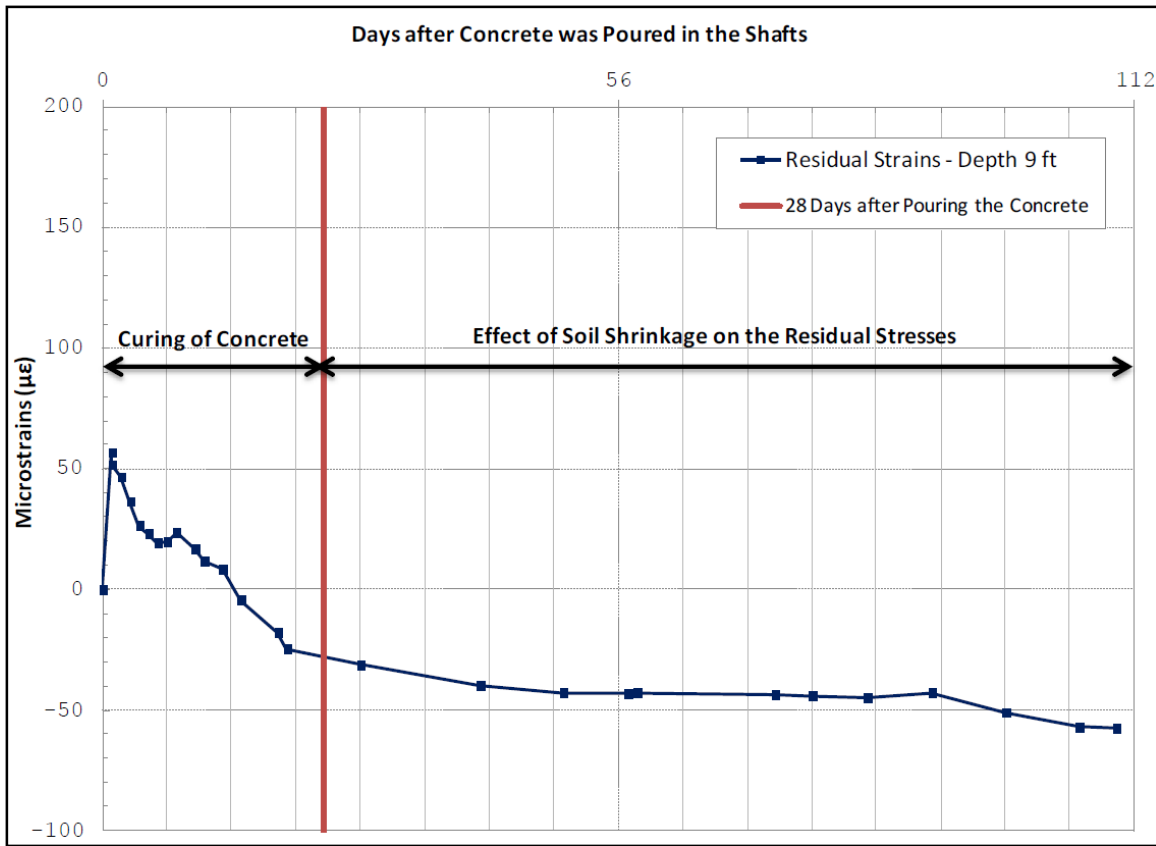


Figure 4.20: Development of residual strains at a depth of 9 feet between shaft construction and excavation (after Koutrouvelis, 2012).

During the first three to four weeks after concrete placement, the development of residual strains is governed by the concrete curing. After most of the activity associated with concrete curing subsided, moisture changes in the expansive clay may have contributed to the development of residual compressive strains in the shaft before excavation (Koutrouvelis, 2012). The existence of residual stresses and strains can lead to difficulties in data interpretation, and may influence the shafts' response to loading. While stresses and strains in the shaft are generally assumed to be negligible prior to excavation, in some cases, it may be necessary to consider the effects of residual stresses and strains on the shafts when interpreting wall performance data.

## 4.5: Summary and Conclusions

An examination of test wall behavior between shaft construction and excavation has shed light on the processes which occur in drilled shaft retaining walls prior to excavation. Key findings include:

- Prior to shaft construction, the test site experienced approximately eight months of above average rainfall. Between shaft construction and excavation, the wall experienced two months of below average rainfall, followed by two months of above average rainfall.
- Axial strains developed in the shafts prior to construction due to a combination of concrete curing and expansive soil movement. In many cases, the development of axial strains suggests that tension cracks developed throughout the shaft.
- Residual stresses and strains are present in the shafts prior to excavation. The distribution of residual stresses and strains is highly variable within each shaft.

## CHAPTER 5: TEST WALL PERFORMANCE DURING EXCAVATION (AUGUST 2010 – SEPTEMBER 2010)

*Note: Portions of this section have been previously published by the author (Brown et. al., Geo-Frontiers 2011).*

### 5.1: Overview

#### 5.1.1: SUMMARY OF EXCAVATION PROGRESS

Excavation of the test wall began on July 29, 2010 and took place over a period of approximately four weeks. The full cantilever height of 14 to 15 feet was reached on August 13, 2010, and the preliminary slopes were completed on August 19, 2010. The slopes were improved on September 30, 2010, and facing was installed on October 8, 2010. Photos of the excavation progress are provided in Figure 5.1 - Figure 5.2.



Figure 5.1: Photos of initial excavation progress (7/29/2010 – 8/5/2010).



Figure 5.2: Photos of later excavation progress (8/23/2010 - 10/1/2010).

### 5.1.2: CLIMATIC INFORMATION

Prior to the start of excavation, the project site had experienced a relatively dry spring, followed by a summer with above average rainfall. During excavation, hot, dry weather during August was followed by above average rainfall during the month of September (Figure 5.3), punctuated by approximately 1.9 inches of rain on September 7 (Figure 5.4). Average daily temperatures decreased from about 85 degrees Fahrenheit at the start of excavation to about 65 degrees at the installation of facing, a decrease of approximately 20 degrees (Figure 5.5).

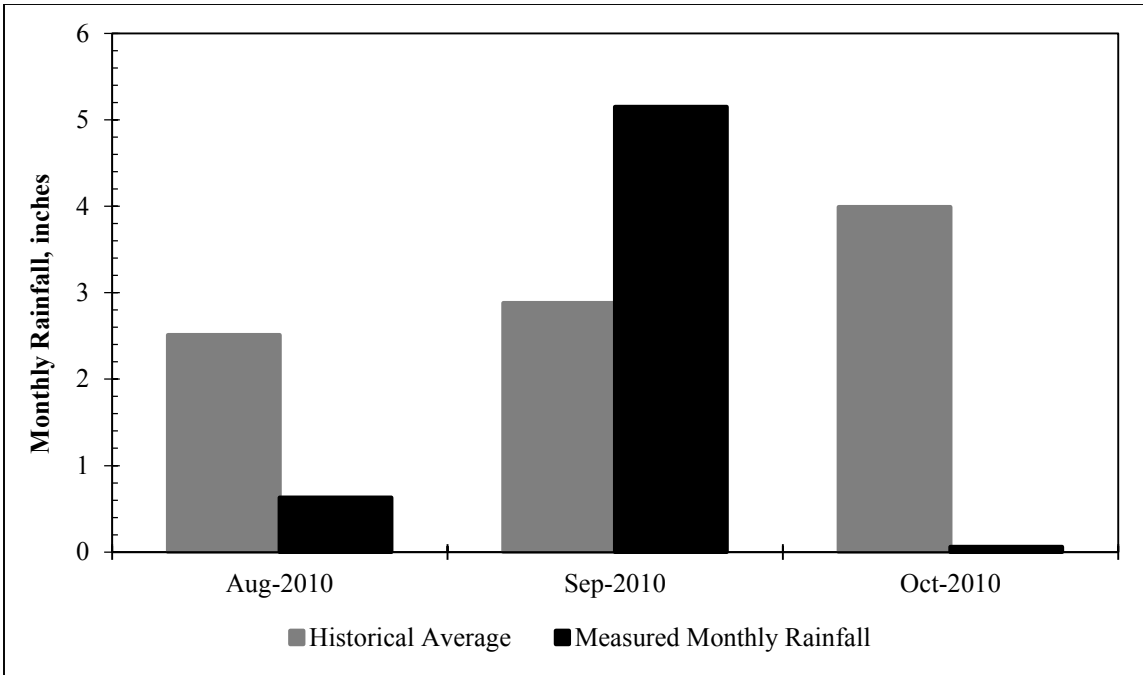


Figure 5.3: Monthly rainfall totals for Austin, Texas (Jul. 2010 – Oct. 2010; data from [www.wunderground.com](http://www.wunderground.com)).

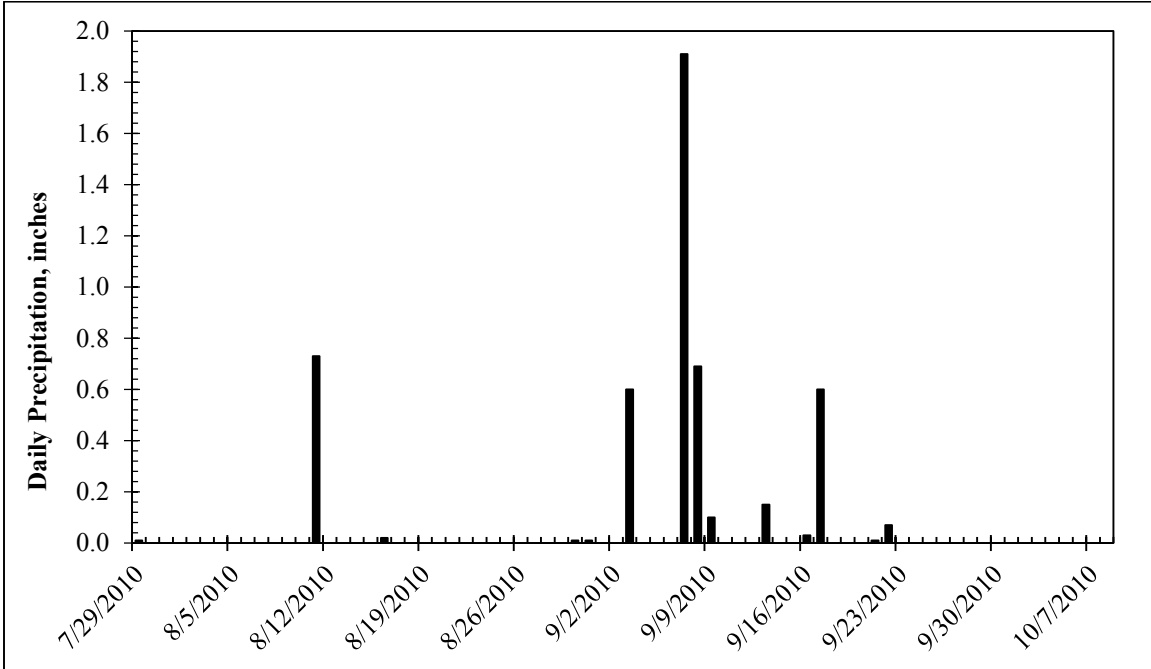


Figure 5.4: Daily precipitation for Manor, Texas (Jul. 2010 – Oct. 2010; data from [www.wunderground.com](http://www.wunderground.com)).

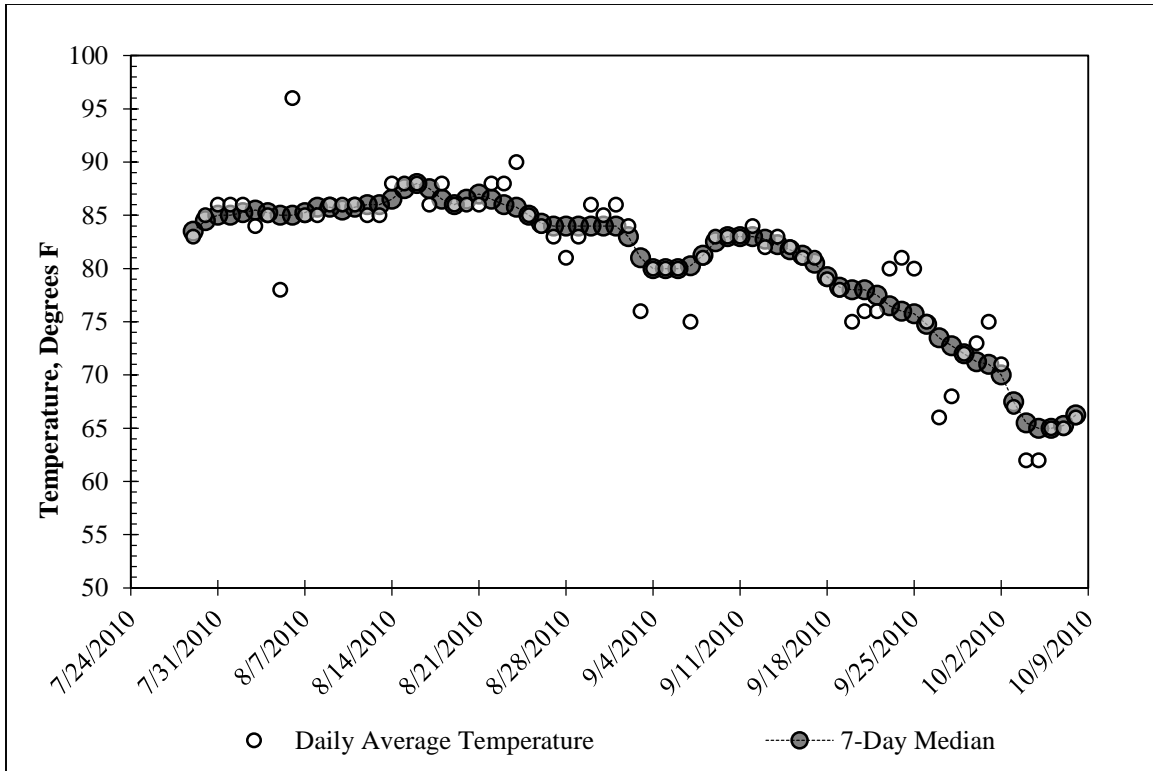


Figure 5.5: Daily temperature data for Manor, Texas (Jul. 2010 – Oct. 2010; data from [www.wunderground.com](http://www.wunderground.com)).

## 5.2: Summary of Field Instrumentation Data

### 5.2.1: INCLINOMETER DATA

Beginning on July 27, 2010, inclinometer data from the east instrumented shaft was recorded at regular intervals throughout the excavation process. Lateral deflections at ground surface and a depth of 14 feet, along with a summary of key excavation events, are shown in Figure 5.6. Deflected shapes at various points during excavation are provided in Figure 5.7, and cumulative deflections in the soil 5.5 feet behind the centerline of the wall are provided in Figure 5.8.

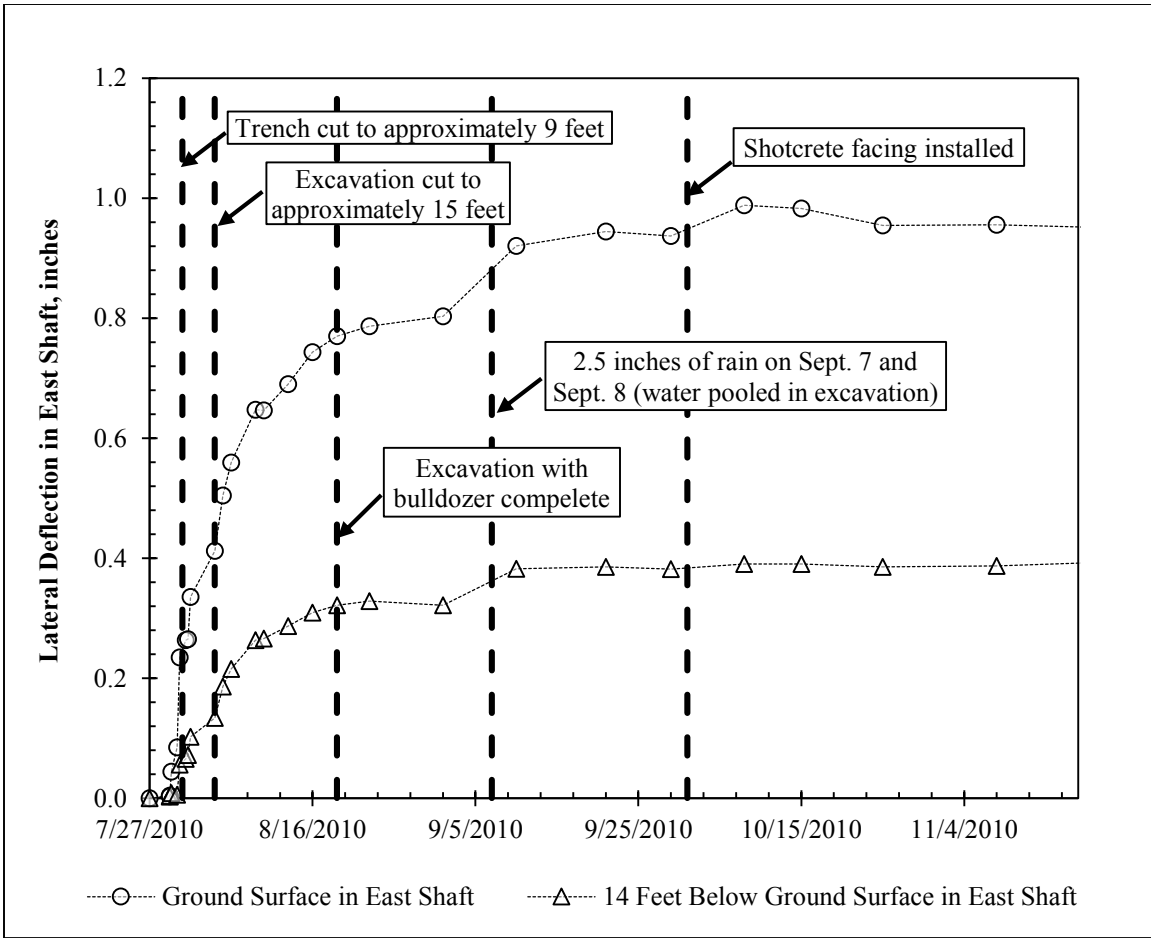


Figure 5.6: Progression of lateral deflections and key events during excavation.

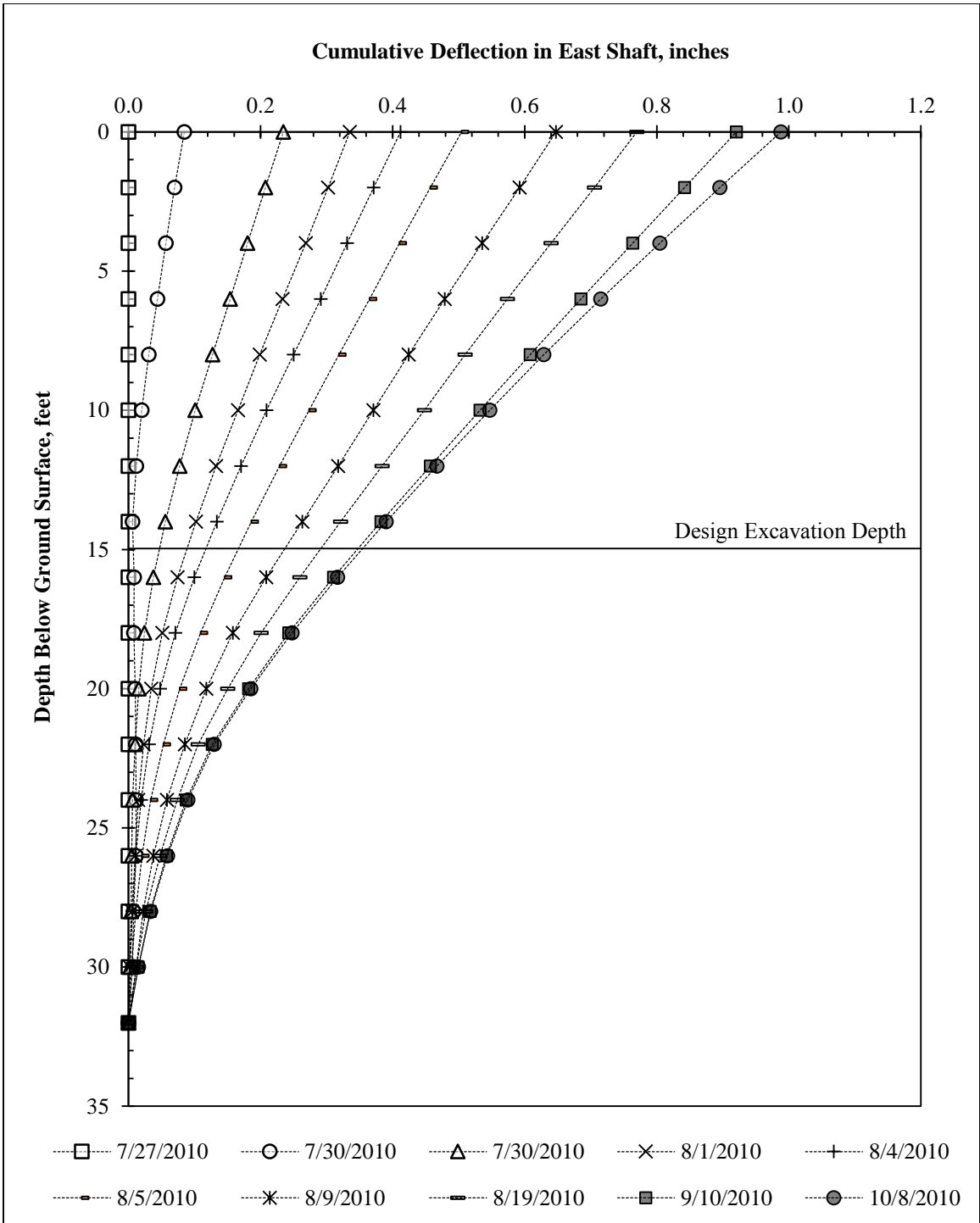


Figure 5.7: Deflected shape of east instrumented shaft at various dates during excavation.



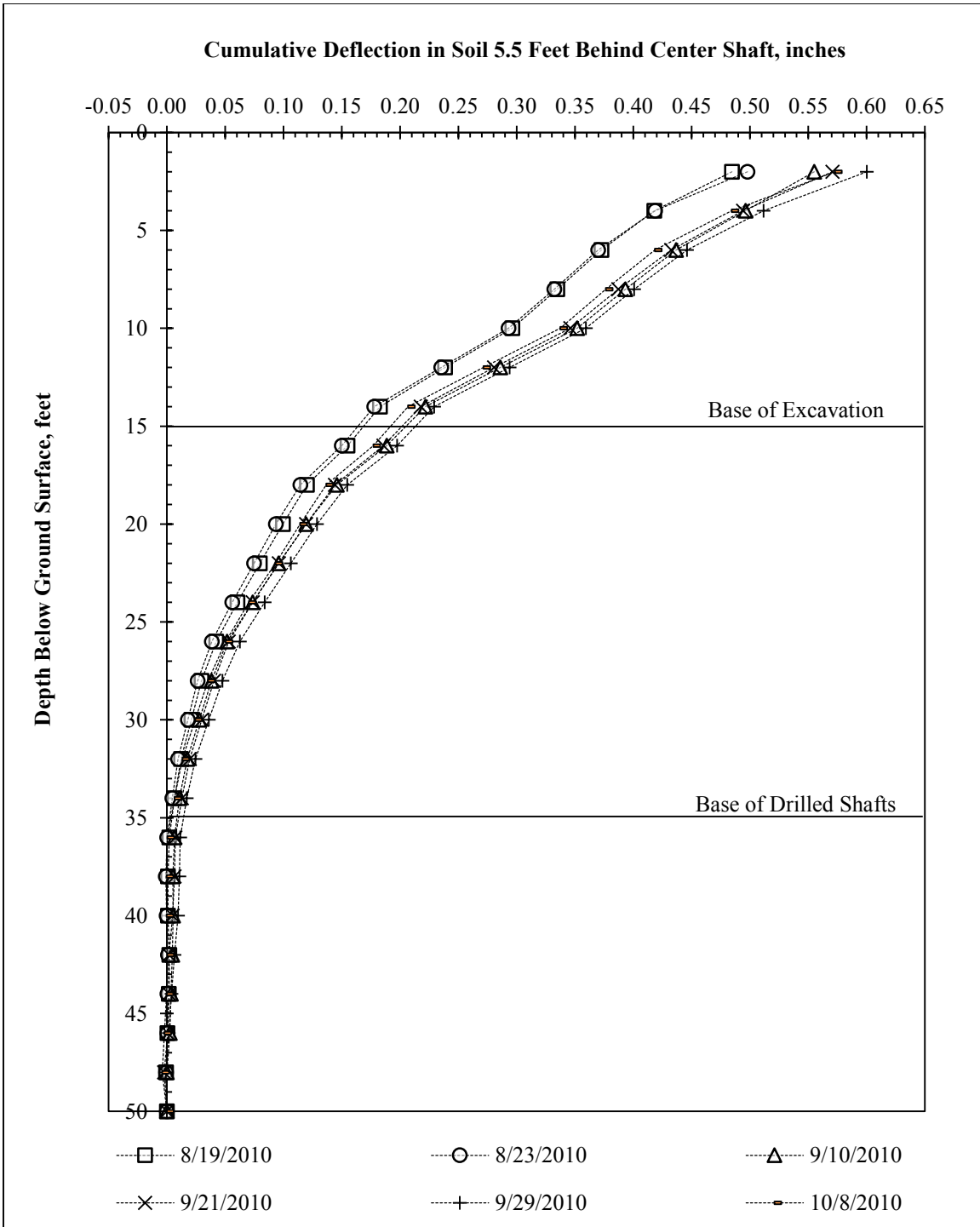


Figure 5.8: Cumulative deflections recorded in inclinometer installed through the soil 5.5 feet behind the center instrumented shaft.

### 5.2.2: LINEAR POTENTIOMETER DATA

A linear potentiometer was installed prior to excavation. It was attached to shaft #16, adjacent to the west instrumented shaft (shaft #15). It provides continuous data on top-of-wall deflection and redundancy with the inclinometer data. Linear potentiometer data during the first month of excavation, along with top-of-wall deflections for the three instrumented shafts, is provided in Figure 5.9.

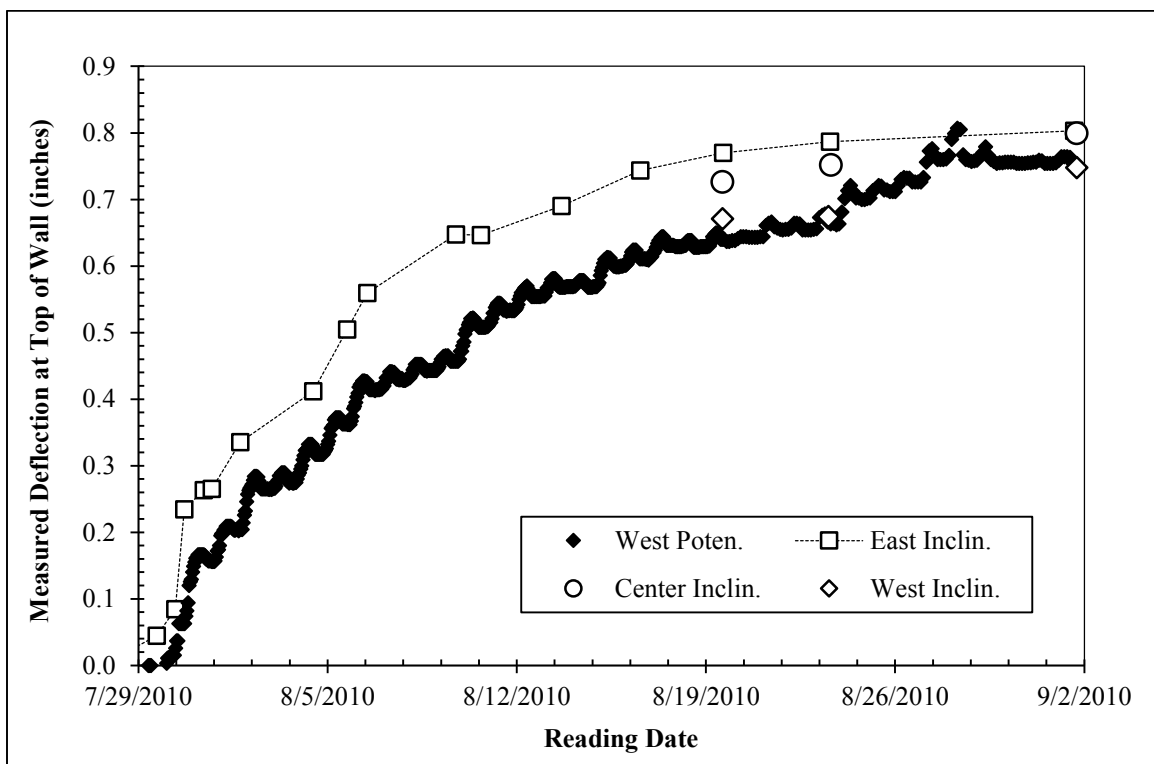


Figure 5.9: Deflection measured at top of wall during excavation. Excavation began on July 29 and continued through August 27.

### 5.2.3: STRAIN GAUGE DATA

Throughout the excavation progress, strain gauges were monitored in the three instrumented shafts. Strain data is presented in Figure 5.10 - Figure 5.24. In the following figures, strain data is zeroed on July 27, 2010.

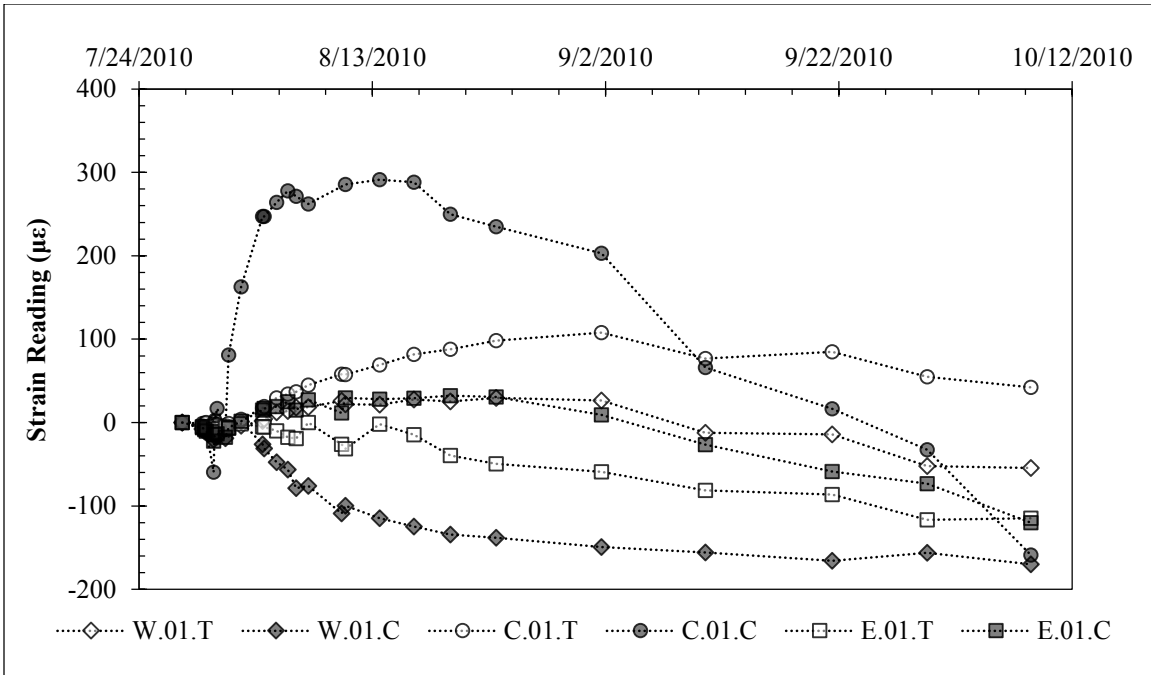


Figure 5.10: Strain Data 1 Foot Below Ground Surface During Excavation.

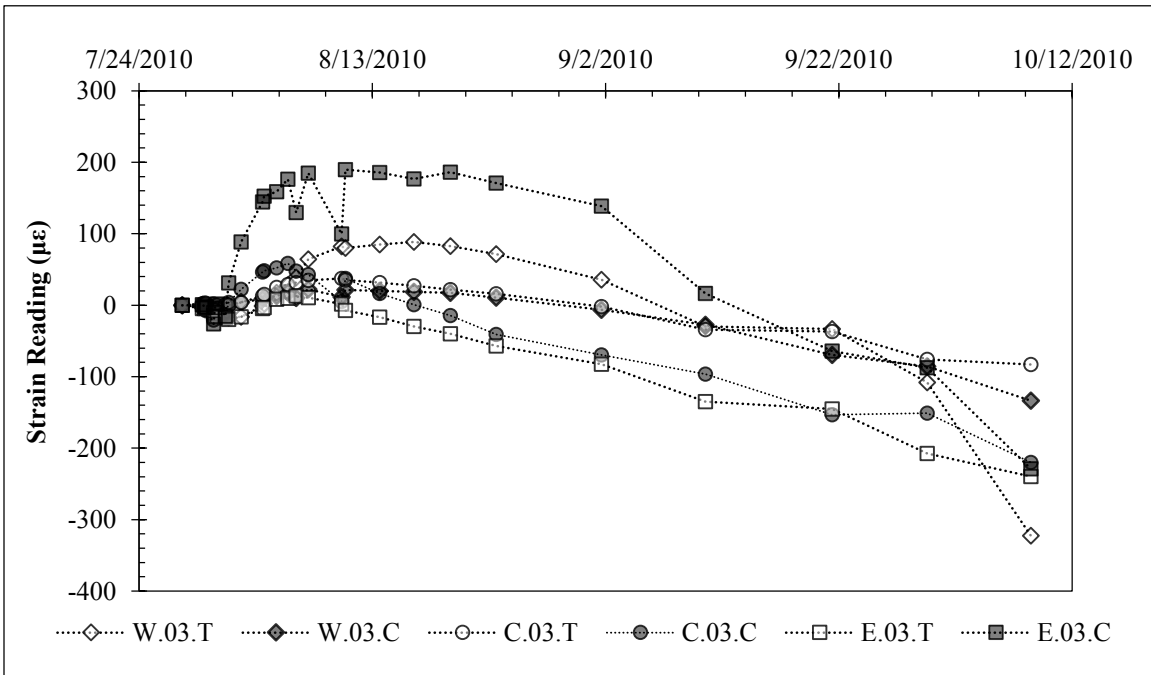


Figure 5.11: Strain Data 3 Feet Below Ground Surface During Excavation.

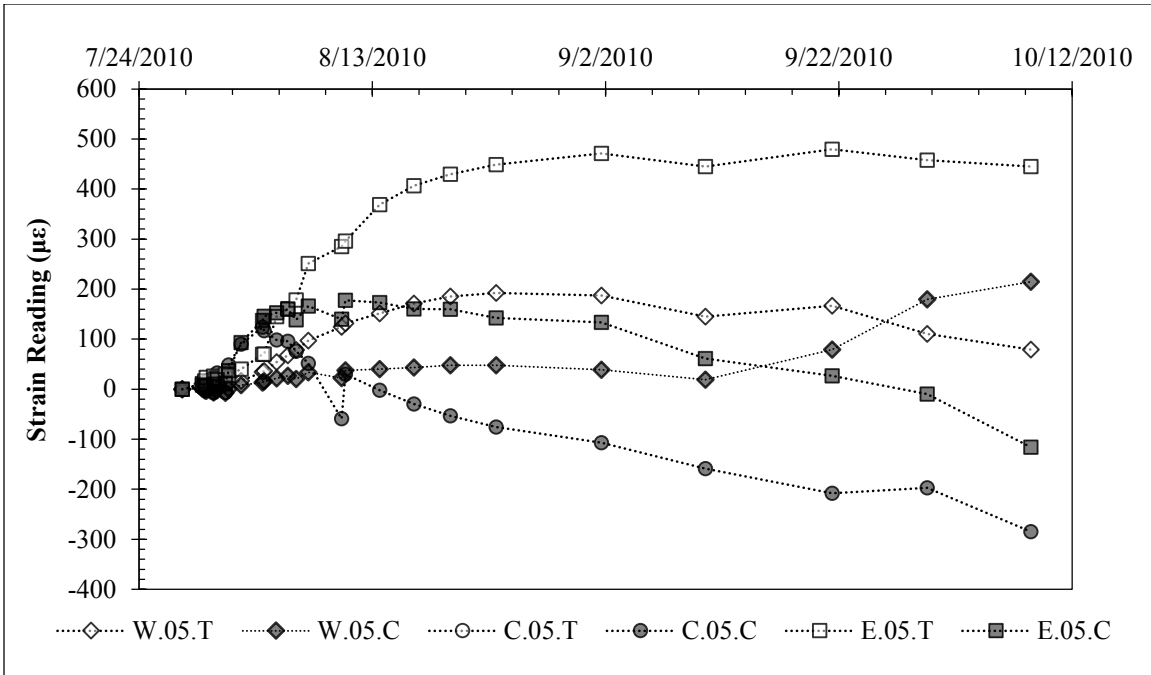


Figure 5.12: Strain Data 5 Feet Below Ground Surface During Excavation.

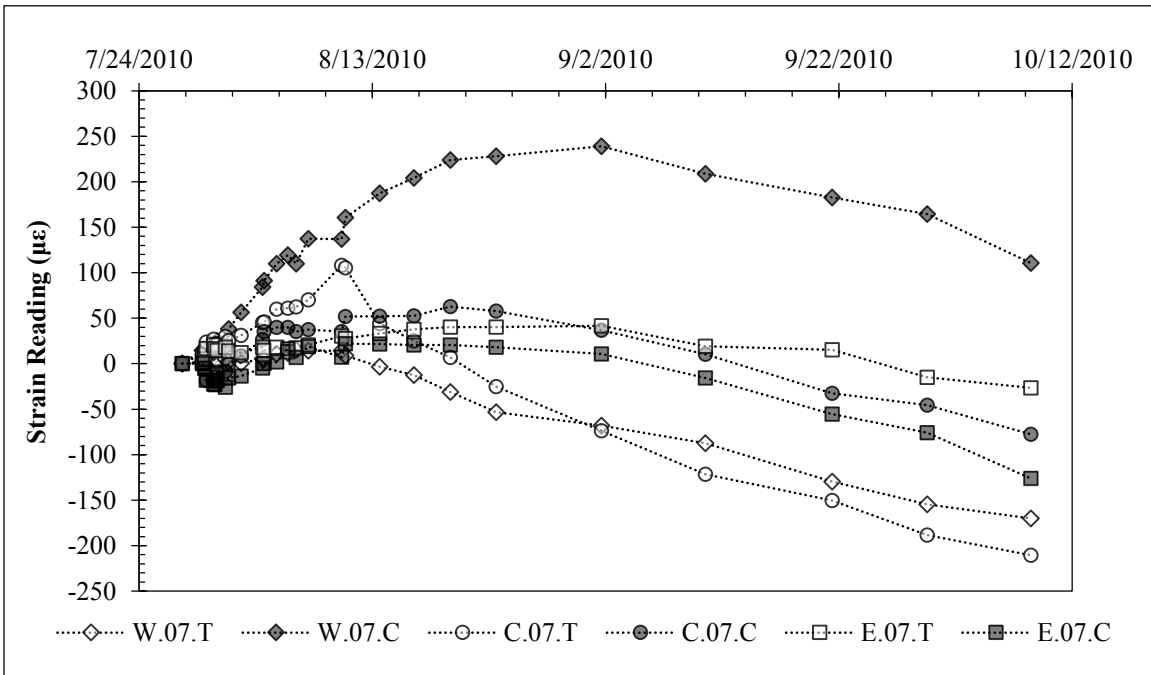


Figure 5.13: Strain Data 7 Feet Below Ground Surface During Excavation.

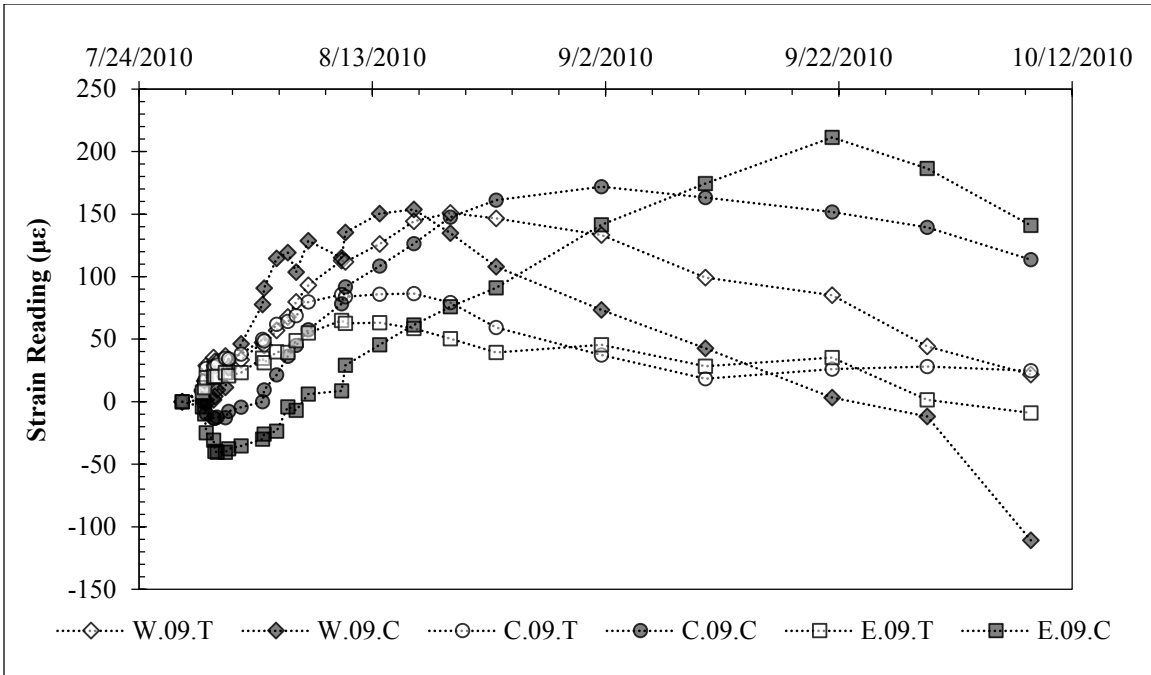


Figure 5.14: Strain Data 9 Feet Below Ground Surface During Excavation.

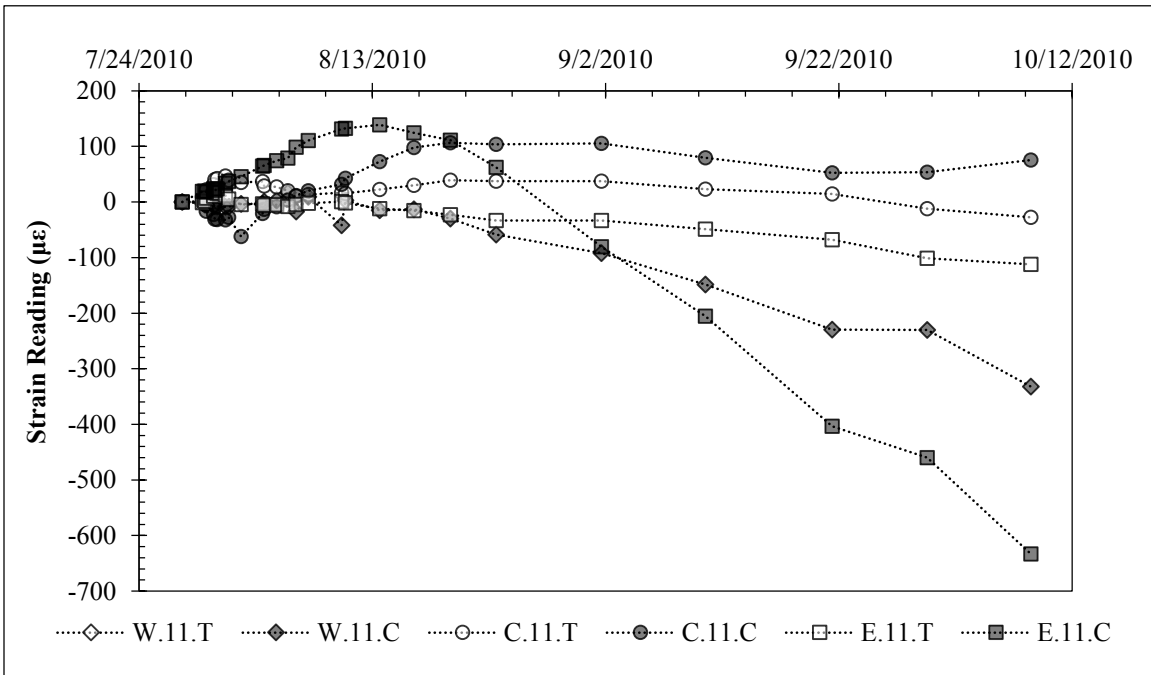


Figure 5.15: Strain Data 11 Feet Below Ground Surface During Excavation.

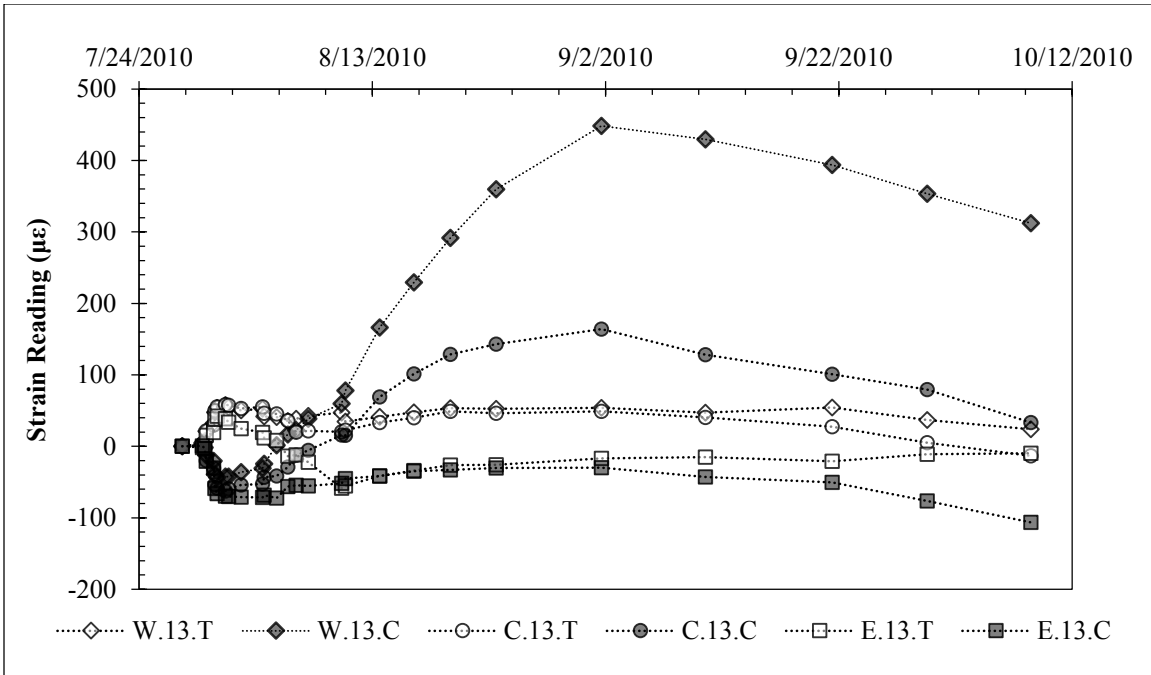


Figure 5.16: Strain Data 13 Feet Below Ground Surface During Excavation.

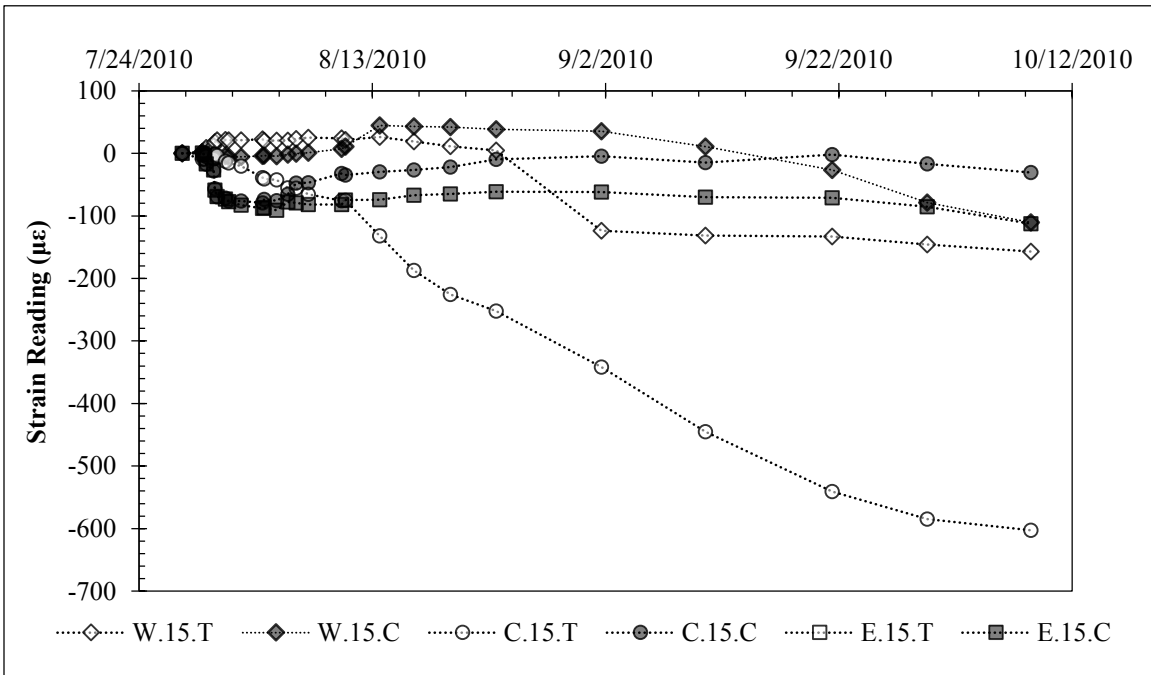


Figure 5.17: Strain Data 15 Feet Below Ground Surface During Excavation.

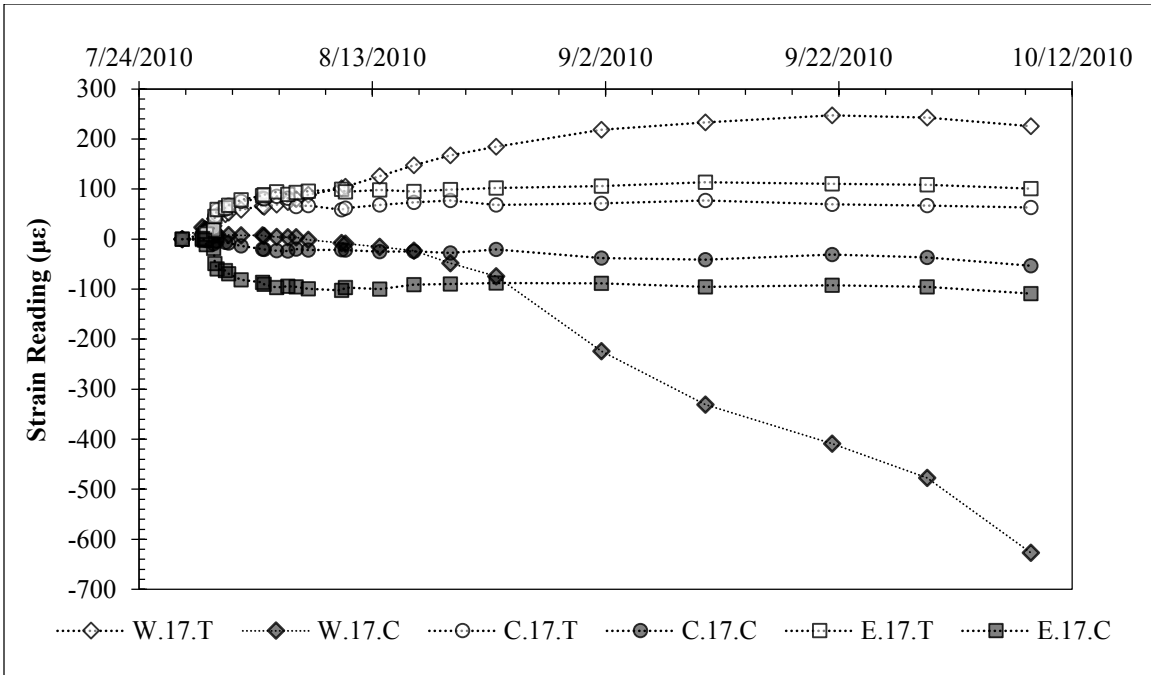


Figure 5.18: Strain Data 17 Feet Below Ground Surface During Excavation.

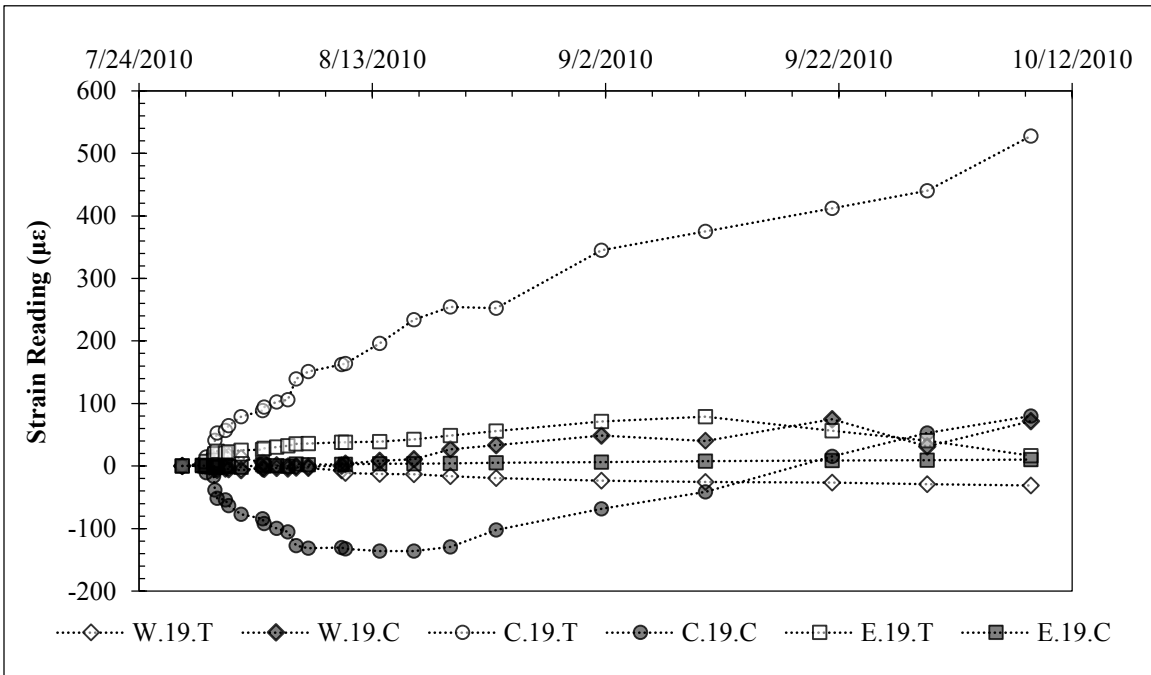


Figure 5.19: Strain Data 19 Feet Below Ground Surface During Excavation.

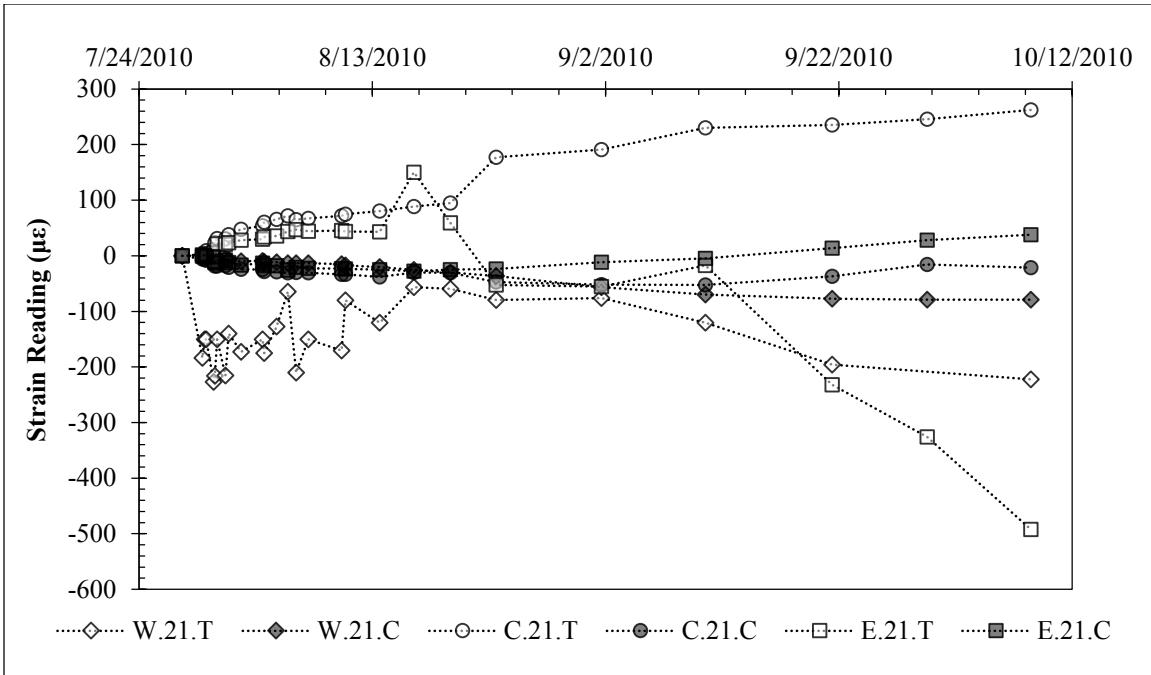


Figure 5.20: Strain Data 21 Feet Below Ground Surface During Excavation.

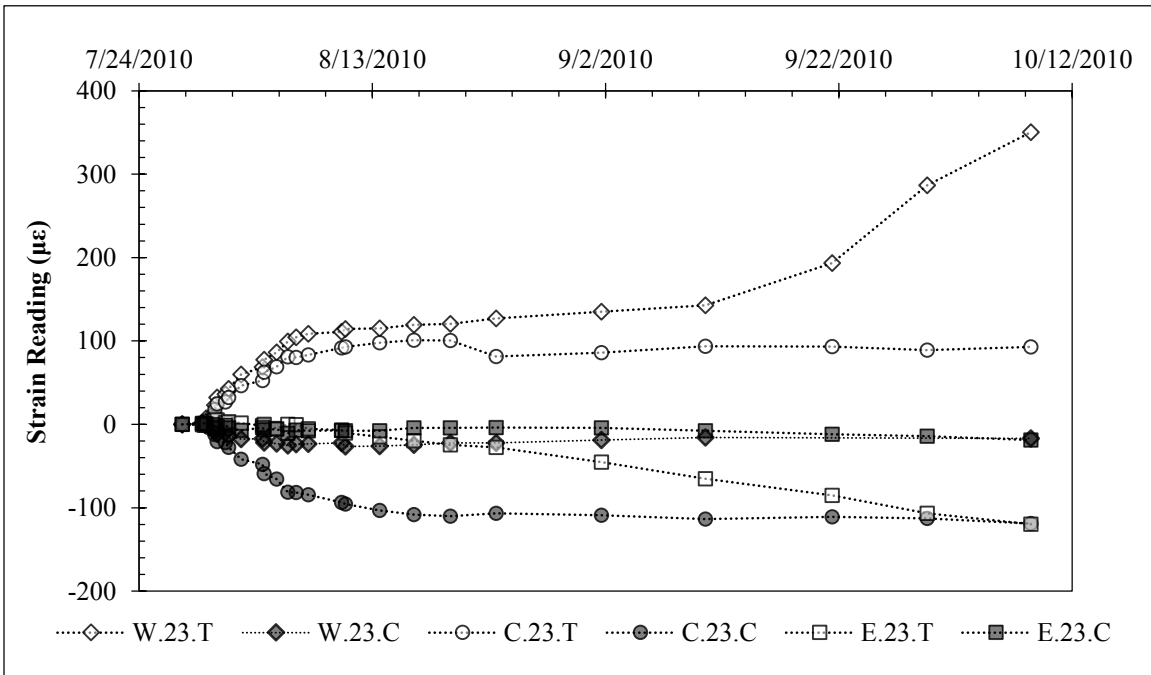


Figure 5.21: Strain Data 23 Feet Below Ground Surface During Excavation.



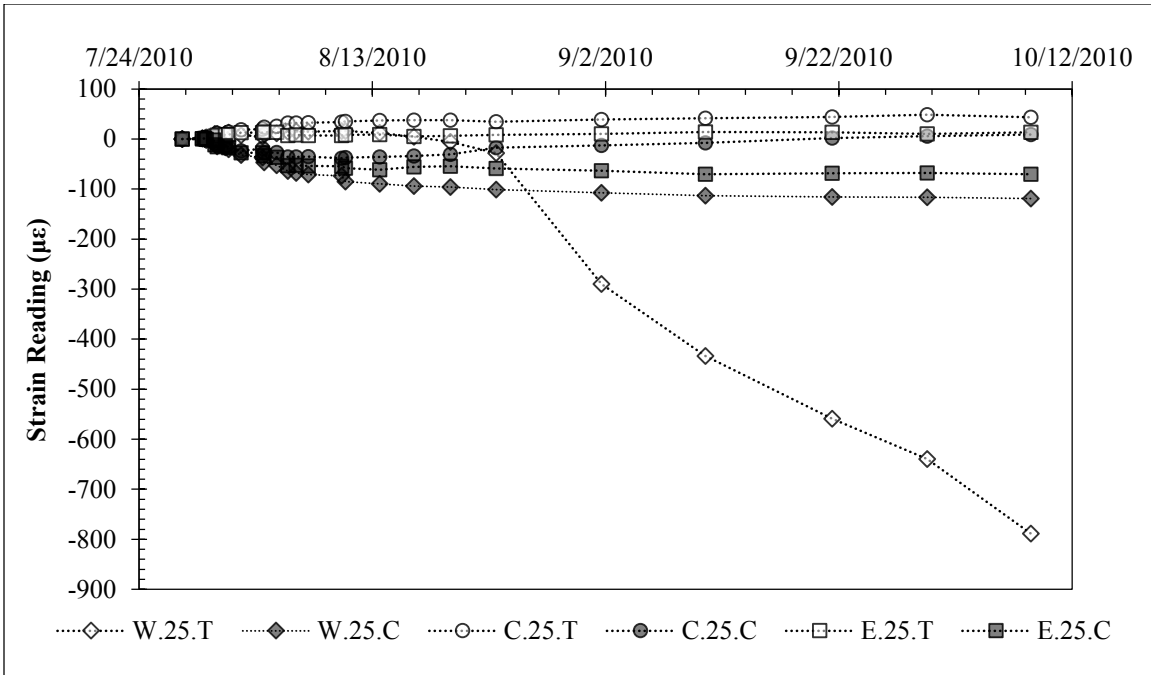


Figure 5.22: Strain Data 25 Feet Below Ground Surface During Excavation.

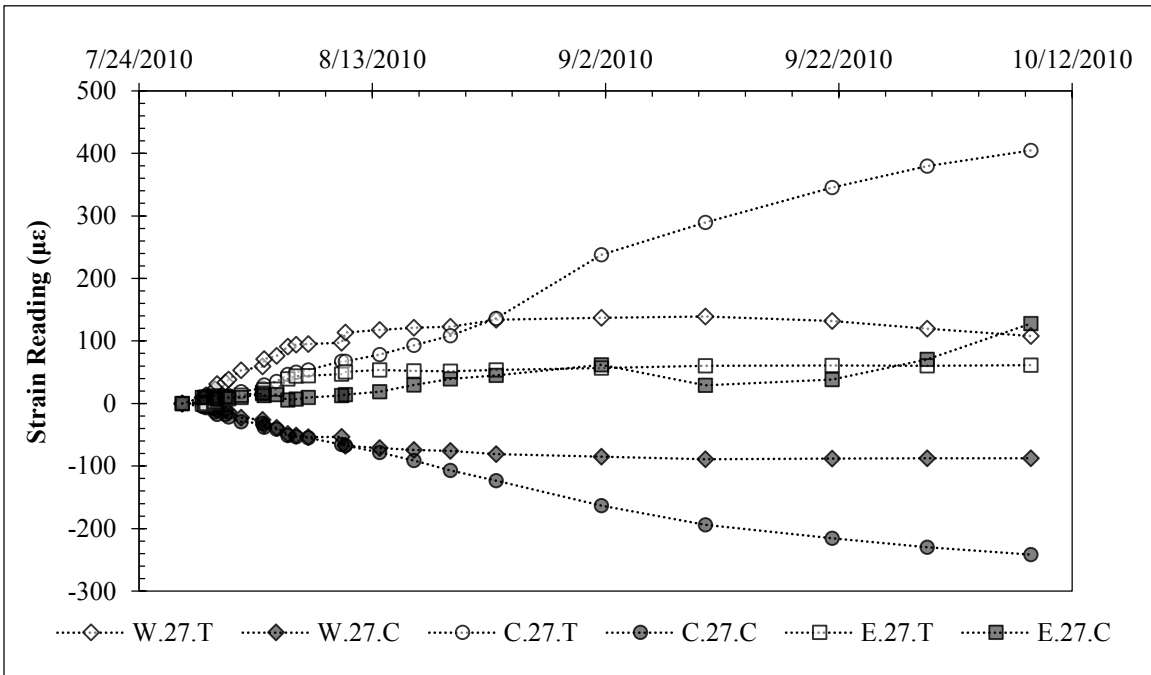


Figure 5.23: Strain Data 27 Feet Below Ground Surface During Excavation.

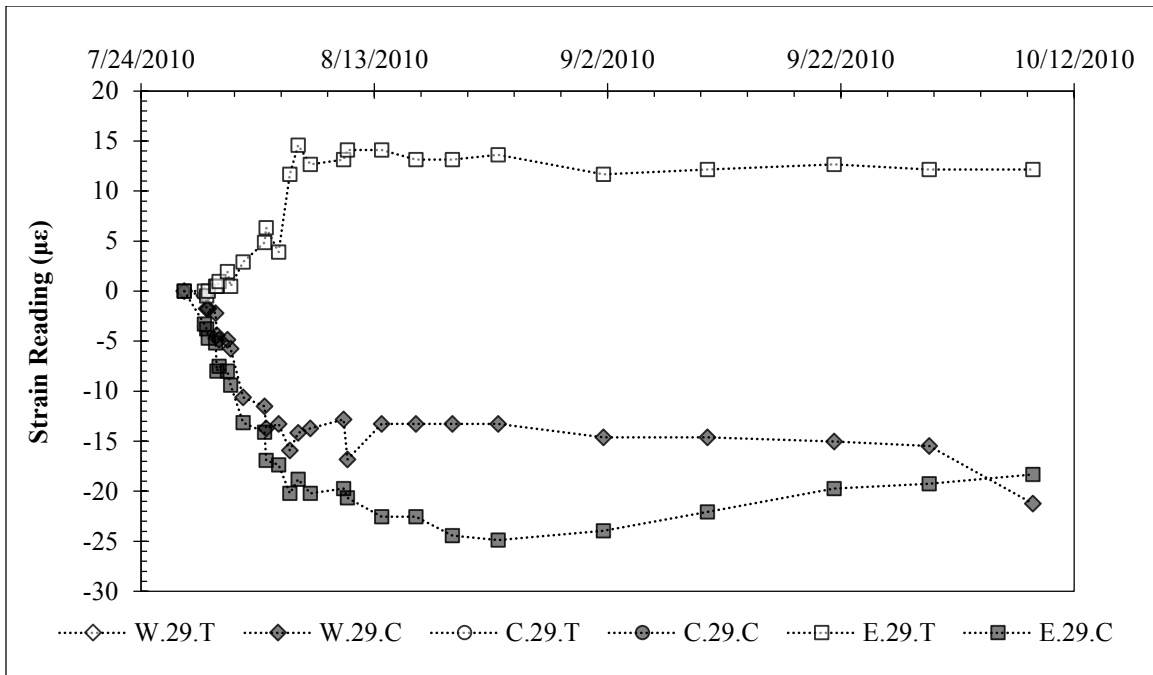


Figure 5.24: Strain Data 29 Feet Below Ground Surface During Excavation.

### 5.3: Data Interpretation

#### 5.3.1: IMMEDIATE RESPONSE TO STRESS RELIEF

During excavation, the wall responded almost immediately to the relief of stress. The deflection at the top of the wall, measured directly with a linear potentiometer and in three inclinometers, is shown on Figure 5.9. The top-of-wall deflections developed more quickly on the east versus the west side because a larger volume of soil was initially removed from the east side (Figure 5.25). The final excavation dimensions at the centerline of the wall were, on average, reasonably close to the design values (Figure 5.26). The final deflections immediately after the excavation was completed were similar between the three shafts (Figure 5.9).

Between depths of 20 and 30 feet below the original ground surface (5 to 15 feet below the cantilever), the shafts developed a bending moment. Figure 5.27 shows axial

strains from a pair of strain gauges on either side of the shaft's neutral axis at the approximate location of the maximum bending moment. The strains are nearly equal and opposite, and their development is qualitatively similar to the increase in deflection with time at the top of the wall (Figure 5.9).

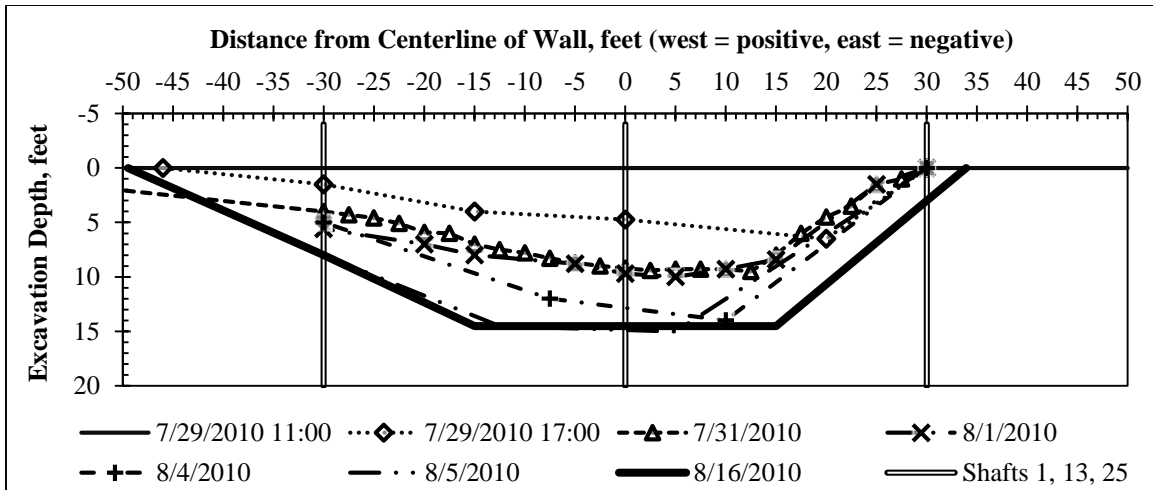


Figure 5.25: Progression of excavation depth along wall face.

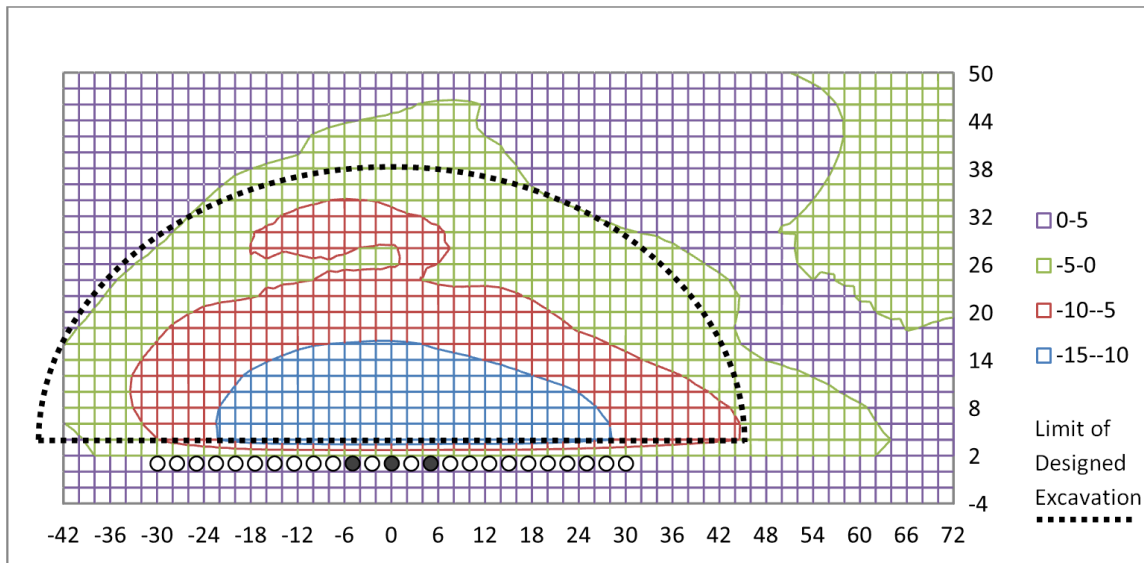


Figure 5.26: Contour plot of final surveyed excavation dimensions (all units in feet).

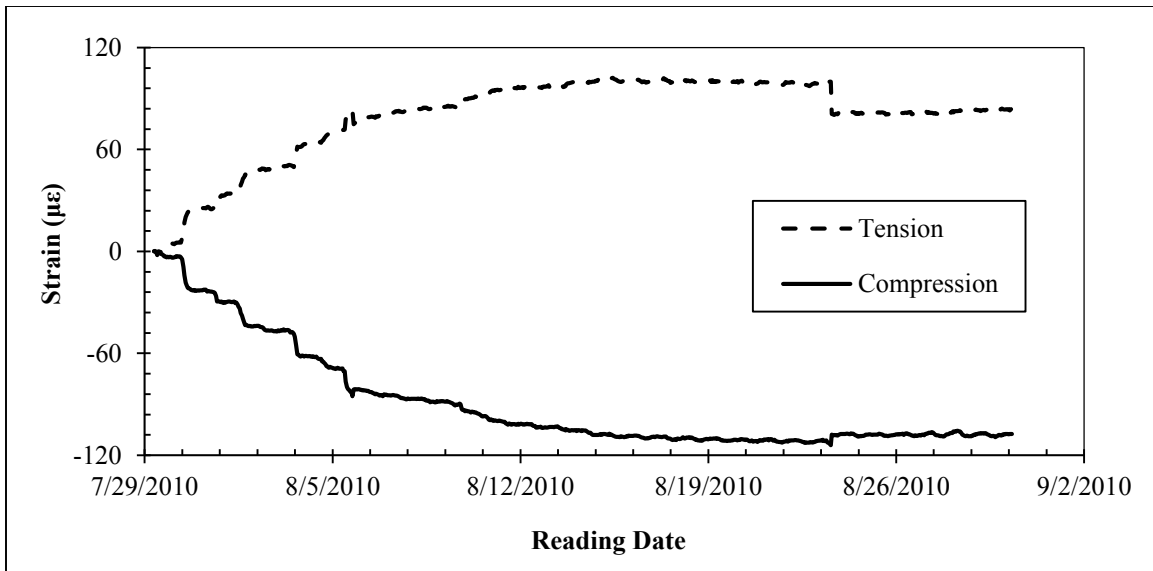


Figure 5.27: Development of bending strains in a pair of strain gauges located 23 feet below ground surface in the center shaft.

### 5.3.2: STRAIN GAUGE BEHAVIOR

#### 5.3.2.a: Thermal Strains

As concrete was exposed to temperature changes during excavation, gauges on the exposed side of the wall began to register strains consistent with daily temperature fluctuations (Figure 5.28). Additionally, the average daily strain value increased as the shafts were exposed to the high ambient temperatures encountered during excavation. At a depth of 1 foot below ground surface, predicted bending moments are relatively small; the majority of the measured strains at shallow depths appear to be related to temperature increases, rather than increases in bending curvature caused by earth pressure loading. When strain gauge data are compared with daily temperature data, the strain gauges on the exposed side of the test wall register approximately 7 to 8 microstrains per degree Fahrenheit. Thermal strains will be analyzed in more detail in subsequent chapters.

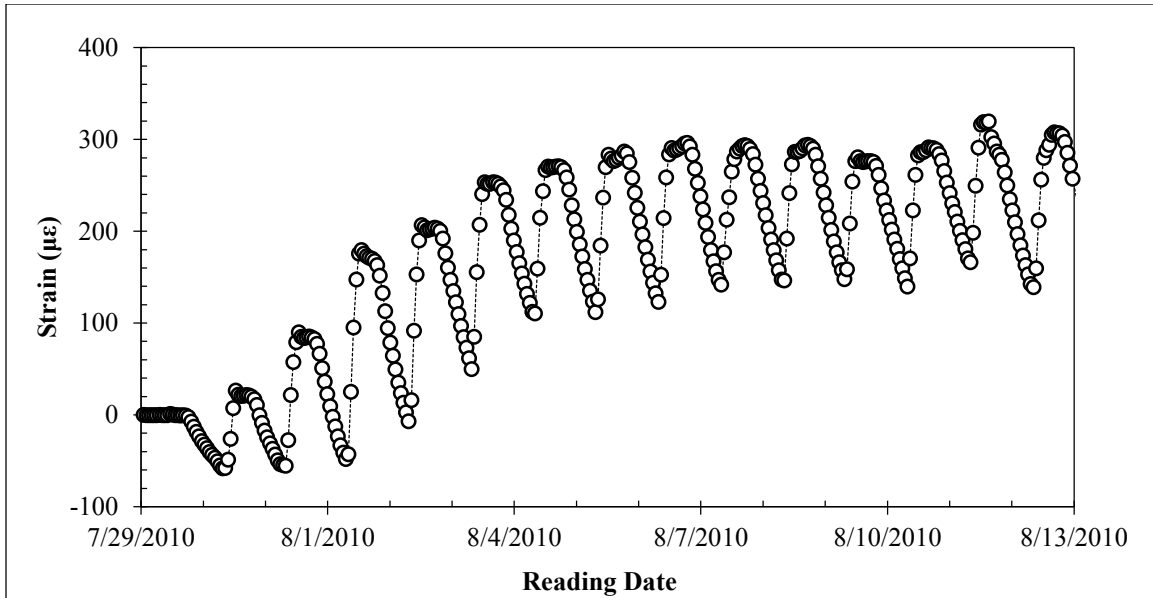


Figure 5.28: Strains related to temperature changes in exposed concrete. Gauge located 1 foot below ground surface on exposed side of wall. Soil at gauge location was excavated on July 29-31.

### 5.3.2.b: Gauges Above Excavation Line (1-13 feet below ground surface)

As a group, the strain gauges above the excavation line exhibited a response consistent with other data. Every functional gauge showed a response within days of the start of excavation. In general, this response was marked by a combination of bending curvature (tension gauge shows positive strain; compressive gauge shows a similar negative strain) and thermal strains. Some gauges (e.g. C.01.C, W.07.C) exhibited signs of tension cracking, despite being under primarily compressive loads. Additionally, some other pairs of gauges (e.g. C.03.T / C.03.C and E.07.T / E.07.C) exhibited signs of axial strains while maintaining a constant bending curvature. Effects such as these could be an indication of residual stresses developed prior to excavation influencing gauge response during excavation.

### **5.3.2.c: Gauges Below Excavation Line (15-29 feet below ground surface)**

Below the excavation line, where predicted bending moments were higher and the concrete was not exposed by removal of soil, gauges showed more pronounced bending strains and minimal thermal effects. Some pairs of gauges (e.g. E.17.T / E.17.C and C.23.T / C.23.C) showed bending strains which are very close to ideal behavior for the observed deflection profile; these ideal gauges can be used to monitor relatively small changes in bending moment at those depths over time. Other pairs of gauges (e.g. C.19.T / C.19.C) maintained a consistent bending strain, but display axial strains that steadily increased in a tensile direction. Similar to the shallow gauges, some peculiar gauge behavior was observed, such as gauges steadily moving toward unusually large compressive strains (e.g. C.15.T, W.17.C, W.25.T), or large tensile strains in gauges that should be under compression (e.g. W.13.C). It is likely that unusual gauge behavior such as this was a result of residual stresses, tension cracking, or simply damage to the gauge. The deepest pair of functional gauges (E.29.T / E.29.C) displayed a small but measurable bending curvature which is consistent with estimates from inclinometer data.

### **5.3.3: DESIGN PREDICTIONS VERSUS OBSERVED BEHAVIOR**

At the conclusion of excavation, the measured top-of-wall deflections were consistent with the initial design analysis predicted by a p-y analysis using a triangular earth pressure distribution of 40 psf per foot of depth (the current standard of practice in Texas). The input parameters for this analysis are summarized in Table 5.1: Baseline assumptions and design parameters for short-term LPILE analysis.. However, while the predicted and measured top-of-wall deflections are similar, the deflected shapes show significant differences (Figure 5.29).

Table 5.1: Baseline assumptions and design parameters for short-term LPILE analysis.

<b>Parameter</b>	<b>Value</b>
Total Unit Weight of Soil, $\gamma_t$	125 pcf
Equivalent Fluid Pressure Loading, $\gamma_{EF}$	40 psf/ft
Coefficient of Active Earth Pressure, $k_a$	0.31 (from $\gamma_{EF} / \gamma_t$ )
Undrained Shear Strength, $S_U$	3,200 psf
Foundation Soil p-y Curves	Stiff Clay Without Free Water
Cracking Moment, $M_{Cr}$	680 k-in.
Yielding Moment, $M_y$	3,200 k-in.
Uncracked Bending Stiffness, $EI_{uc}$	$67 \times 10^6$ k-in.
Cracked Bending Stiffness, $EI_{cr}$	$18 \times 10^6$ k-in.
Soil Strength Reduction Due to Clear Spacing	0.5
Shaft Diameter	24 in.
Height of Retained Soil, H	180 in.
Reinforcement	12 #7 bars (1.6% of gross area)

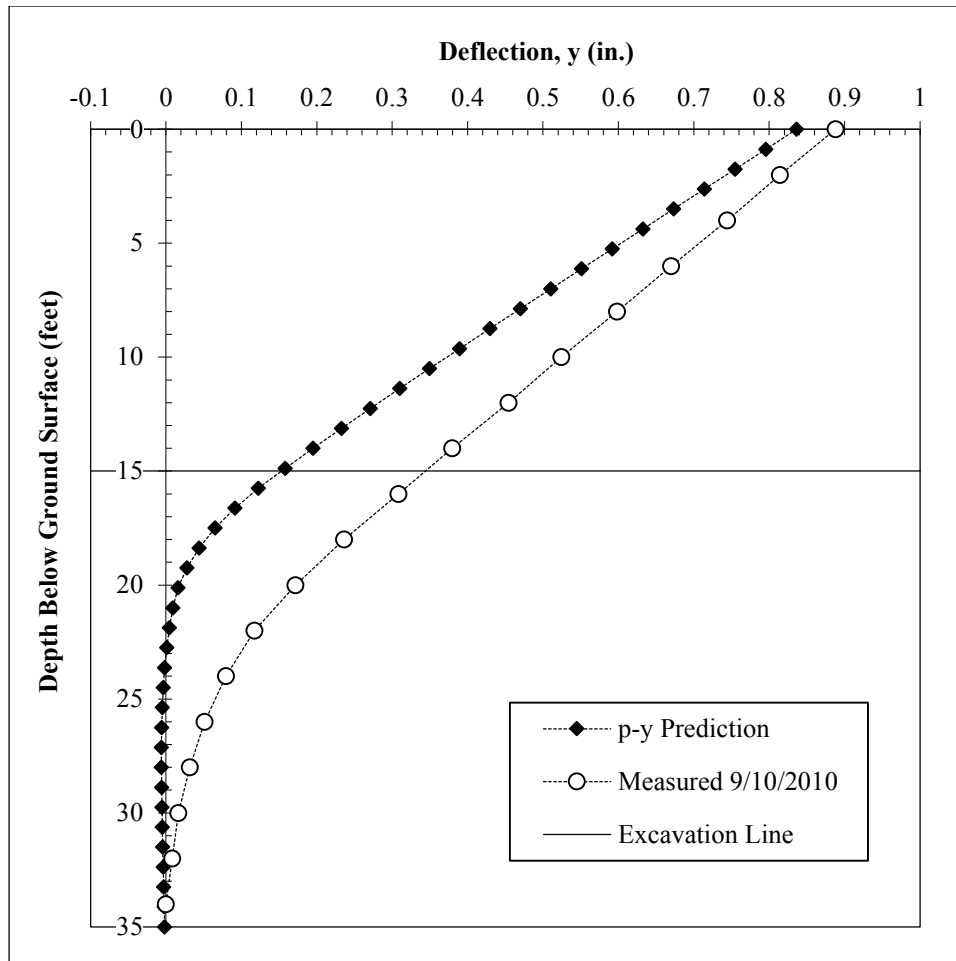


Figure 5.29: Comparison of p-y prediction with measured field data. P-y analysis used a triangular earth pressure distribution of 40 psf/ft.

Further examination of the field inclinometer data indicates that a significant amount of shaft base rotation occurred during excavation (Figure 5.30). This contrasts with the typical p-y formulation, in which the shaft base remains fixed and the shaft behavior is governed by an external load.



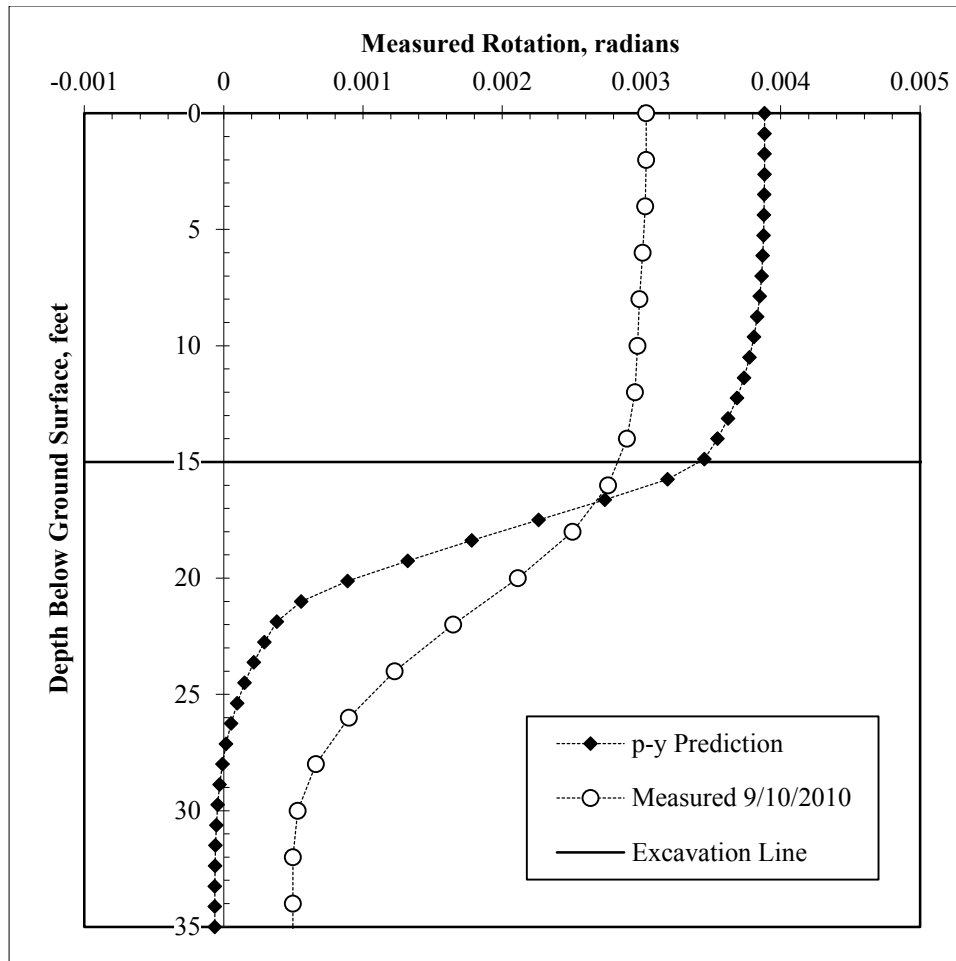


Figure 5.30: Comparison of predicted and measured shaft rotation profiles induced by removal of soil during excavation.

Because a significant amount of the measured top-of-wall deflection is the result of global soil/shaft movement and shaft base rotation, neither of which directly stress the shaft, the observed bending moments in the test wall are lower than those predicted by the p-y formulation (Figure 5.31). In a typical p-y formulation, where the deflection and rotation at the shaft base are taken to be zero, every increase in shaft deflection is accompanied by a corresponding increase in stress within the shaft. In the test wall, however, the presence of base rotation and global soil/shaft movement allows the shaft to

accommodate movements in other ways besides an increase in bending moment. As a result, our measured maximum bending moments are approximately 50% of the predicted value at a top-of-wall deflection of 0.9 inches (Figure 5.31). While deflection requirements often govern design and performance considerations, it is important to note that for a given top-of-wall deflection in our test wall, there may be more remaining bending moment capacity than a traditional p-y analysis would suggest.

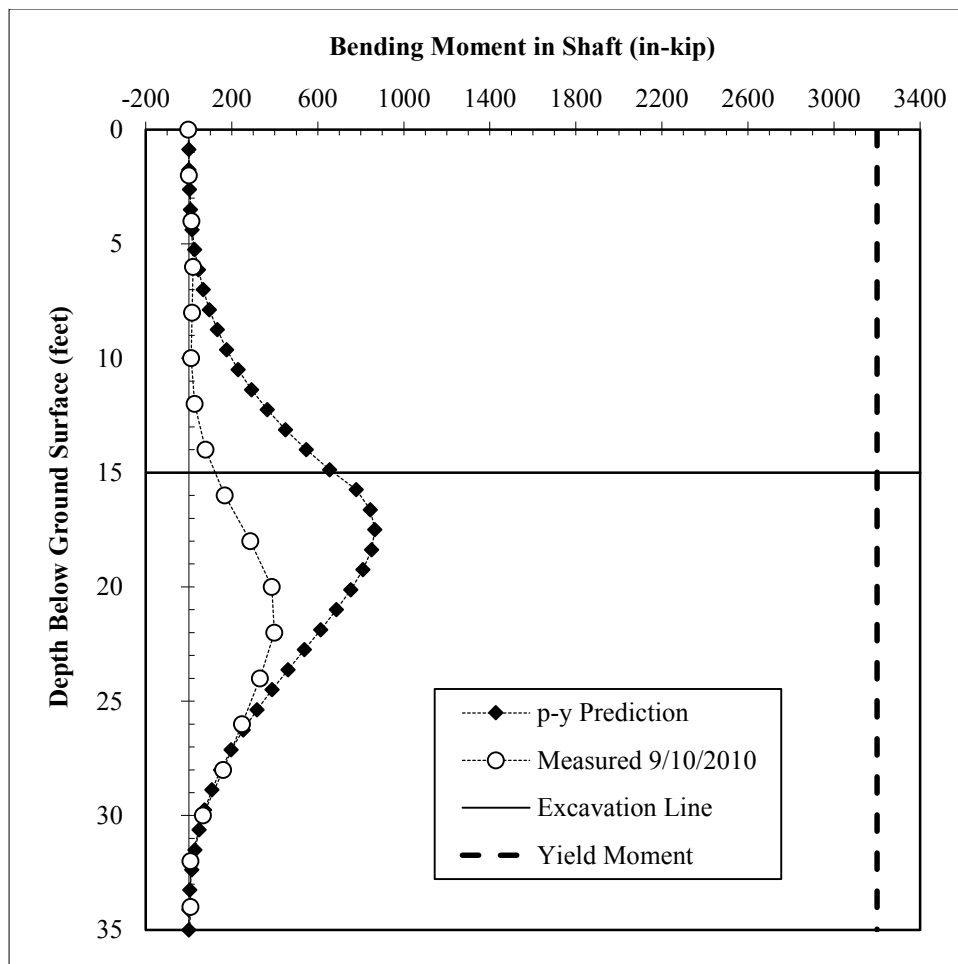


Figure 5.31: Comparison of predicted and measured bending moment profiles induced by removal of soil during excavation.

#### **5.3.4: FINITE ELEMENT MODEL**

It is possible that the differences between measured and predicted data are primarily due to global movements of the shaft/soil system in response to stress relief during excavation. To illustrate this concept, a simple linear elastic finite element model was used to represent the process of soil removal during excavation. In this model, the removal of excavated soil initiated a global response that extended well beyond the shaft base (Figure 5.32 - Figure 5.33). The quality of these global motions is consistent with the observed data, and with some adjustment of model soil parameters, the finite element model is consistent with the measured field inclinometer data (Figure 5.34).

The finite element model, although it is tremendously oversimplified, may provide some insight into the nature of soil response during excavation. In a sensitivity analysis, using commonly reported values of  $K_o$  for overconsolidated clays in Texas ( $K_o = 2$  to  $3$ ), to achieve a deflected shape similar to the field measurement, average values of  $E/S_u$  were between 100 and 500 (Figure 5.34). The soil stiffness suggested by the finite element model is softer than our measured stiffness data from Spectral Analysis of Surface Waves (SASW) testing on the project site (Figure 5.35 – Figure 5.36) and the commonly used  $E/S_u$  value of 1000 for stiff clays, but is consistent with our stiffness data from UU testing and the general observation that stiff-fissured clays experience significant stiffness reductions during and after unloading (e.g. Cripps and Taylor, 1981).

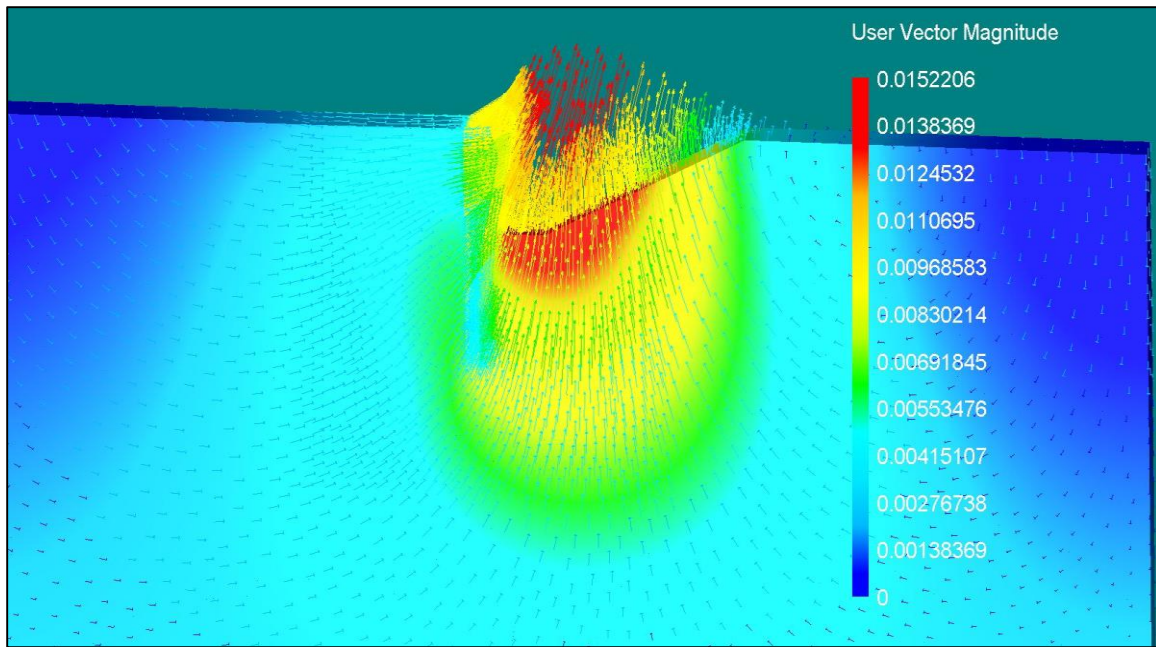


Figure 5.32: Global response to removal of soil in linear elastic FEM.

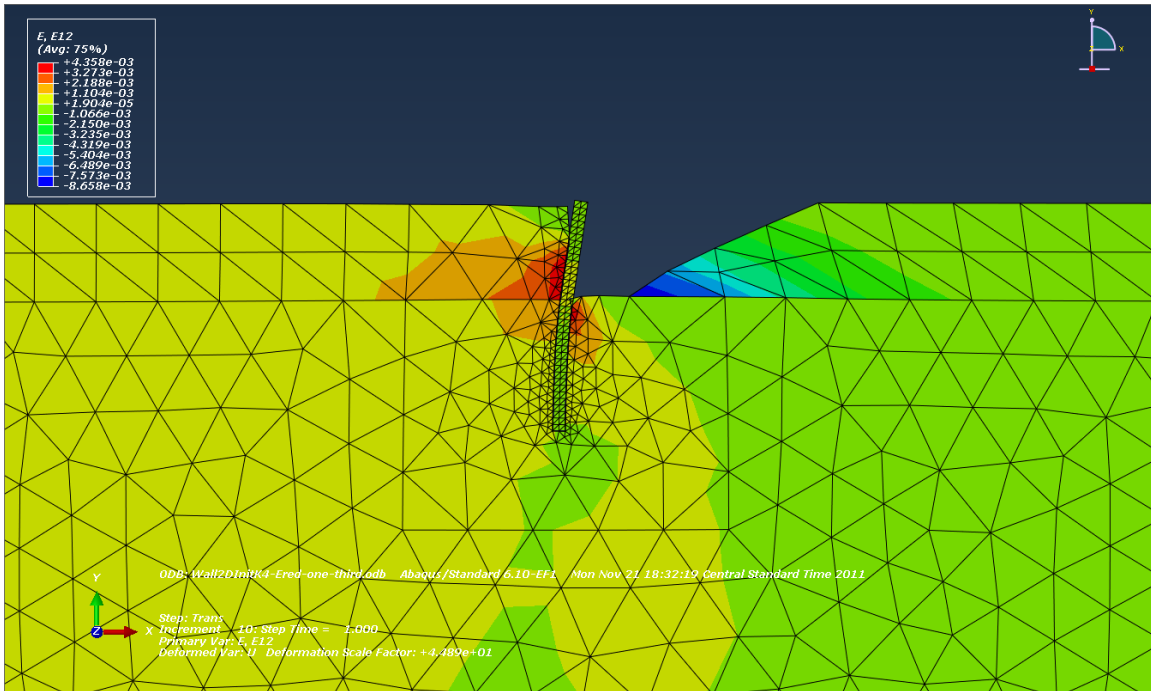


Figure 5.33: Global shear strains in response to removal of soil in linear elastic FEM.

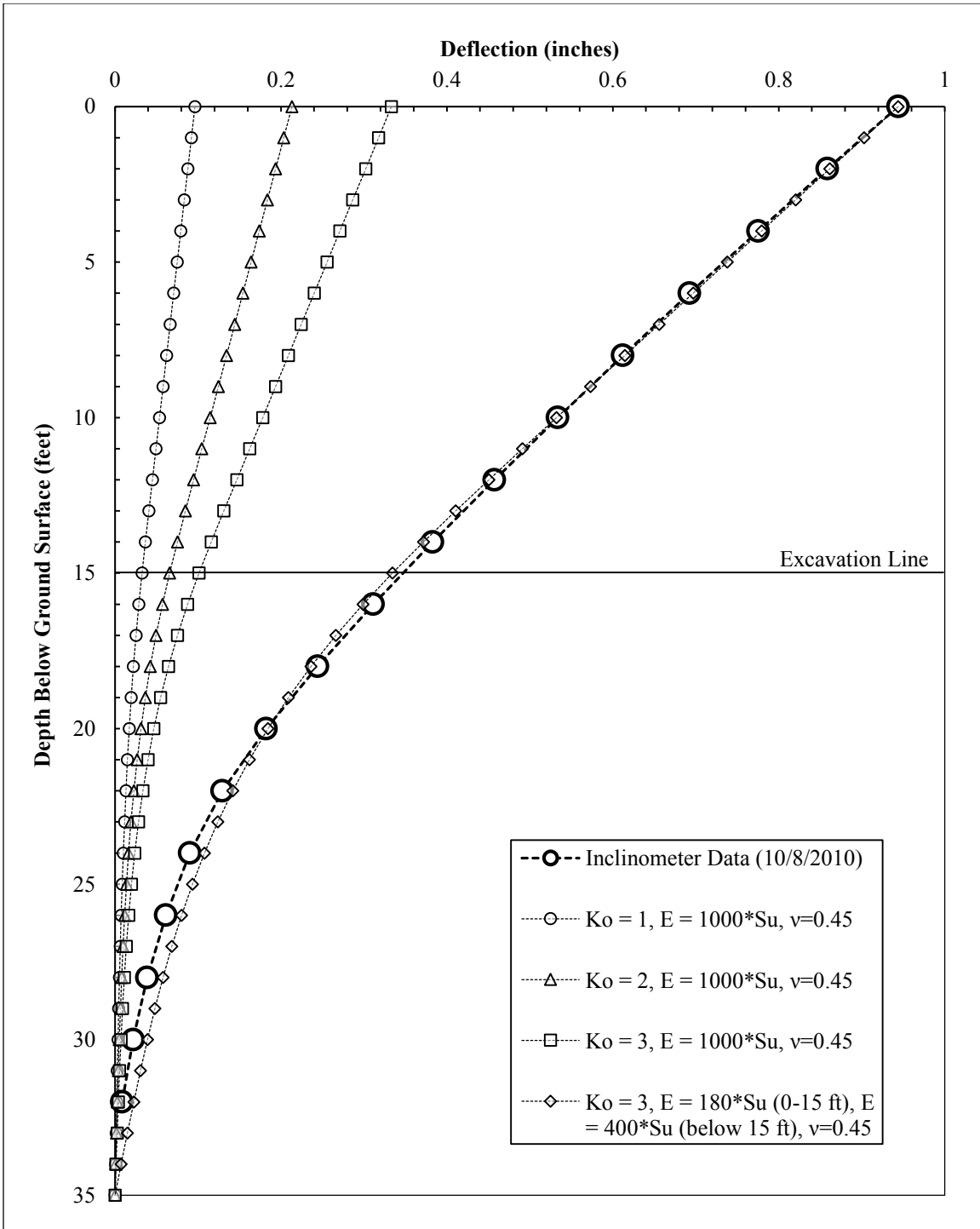


Figure 5.34: Comparison of linear elastic finite element model predictions with measured field data.



Figure 5.35: SASW testing at the test wall prior to excavation, June 2010.

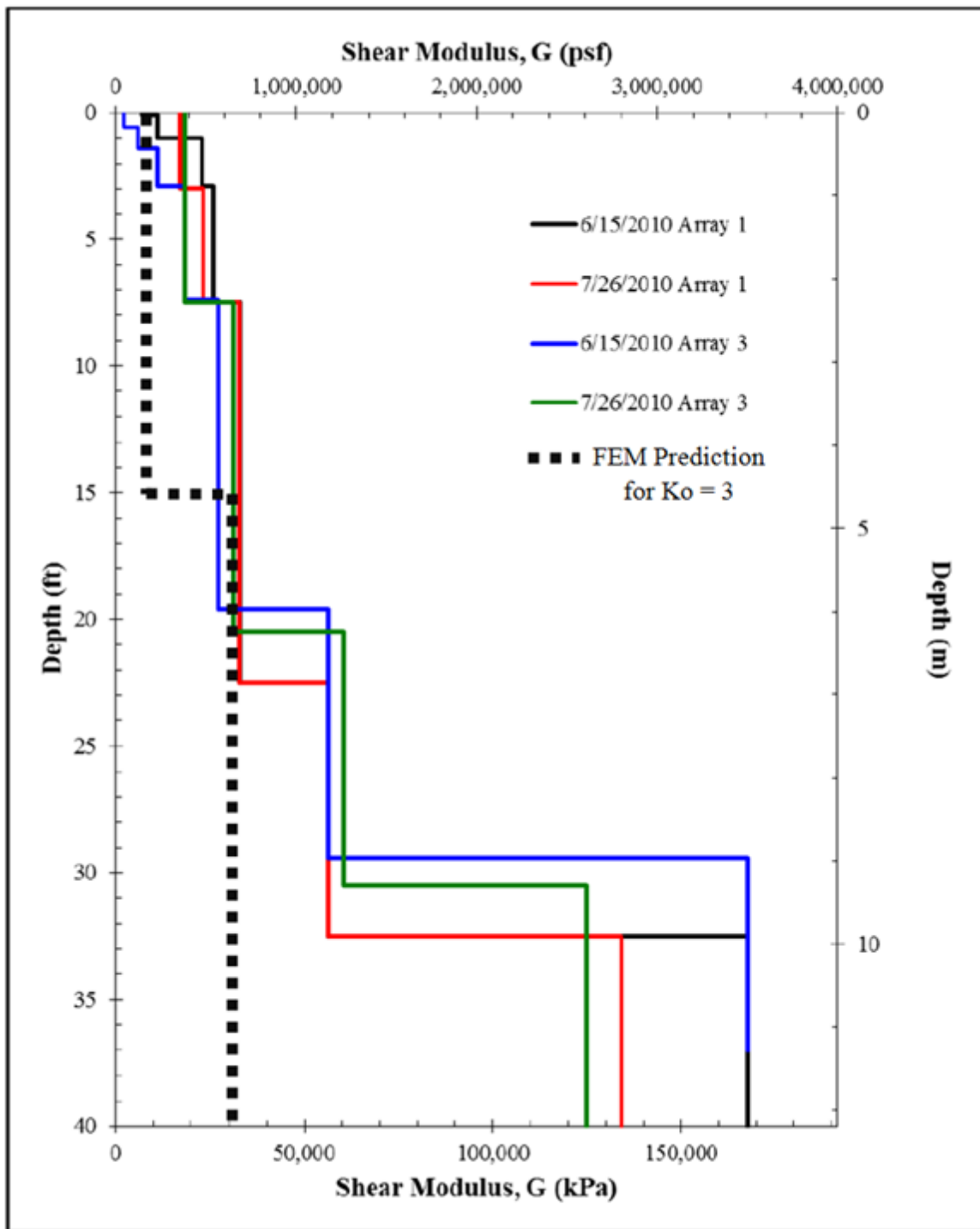


Figure 5.36: Comparison of measured shear modulus profiles from SASW testing with finite element model prediction (after Ellis, 2011).

### **5.3.5: MODIFIED LPILE ANALYSIS**

#### **5.3.5.a: Selection of Loading Conditions and p-y Curves**

Based on the results of the finite element model and differentiation of the bending moment curves estimated from field data, a modified LPILE analysis was conducted. To minimize the effects of thermal deformations on data interpretation, the survey taken on September 10, 2010 is used for analysis. Additional discussion of thermal deformations is provided in the next chapter. Estimated values of bending moment and soil resistance are presented in Figure 5.37. The input earth pressure envelope for the LPILE analysis was defined using the calculated earth pressures from Figure 5.37 at depths of 0 to 14 feet. To simulate the effects of small thermal bending curvatures on wall movement, a bending moment of 40 in-kip was applied at the top of the shaft to provide consistency with the measured bending moment diagram above the excavation line (the development of this process is discussed in Chapter 6). A “thermal moment” of 40 in-kip is consistent with a small positive bending curvature due to the front of the wall being cooler than the back of the wall (it is important to note, however, that thermal curvatures do not directly stress the wall). The excavation depth was set at 14 feet for consistency with the as-built measurements of the excavation.

The p-y curves calculated from the field inclinometer data are compared with representative curves at depths between 16 and 22 feet below the original ground surface in Figure 5.38 to Figure 5.43. Of the proposed curves surveyed, the curves based on drained, fully softened strength parameters ( $\phi = 24$ ) with effective weights and non-default values of initial stiffness ( $k_{py} = 375 \text{ lb/in}^3$ ) provide a reasonable approximation of the foundation soil response. Based on the heavily fissured structure of the soil, the presence of stress relief due to unloading, and the softer-than-expected soil response, it is possible that the stiff-fissured clay in the base of the excavation has already reached drained



conditions. In the subsequent LPILE analysis during excavation, drained, fully softened curves with non-default initial stiffness values are used to model the foundation soil behavior. A summary of input parameters for the modified LPILE analysis is provided in Table 5.2.

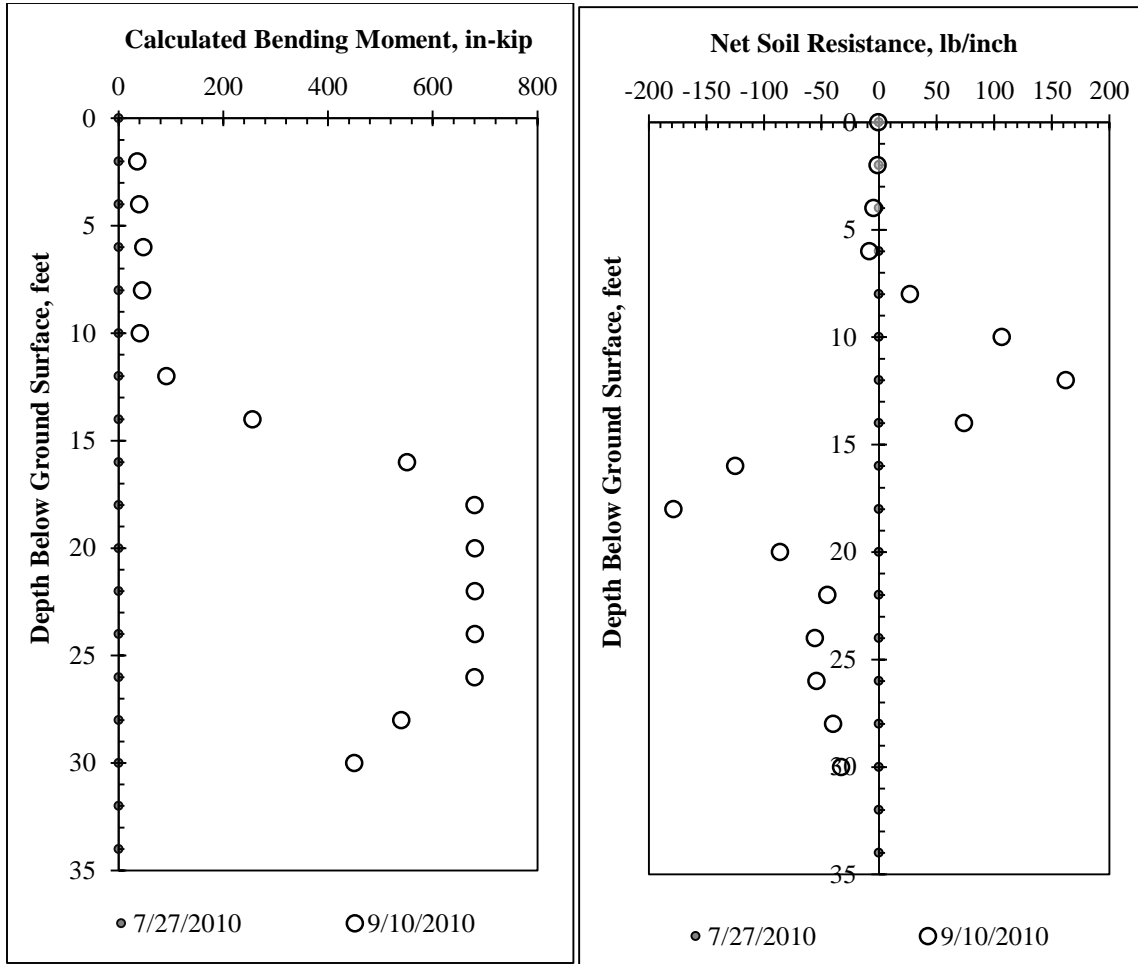


Figure 5.37: Calculated values of bending moment and net soil resistance during excavation, based on measured rotation profiles from inclinometer data.

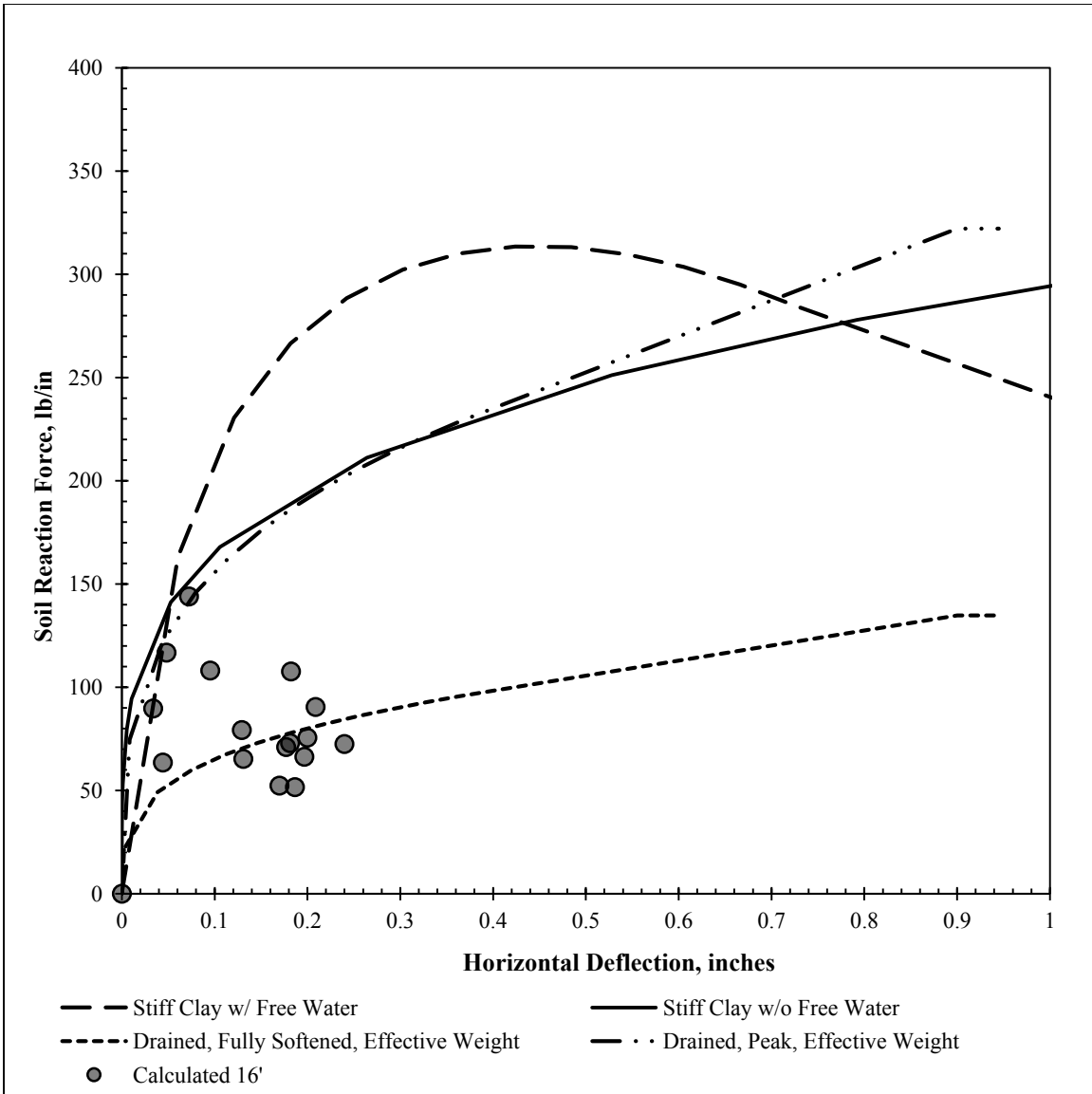


Figure 5.38: Comparison of calculated p-y curves during excavation with proposed p-y curves at a depth of 16 feet below original ground surface.

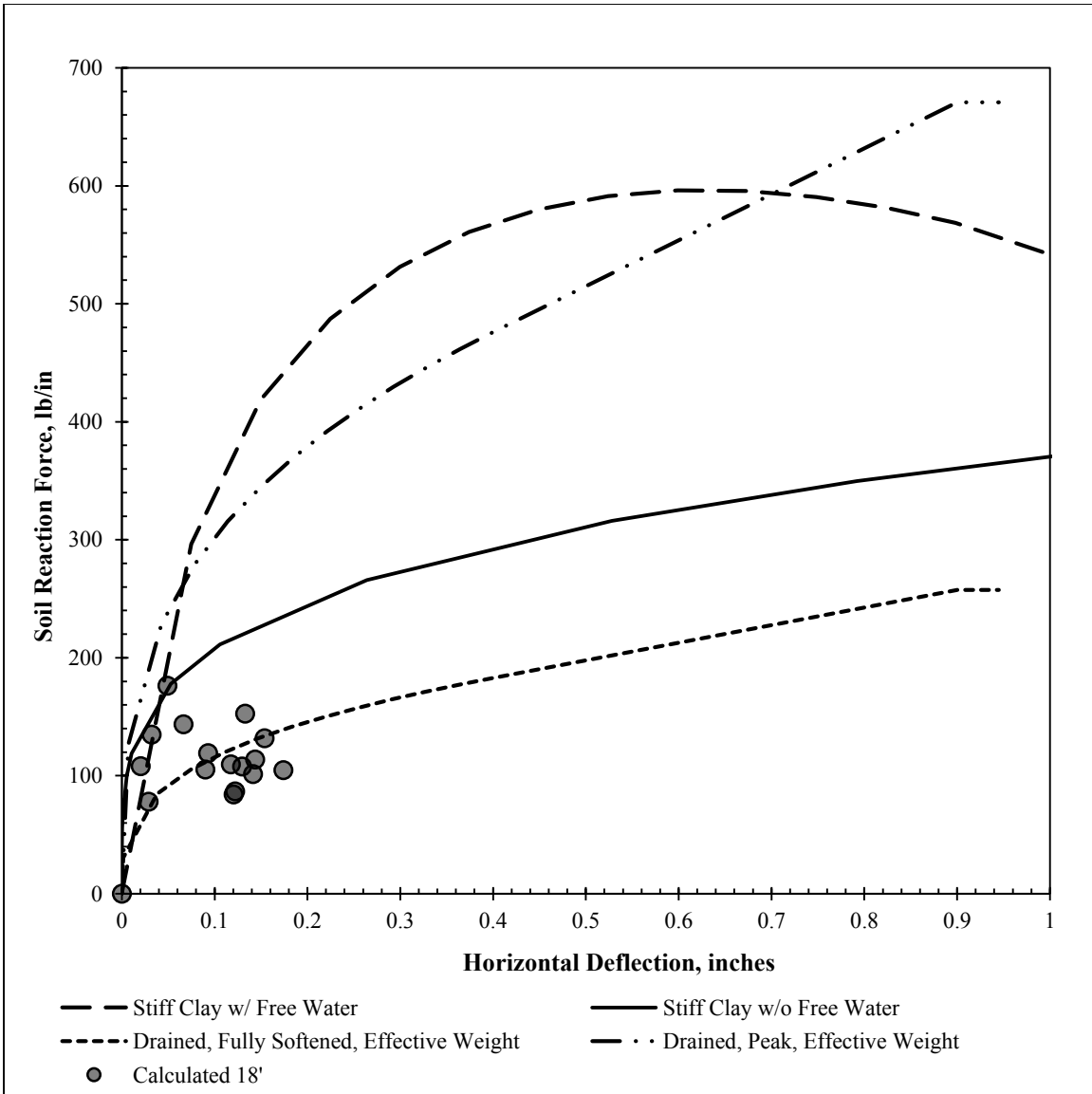


Figure 5.39: Comparison of calculated p-y curves during excavation with proposed p-y curves at a depth of 18 feet below original ground surface.

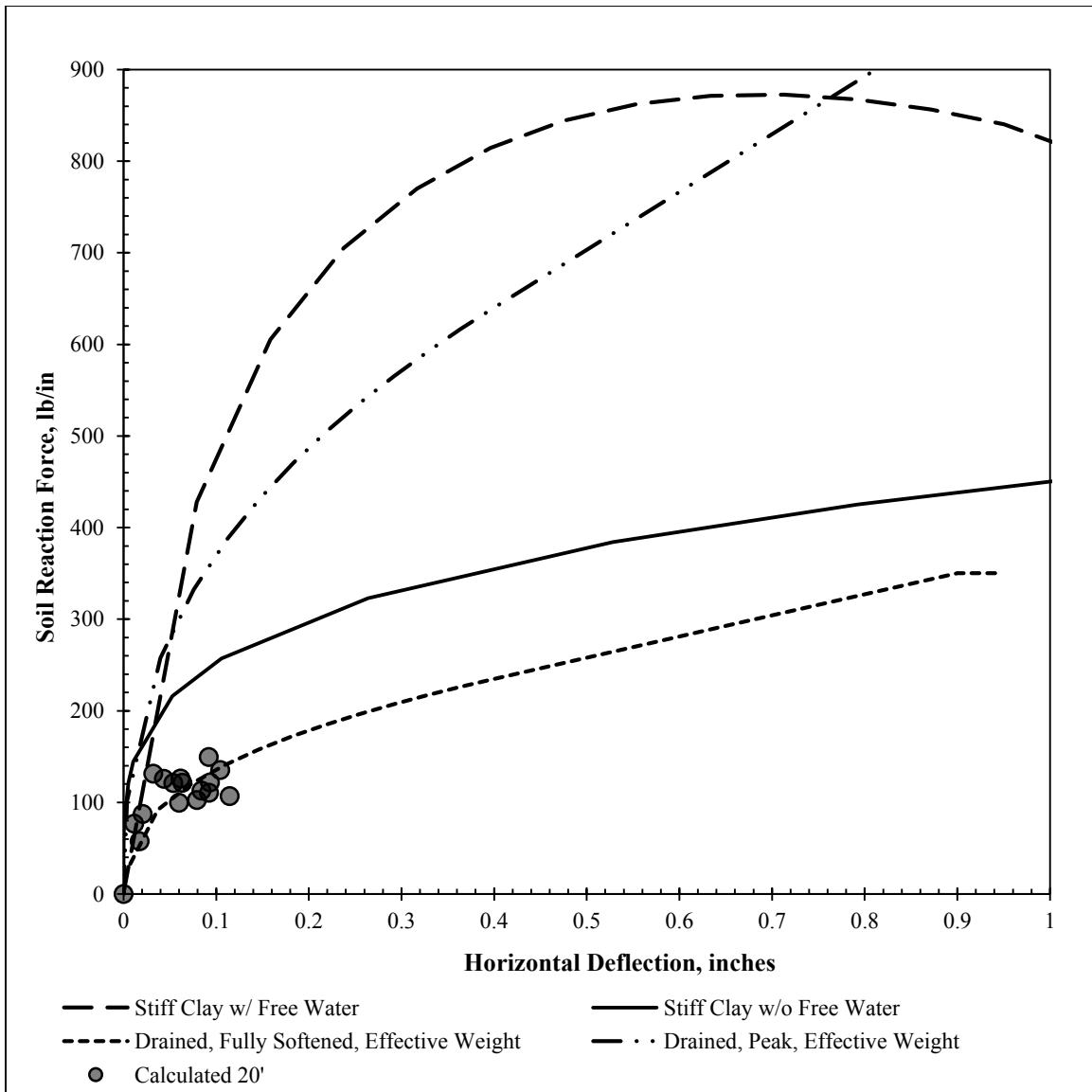


Figure 5.40: Comparison of calculated p-y curves during excavation with proposed p-y curves at a depth of 20 feet below original ground surface.

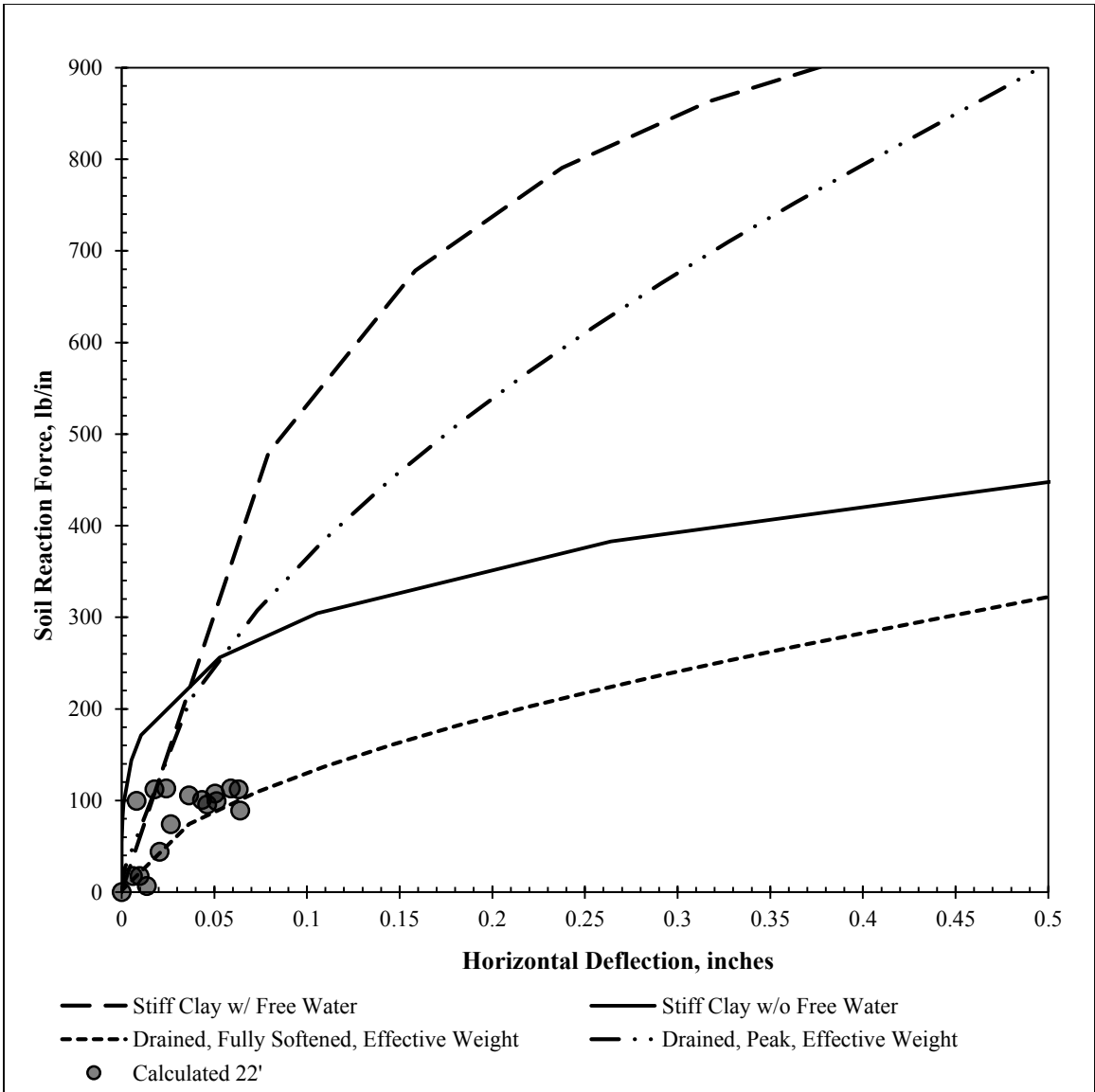


Figure 5.41: Comparison of calculated p-y curves during excavation with proposed p-y curves at a depth of 22 feet below original ground surface.

Table 5.2: Baseline assumptions and design parameters for modified LPILE analysis.

Parameter	Value
Effective Unit Weight of Soil, $\gamma$	62.6 pcf
Earth Pressure Loading	Input Envelope from Calculated $p_{net}$
Additional Moment Applied at Top for Thermal Effects	40 k-in
Friction Angle of Foundation Soil	24 degrees
Foundation Soil p-y Curves	Sand (Reese)
Non-Default Initial Stiffness, $k_{py}$	375 lb/in <sup>3</sup>
Cracking Moment, $M_{Cr}$	680 k-in.
Yielding Moment, $M_y$	3,200 k-in.
Uncracked Bending Stiffness, $EI_{uc}$	$67 \times 10^6$ k-in.
Cracked Bending Stiffness, $EI_{cr}$	$18 \times 10^6$ k-in.
Shaft Diameter	24 in.
Height of Retained Soil, H	168 in.
Reinforcement	12 #7 bars (1.6% of gross area)

### 5.3.5.b: Results of Modified LPILE Analysis

Based on the results of the modified LPILE analysis, measured values of bending moments (Figure 5.42) and soil reaction forces (Figure 5.43) are slightly larger than those predicted by LPILE. The use of fully softened strengths for p-y curves may influence this discrepancy, as the field behavior of the soil has likely not degraded to fully softened conditions over the entire shaft depth. The consistency in bending moments, earth pressures, and soil reaction forces between the measured values and the LPILE analysis suggests that the loading conditions on the pile have been modeled reasonably well; despite this, the measured and predicted deflection profiles show considerable differences (Figure

5.42). This is likely due to global movements of the soil-shaft system similar to those predicted by the FEM.

By subtracting the measured deflection profile from the profile predicted by LPILE under similar loading conditions, a profile of global soil movements can be estimated. The results of this analysis are presented in Figure 5.44. The profile of global horizontal soil movement with depth can be nearly bounded between two straight lines corresponding to top-of-wall deflections of 0.10 and 0.15 percent of the wall height, extending to zero at the shaft base (Figure 5.44). The influence of horizontal deflection becomes slightly less pronounced near the shaft base, further from the stress relief of the excavation. Based on the results of this analysis, global movements of the soil-shaft system may account for approximately 30% of the measured top-of-wall deflection.

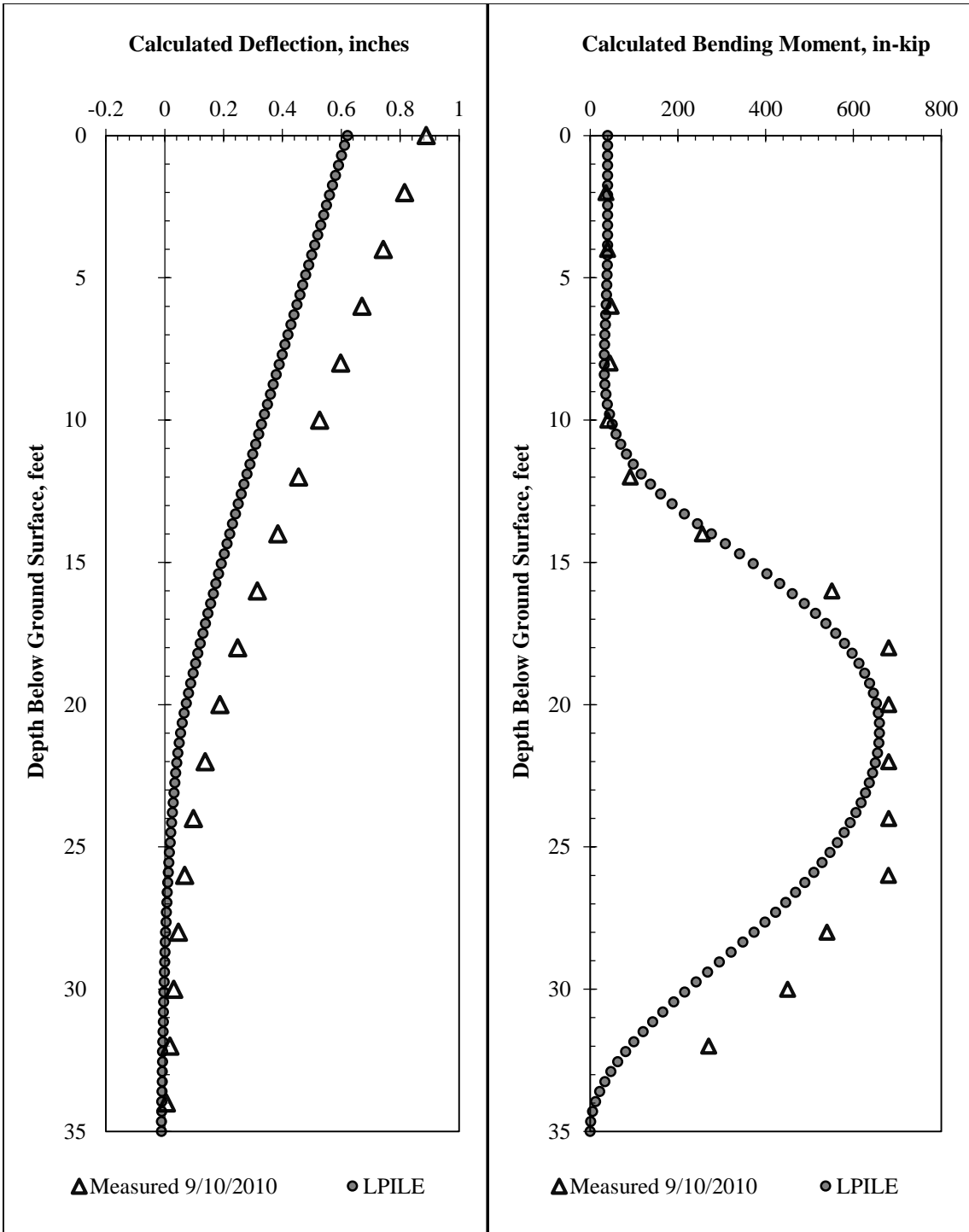


Figure 5.42: Comparison of measured and calculated profiles of deflection and bending moment in advanced LPILE analysis.



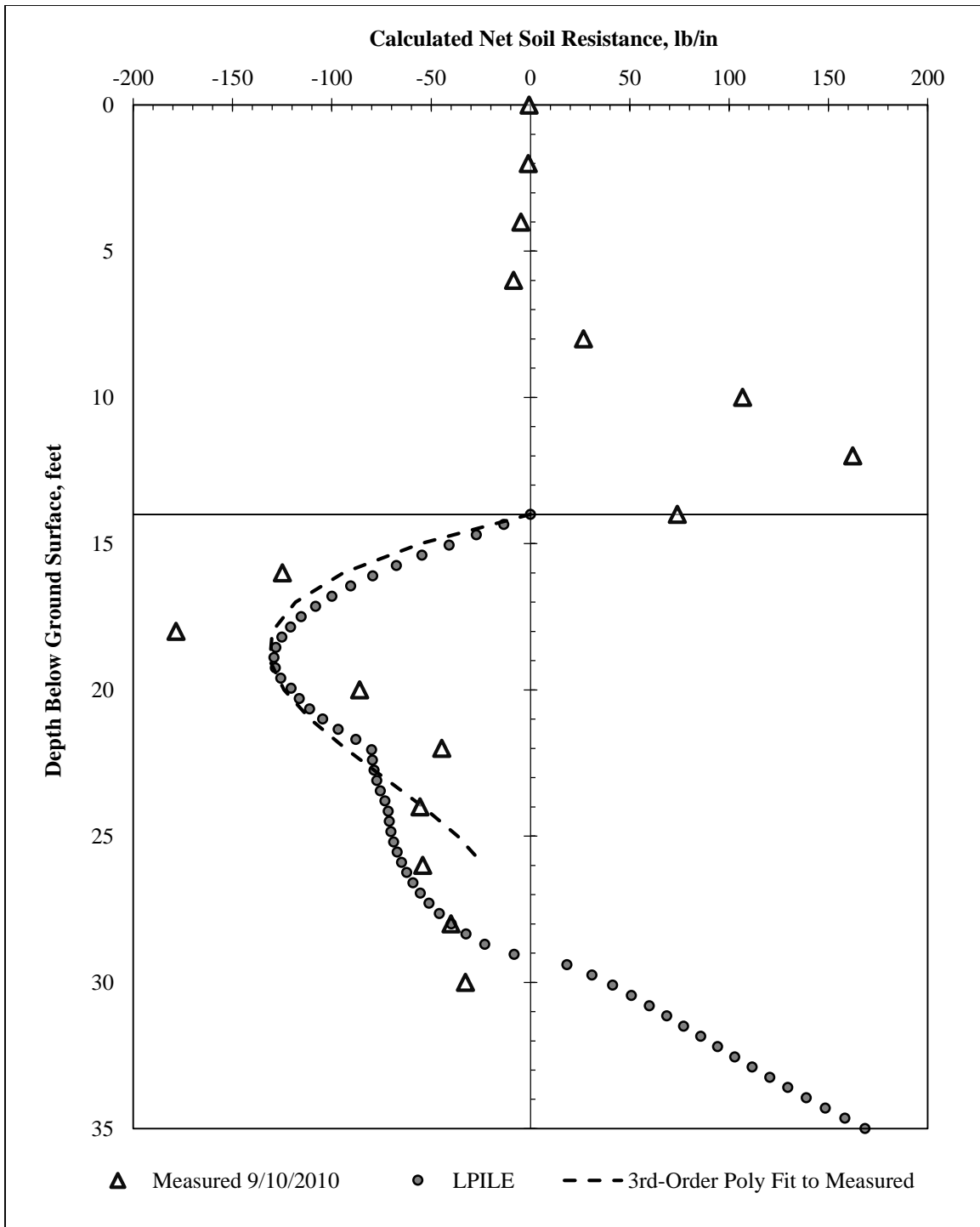


Figure 5.43: Comparison of measured and calculated profiles of soil resistance in advanced LPILE analysis.

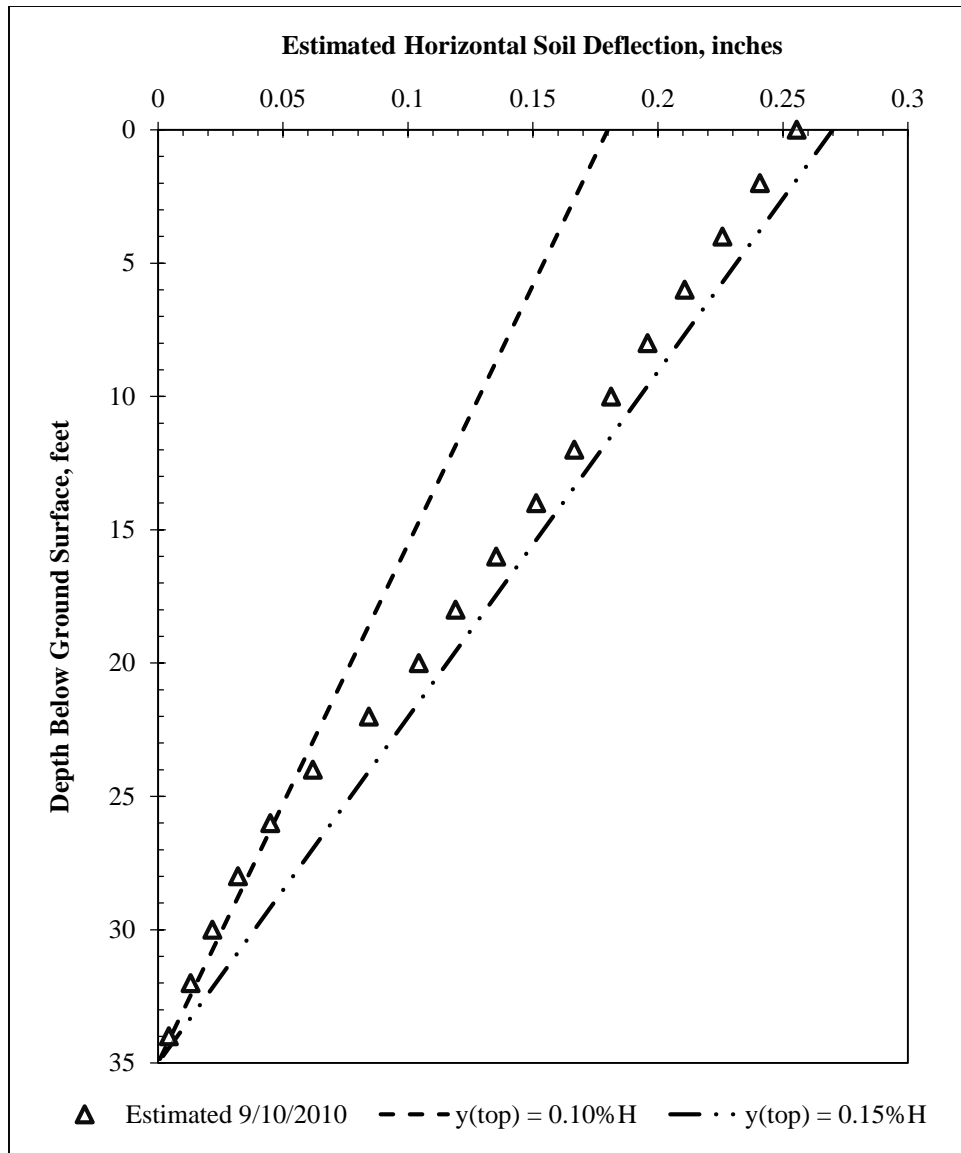


Figure 5.44: Estimated horizontal deflection due to global movements of the soil-shaft system during excavation.

### 5.4: Summary and Conclusions

The behavior of the Lymon C. Reese wall suggests that standard of practice design methods may not accurately account for what occurs during excavation. Based on the results of the instrumentation and data analysis program, several conclusions can be drawn:

- The standard design procedure for stiff clay predicts top-of-wall deflections fairly well for the test wall. However, it does not accurately predict the deflected shape at depth, and significantly overestimates the bending stresses in the shaft.
- The response of the foundation soil is much softer than the design prediction. Additionally, calculated values of earth pressure above the excavation line are smaller than the typically assumed design values.
- Within the time frame of excavation for the test wall (approximately 6 weeks), foundation soil response can be approximated with p-y curves using drained strength parameters, with initial curve stiffness ( $k_{py}$ ) defined by the measured profile of undrained shear strength with depth. In a heavily overconsolidated, fissured clay such as the Taylor formation, stress relief during excavation may lead to relaxation of stresses along the fissures, dramatically shortening both drainage path lengths and drainage times.
- A significant amount of the measured test wall deflection was due to a combination of global movement of the soil-shaft system and shaft base rotation, neither of which directly stress the wall. These motions are not accounted for in the design analysis, and because they are visually obscured by the application of facing material, they may not be noticed without careful monitoring. While estimates of global movements for the test wall are provided, additional data from other drilled shaft walls in expansive soils are required to formulate reliable recommendations for design.
- Deformations prior to the application of facing accounted for approximately 50% of the test wall's allowable top-of-wall deflections. As pore pressures dissipate and earth pressures above the excavation line increase, top-of-wall deflections are expected to increase further. Because deflection requirements often govern design

in practice, an understanding of the soil and shaft deformations during excavation may be important in some cases to ensure adequate wall performance.

## CHAPTER 6: TEST WALL BEHAVIOR DURING NATURAL MOISTURE CYCLES (OCTOBER 2010 – APRIL 2012)

### 6.1: Overview

After the completion of excavation in September 2010, shotcrete facing material was installed on October 1, 2010. Between October 2010 and April 2012, the wall experienced a range of climatic conditions, which were reflected in the observed wall movements. Because the application of facing represents a practical “zero” value for field measurements, subsequent test wall measurements are referenced to the October 8, 2010 survey (the most recent survey after facing installation).

### 6.2: Important Events and Qualitative Observations

#### 6.2.1: INSTALLATION OF SHOTCRETE FACING

To prevent soil erosion from between the shafts and provide consistency with design practice, shotcrete facing material was installed on October 1, 2010 (Figure 6.1).



Figure 6.1: Installation of Shotcrete Facing on October 1, 2010.

### 6.2.2: INSTALLATION OF TIME-DOMAIN REFLECTOMETRY PROBES

Prior to the application of shotcrete facing, time-domain reflectometry probes were installed. A total of 10 probes were installed through the wall facing on September 30 – October 1, 2010 (as shown in Figure 6.2), and 10 were installed through the ground surface on October 14 (as shown in Figure 6.3). The approximate locations of all installed TDR probes are shown in Figure 6.4. Additional discussion of TDR probe installation, calibration, and data analysis can be found in Dellinger (2011).



Figure 6.2: Installation of TDR Moisture Probes Behind Wall Facing.



Figure 6.3: Installation of TDR Moisture Probes Through Ground Surface.

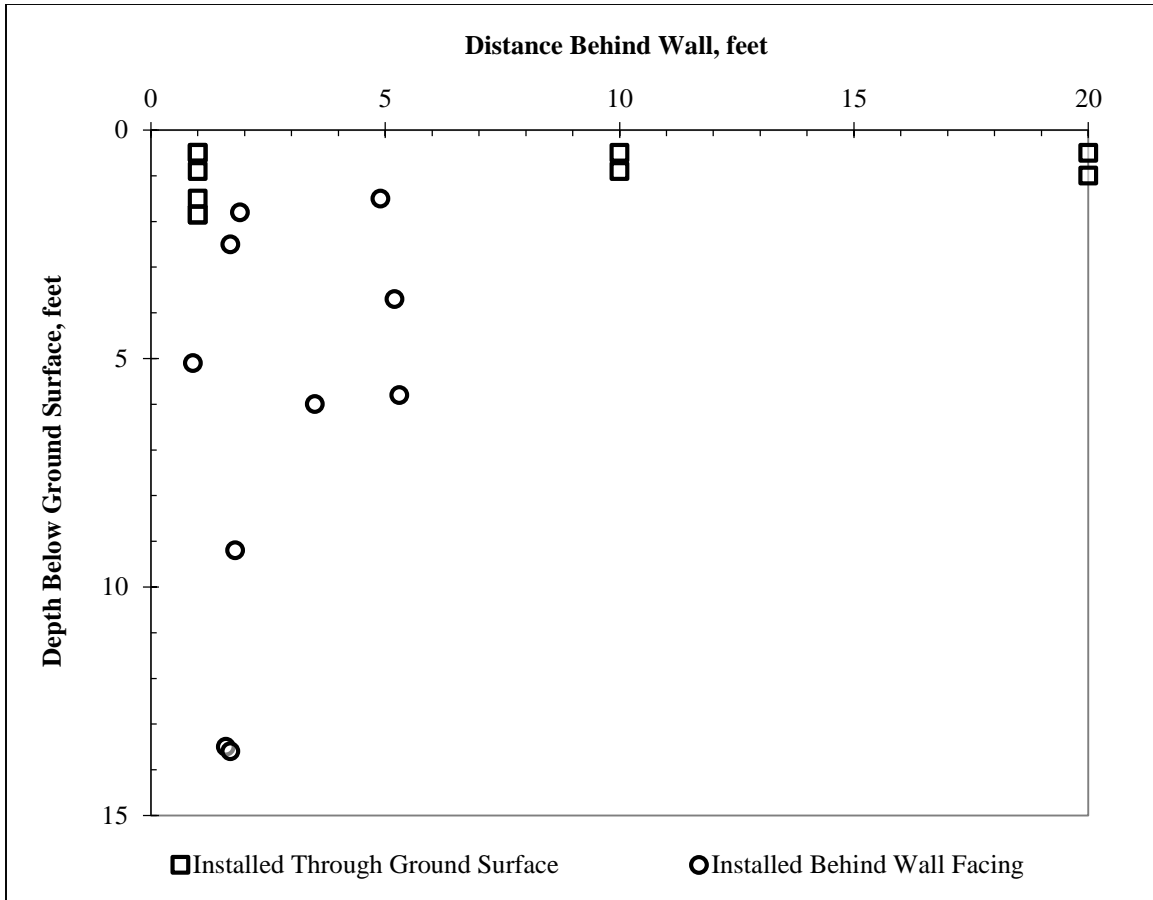


Figure 6.4: Approximate Locations of TDR Moisture Probes.

### 6.2.3: EXCAVATION SLOPE REPAIR AND EROSION CONTROL

On August 17, 2011, the slopes were reshaped to reduce erosion and prevent surface water from draining into the excavation (Figure 6.5). On October 8, 2011, erosion control material was installed (Figure 6.6).



Figure 6.5: Excavation slopes are reshaped on August 17, 2011.



Figure 6.6: Erosion control material is installed on October 18, 2011.

#### **6.2.4: CLIMATIC INFORMATION**

After facing installation was completed in October 2010, the test wall experienced approximately three months of below average rainfall, followed by a series of storms in January 2011. During the spring and summer of 2011, the test wall experienced an extended period of below average rainfall, widely reported to be the most severe drought Austin, Texas had experienced since record keeping had begun over 100 years before. During the fall and winter of 2011 and early 2012, rainfall totals were above average, and the project site was frequently flooded by heavy rains. By the time controlled inundation



testing had begun in early May, 2012, the project site had seen several weeks with high temperatures and minimal rainfall. Rainfall patterns are summarized in Figure 6.7; daily temperature data is presented in Figure 6.8.

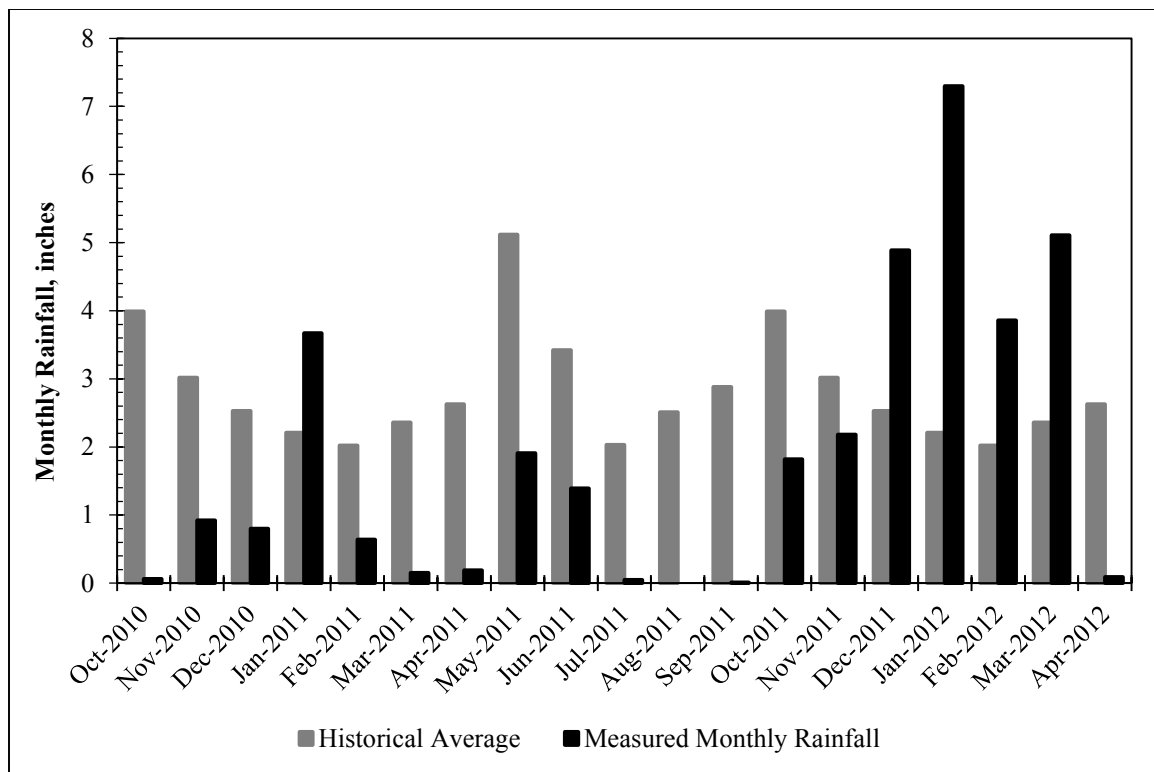


Figure 6.7: Monthly Rainfall Totals for Austin, Texas (Oct. 2010 – Apr. 2012; data from [www.wunderground.com](http://www.wunderground.com)).

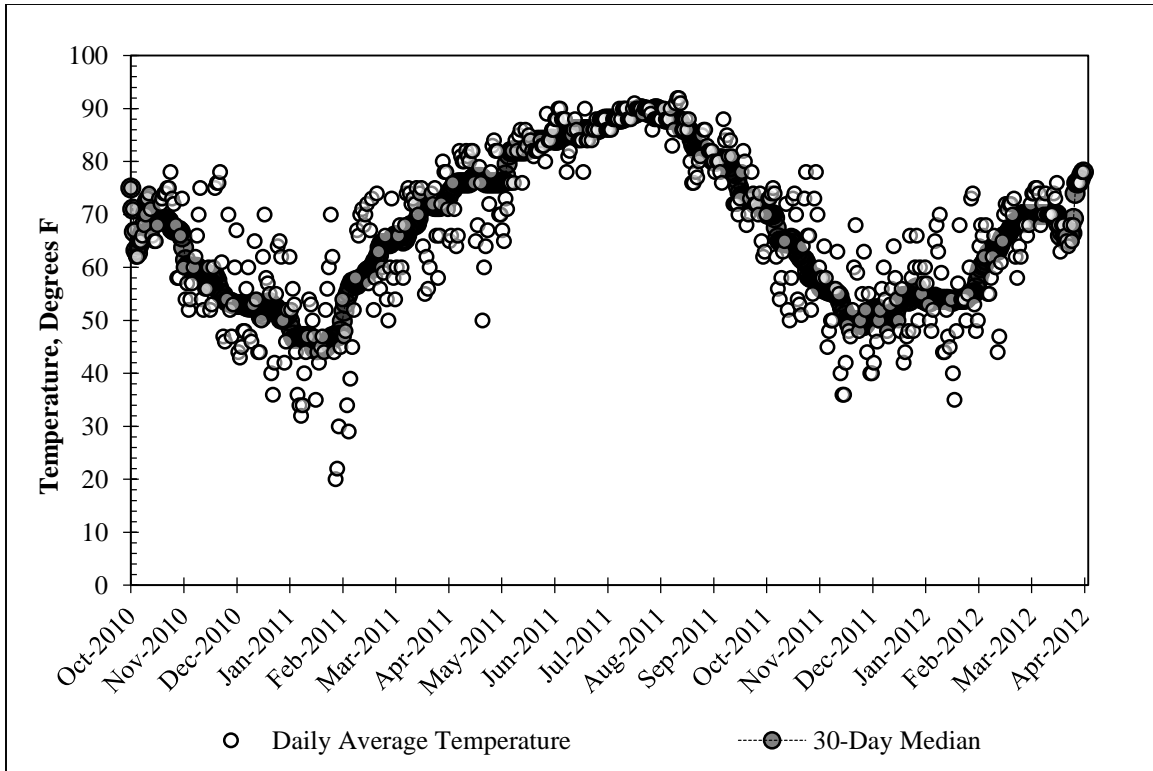


Figure 6.8: Daily Temperature Data for Manor, Texas (Oct. 2010 – Apr. 2012; data from [www.wunderground.com](http://www.wunderground.com)).

### 6.3: Summary of Field Instrumentation Data

#### 6.3.1: INCLINOMETER DATA

At the time of facing installation, the total top-of-wall deflection was approximately 0.97 inches relative to the beginning of excavation. In practice, the application of facing often represents the de facto “zero” date for a wall in service, because any deformations that have occurred during excavation will be visually obscured by the facing material. Without any internal instrumentation, subsequent wall assessments will rely largely on observed deformations and distress in the facing. For this reason, test wall deformations in response to natural soil moisture fluctuations are referenced to our facing installation date of October 8, 2010. The influence of natural moisture cycles on our measured top-of-

wall deflection is illustrated in Figure 6.9. In general, top-of-wall deflections tend to increase with increased rainfall, and stabilize or decrease during periods of drought (rainfall data is presented in Figure 6.7).

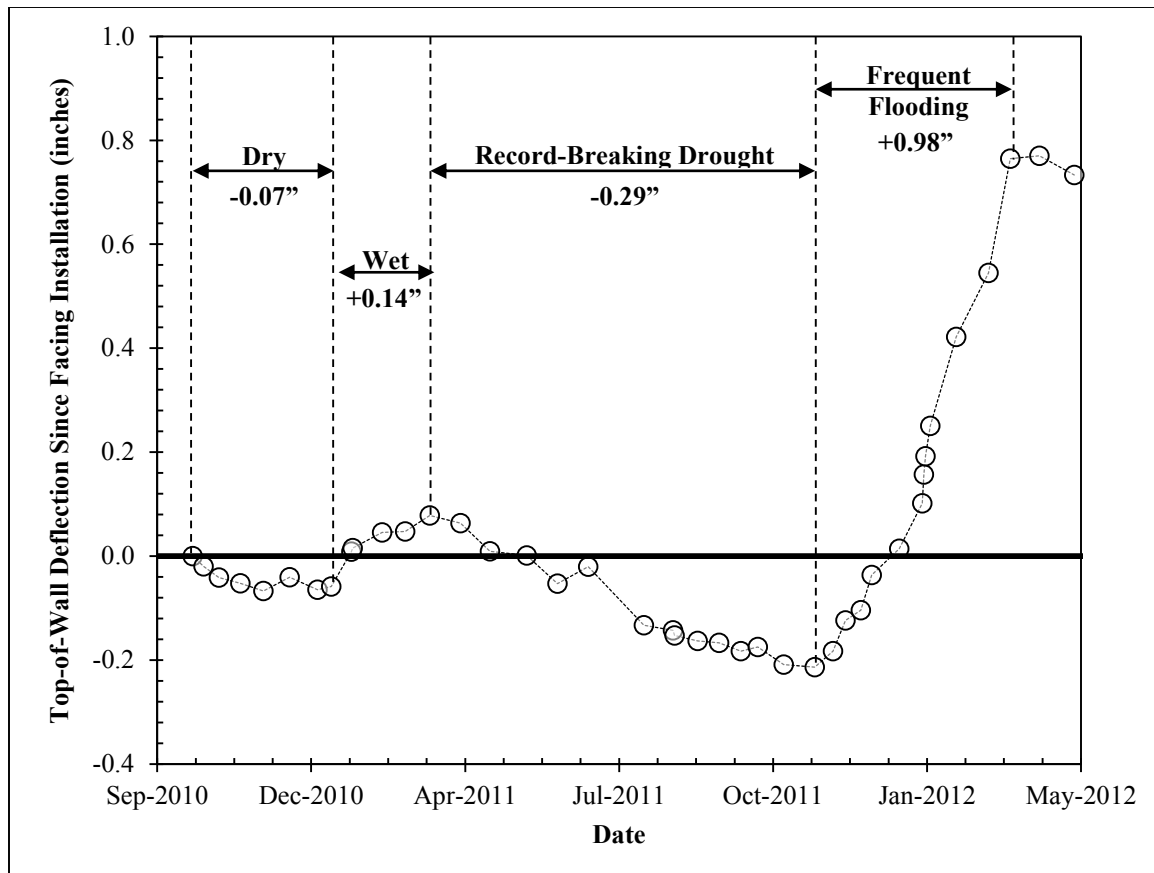


Figure 6.9: Variation of top-of-wall deflection with natural moisture cycles. Deflections are referenced to installation of facing on October 8, 2010.

### 6.3.2: TIME DOMAIN REFLECTOMETRY (TDR) PROBE DATA

Data from the most functional TDR probe, which was installed 1 foot behind the wall through the ground surface to a depth of 1.5 feet, is presented in Figure 6.10. Because large variations in electrical conductivity readings were observed during natural moisture cycles, the same data set is presented on a logarithmic scale in Figure 6.11. After

installation in October, 2010, values remained generally consistent before decreasing dramatically in April, 2011. The sudden decrease in electrical conductivity values occurred approximately one month into a severe drought, and most likely represent the loss of soil contact with the TDR probe rods as the soil decreases in volume and shrinks away from the probe (Figure 6.11). The decrease in electrical conductivity values also occurred at the same time the top-of-wall deflections began to decrease significantly (Figure 6.9), which suggests that soil shrinkage during drying cycles is responsible for both events. After the dramatic drop in April, 2011, electrical conductivity values continued to decrease until November, 2011, when rainfall returned to the project site and the electrical conductivity values increased in response (Figure 6.11). The increase in electrical conductivity values occurred at approximately the same time top-of-wall deflections began to increase in response to rainfall (Figure 6.9), and values remained fairly consistent until the commencement of controlled inundation testing in May, 2012. In late May and April, 2012, a small decrease in top-of-wall deflections was accompanied by a slight, but qualitatively similar, decrease in electrical conductivity values during the same time period (Figure 6.9, Figure 6.11).

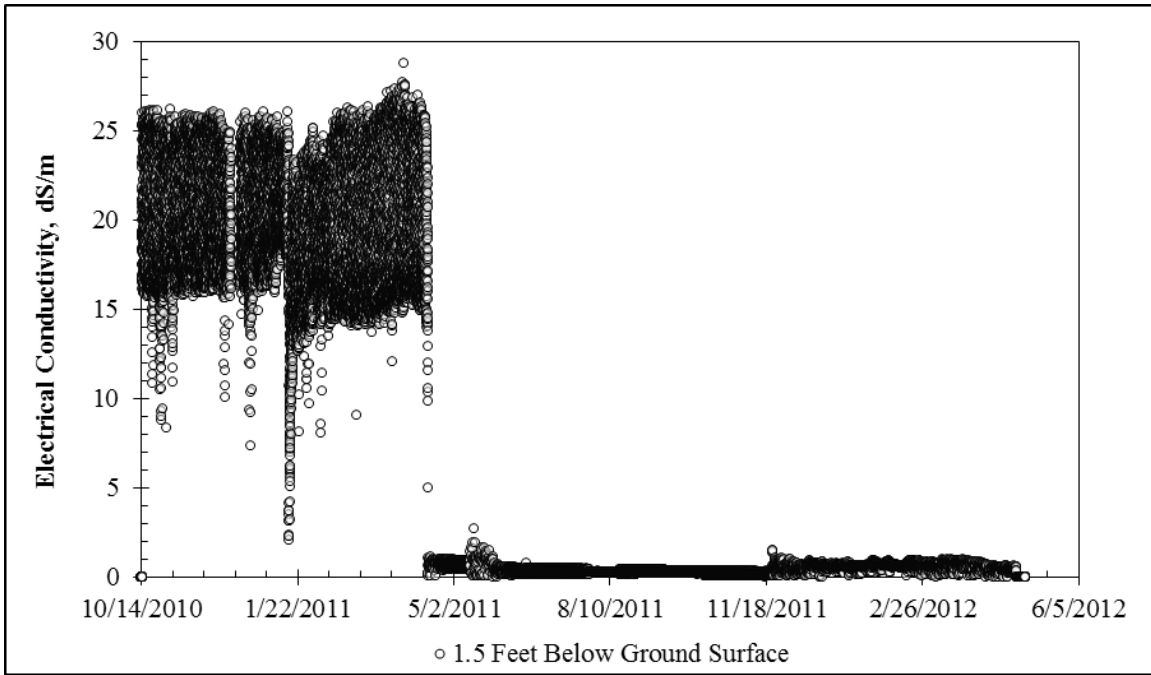


Figure 6.10: Electrical conductivity data from a TDR probe located 1.5 feet below ground surface (Oct. 2010 – Apr. 2012).

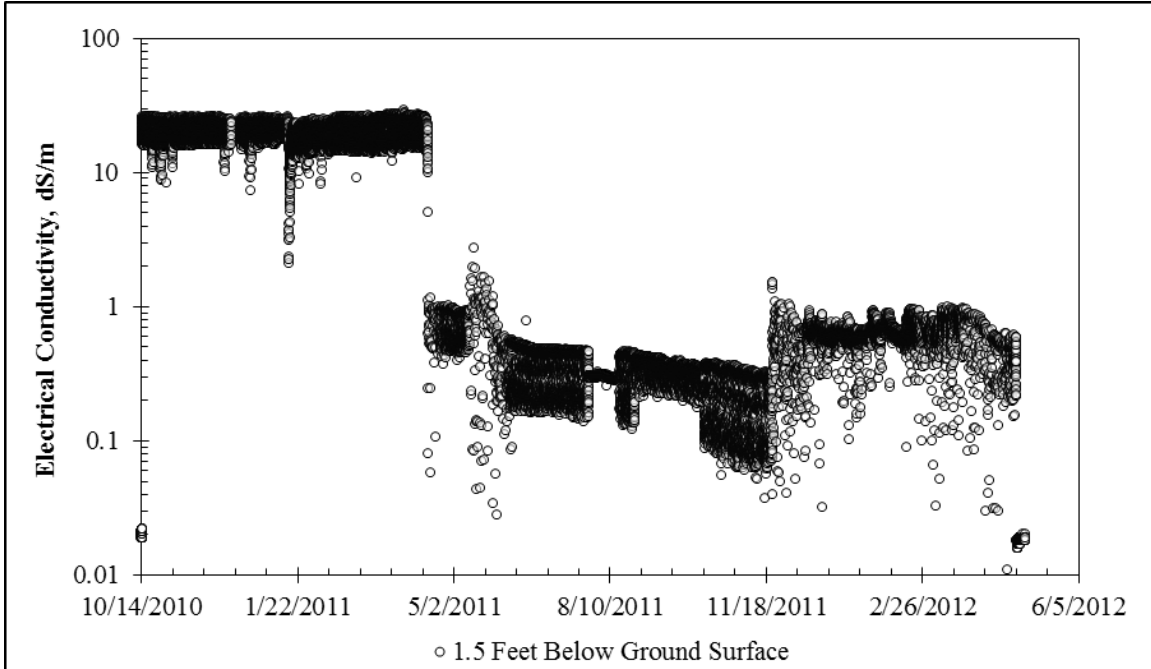


Figure 6.11 Electrical conductivity data from a TDR probe located 1.5 feet below ground surface, presented on a logarithmic scale (Oct. 2010 – Apr. 2012).

### 6.3.3: STRAIN GAUGE DATA

Strain data is presented in Figure 6.12 - Figure 6.26. In the following figures, strain data is zeroed at the first measurement after installation of facing (October 8, 2010). Strain gauge nomenclature indicates which instrumented shaft the gauge is installed in (East, Center, or West), the depth of the strain gauge below original ground surface (1 – 29 feet), and which side of the neutral axis the gauge is installed on (Tension or Compression; tensile strains are positive). Using this nomenclature, gauge E.17.T is located in the east instrumented shaft, 17 feet below ground surface, on the tensile side of the neutral axis.

In shallow gauges from 0 to 13 feet below the original ground surface, small bending strains consistent with the observed inclinometer data exist in many of the gauges. However, the influence of tension cracking seems to increase as more tension cracks appear to develop during this time (e.g. C.09.C). Axial strains consistent with seasonal temperature fluctuations are seen in the majority of shallow gauges, but relative values of bending curvature between pairs of gauges seem to be generally unaffected by seasonal temperature fluctuations (e.g. E.01.T / E.01.C). Some evidence of the development of negative bending curvatures during cycles of soil shrinkage can be seen (e.g. E.01.T / E.01.C, E.03.T / E.03.C). Some gauges display erratic behavior or strain readings outside their range of measurement, which likely indicates the gauge has been damaged and can no longer be used for data interpretation (e.g. C.01.C).

Data from gauges below the excavation line, from 15 – 29 feet below the original ground surface, shows gauge behavior which is generally similar to data from the shallow gauges. The influence of thermal strains is less pronounced due to the insulating presence of the overburden soil. Several of the gauges below the excavation line show evidence of tension cracking. The appearance of cracks is consistent with the measured bending curvatures from inclinometer data; the measured bending curvatures correspond to bending

moments close to the shaft's cracking moment of approximately 680 in-kip. Some gauges continue to show behavior that is very similar to the theoretical expectations (e.g. C.23.T / C.23.C, W.25.T, E.29.C). In addition to the development of cracks in the concrete, several gauges failures were observed. Gauge failures were generally preceded by erratic behavior, and failure was usually indicated by a sharp dive in a tensile or compressive direction before losing the gauge signal (e.g. C.21.C).

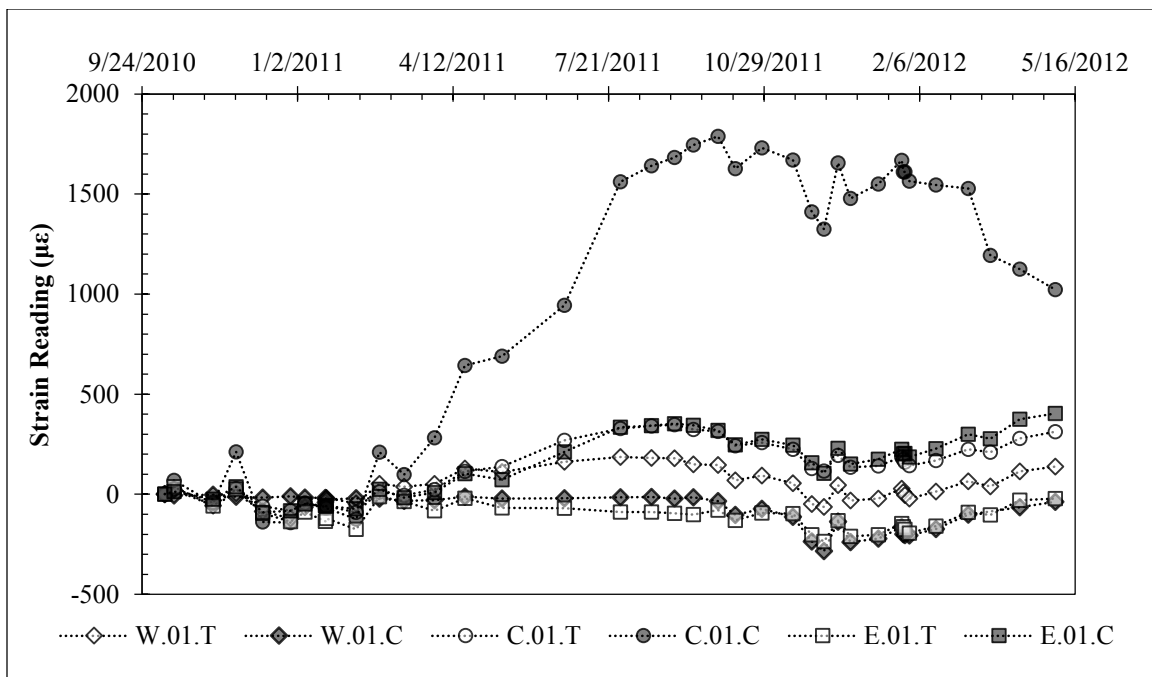


Figure 6.12: Strain Data 1 Foot Below Ground Surface (Oct. 2010 – Apr. 2012).

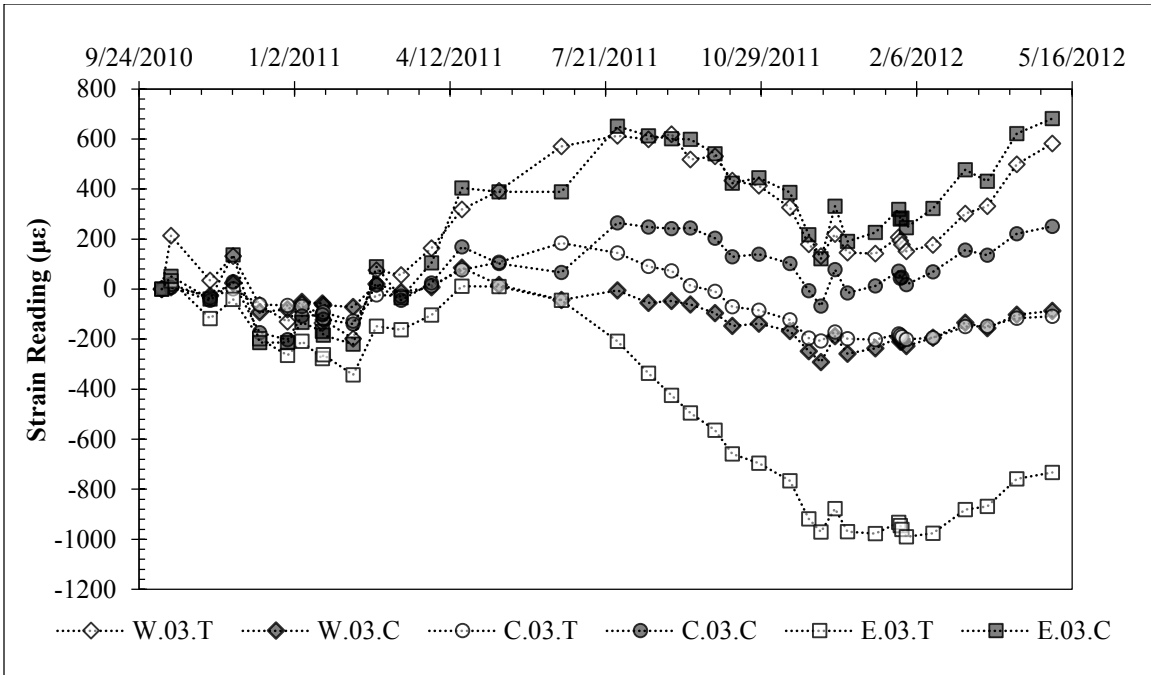


Figure 6.13: Strain Data 3 Feet Below Ground Surface (Oct. 2010 – Apr. 2012).

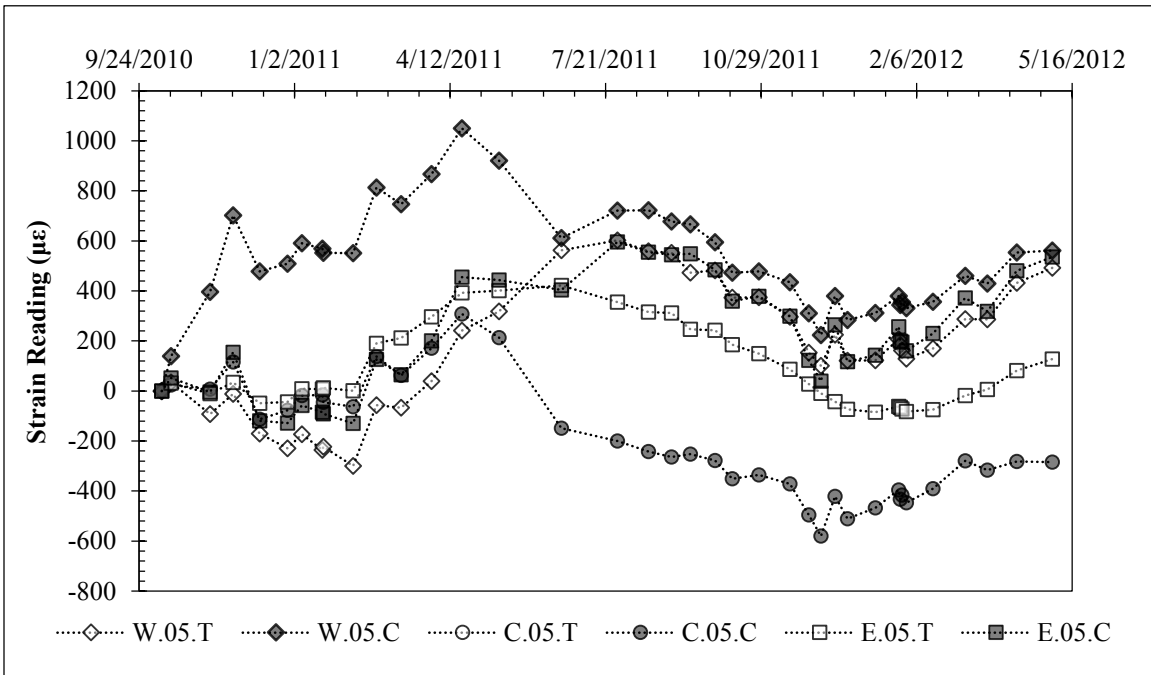


Figure 6.14: Strain Data 5 Feet Below Ground Surface (Oct. 2010 – Apr. 2012).



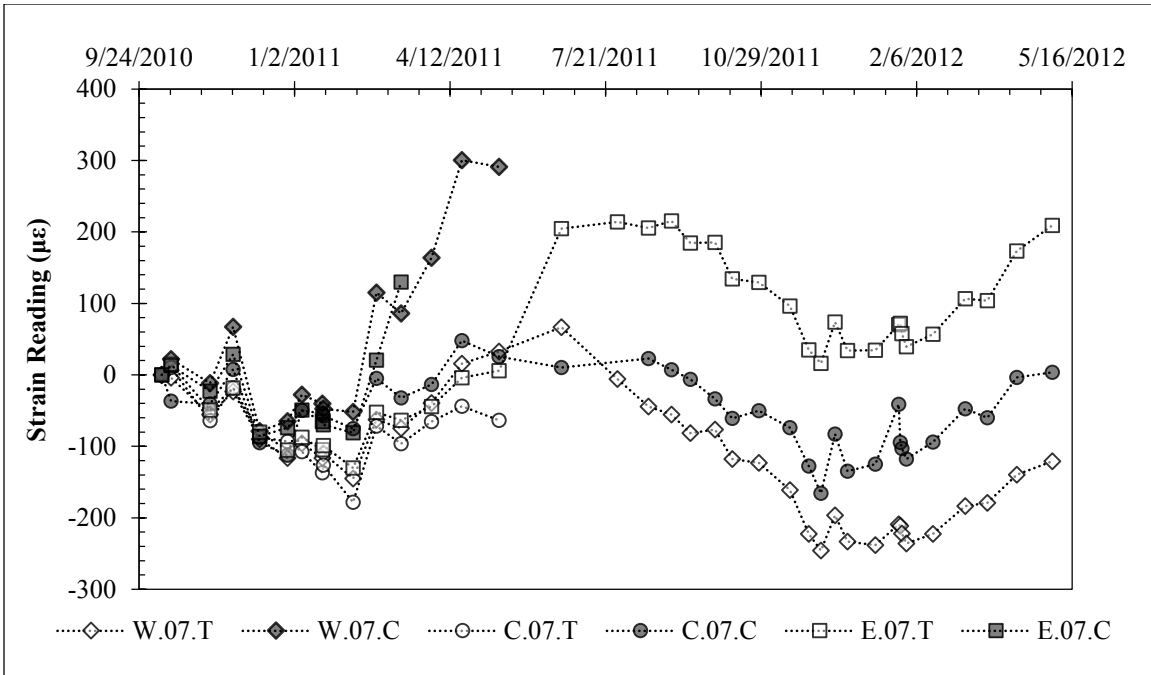


Figure 6.15: Strain Data 7 Feet Below Ground Surface (Oct. 2010 – Apr. 2012).

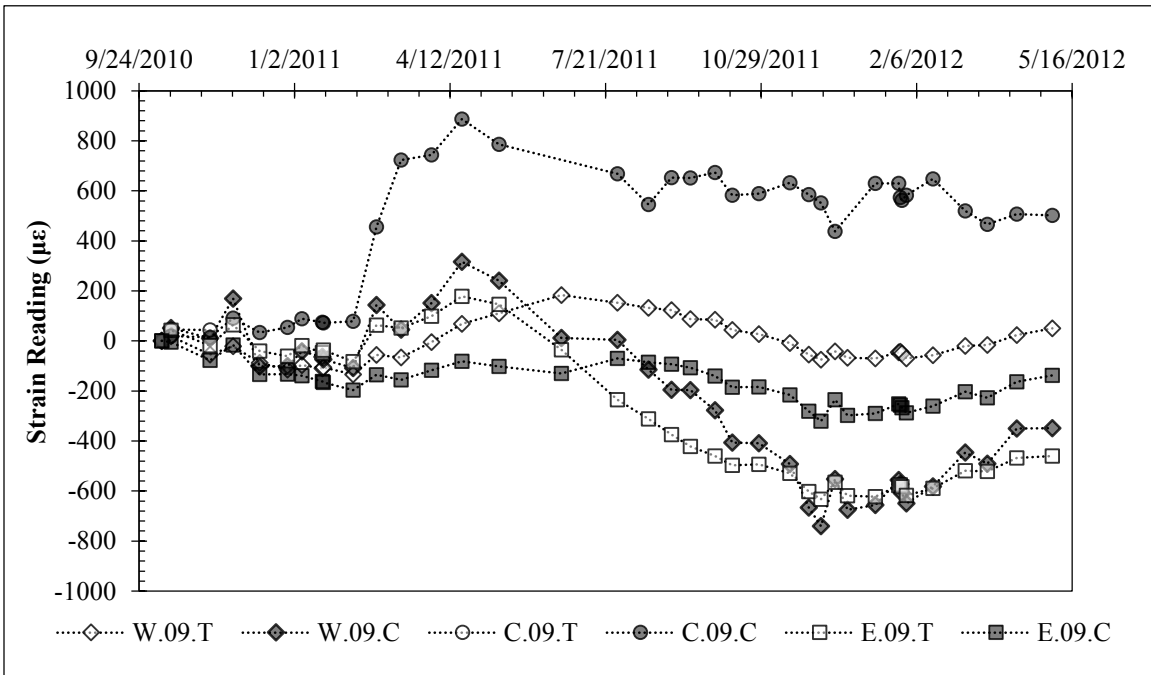


Figure 6.16: Strain Data 9 Feet Below Ground Surface (Oct. 2010 – Apr. 2012).

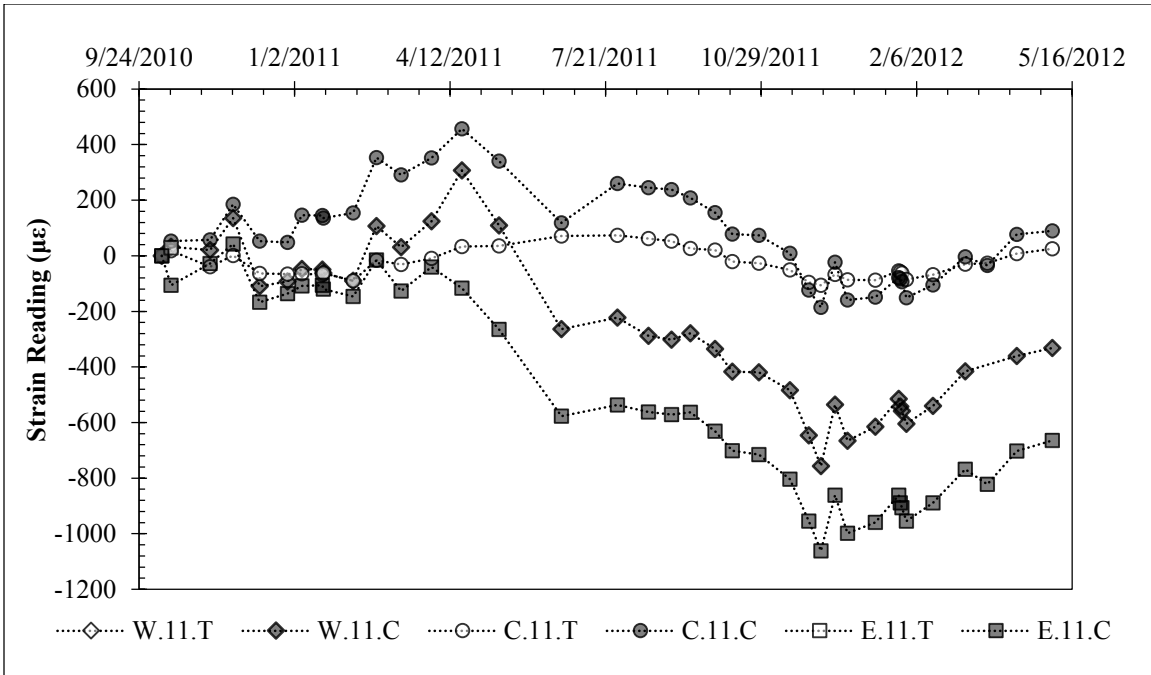


Figure 6.17: Strain Data 11 Feet Below Ground Surface (Oct. 2010 – Apr. 2012).

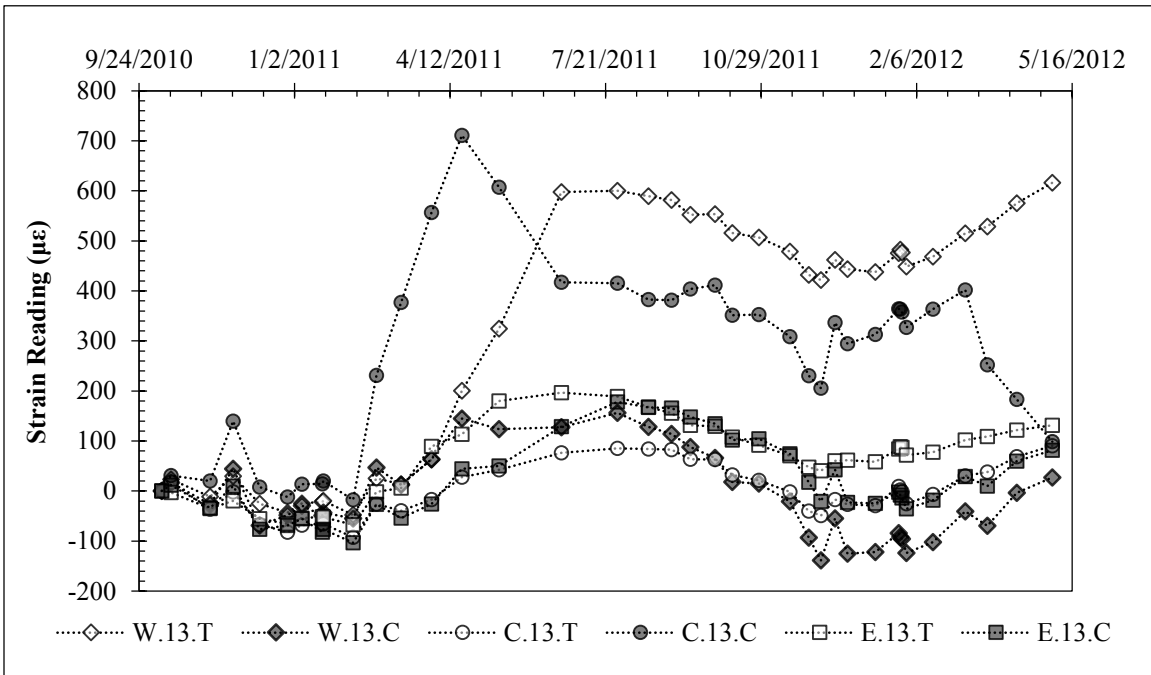


Figure 6.18: Strain Data 13 Feet Below Ground Surface (Oct. 2010 – Apr. 2012).

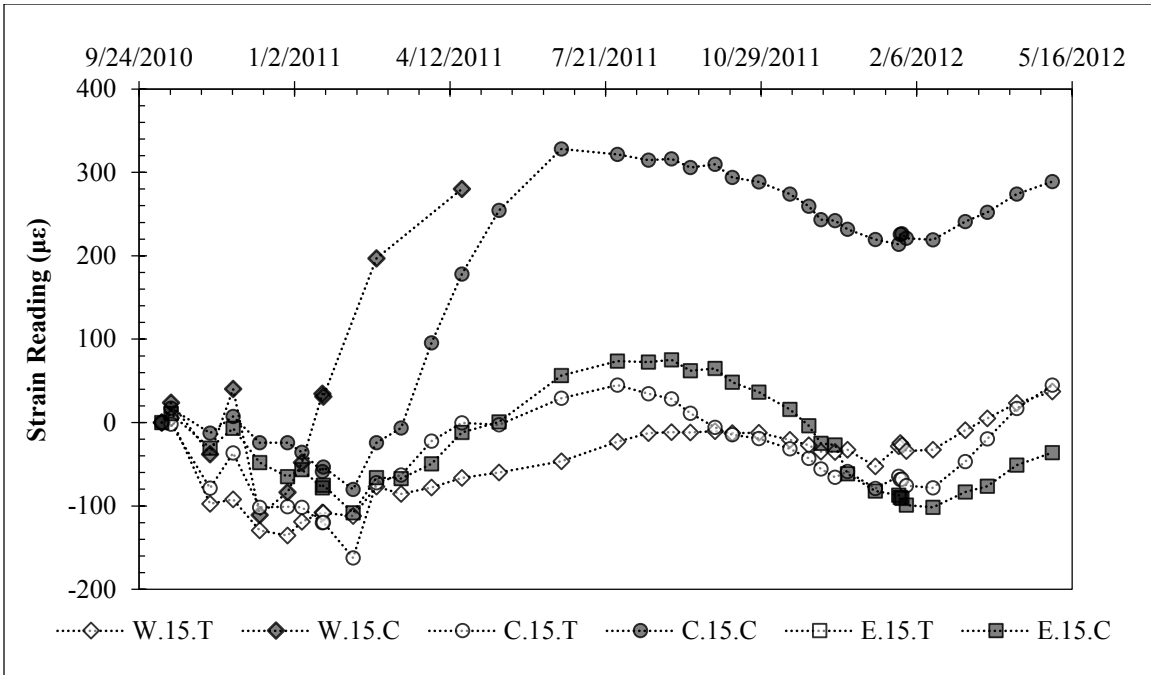


Figure 6.19: Strain Data 15 Feet Below Ground Surface (Oct. 2010 – Apr. 2012).

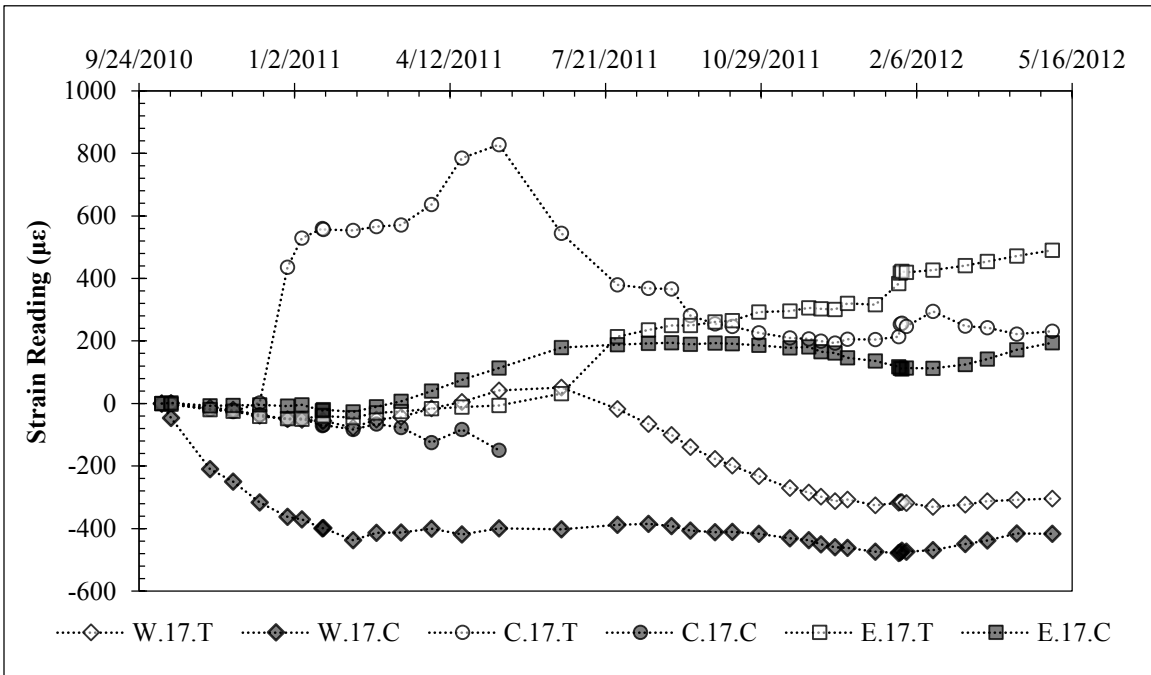


Figure 6.20: Strain Data 17 Feet Below Ground Surface (Oct. 2010 – Apr. 2012).

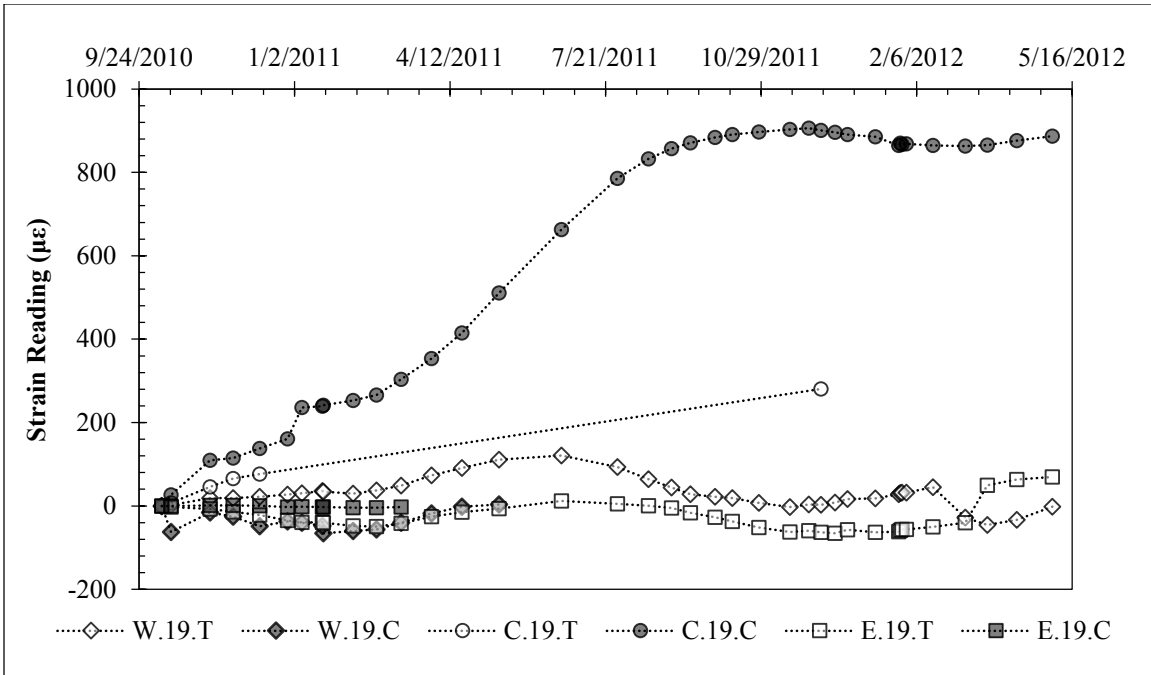


Figure 6.21: Strain Data 19 Feet Below Ground Surface (Oct. 2010 – Apr. 2012).

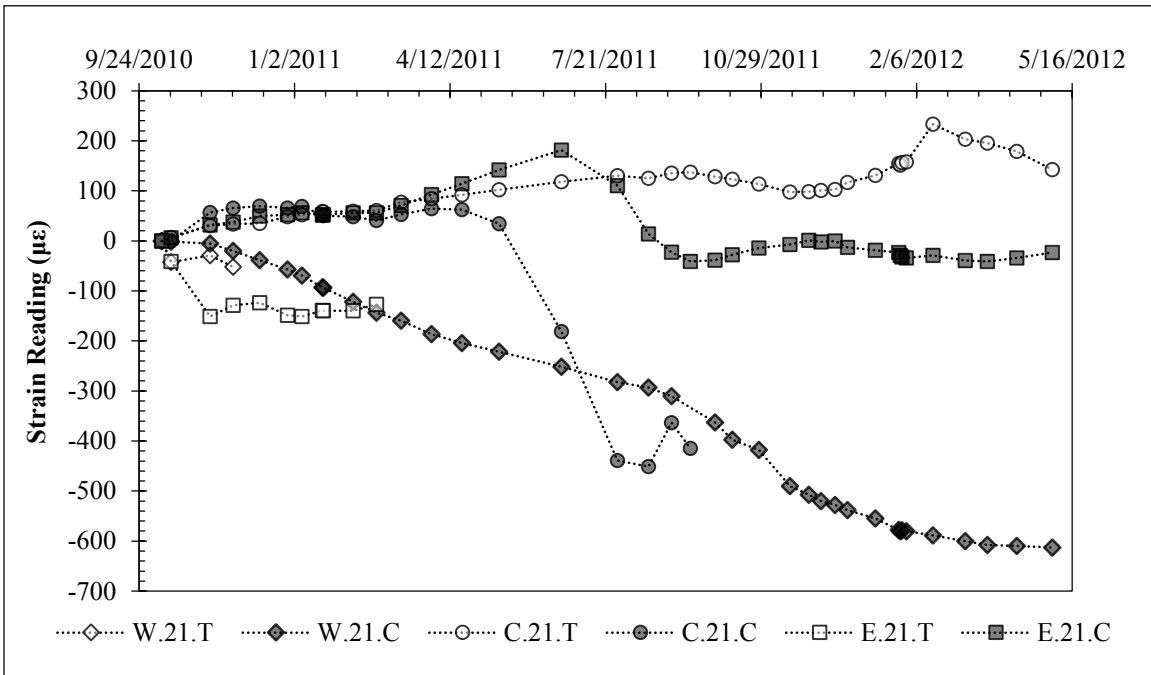


Figure 6.22: Strain Data 21 Feet Below Ground Surface (Oct. 2010 – Apr. 2012).

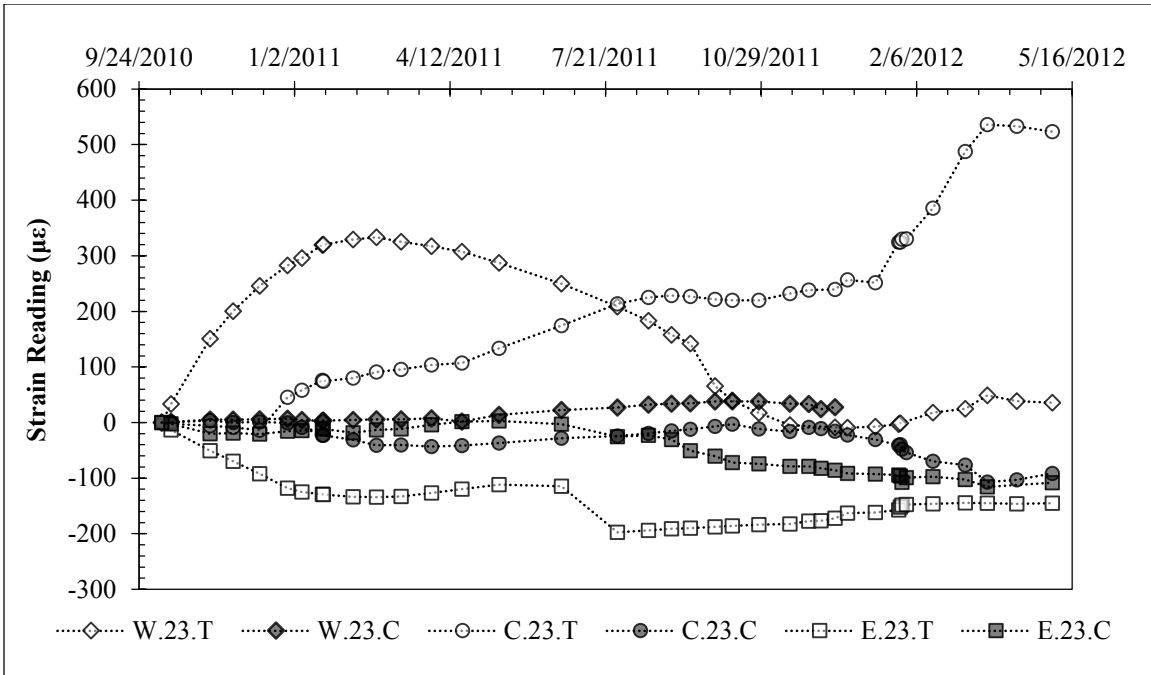


Figure 6.23: Strain Data 23 Feet Below Ground Surface (Oct. 2010 – Apr. 2012).

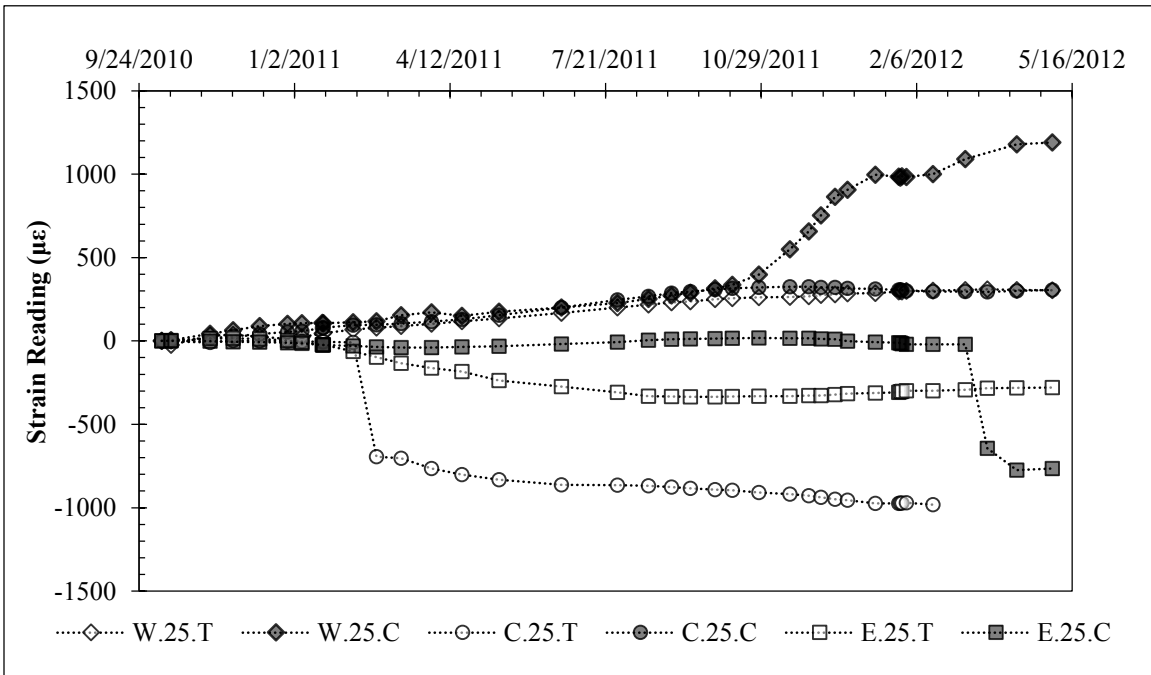


Figure 6.24: Strain Data 25 Feet Below Ground Surface (Oct. 2010 – Apr. 2012).

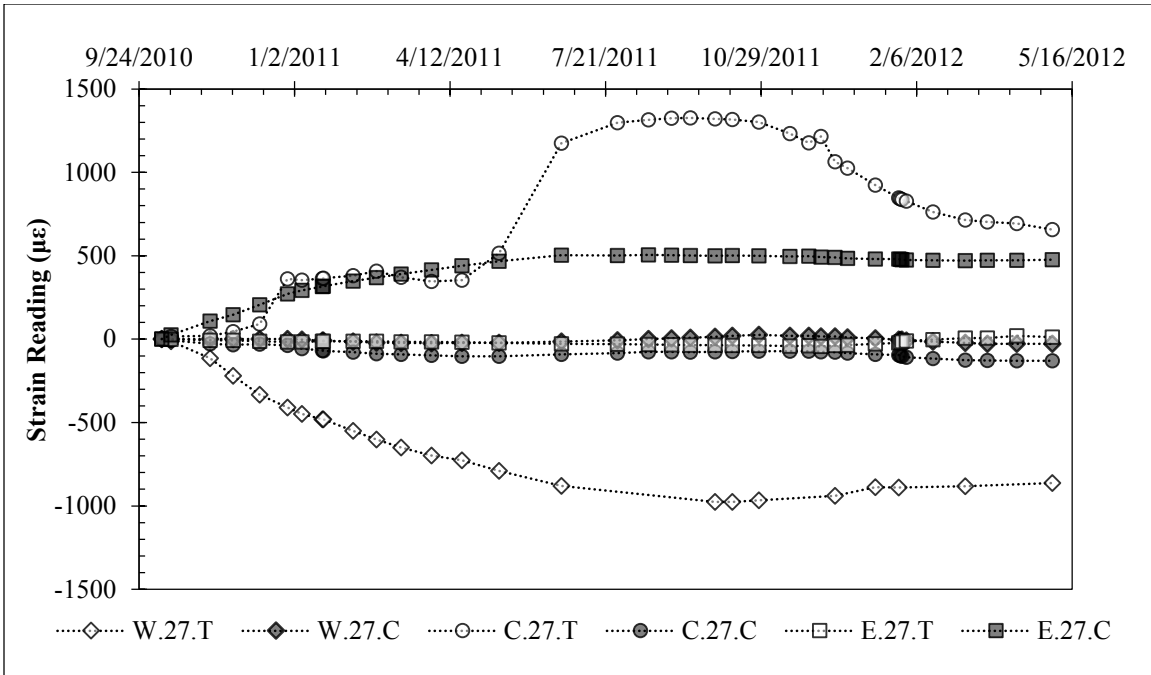


Figure 6.25: Strain Data 27 Feet Below Ground Surface (Oct. 2010 – Apr. 2012).

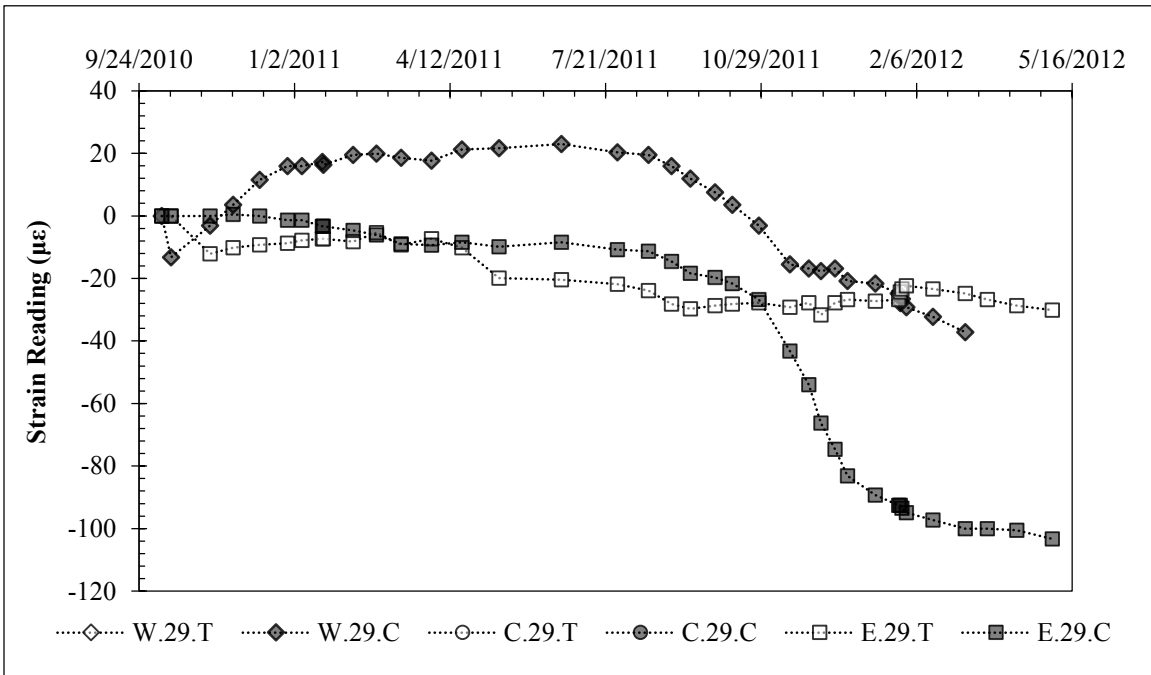


Figure 6.26: Strain Data 29 Feet Below Ground Surface (Oct. 2010 – Apr. 2012).

## **6.4: Data Interpretation**

### **6.4.1: PHASES OF WALL MOTION**

Over the 22 months in which wall deflection was monitored, the test wall experienced a range of climatic conditions and corresponding deflections. These can be simplified into four basic phases of wall motion, using the variation in top-of-wall deflections as the parameter of interest. In the following sections, inclinometer data is presented as a profile of cumulative deflections versus depth; beneath the deflection profile, a plan view of the A- and B-axis of the inclinometer probe is shown. While wall motion can generally be assumed to be one-dimensional and perpendicular to the wall, inspection of plan view data can provide some insights on the nature of wall movement. It is important to note that in each instrumented shaft, the as-built inclinometer casing alignments are slightly different; this is normal and does not indicate the shafts are moving in different directions.

#### **6.4.1.a: Drying Cycle 1: October 8, 2010 – January 6, 2011 (3 months)**

After the installation of the wall facing on October 8, the top-of-wall deflections decreased by a small amount, around 0.07 inches in three months. In this phase, the first possible effects of soil shrinkage are observed.

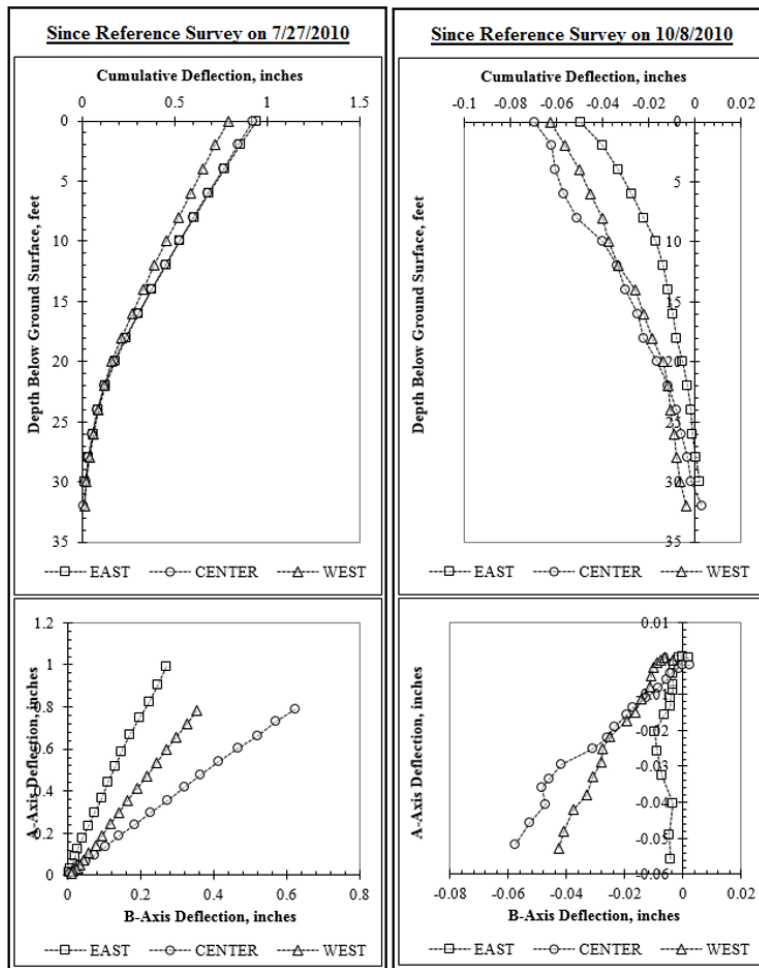


Figure 6.27: Inclinometer Data from January 6, 2011.

**6.4.1.b: Wetting Cycle 1: January 6, 2011 – March 11, 2011 (2 months)**

After a dry fall with below average rainfall, two large rainfall events in January led to flooding in the excavation and access to moisture for the retained and foundation soil. In response to these events, the average top-of-wall deflections increased by approximately 0.14 inches over two months.



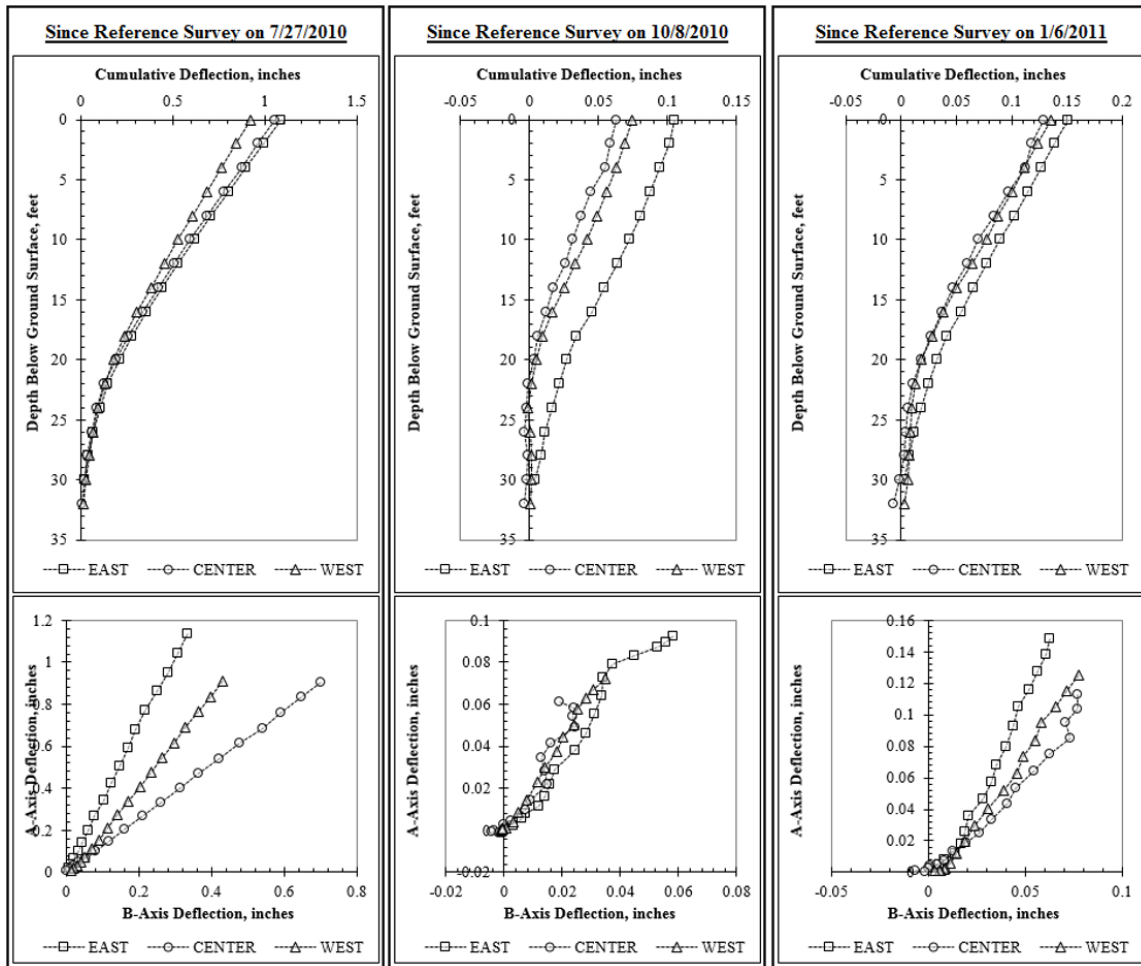


Figure 6.28: Inclinometer Data from March 11, 2011.

**6.4.1.c: Drying Cycle 2: March 11, 2011 – November 16, 2011 (8 months)**

During this phase, a record-breaking drought caused the soil on the project to dry and shrink significantly. In response, the top-of-wall deflections decreased by approximately 0.29 inches over eight months. As an indication of drying-related soil shrinkage on the project site, noticeable differential settlement between the inclinometer casing (installed to a depth of 50 feet) and its surrounding concrete pad (connected to the ground surface independently of the casing) was observed. While this is far from a perfect

measurement, it does indicate significant shrinkage of the retained soil occurred (Figure 6.29). The top-of-wall deflections reach a minimum during this phase.

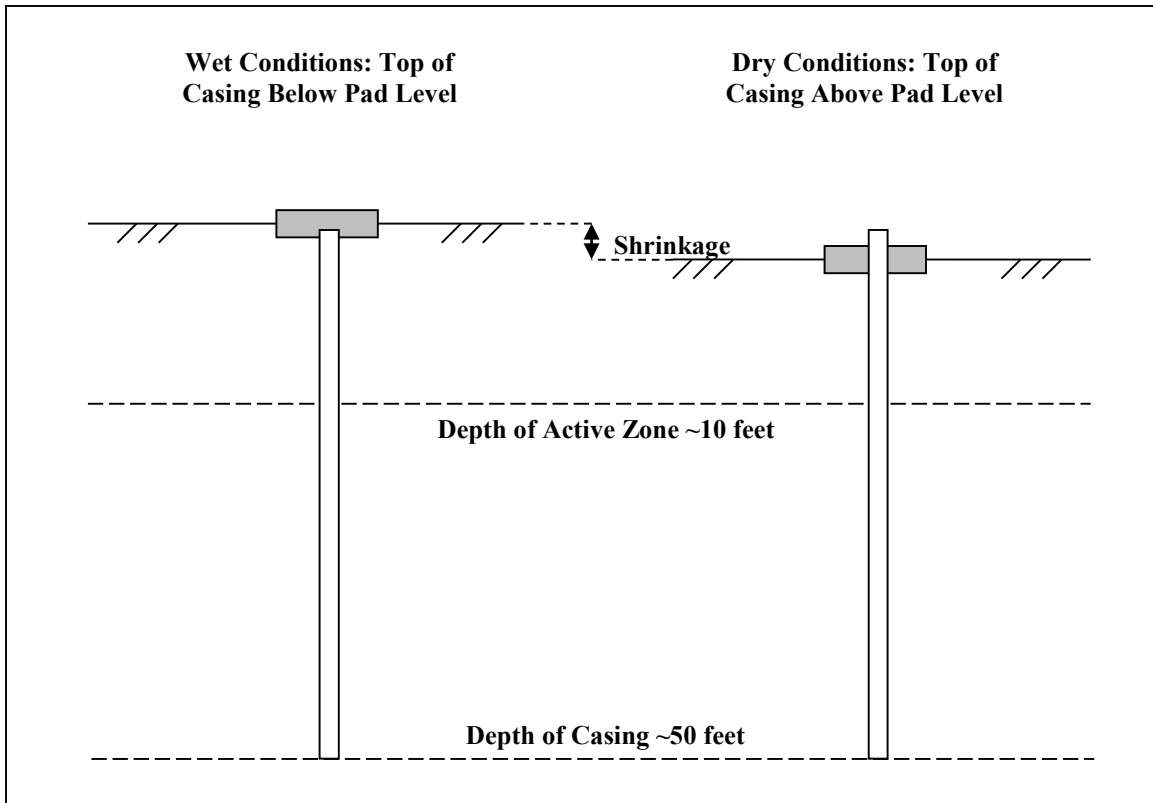


Figure 6.29: The use of a deep inclinometer casing and concrete pad as a qualitative indicator of soil shrinkage near the test wall (not to scale).

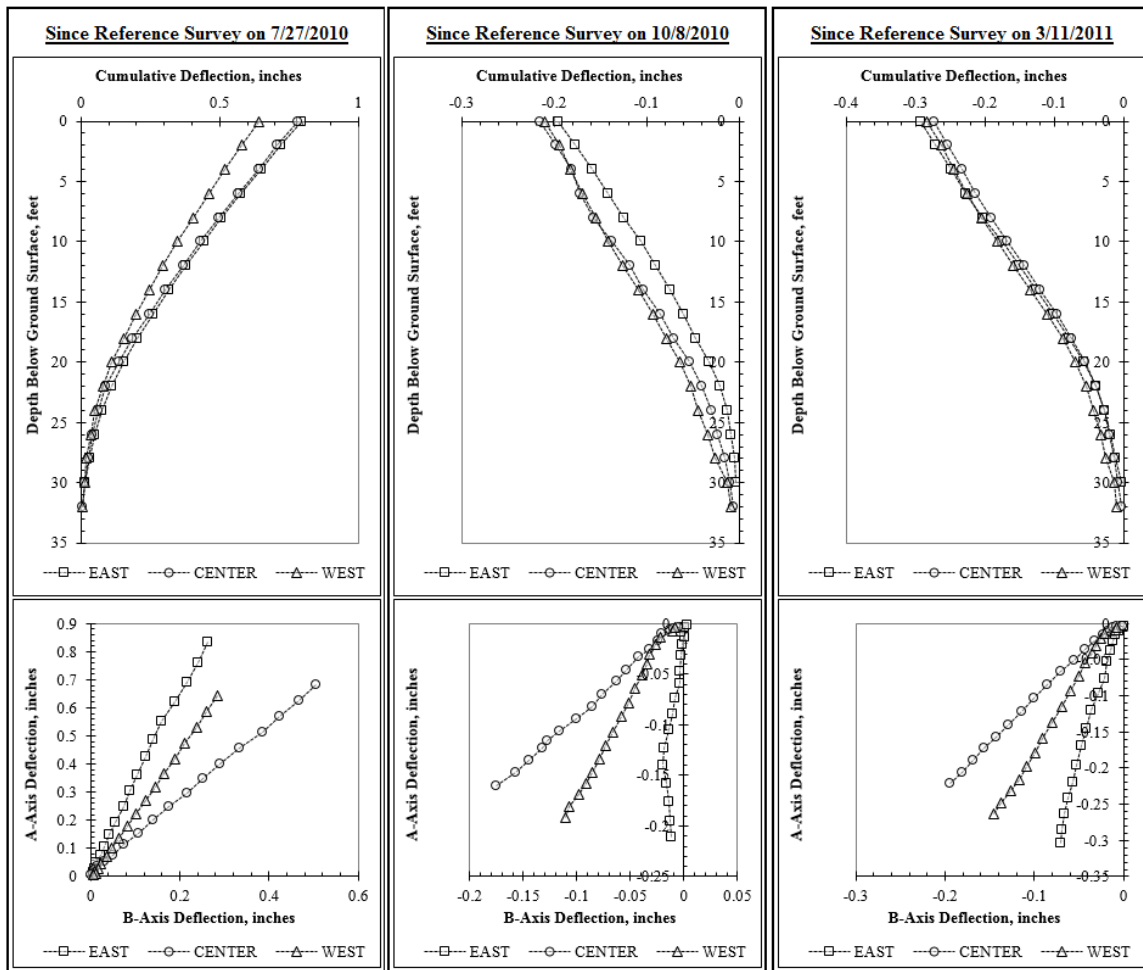


Figure 6.30: Inclinometer Data from November 16, 2011.

#### 6.4.1.d: Wetting Cycle 2: November 16, 2011 – April 10, 2012 (5 months)

During this phase, a very wet winter with two exceptionally large rainfall events caused top-of-wall deflections to increase to their maximum values. In response to the continued presence of water in the excavation and frequent access to moisture for the retained soil during rainfall events, the top-of-wall deflections increased by approximately 0.98 inches over five months. Between April 10, 2012 and the start of the artificial inundation test on May 2, 2012, the top-of-wall deflections stabilized and began to decrease after a short period of hot, dry weather.

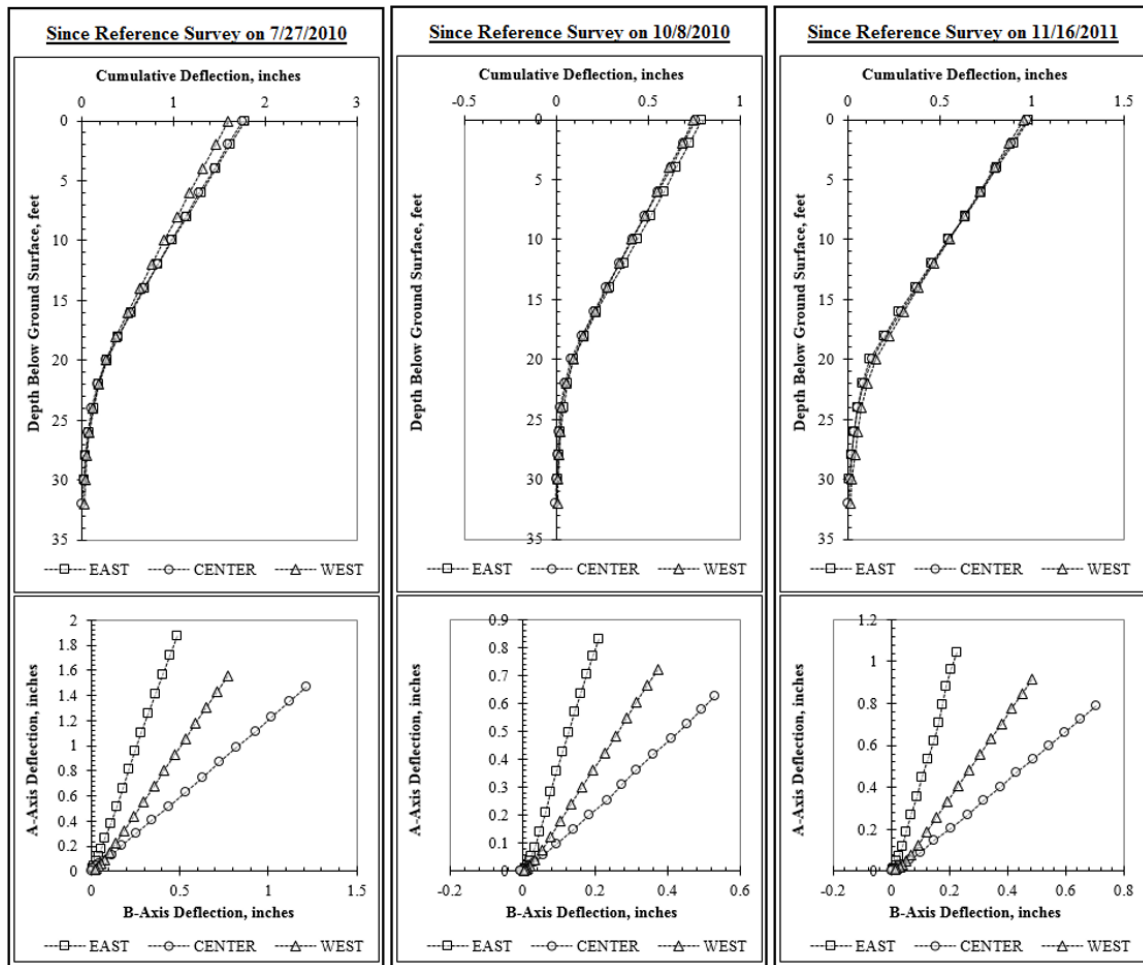


Figure 6.31: Inclinometer Data from April 10, 2012.

#### 6.4.2: DEFLECTED SHAPES AT KEY DATES

During each of the phases of wall motion described above, the deflected shape of the shaft varied in ways that cannot be easily modeled using a typical p-y analysis. In Figure 6.32, the deflected shape of the shaft at the conclusion of each phase of motion is plotted. When these are compared with the deflected shape predicted by the original design p-y analysis using a commonly assumed earth pressure of 40 psf/ft and stiff clay curves for the foundation soil, the qualitative differences in the predicted and measured values are similar to the differences observed during excavation. Throughout both wetting and drying

cycles, the observed foundation soil response is softer than the response predicted by the stiff clay curves. More complex loading mechanisms, the influence of shaft base rotation, weakening of the soil in the base of the excavation, and various other factors may all influence these discrepancies.

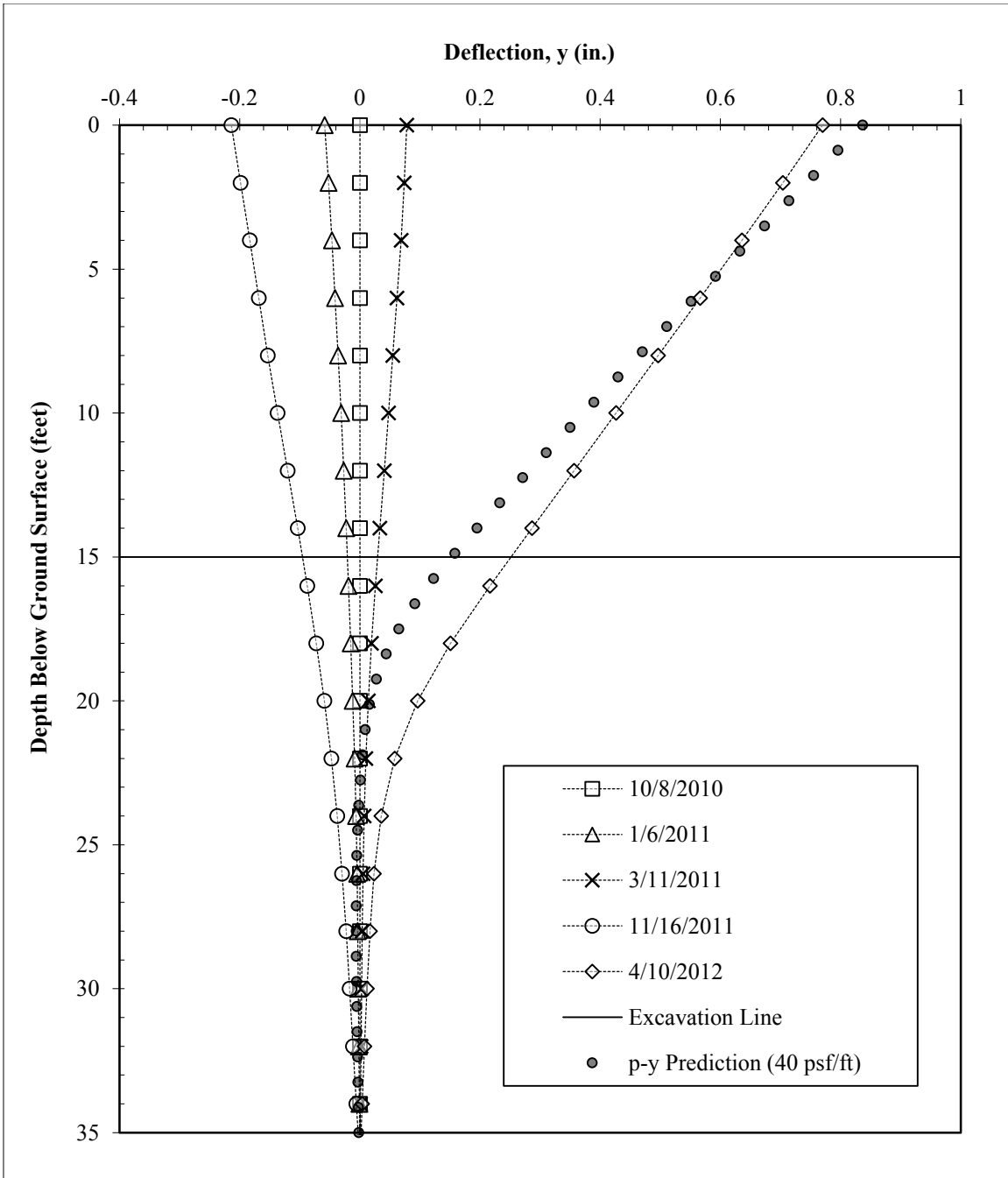


Figure 6.32: Deflected shapes of test wall at key dates, referenced to the installation of facing on October 8, 2010, compared with the initial p-y design analysis.

### **6.4.3: EARTH PRESSURE REDUCTIONS FROM SOIL SHRINKAGE**

The maximum negative wall movement was observed between March 11, 2011 and November 16, 2011, in which top-of-wall deflections decreased by approximately 0.3 inches. Rotation profiles for the three instrumented shafts were differentiated to obtain an envelope of bending moments and equivalent soil reactions in response to soil shrinkage (Figure 6.33). The change in earth pressures corresponds to a reduction in equivalent fluid pressure of approximately 20 psf/ft (defined as the triangular distribution which will produce a profile of bending moments and deflections similar to the results of the calculated earth pressure distribution). The results of an LPILE analysis using the input parameters from Table 6.1 is presented in Figure 6.34. While top-of-wall deflections are fairly well predicted, wall behavior at depth is somewhat stiffer in the LPILE prediction. Additionally, the bending moment diagram appears to be shifted in a positive direction by approximately 120 in-kip at ground surface, and an average of 150 in-kip over the depth of the shaft (Figure 6.34).

Table 6.1: Baseline assumptions and design parameters for initial soil shrinkage LPILE analysis.

Parameter	Value
Effective Unit Weight of Soil, $\gamma$	62.6 pcf
Earth Pressure Loading	Input Envelope from Calculated $p_{net}$
Additional Moment Applied at Top for Thermal Effects	N/A
Friction Angle of Foundation Soil	24 degrees
Foundation Soil p-y Curves	Sand (Reese)
Non-Default Initial Stiffness, $k_{py}$	375 lb/in <sup>3</sup>
Cracking Moment, $M_{Cr}$	680 k-in.
Yielding Moment, $M_y$	3,200 k-in.
Uncracked Bending Stiffness, $EI_{uc}$	$67 \times 10^6$ k-in.
Cracked Bending Stiffness, $EI_{cr}$	$18 \times 10^6$ k-in.
Shaft Diameter	24 in.
Height of Retained Soil, H	168 in.
Reinforcement	12 #7 bars (1.6% of gross area)



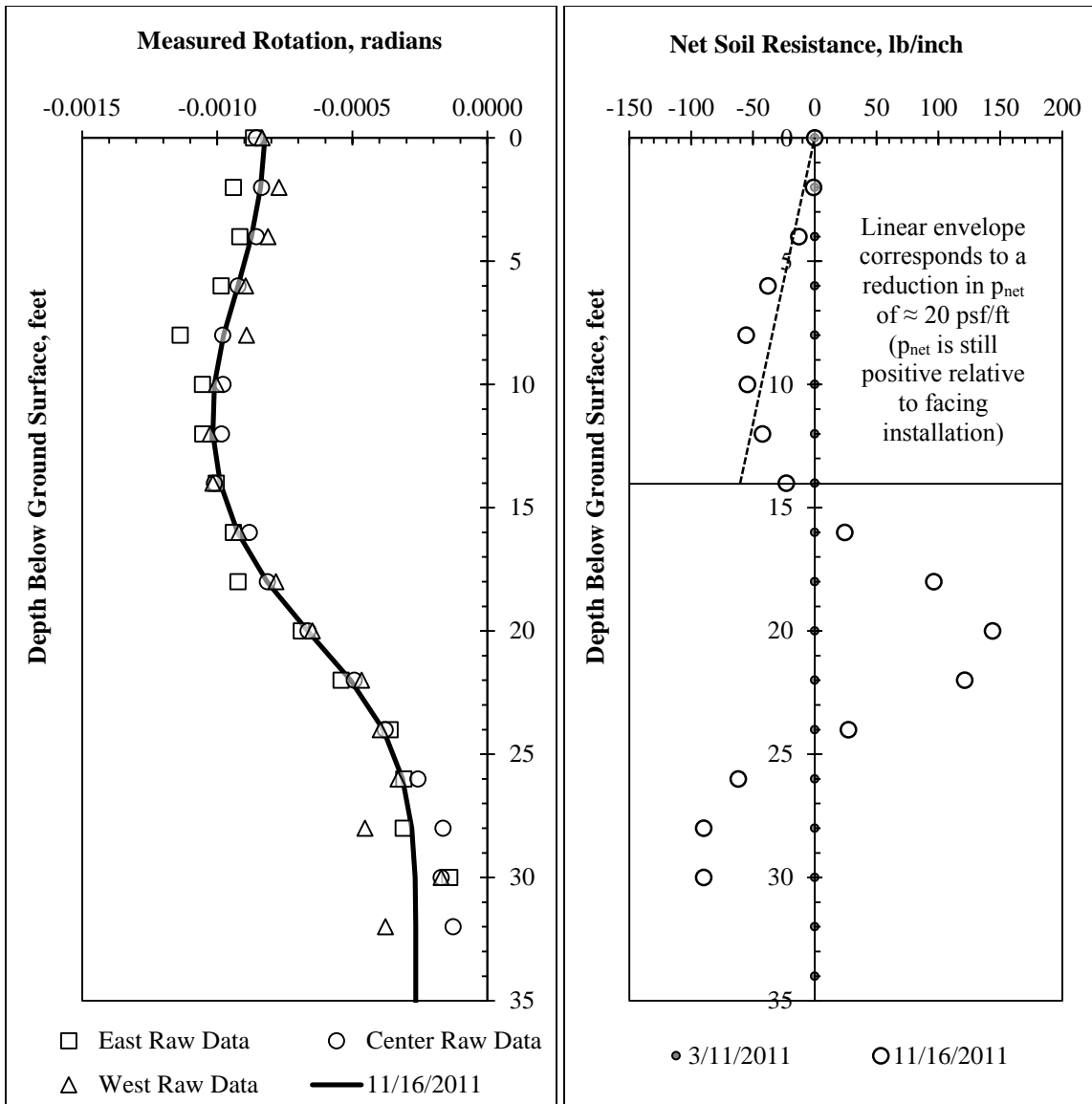


Figure 6.33: Profiles of shaft rotation and estimated reduction in net earth pressures in response to soil shrinkage between March 11 and November 16, 2011.

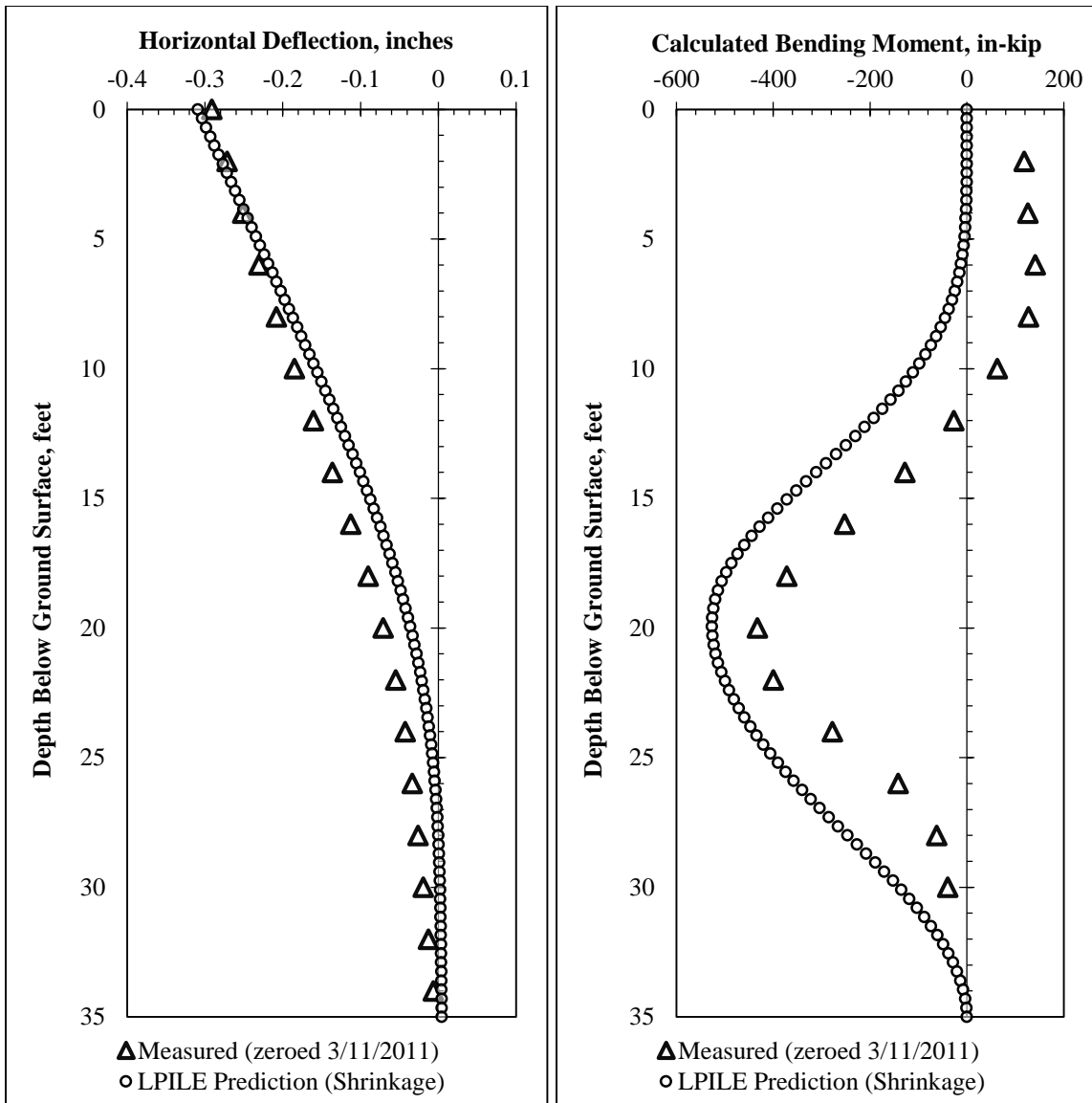


Figure 6.34: Comparison of LPILE prediction with horizontal deflections and bending moments between March 11 and November 16, 2011.

#### 6.4.4: THERMAL STRAINS AND BENDING CURVATURES

The discrepancy in measured and predicted bending moments in Figure 6.34 can be partially explained by thermal strains. Temperature differentials between the front and back side of the shaft can lead to the appearance of bending curvatures. As the exposed

side of the shaft heats up and expands, the back of the shaft moves less because of the insulating presence of the retained soil. The difference in thermal strains on the front and back sides of the shaft results in the development of a bending curvature. Although thermal deformations do not directly stress the shaft, the influence of thermal strains on recorded values of bending curvature can be mistaken for an applied bending moment in the loading analysis.

While the ambient air temperatures at the time of data recording were the same on March 11 and November 16, the temperature conditions preceding each reading were different. At the reference survey on March 11, a temperature increase of approximately 30 degrees Fahrenheit occurred in the four hours prior to the inclinometer survey. On November 16, the temperature increase during the same time period was approximately 13 degrees. Air temperature readings from a weather station near the test wall site are presented in Figure 6.35.

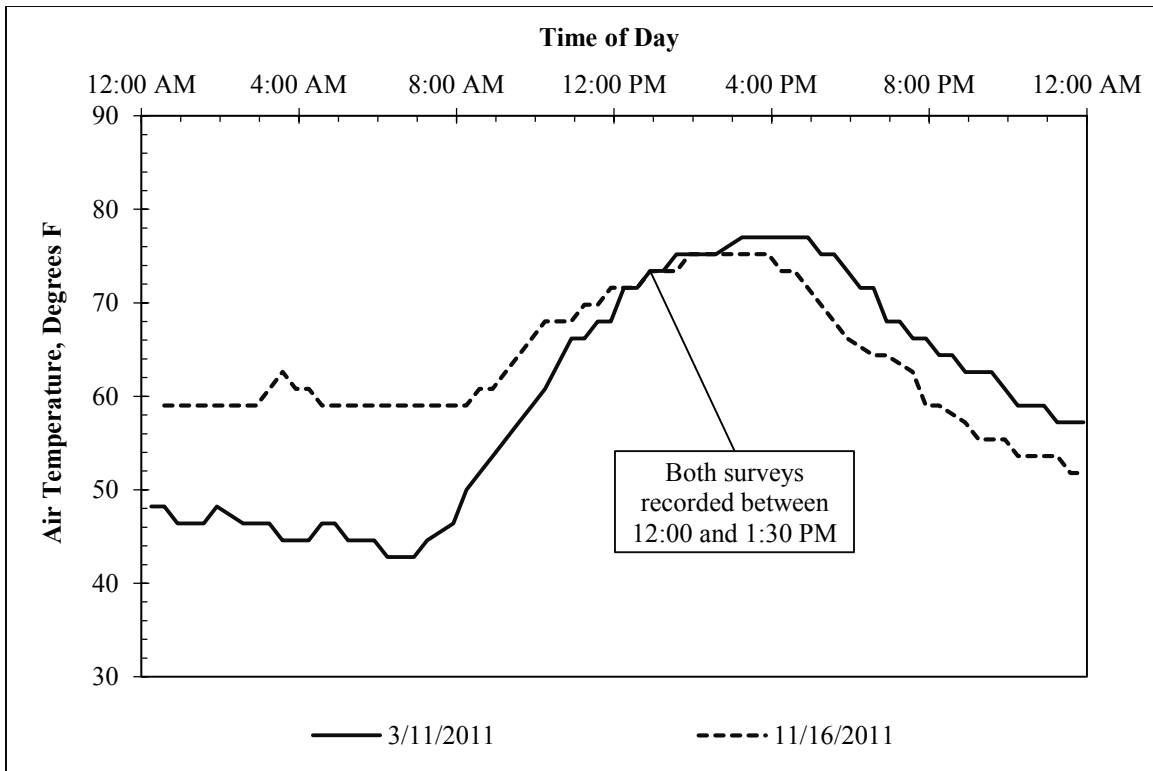


Figure 6.35: Air temperature in Manor, Texas on March 11 and November 16, 2011 (data from [www.wunderground.com](http://www.wunderground.com)).

#### 6.4.4.b: Daily Variation in Temperature and Bending Strains

To illustrate the daily effects of temperature fluctuation on the test wall, strain data from the center shaft can be compared with temperature data from a nearby weather station. To minimize the effects of wall deformation and seasonal temperature changes on data interpretation, five days of data from October 22 to October 27, 2011 are presented. During this time, the wall experienced minimal changes in deflection, and the daily values of maximum, minimum, and average temperature were similar. Results are presented in Figure 6.36.

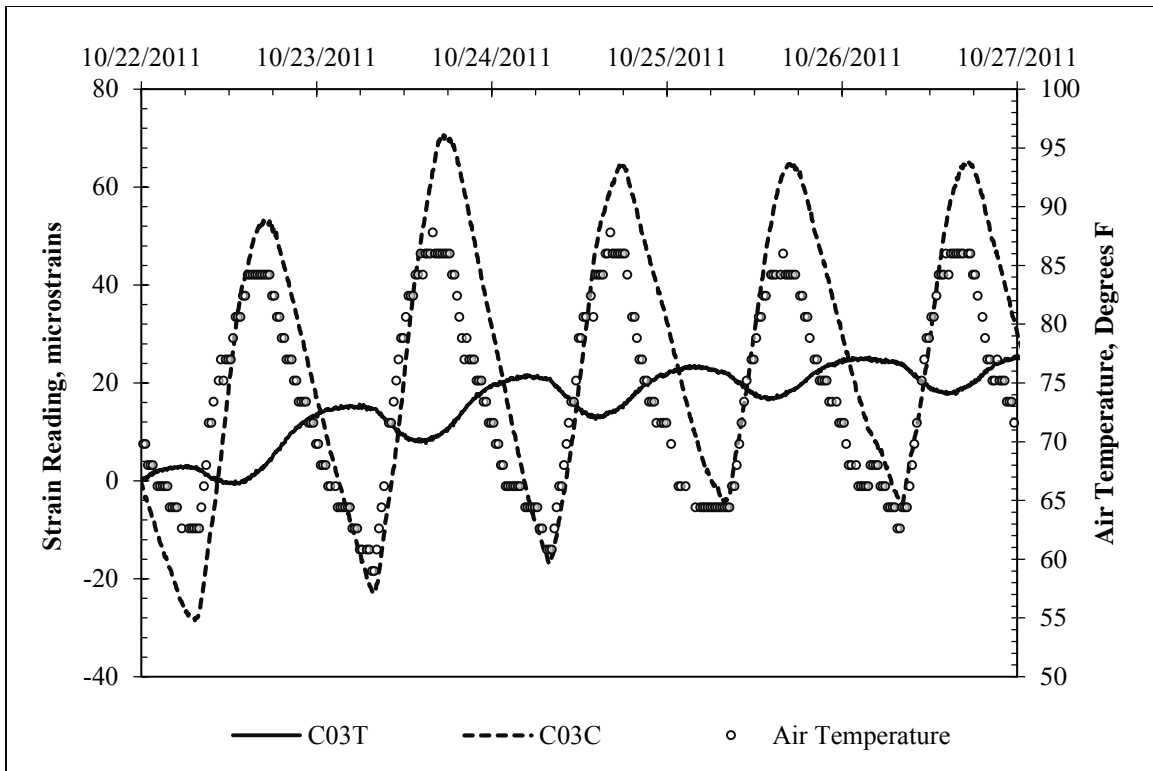


Figure 6.36: Comparison of air temperature in Manor, Texas and strain data at a depth of 3 feet in the center instrumented shaft (October 22 – October 27, 2011; weather data from [www.wunderground.com](http://www.wunderground.com)).

The wall responds relatively quickly to daily temperature fluctuations. The gauges on the compression side of the wall (3 inches from the exposed surface) reach their maximum strain within 3 to 4 hours after the air temperature reaches its maximum. The gauges on the tension side (21 inches from the exposed surface), however, do not reach their maximum until around 9 to 10 hours after the maximum air temperature. By this point, the air temperature has begun to decrease and reaches a minimum value soon after the tension side of the shaft reaches its maximum. Because bending curvatures in the shaft are related to the difference in strains between the front and back sides of the shaft, bending curvatures are affected by this hysteresis. Comparisons of bending curvature fluctuations in the test wall at depths of 3, 11, and 13 feet are presented in Figure 6.37.

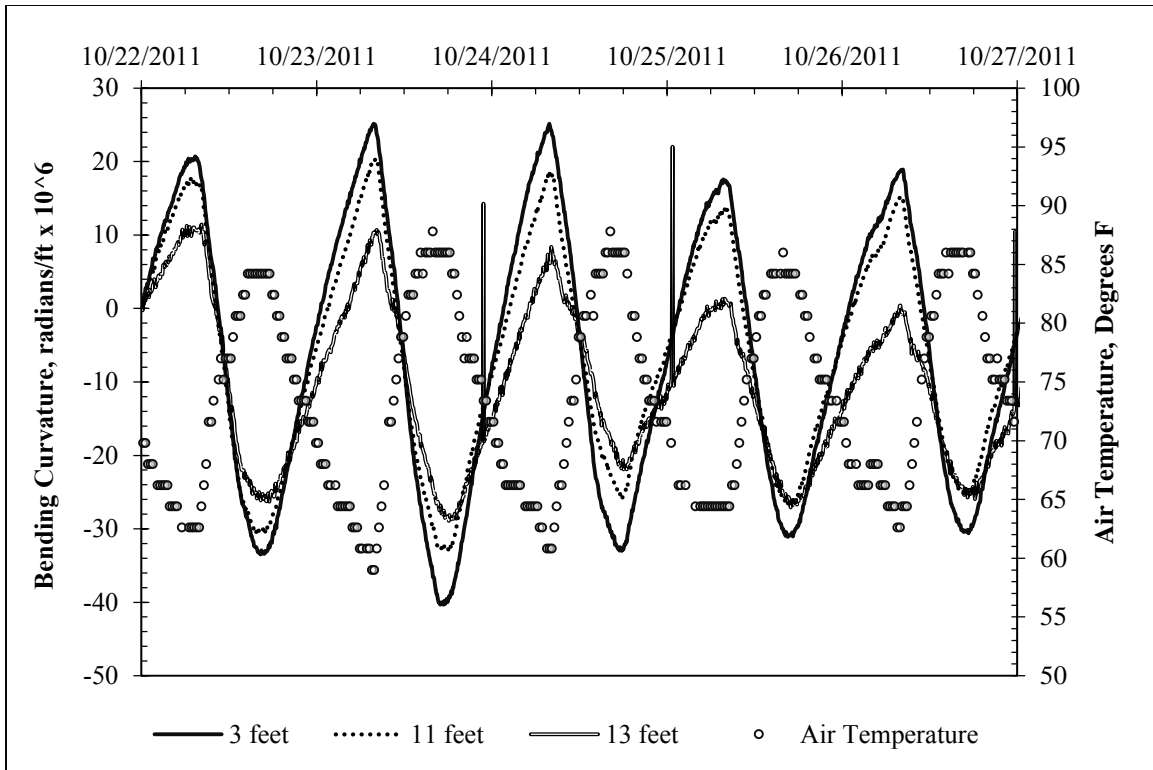


Figure 6.37: Comparison of air temperature in Manor, Texas and measured bending curvature in the test wall at various depths in the center shaft (temperature data from [www.wunderground.com](http://www.wunderground.com)).

From October 22 – 27, 2011, the daily temperature fluctuation ranged from 22 to 28 degrees Fahrenheit. During the same time, the average measured bending curvatures in the shaft above the excavation line were approximately  $40 \times 10^{-6}$  to  $50 \times 10^{-6}$  radians per foot. Although all gauges are the same distance from the exposed side of the shaft, the bending curvature induced by a given temperature change appears to decrease with depth below original ground surface (Figure 6.37). The maximum and minimum values of thermal bending curvature occur, respectively, at approximately the same time as the minimum and maximum values of air temperature (e.g. if temperatures are at their maximum at 5:00 PM, bending curvatures and wall deflections are at their minimum).

Based on the moment-curvature relationship for the test wall, the range of measured thermal bending curvatures are equivalent to applied “moment” fluctuations of approximately 250 to 300 in-kip.

If the measured bending curvatures are applied above the excavation line only (from 0 to 15 feet) and integrated twice, they correspond to a daily variation in top-of-wall deflection of approximately 0.05 to 0.10 inches (0.03 to 0.06% of the wall height). Over the entire monitoring period of three years, the test wall experienced an average daily temperature fluctuation of 22 degrees Fahrenheit, with a maximum recorded daily fluctuation of 48 degrees.

#### **6.4.4.c: Analysis of Thermal Deformations on March 11, 2011 and November 16, 2011**

On March 11, 2011, the bending curvatures induced by temperature change were relatively high, corresponding to a short-term increase of approximately 30 degrees Fahrenheit. On November 16, the temperature increase was much smaller, approximately 13 degrees, and the thermal bending curvatures were accordingly smaller. When March 16, 2011 is used as the reference survey, the reduced thermal bending curvatures on November 16 appear in the analysis as additional bending moments of between 100 and 150 in-kip. Based on the data from Figure 6.37, an air temperature difference of approximately 18 degrees is consistent with a bending curvature corresponding to a bending moment of about 150 in-kip.

To simulate the effects of thermal bending curvatures in the LPILE analysis, a bending moment of 150 in-kip (equivalent to the average difference between measured and predicted moment curves) was applied to the top of the shaft. Input parameters for the LPILE analysis are summarized in Table 6.2. Results of the LPILE analysis are provided in Figure 6.38 and Figure 6.39.

Table 6.2: Baseline assumptions and design parameters for soil shrinkage LPILE analysis, accounting for thermal bending curvatures.

Parameter	Value
Effective Unit Weight of Soil, $\gamma$	62.6 pcf
Earth Pressure Loading	Input Envelope from Calculated $p_{net}$
Additional Moment Applied at Top for Thermal Effects	150 k-in
Friction Angle of Foundation Soil	24 degrees
Foundation Soil p-y Curves	Sand (Reese)
Non-Default Initial Stiffness, $k_{py}$	375 lb/in <sup>3</sup>
Cracking Moment, $M_{Cr}$	680 k-in.
Yielding Moment, $M_y$	3,200 k-in.
Uncracked Bending Stiffness, $EI_{uc}$	67 x 10 <sup>6</sup> k-in.
Cracked Bending Stiffness, $EI_{cr}$	18 x 10 <sup>6</sup> k-in.
Shaft Diameter	24 in.
Height of Retained Soil, H	168 in.
Reinforcement	12 #7 bars (1.6% of gross area)



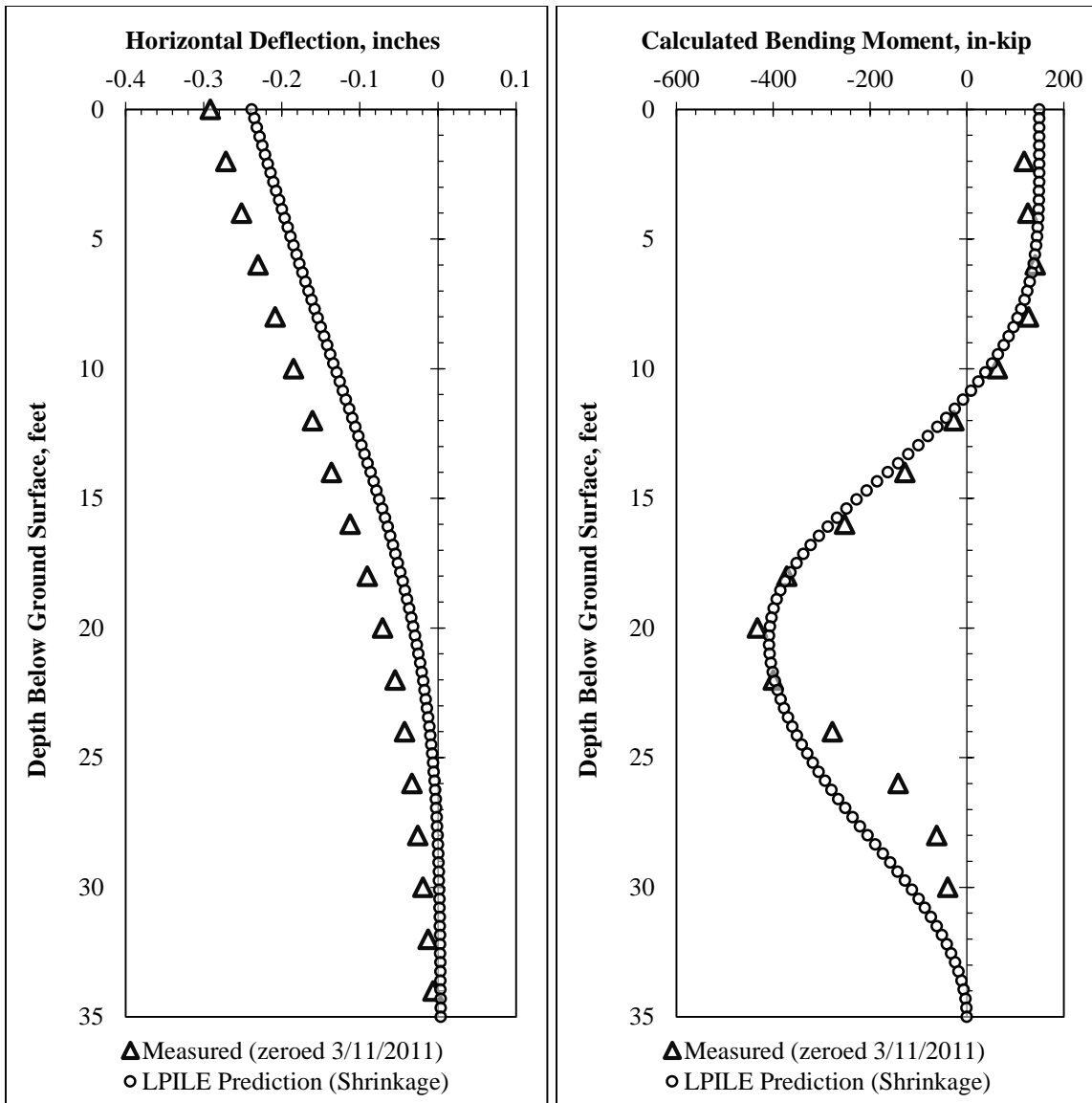


Figure 6.38: Comparison of LPILE prediction with horizontal deflections and bending moments between March 11 and November 16, 2011. A bending moment of 150 in-kip was applied at the top of the shaft to simulate thermal effects.

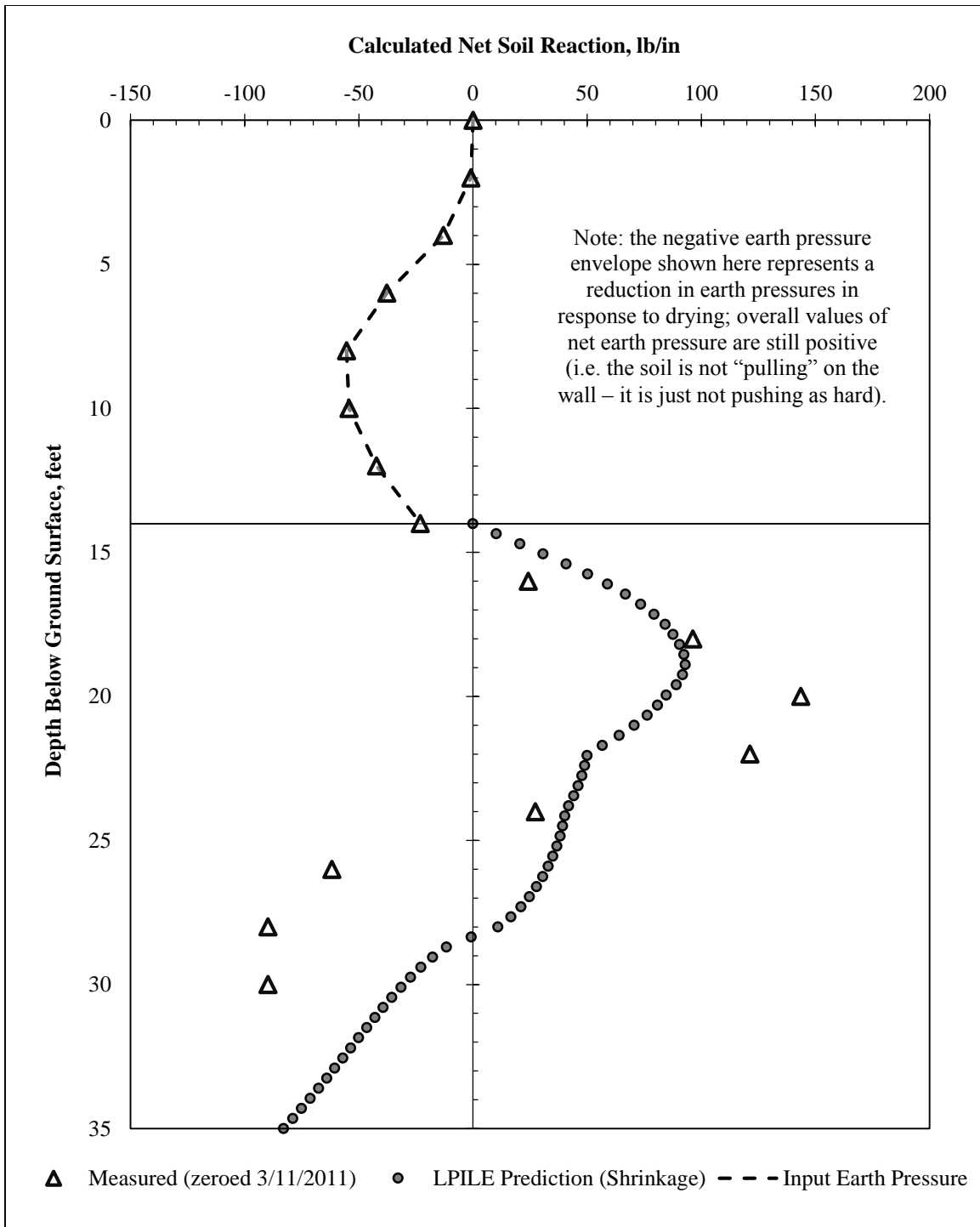


Figure 6.39: Comparison of measured and calculated soil reaction forces due to expansive soil shrinkage.

#### **6.4.5: EARTH PRESSURE INCREASES FROM SOIL EXPANSION**

The analysis of earth pressures induced by soil wetting during inundation testing (discussed in Chapter 7) suggests that the increases in wall deflections due to wetting are due to the presence of water causing softening of the retained soil and loss of resistance in the foundation soil. The increase in deflections with increased moisture content is gradual and takes place over a period of months. There is limited evidence to suggest that extremely high earth pressures due to soil expansion exist at the test wall (in the upper three to five feet of soil, where the theoretical potential for large swell pressures exists, calculated earth pressures are consistently low). Because the response of the test wall to natural wetting cycles is similar to the response during controlled inundation testing, earth pressure increases due to soil expansion are covered in the following chapter.

### **6.5: Summary and Conclusions**

Data recorded at the Lymon C. Reese research wall during natural moisture cycles has provided some insight into the behavior of drilled shaft retaining walls during cycles of wetting and drying. Conclusions include:

- During cycles of drying, wall deflections decreased. This is primarily due to volumetric shrinkage of the soil, which leads to an equivalent reduction in earth pressures. After 8 months of extreme drought, deflections at the test wall decreased by approximately 0.3 inches, and the earth pressure reduction corresponds to a decrease in equivalent fluid pressure of approximately 20 psf/ft. The effects of soil shrinkage can be approximated with the use of an equivalent “negative earth pressure” envelope with p-y curves using fully softened, drained strength parameters with initial stiffness  $k_{py}$  defined by the original profile of undrained

- shear strength. This method provides approximations close to the measured values, but does not account for the increase in soil stiffness with drying.
- During cycles of wetting, wall deflections increased. This is primarily due to a combination of soil swelling and the dissipation of negative pore pressures. The presence of water contributes to both increased earth pressures (softening of the retained soil) and decreased resistance (softening of the foundation soil). There is little evidence at the test wall to suggest that high lateral earth pressures due to soil expansion are imposed.
  - The use of Time Domain Reflectometry (TDR) probes to measure moisture content in expansive clay is problematic because of the soil's high electrical conductivity and tendency to pull back from the probe rods during drying cycles. However, electrical conductivity measurements from one TDR probe appear to correlate with moisture contents and top-of-wall deflections. While the electrical conductivity data cannot be directly related to moisture content, it can provide a qualitative indicator of the moisture conditions on the project site.
  - The direct use of strain gauge data for the determination of bending curvature generally requires more advanced data interpretation than simply taking the first derivative of rotation profiles measured from inclinometer data. This difficulty is primarily due to the heterogeneous behavior of the concrete with depth, the appearance of tension cracks at bending moments close to the cracking moment, and the tendency of strain gauges to measure a variety of processes in addition to wall deformations resulting from lateral loads. While individual strain gauges measure localized, variable processes within the shaft, the inclinometer casing measures global behavior that can be more easily used directly without subjective data analysis.

- Daily cycles of thermal strains can influence data interpretation. If the climatic conditions on survey dates are substantially different, bending curvatures induced by daily temperature differences can be mistaken for bending moments caused by changes in earth pressure. The test wall experiences an average daily temperature fluctuation of approximately 22 degrees Fahrenheit, which corresponds to a daily variation in top-of-wall deflection of approximately 0.05 to 0.1 inches. Daily temperature fluctuations as high as 48 degrees have been recorded at the test site.
- Because thermal deformations are tedious to model without detailed weather data, and their effect on wall behavior is relatively small, large-scale corrections to the data set for temperature effects are generally not practical. However, if isolated surveys with unusual deflection, rotation, or bending curvatures are observed in the data, consideration of thermal effects is needed.

## **CHAPTER 7: TEST WALL BEHAVIOR DURING CONTROLLED INUNDATION TESTING (MAY 2012 – JULY 2013)**

### **7.1: Overview**

During the extremely dry summer of 2011, the research plan was modified to include cycles of artificial inundation of the retained soil. Based on climatic history and the available long-term weather forecasting, it was deemed unlikely that the soil on the project site would ever sustain the high moisture contents necessary to investigate the effects of soil expansion on wall behavior. By increasing soil moisture content behind the wall to an upper-bound condition, the influence of soil wetting and expansion on the earth pressures can be more readily estimated. Beginning in May 2012, the retained soil was provided unlimited access to water for two months, followed by a seven month drying cycle. In February 2013, the retained soil was inundated until the top-of-wall deflections reached equilibrium, a period of approximately four additional months.

### **7.2: Summary of Key Events**

#### **7.2.1: SITE INVESTIGATION AND INSTALLATION OF INUNDATION BERM AND PIEZOMETERS**

On February 23, 2012, a site investigation was conducted and four stand pipe piezometers were installed as shown in Figure 7.1. On April 26, 2012, the inundation berm was constructed as shown in Figure 7.2 – Figure 7.3.

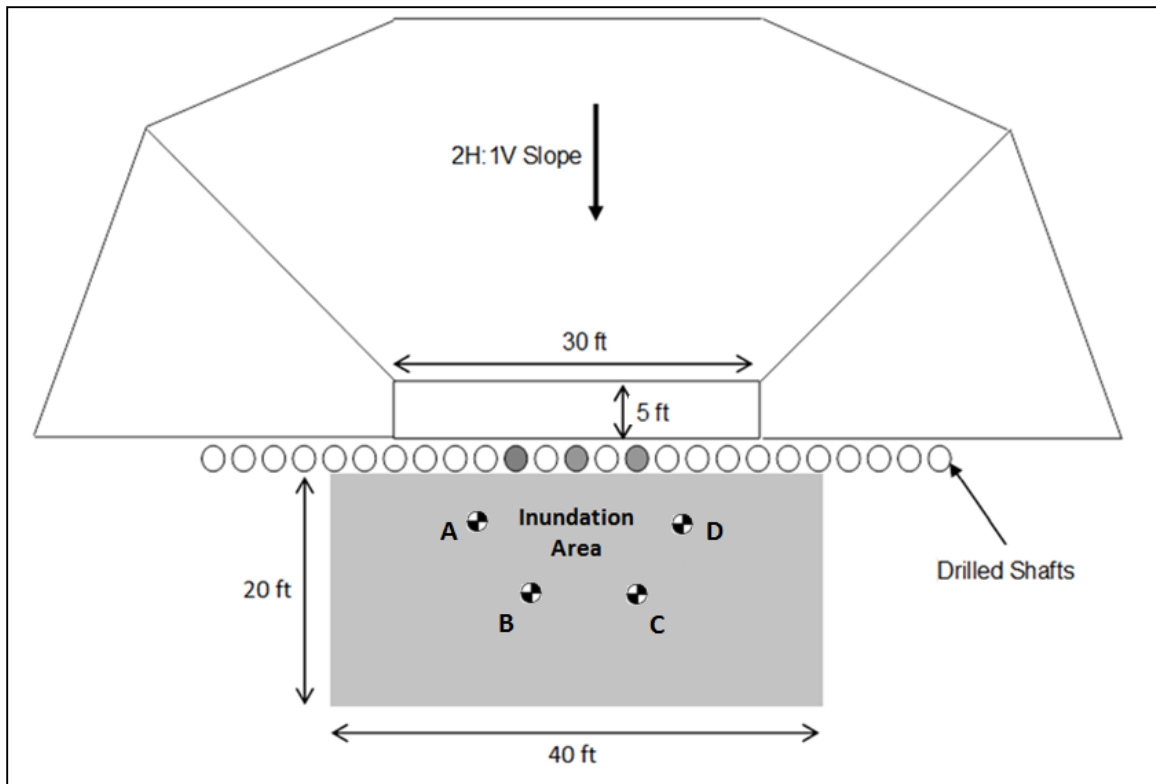


Figure 7.1: Location of inundation zone and stand pipe piezometers. Piezometers A and C are screened from 5 to 15 feet; piezometer B is screened between 3.4 and 4.6 feet; piezometer D is screened between 3.6 and 4.8 feet.

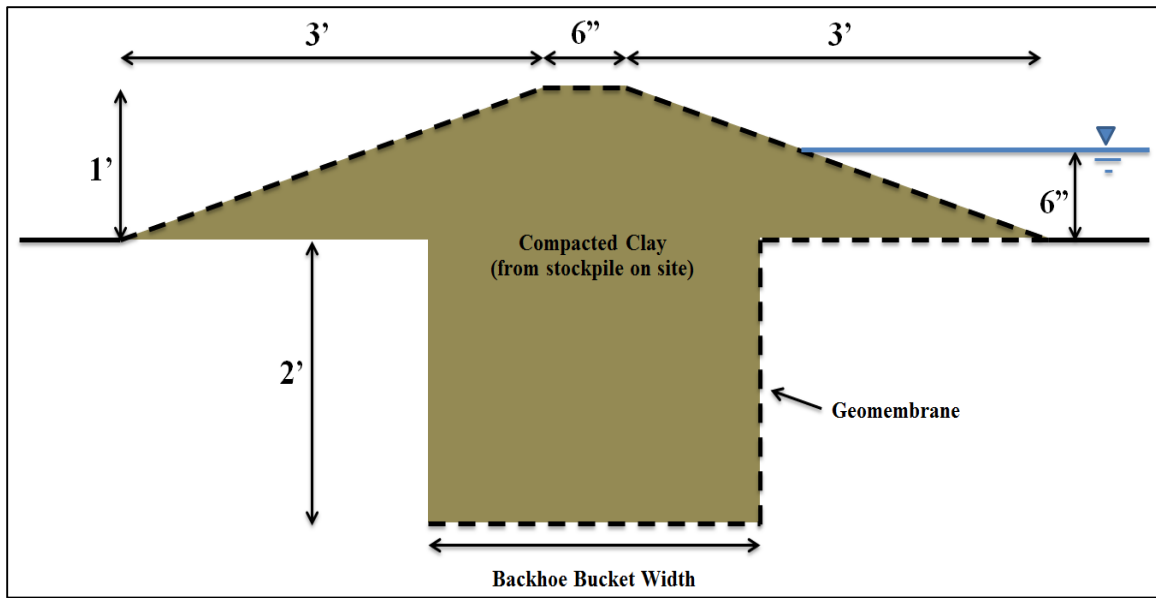


Figure 7.2: Schematic of inundation berm.

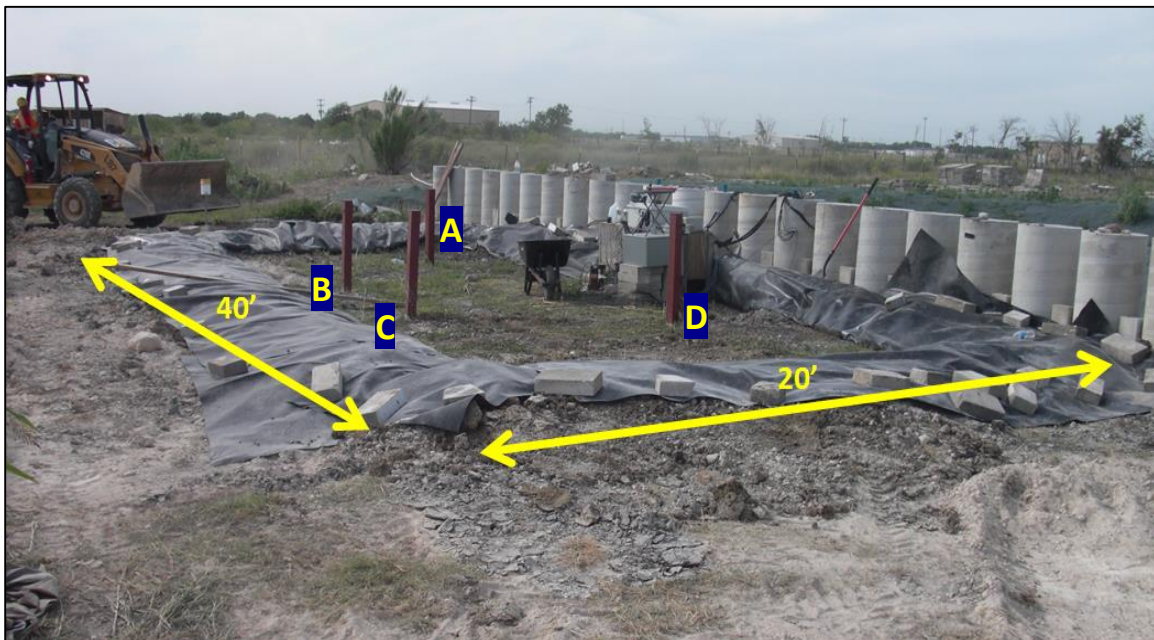


Figure 7.3: Inundation berm and stand pipe piezometers (April 26, 2012).



## **7.2.2: SUMMARY OF INUNDATION CYCLES**

### **7.2.2.a: First Inundation Cycle (May 2012 – July 2012)**

Beginning on May 3, 2012, the inundation zone was filled. Wall deflections increased steadily for approximately two months until July 2, 2012, when the water supply to the pond was stopped and the wall was allowed to return to its natural state.

### **7.2.2.b: First Drying Cycle (July 2012 – February 2013)**

From July 2012 to February 2013, the wall was not provided access to moisture beyond naturally occurring rainfall on the project site. Over this time period, deflections fluctuated slightly, but did not increase or decrease to a degree consistent with a significant change in loading conditions.

### **7.2.2.c: Second Inundation Cycle (February 2013 – June 2013)**

Beginning on February 5, 2013, the inundation zone was filled a second time. After approximately four months of inundation, the wall deflections and piezometer water levels stabilized. In response to a large storm event, a major flood occurred in which the water level in the excavation reached the ground surface prior to the inclinometer and strain gauge data surveys recorded on May 6, 2013 (Figure 7.4). During this flood event, significant erosion of the excavation slopes occurred; due to additional soil transported to the excavation base, the excavation depth had decreased to approximately 13.5 feet below ground surface.



Figure 7.4: Flooding in response to a large storm before the May 6, 2013 data surveys. Water level in the excavation reached ground surface.

#### **7.2.2.d: Second Drying Cycle (June 2013 – July 2013)**

On June 3, 2013, a second drying cycle began. Water moved out of the soil quickly, and shrinkage cracks appeared in the surface soil (Figure 7.5). As water moved out of the soil, top-of-wall deflections began to decrease fairly quickly. At the time of this writing, the wall deflections had been monitored during drying for a period of approximately two months. At the conclusion of data recording in July 2013, top-of-wall deflections and stand pipe piezometer levels had nearly stabilized, but had not completely reached equilibrium. Based on previous observations, it is likely that when water levels return to their natural values of approximately 8 feet below ground surface, the top-of-wall deflections will stabilize.



Figure 7.5: Inundation zone on June 17, 2013, two weeks into second drying cycle. Stand pipe piezometer casing is 4" across.

### **7.2.3: CLIMATIC INFORMATION**

Monthly rainfall totals for Austin, Texas during controlled inundation testing are presented in Figure 7.6. Daily temperature measurements for Manor, Texas are presented in Figure 7.7. While rainfall data during periods of wall inundation is useful to get a sense of the soil conditions outside the influence of the inundation zone, rainfall data during the drying cycle from July 2012 to February 2013 is of most interest. For the first three months of the drying cycle during July through September 2012, rainfall totals were above average, followed by four months of below average rainfall between October and December, 2012. During January 2013, rainfall totals began to increase before the beginning of the second inundation cycle in February 2013.

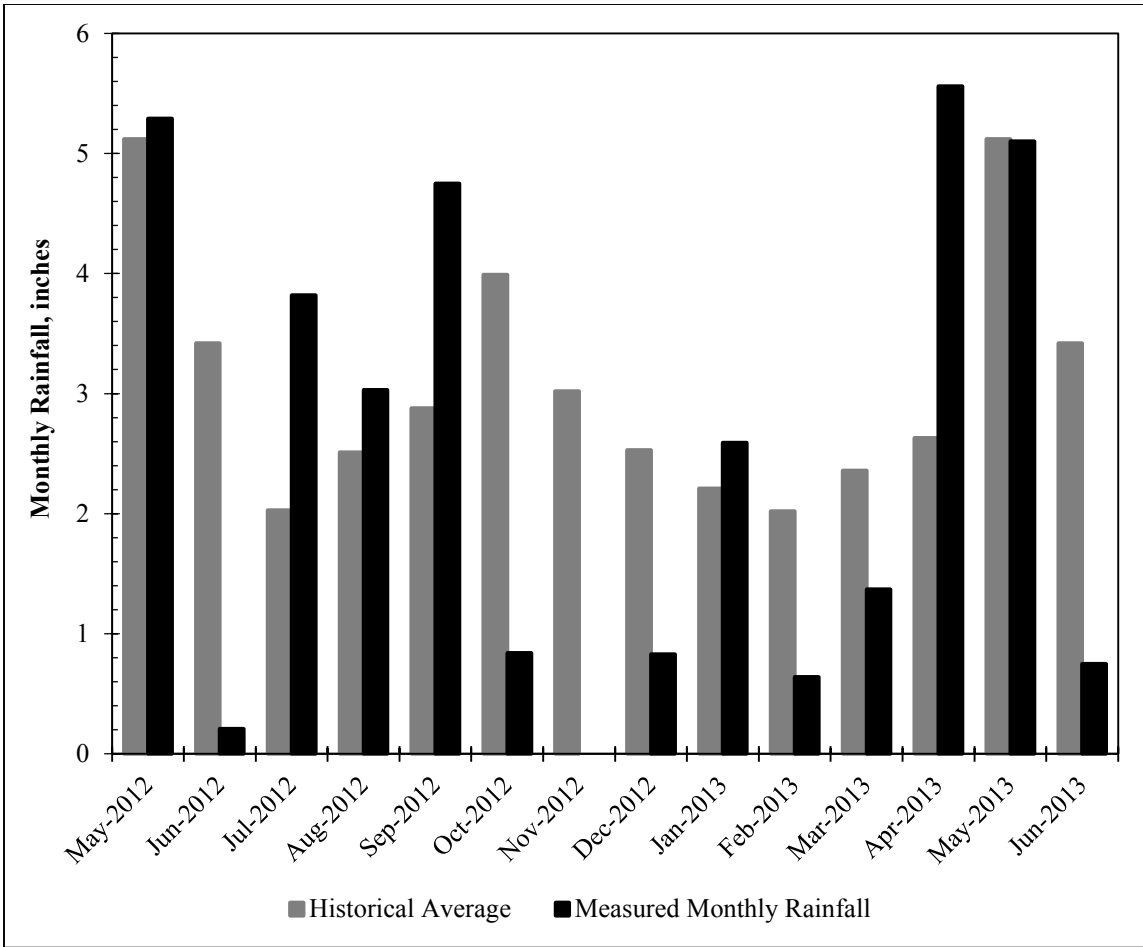


Figure 7.6: Monthly rainfall totals for Austin, Texas (May 2012 - Jun. 2013; data from [www.wunderground.com](http://www.wunderground.com)).

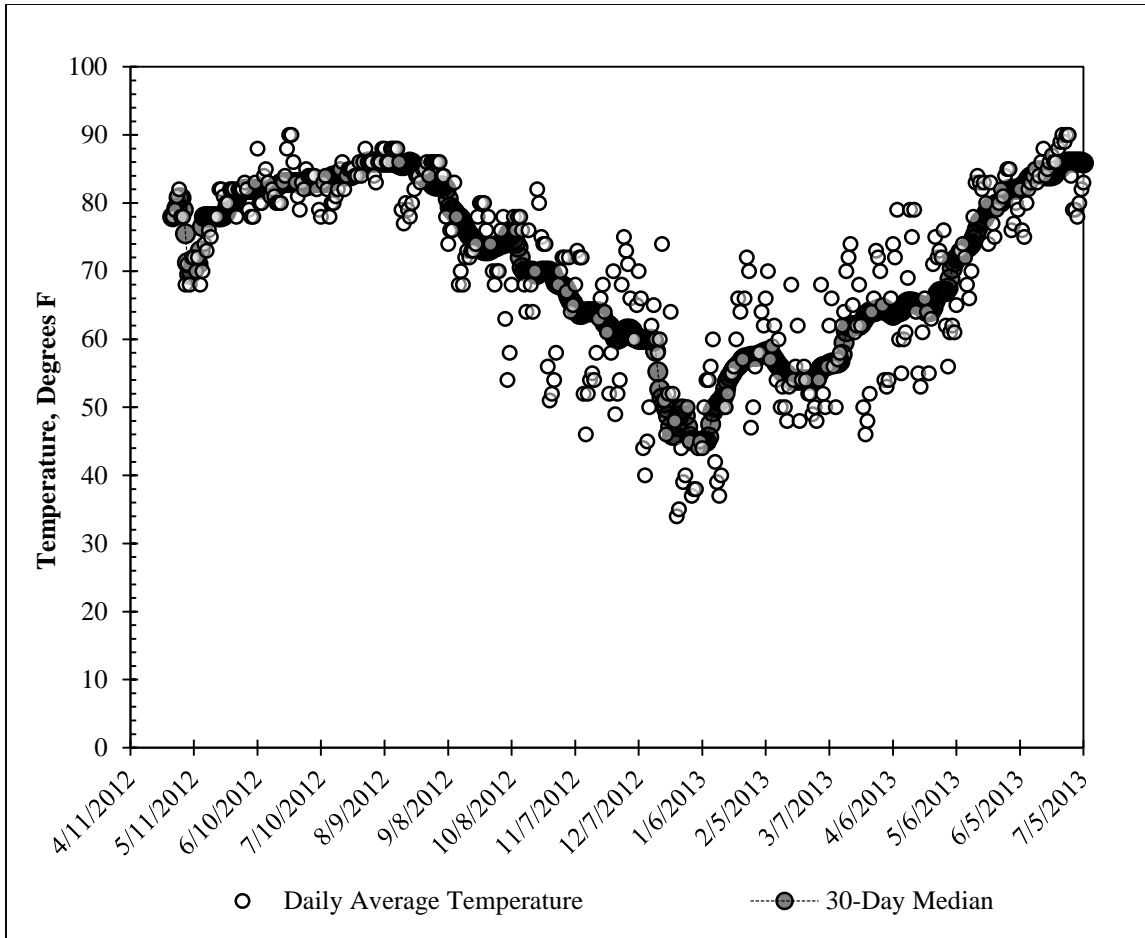


Figure 7.7: Daily average temperature data for Manor, Texas (May 2012 - Jul. 2013; data from [www.wunderground.com](http://www.wunderground.com)).

### 7.3: Summary of Field Instrumentation Data

#### 7.3.1: INCLINOMETER DATA

Inclinometer data is referenced to the installation of facing in October, 2010. Average deflected shapes are presented in Figure 7.8, top-of-wall deflections are presented in Figure 7.9, and the rate of deflection at ground surface is presented in Figure 7.10.

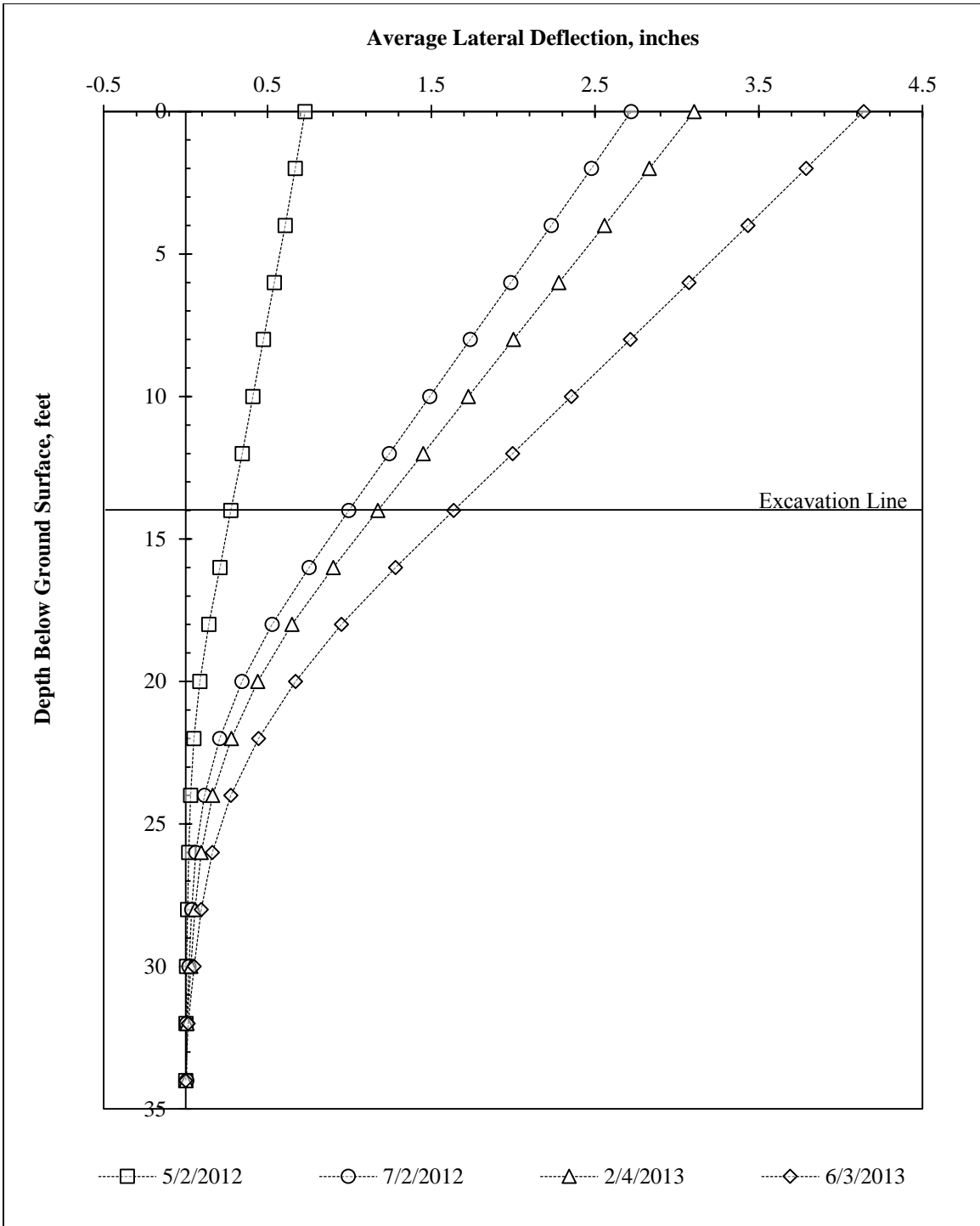


Figure 7.8: Average deflected shapes at key dates during inundation testing. Data is referenced to installation of facing in October, 2010.

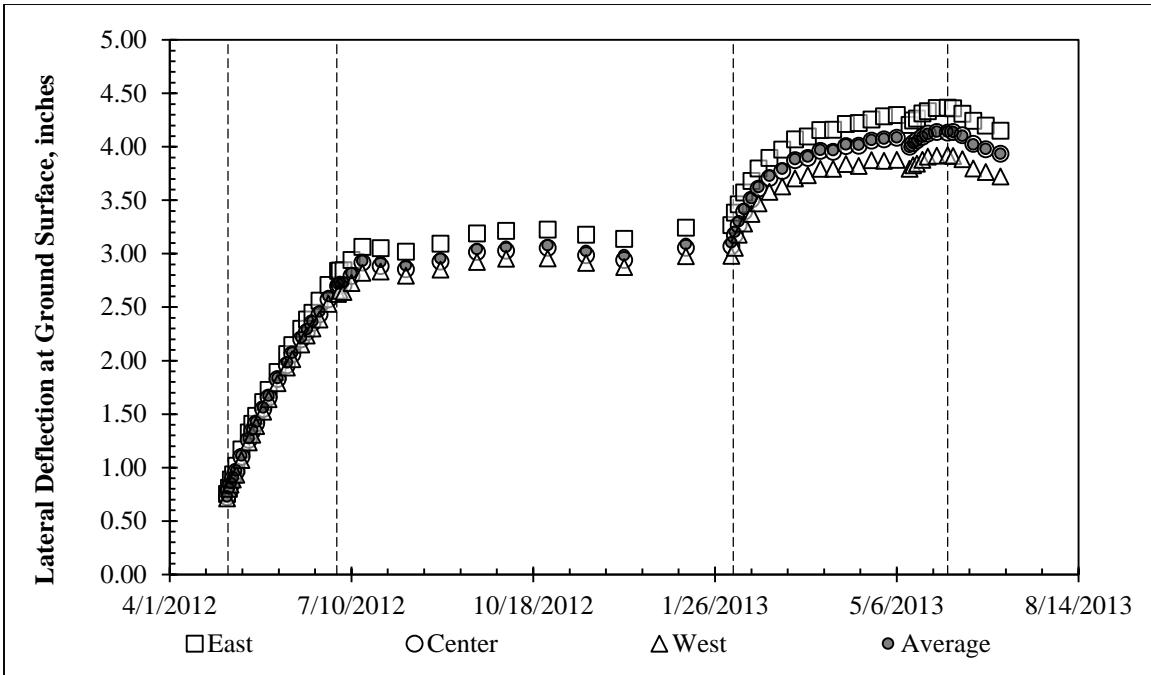


Figure 7.9: Top-of-wall deflections during inundation testing (key dates indicated by vertical dashed lines). Reference survey is facing installation in October, 2010.

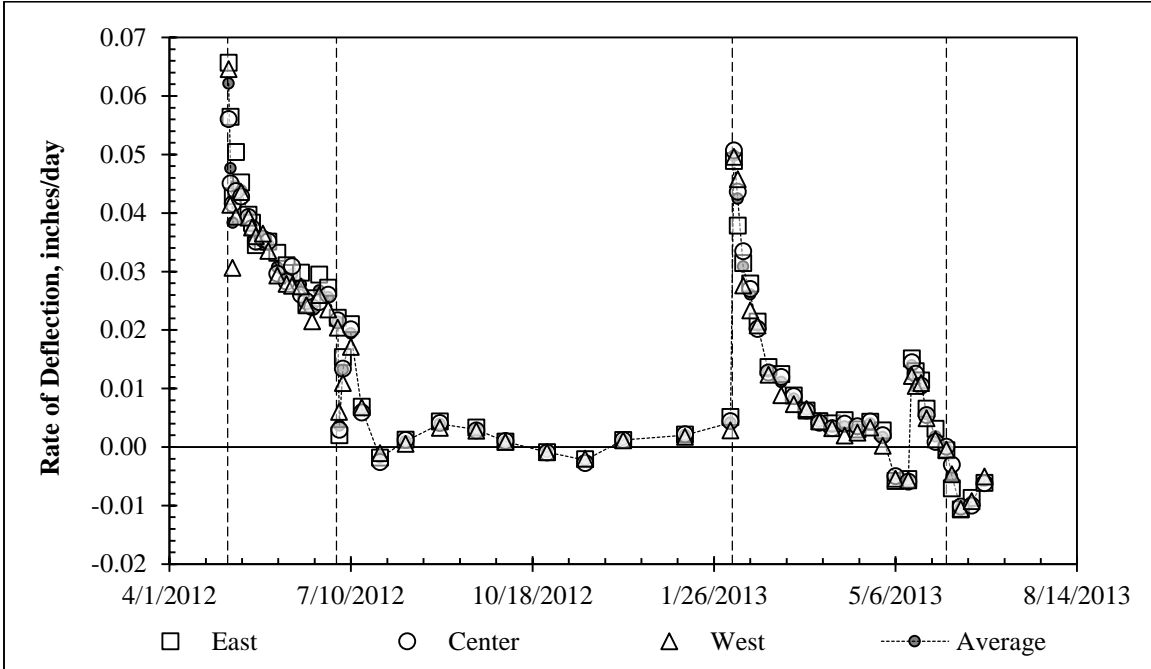


Figure 7.10: Rate of deflection at ground surface during inundation testing (key dates indicated by vertical dashed lines).

### **7.3.2: SOIL MOISTURE CONTENT DATA**

A summary of measured soil moisture contents during controlled inundation testing is provided in Figure 7.11. Data from samples using a hand auger, as well as data from geotechnical investigations conducted by Fugro Consultants, Inc., is provided. While a wide range of moisture contents were measured throughout the testing, in general, measured moisture contents ranged from approximately 15 to 35 percent in the zone above the natural groundwater table. At the conclusion of the second inundation cycle, moisture contents had increased to approximately 30 percent over the entire depth of the active zone (above the natural groundwater table at 8 feet below ground surface). While the final values of moisture content were similar at the conclusion of the first and second inundation cycles between 0 and 4 feet below ground surface, the second inundation cycle resulted in additional wetting of the soil between 4 and 8 feet below ground surface. Below the groundwater table at a depth of 8 feet, the soil transitions from dark brown Taylor clay to tan Taylor clay, and the natural moisture contents increase to between approximately 34 and 40 percent.



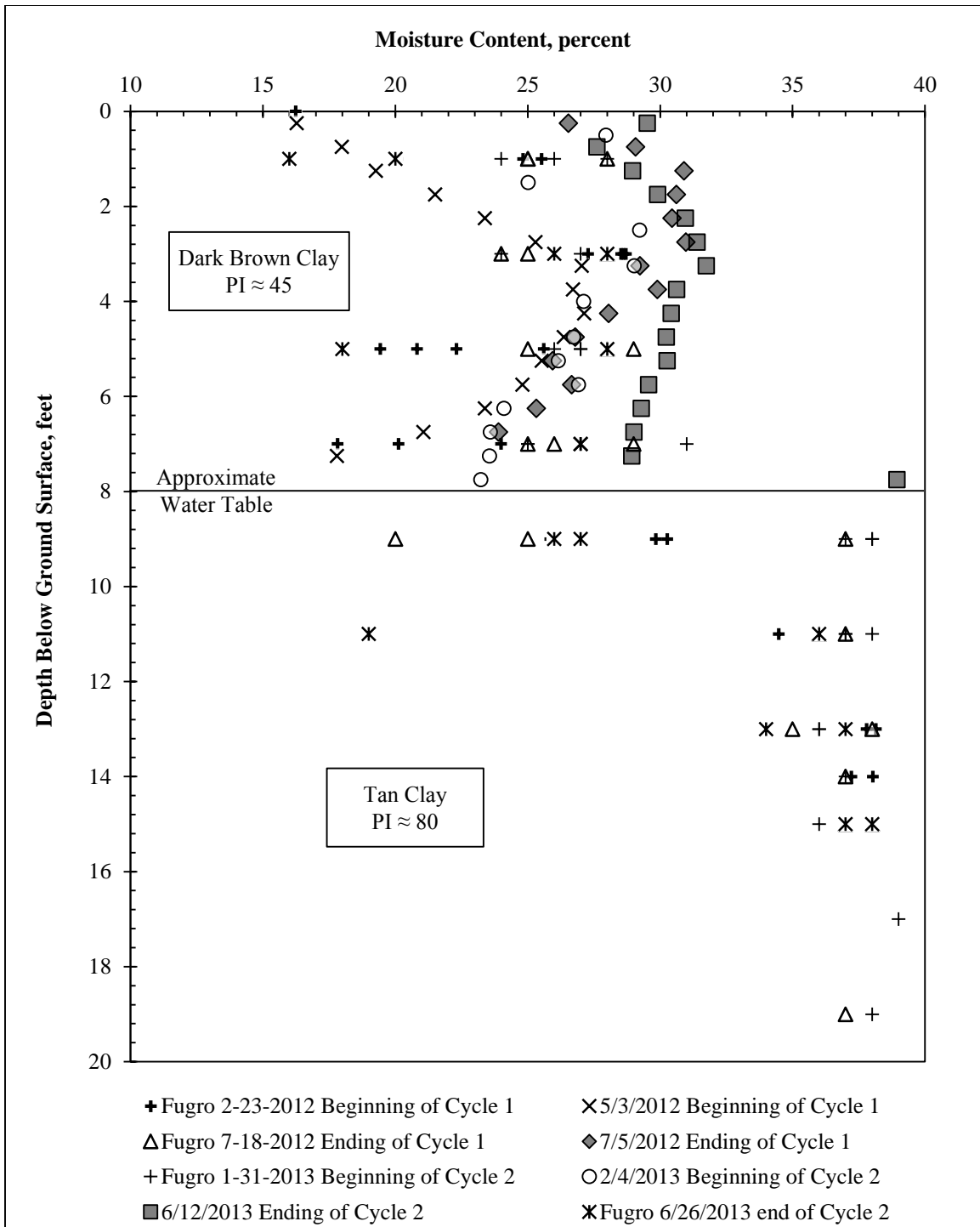


Figure 7.11: Summary of measured soil moisture contents during controlled inundation testing.

### 7.3.3: STAND PIPE PIEZOMETER DATA

Data from the stand pipe piezometers were recorded at regular intervals for the duration of inundation testing. Piezometer B-3 was installed and developed in 2010; consequently, water levels can be plotted for all inundation cycles (Figure 7.12). Piezometers A, B, C, and D were not properly developed after installation and did not show reliable data until the second inundation cycle. Data from the second cycle is presented in Figure 7.13 (piezometers with shallow screen intervals) and Figure 7.14 (piezometers with deeper screen intervals).

The water level in Piezometer B-3 was relatively unaffected by the presence of water in the inundation zone. The increased values in May, 2012 were associated with flooding on the project site that infiltrated the piezometer casing, and most likely do not represent the actual groundwater conditions. At the conclusion of inundation testing in July, 2013, the water level had stabilized at approximately 8.5 to 9 feet below ground surface.

The water levels in the piezometers with shallow screen intervals stabilized at approximately 0.5 and 1.3 feet below ground surface during the second inundation cycle, before increasing during a large flood in May, 2013 by approximately 0.3 feet. After the flood, water levels returned to values slightly higher than their original equilibrium values. The discrepancy in equilibrium water heights may be due to the development of steady-state seepage conditions, in which a cone of depression near the wall face leads to lowered water levels in stand pipe piezometers close to the wall (Figure 7.13). In piezometers with deeper screen intervals, water levels showed a similar trend, with equilibrium water levels increasing slightly after flooding in May, 2013. Water levels were similarly lowered in the piezometer closer to the wall face. At the conclusion of inundation testing, despite the small cone of depression near the wall facing drains, conditions close to hydrostatic pressures had likely developed in much of the retained soil. After the water supply was

stopped in June, 2013, water levels in all piezometers immediately began to decrease toward their pre-inundation values.

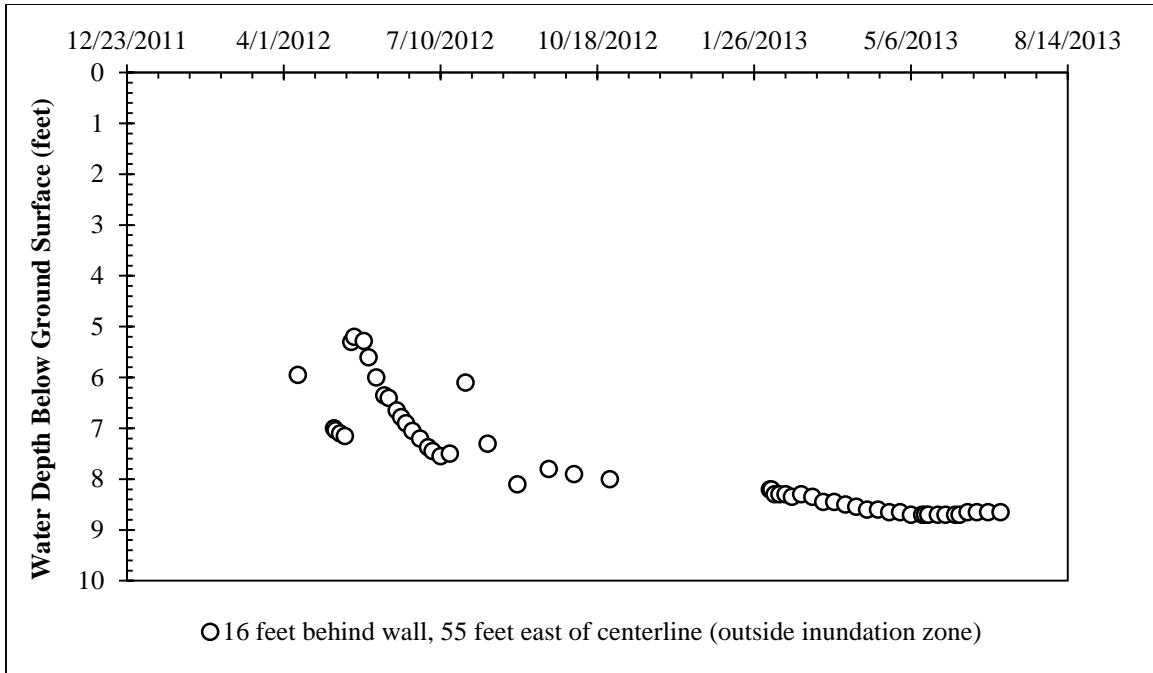


Figure 7.12: Water level in Piezometer B-3 (outside inundation zone) during inundation testing.

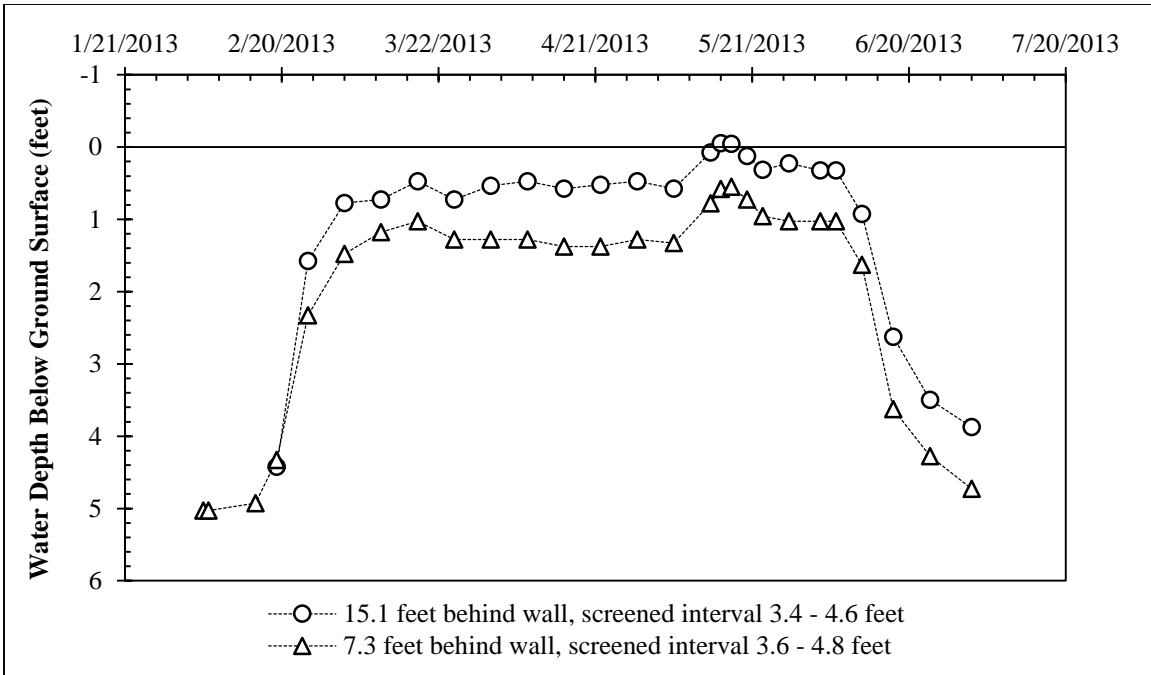


Figure 7.13: Data from shallow-screened stand pipe piezometers during second inundation cycle.

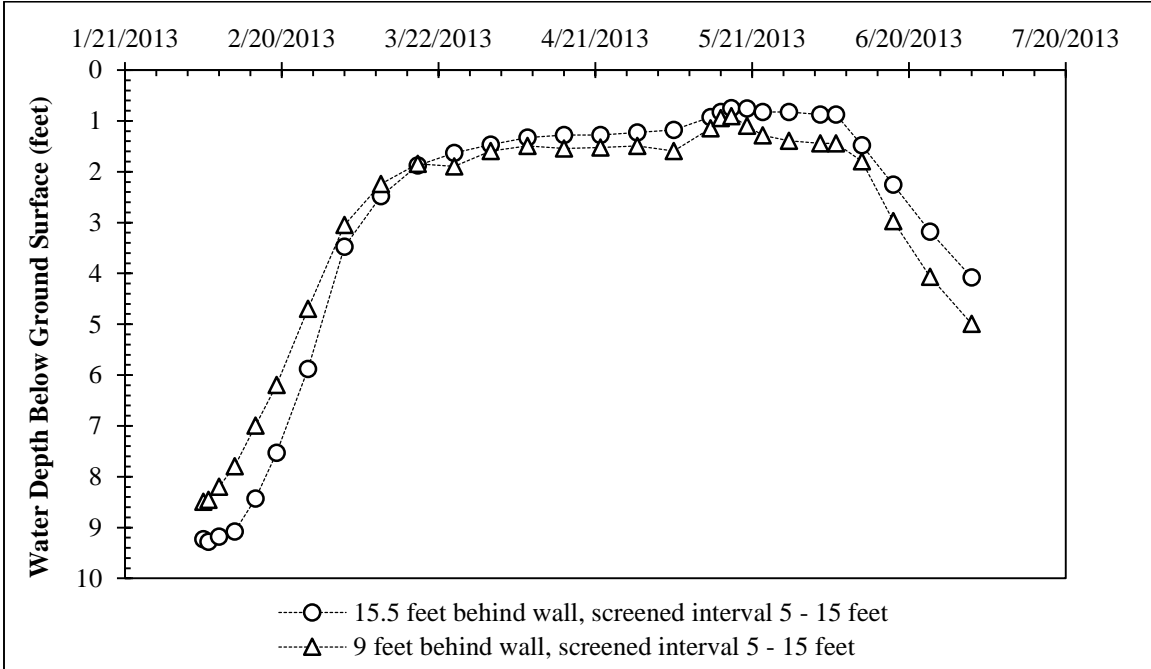


Figure 7.14: Data from deeper-screened stand pipe piezometers during second inundation cycle.

#### **7.3.4: TIME DOMAIN REFLECTOMETRY (TDR) PROBE DATA**

Data from the most functional TDR probe, which was installed 1.5 feet below ground surface, is presented in Figure 7.15 to Figure 7.19. Over the course of inundation testing, measured electrical conductivity values ranged from approximately 1.5 dS/m during the first inundation cycle, to zero during periods of drying (Figure 7.15).

During the first inundation cycle, electrical conductivity values increased immediately in response to the presence of water. Within one month, values had stabilized and had begun to steadily increase at the conclusion of the first inundation cycle (Figure 7.16). During the first drying cycle, values began to decrease quickly after the water supply to the inundation zone was removed, and had reached a zero value within six weeks (potentially indicating soil shrinkage leading to loss of probe rod contact). Rainfall events in August and September, 2012 led to short increases in electrical conductivity, followed immediately by gradual returns to zero during drying (Figure 7.17). The second drying cycle concluded with a period of above average rainfall in January, 2013, in which electrical conductivity values remained above zero for several weeks.

During the second inundation cycle, the probe again showed immediate response to the presence of water. Measured values of electrical conductivity continued to increase throughout the second inundation cycle, though not to values as high as those recorded during the first inundation cycle (Figure 7.18). After wall deflections and water levels stabilized, the second inundation cycle was stopped. Within one week after stopping the water supply to the inundation zone, a sudden decrease in electrical conductivity values occurred (perhaps indicating the local water level dropping below the probe), and within three weeks, values had returned to zero (Figure 7.19).

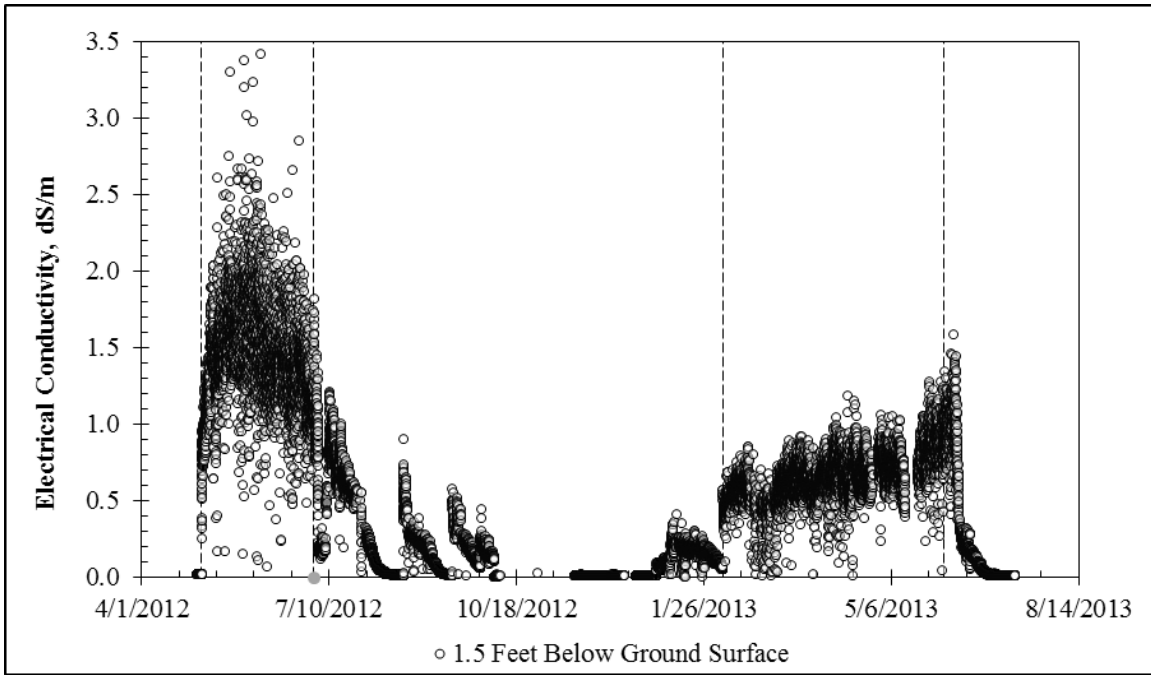


Figure 7.15: Electrical conductivity data from a TDR probe located 1.5 feet below ground surface (May 2012 – Jul. 2013).

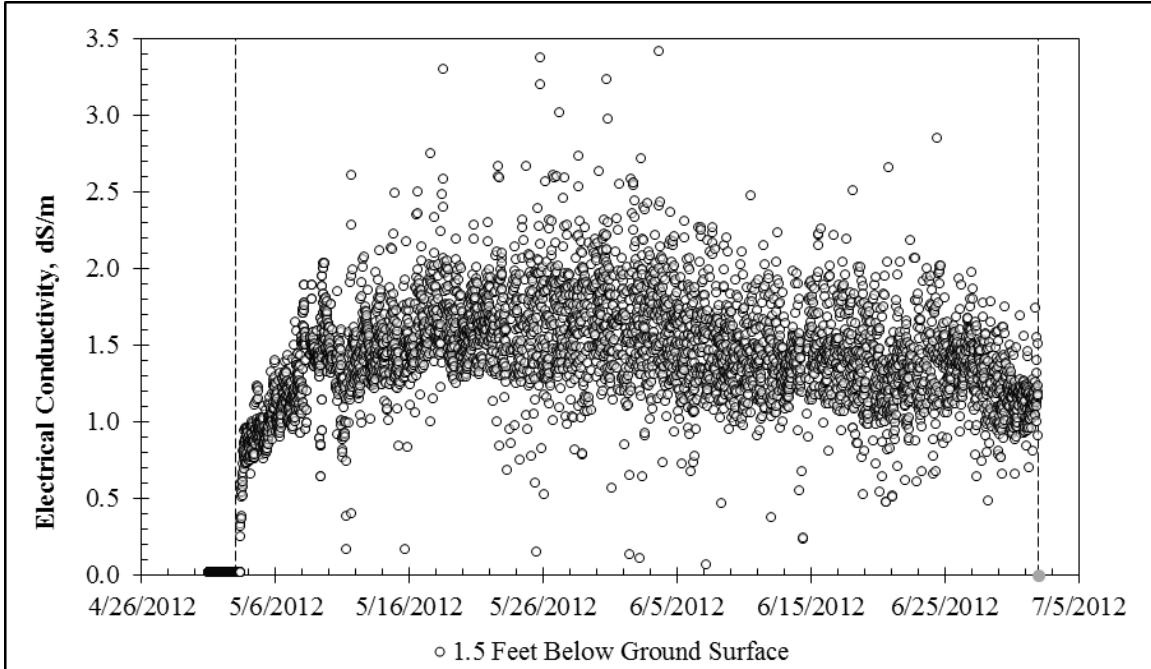


Figure 7.16: Electrical conductivity data from a TDR probe located 1.5 feet below ground surface during first inundation cycle (May – Jul. 2012).

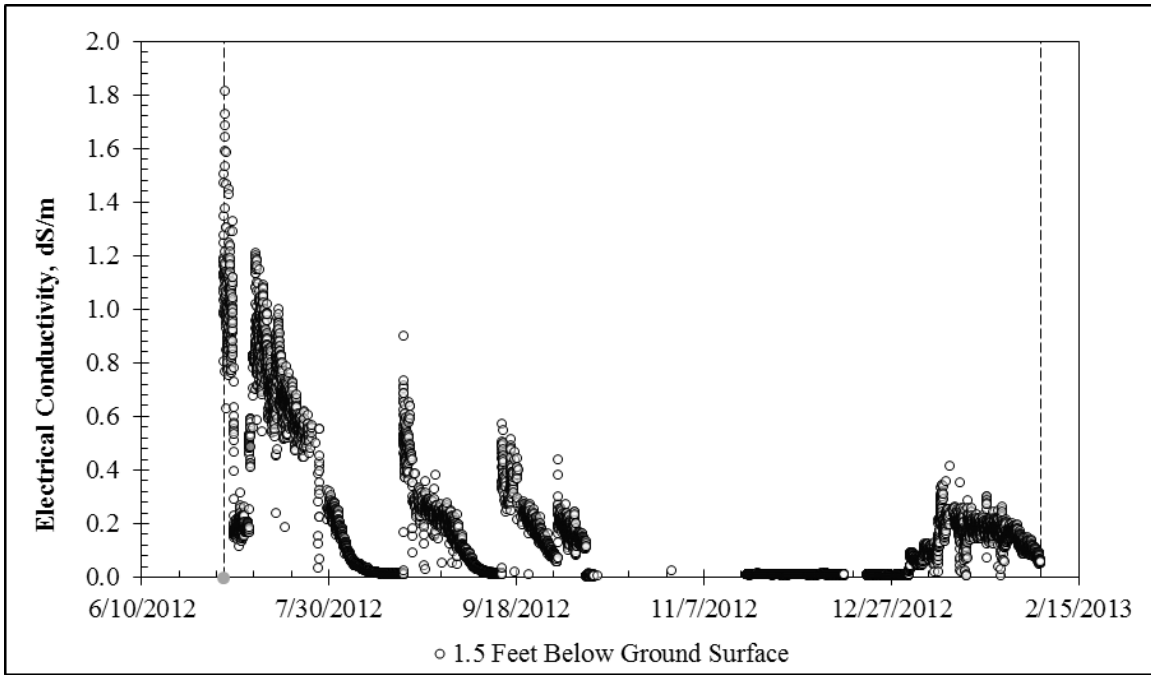


Figure 7.17: Electrical conductivity data from a TDR probe located 1.5 feet below ground surface during first drying cycle (Jul. 2012 – Feb. 2013).

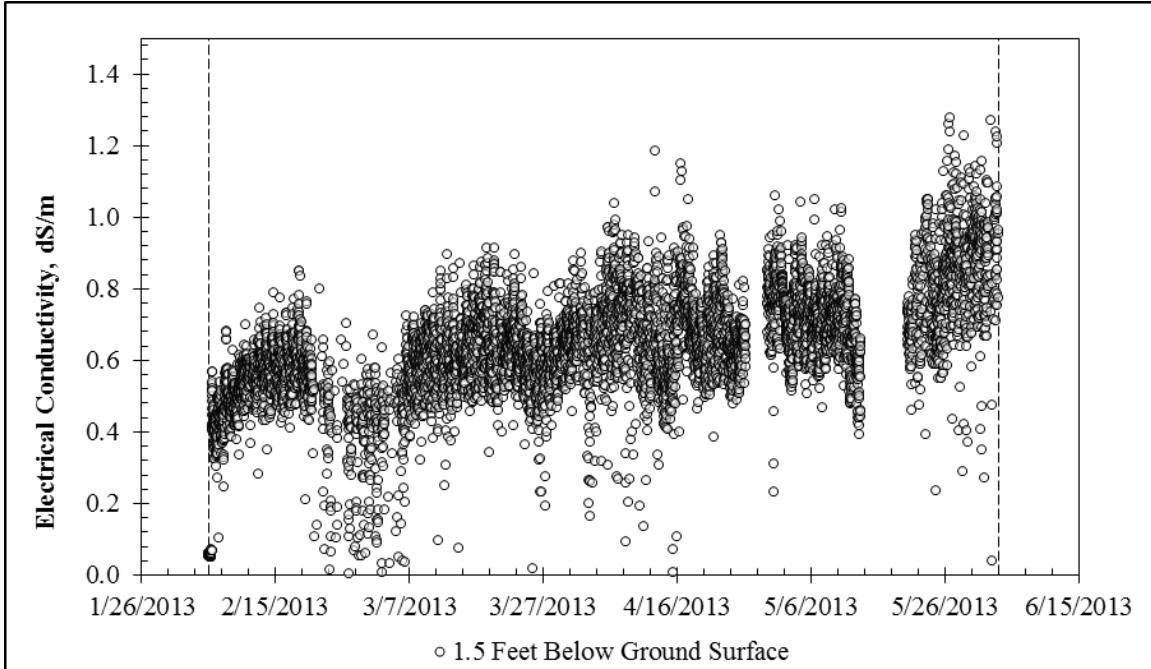


Figure 7.18: Electrical conductivity data from a TDR probe located 1.5 feet below ground surface during second inundation cycle (Feb. – Jun. 2013).

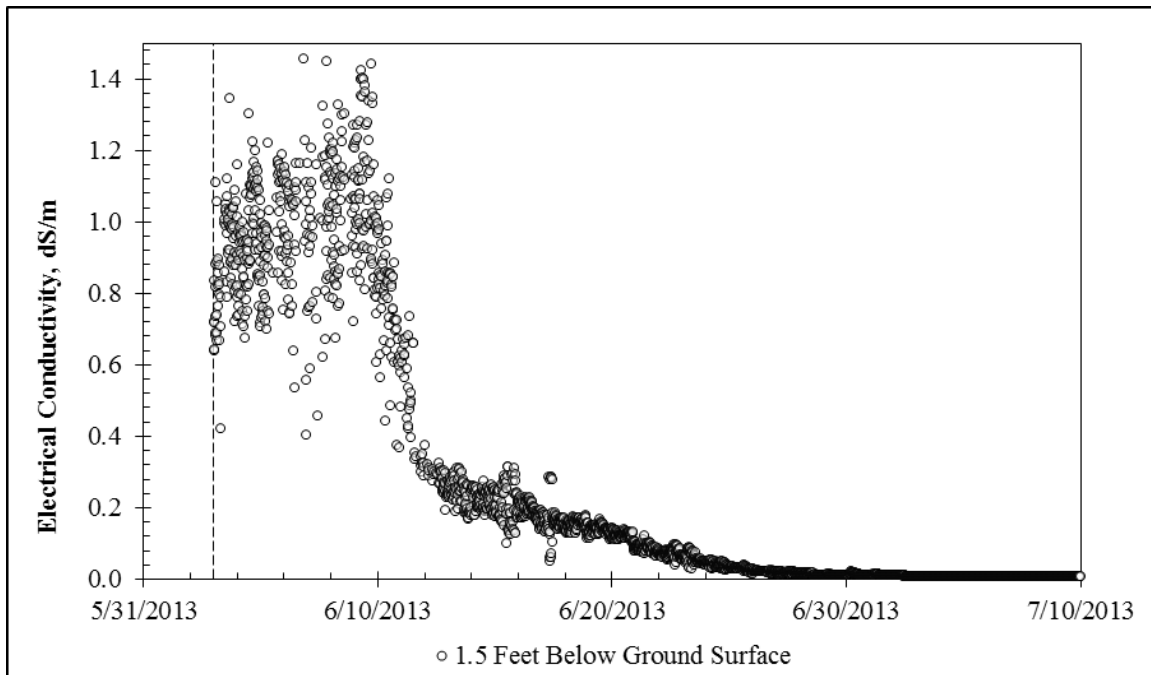


Figure 7.19: Electrical conductivity data from a TDR probe located 1.5 feet below ground surface during second drying cycle (Jun. – Jul. 2013).

### 7.3.5: STRAIN GAUGE DATA

Strain data is presented in Figure 7.20 to Figure 7.34. In the following figures, strain data is zeroed at the beginning of the first inundation cycle on May 3, 2013. Strain gauge nomenclature indicates which instrumented shaft the gauge is installed in (East, Center, or West), the depth of the strain gauge below original ground surface (1 – 29 feet), and which side of the neutral axis the gauge is installed on (Tension or Compression; tensile strains are positive). Using this nomenclature, gauge E.17.T is located in the east instrumented shaft, 17 feet below ground surface, on the tensile side of the neutral axis.

In shallow gauges above the excavation line (from 1 to 13 feet below ground surface), several gauge failures occurred. These failures were similar to those recorded during natural moisture cycles. Thermal effects due to both seasonal and daily temperature fluctuations are observed in gauges near ground surface with minimal bending strains



(Figure 7.20). As gauge depth and bending curvatures due to loading increase, the importance of thermal effects is generally limited to axial strains, with bending curvatures remaining fairly consistent (e.g. C.13.C and C.13.T). During the first and second inundation cycles, most gauges responded quickly to the presence of water; this response was generally more pronounced during the second inundation cycle. The increased magnitude of response during the second inundation cycle may be due to the development of tension cracks during the increasing deflections of the first cycle, which leads to a softer moment-curvature response consistent with cracked section properties (e.g. W.13.T).

In deeper gauges below the excavation line (15 to 29 feet below ground surface), the influence of thermal effects decreases. Several gauges (e.g. E.17.T, E.19.T, W.25.T, etc.) show immediate response during the first inundation cycle, limited activity during the first drying cycle, and immediate response during the second inundation cycle. Some evidence of tension cracking, both before and during the inundation testing, is indicated by larger than average responses to bending (e.g. C.21.T). The development of bending strains in many gauges is qualitatively similar to the development of top-of-wall deflection during inundation.

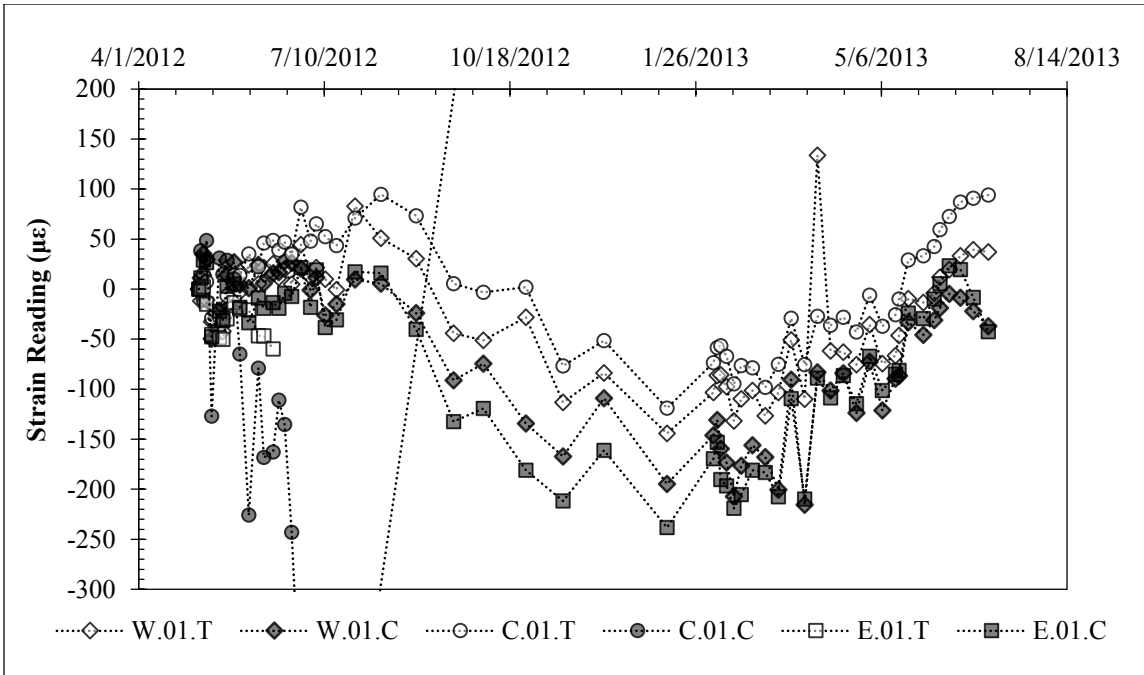


Figure 7.20: Strain Data 1 Foot Below Ground Surface (May 2012 – July 2013).

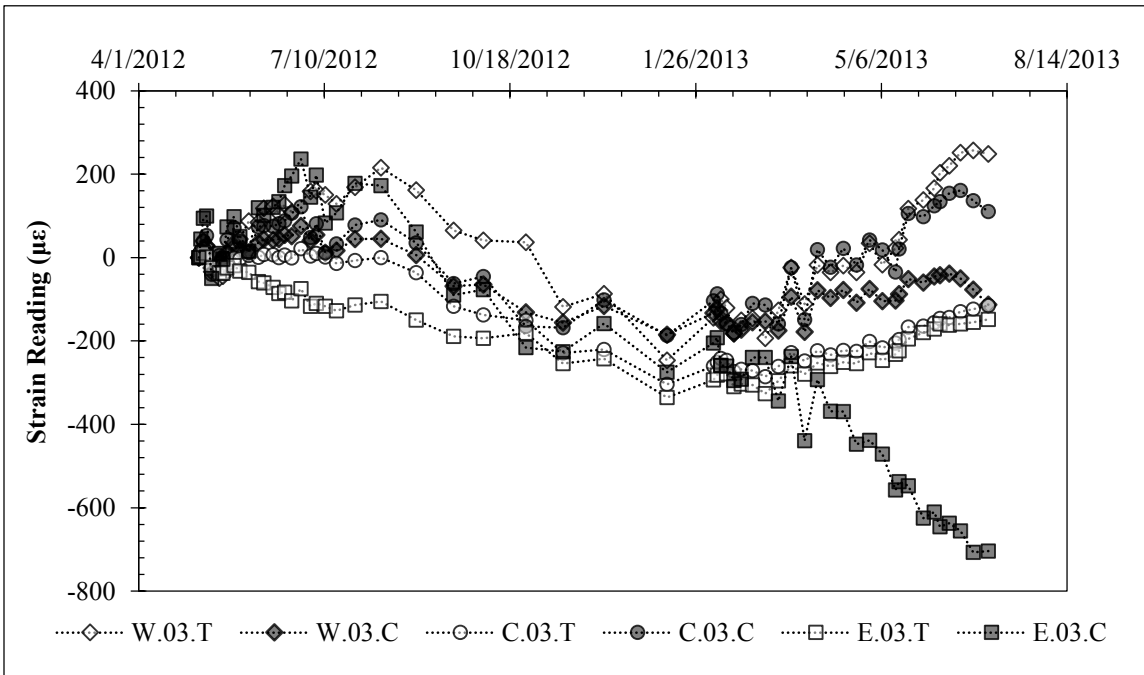


Figure 7.21: Strain Data 3 Feet Below Ground Surface (May 2012 – July 2013).

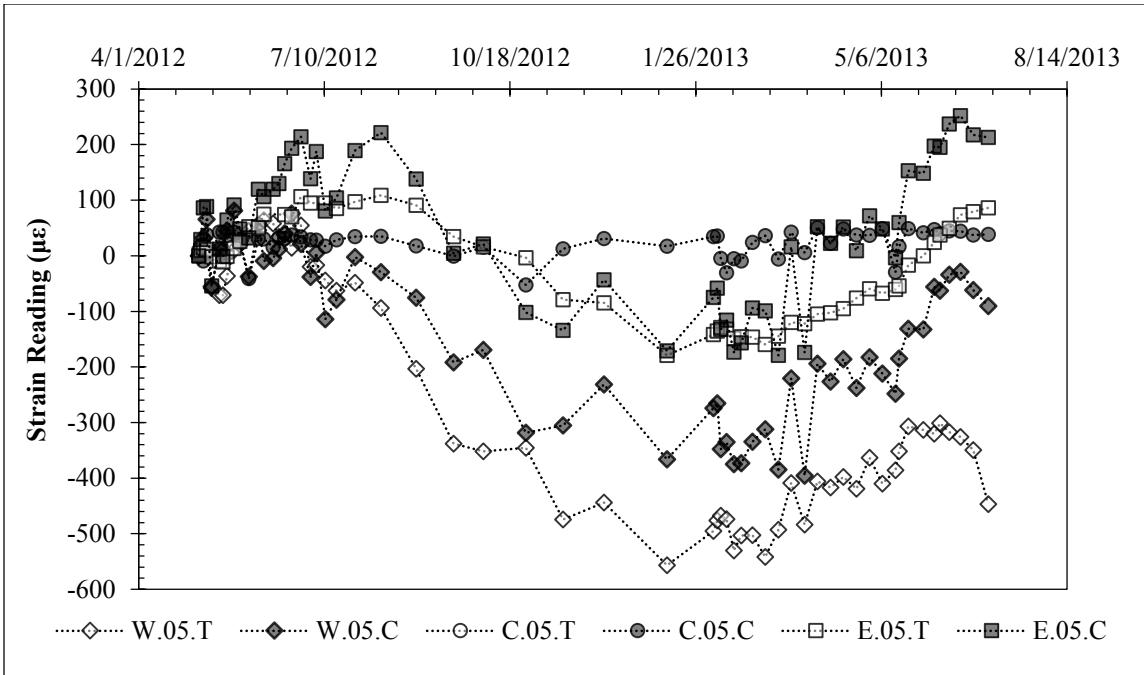


Figure 7.22: Strain Data 5 Feet Below Ground Surface (May 2012 – July 2013).

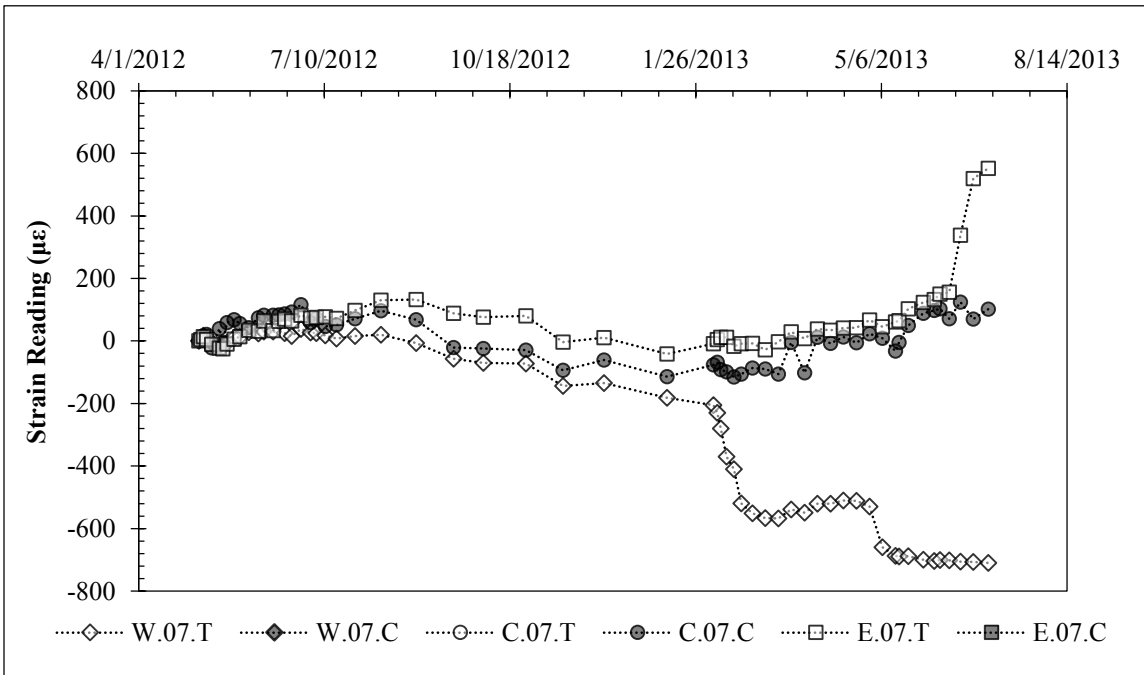


Figure 7.23: Strain Data 7 Feet Below Ground Surface (May 2012 – July 2013).

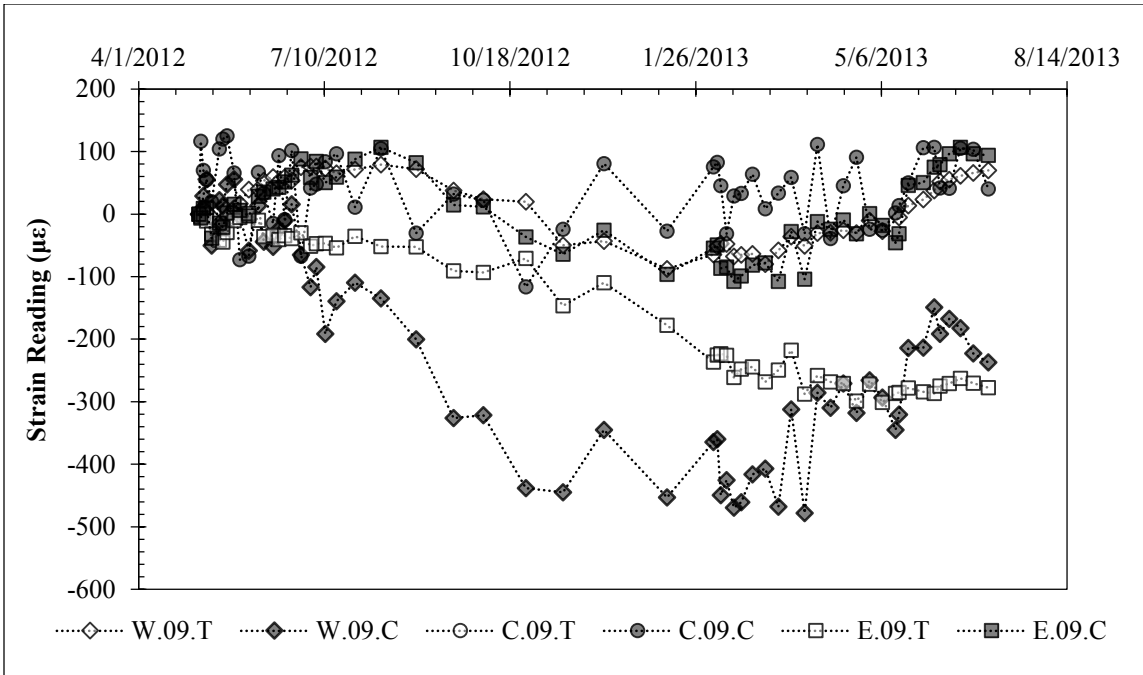


Figure 7.24: Strain Data 9 Feet Below Ground Surface (May 2012 – July 2013).

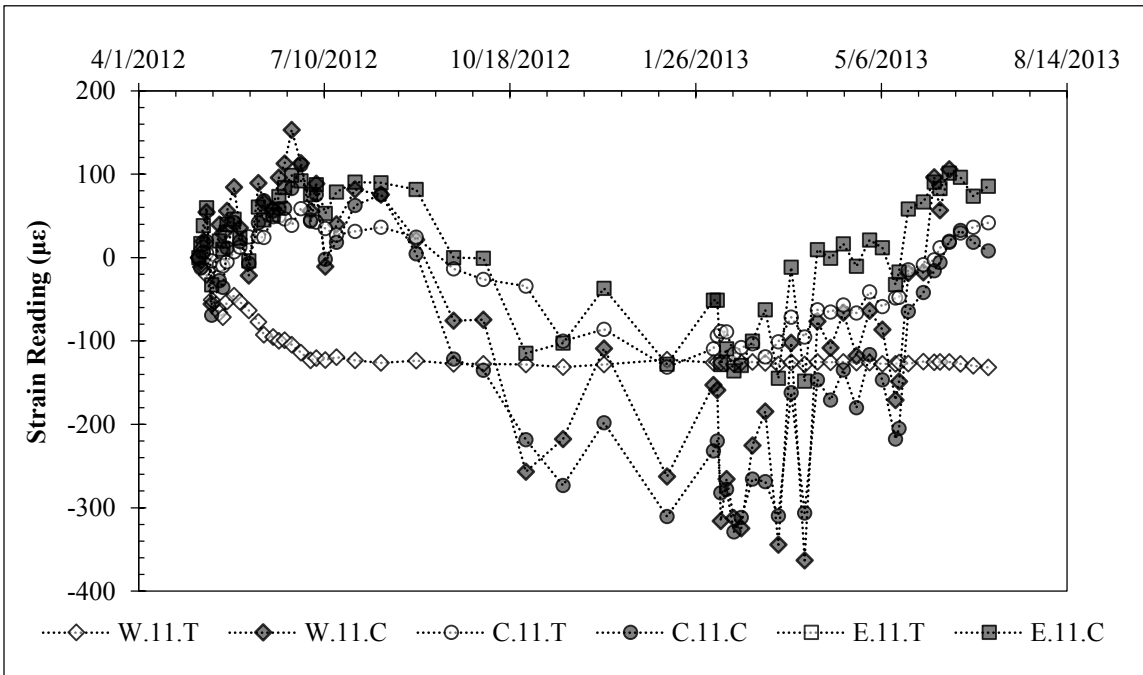


Figure 7.25: Strain Data 11 Feet Below Ground Surface (May 2012 – July 2013).

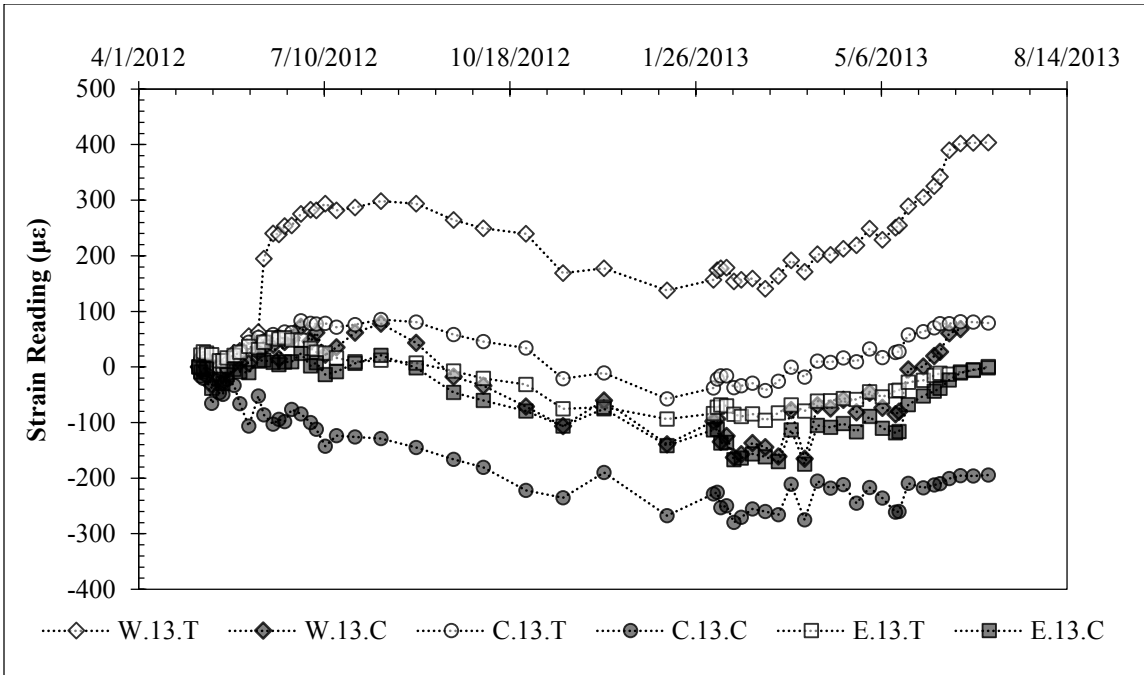


Figure 7.26: Strain Data 13 Feet Below Ground Surface (May 2012 – July 2013).

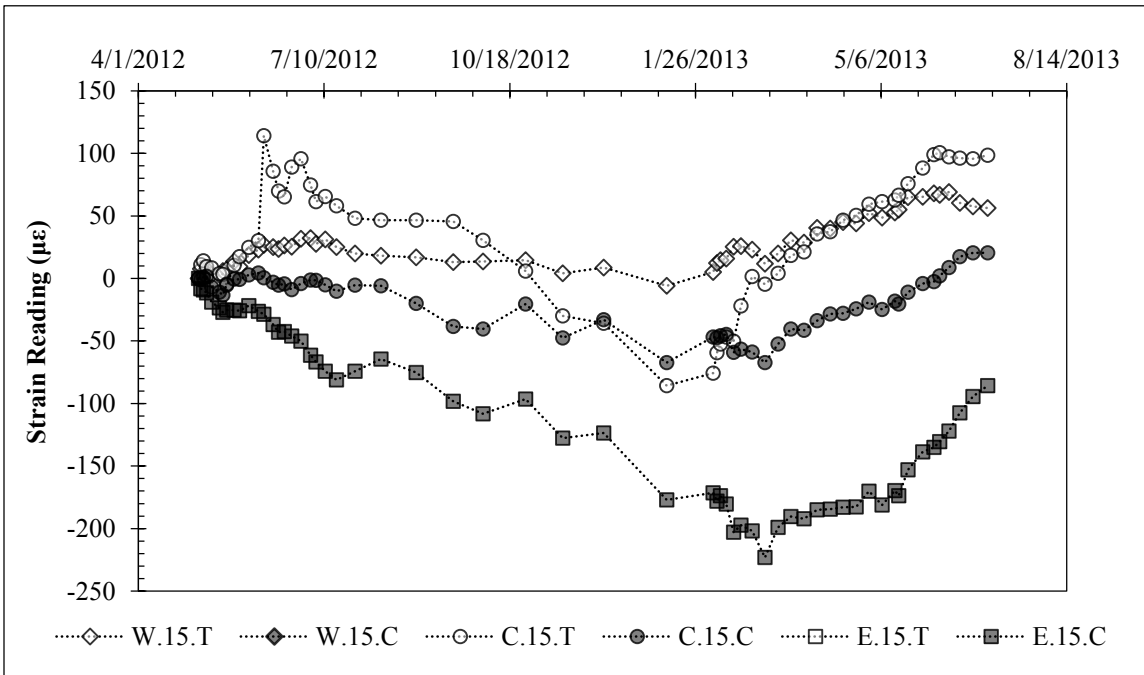


Figure 7.27: Strain Data 15 Feet Below Ground Surface (May 2012 – July 2013).

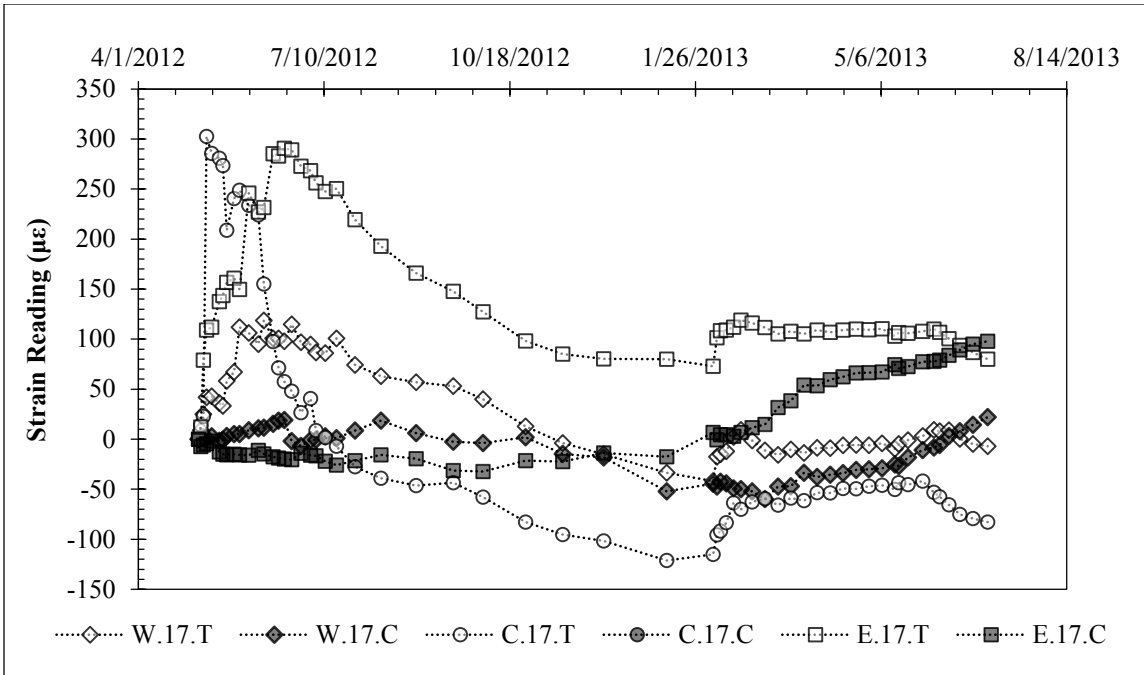


Figure 7.28: Strain Data 17 Feet Below Ground Surface (May 2012 – July 2013).

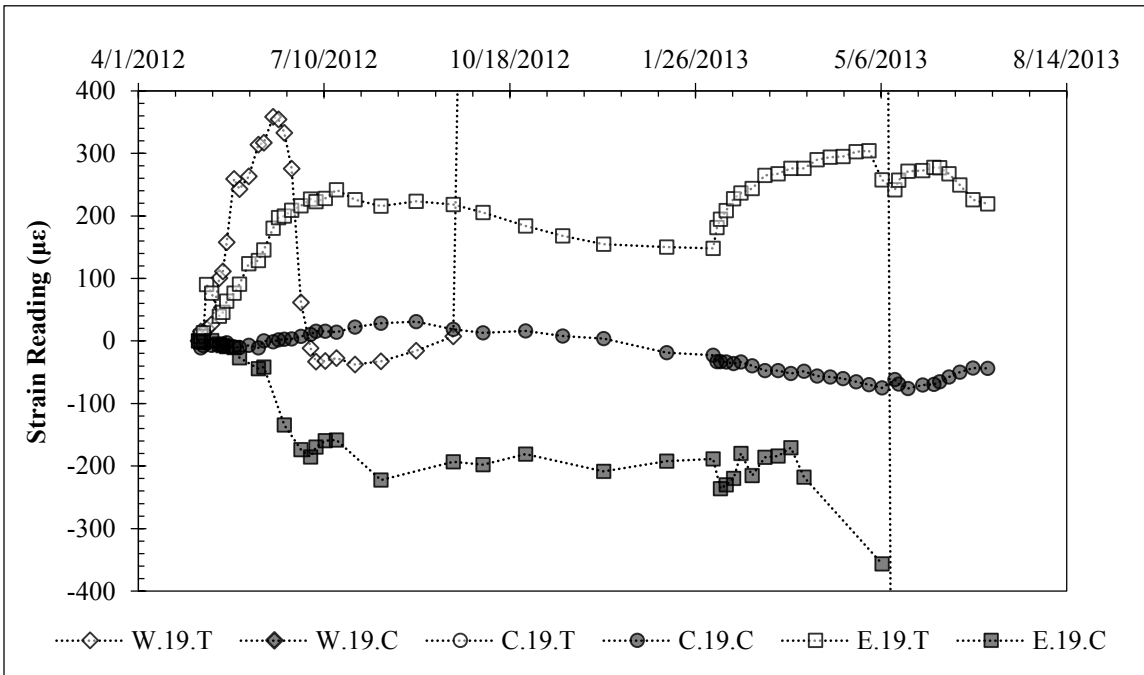


Figure 7.29: Strain Data 19 Feet Below Ground Surface (May 2012 – July 2013).

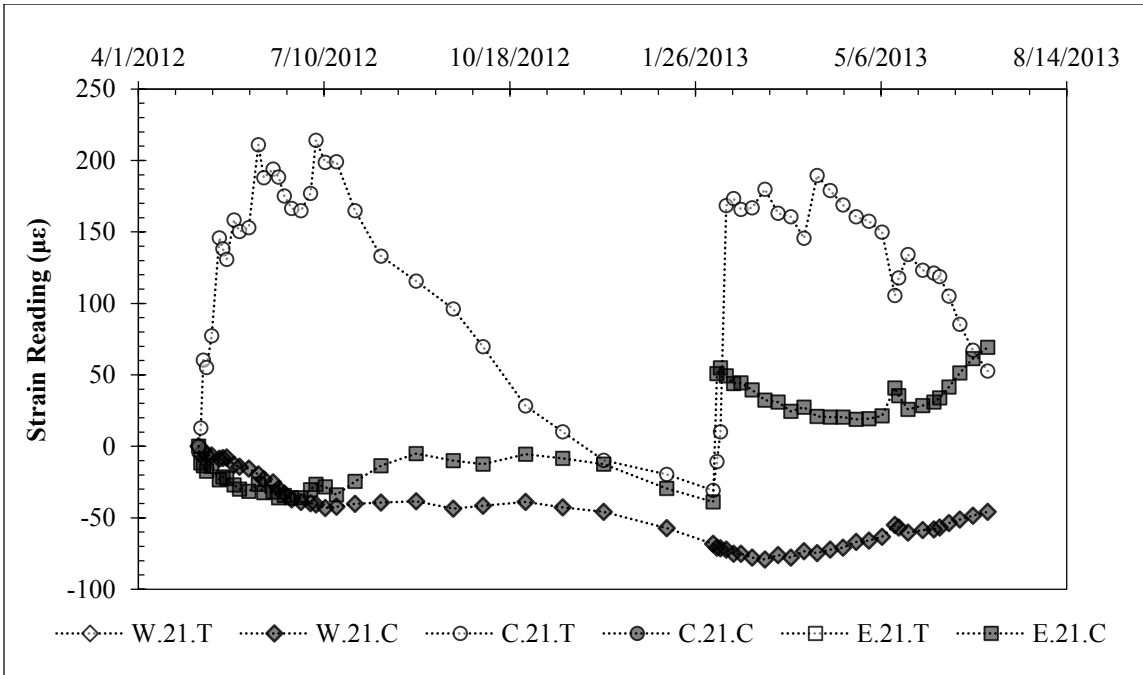


Figure 7.30: Strain Data 21 Feet Below Ground Surface (May 2012 – July 2013).

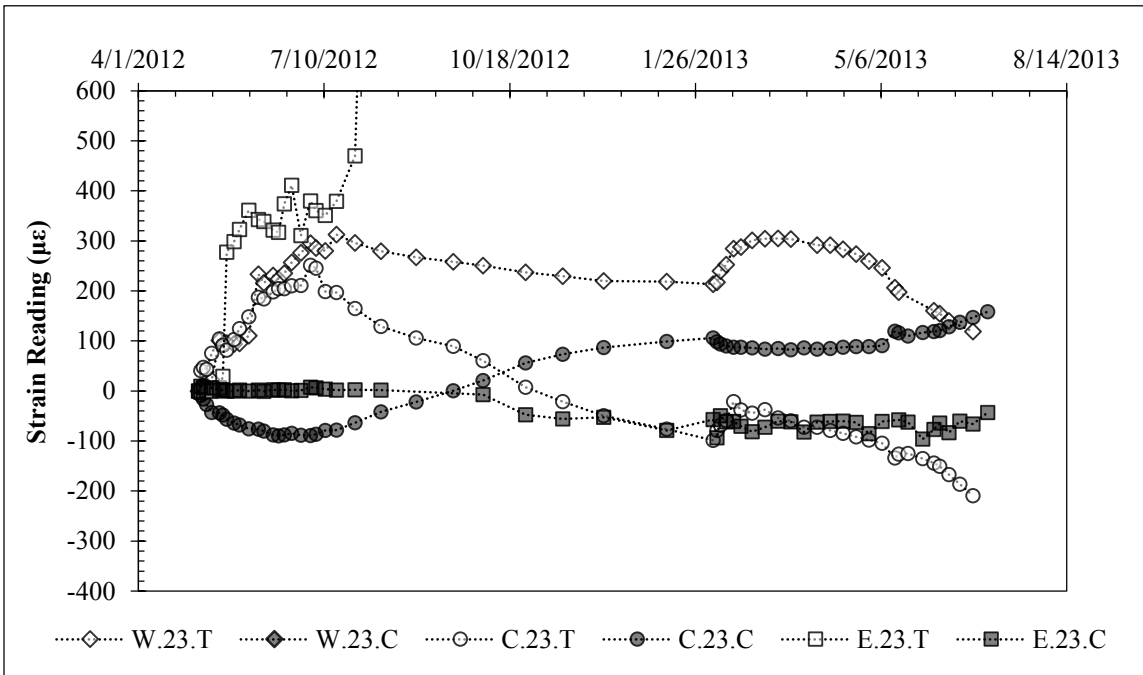


Figure 7.31: Strain Data 23 Feet Below Ground Surface (May 2012 – July 2013).

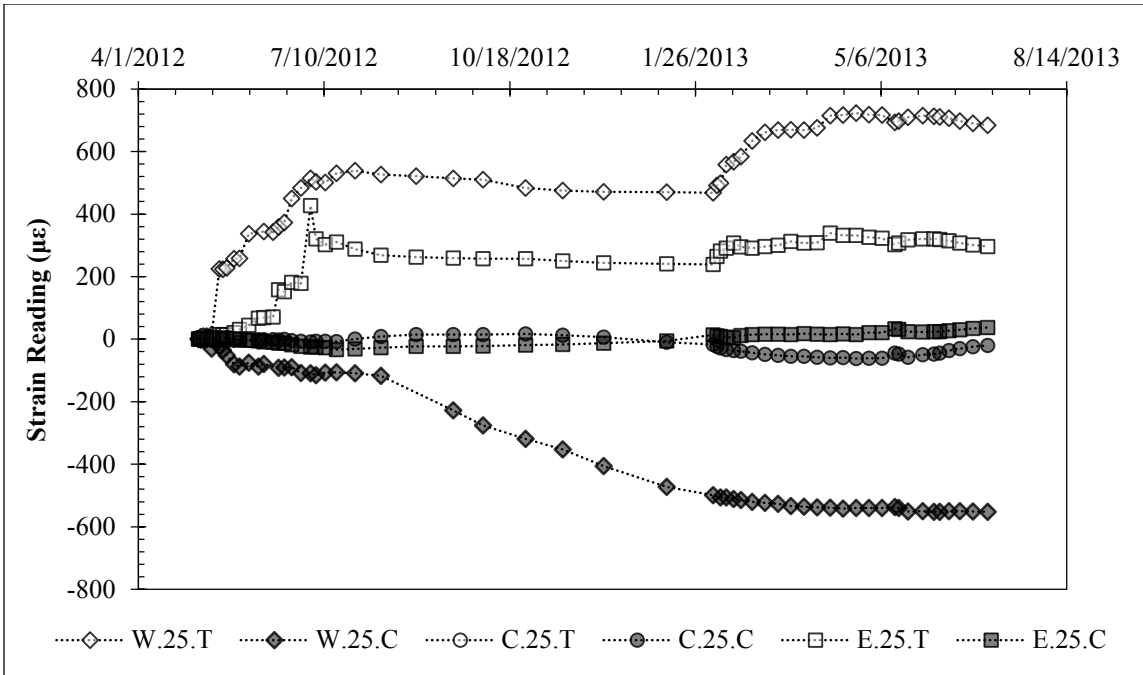


Figure 7.32: Strain Data 25 Feet Below Ground Surface (May 2012 – July 2013).

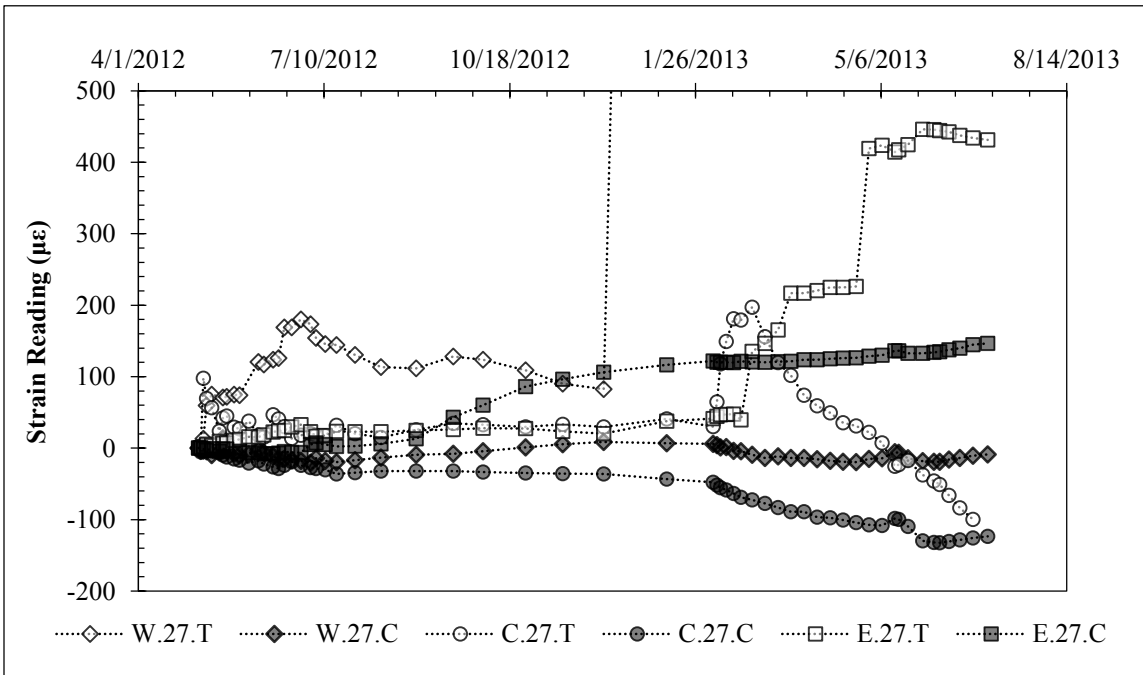


Figure 7.33: Strain Data 27 Feet Below Ground Surface (May 2012 – July 2013).



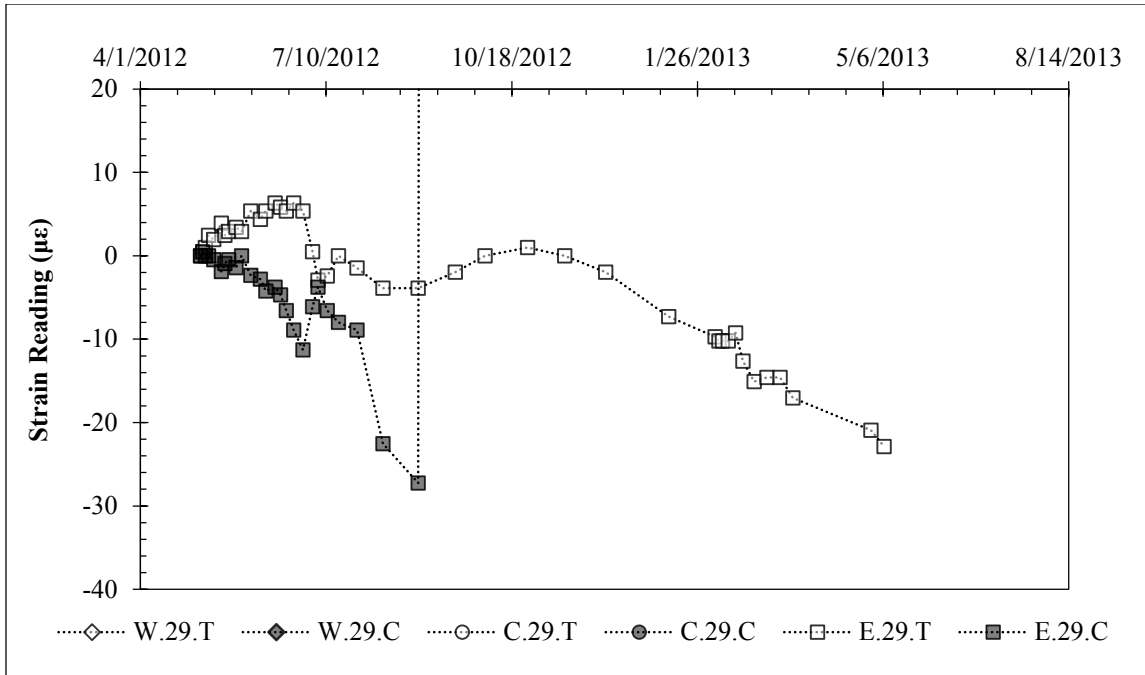


Figure 7.34: Strain Data 29 Feet Below Ground Surface (May 2012 – July 2013).

## 7.4: Data Interpretation

### 7.4.1: IMMEDIATE RESPONSE TO WATER

The inundation test began on May 3, 2012, and the wall and soil responded nearly immediately to the presence of water (Figure 7.35). Within minutes, the TDR probes installed throughout the retained soil registered the presence of free water (Figure 7.36), and within hours, water had begun to infiltrate through the wall drainage system into the excavation (Figure 7.37). This immediate response is consistent with the response observed at the test wall during large rainfall events, and suggests that the fissures present in the expansive clay provide preferential pathways for moisture flow.



Figure 7.35: The inundation zone is filled on May 3, 2012.

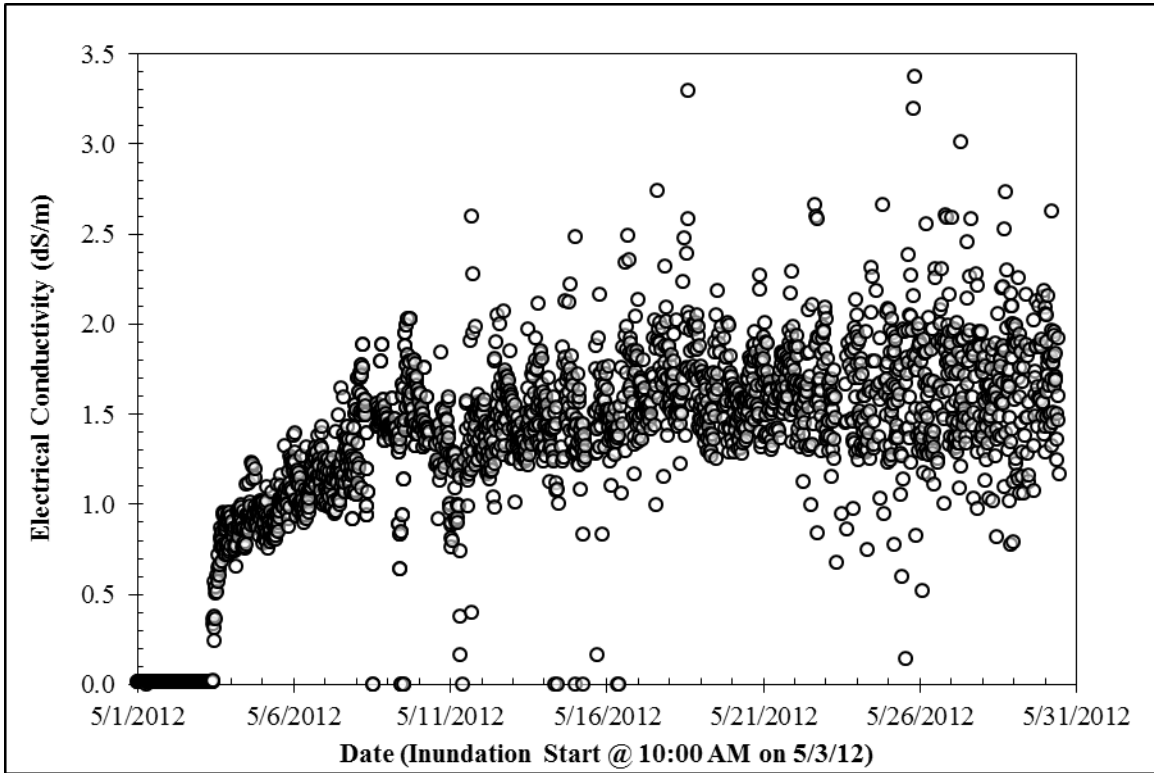


Figure 7.36: Electrical conductivity data from one TDR probe shows a response within minutes of beginning the inundation test. Probe is located 1.5 feet below ground surface.



Figure 7.37: Water infiltration into the excavation was first observed 90 minutes from the start of inundation.

The top-of-wall deflection began to increase almost immediately in response to inundation, and continued at a slightly decreasing rate for the duration of the test (Figure 7.9). Based on the daily rate of deflection, it was inferred that the inundation test would likely need to continue for several additional months before an equilibrium condition was reached (Figure 7.10). Because of this, and in order to allow the soil time to dry out before the next scheduled inundation cycle in January 2013, the first inundation cycle was stopped on July 2, 2012. After the water supply to the inundation area was cut off, the wall deflection stabilized within one day, again suggesting that fissures in the soil mass provide fairly direct access to moisture. Over the two month inundation cycle, the top-of-wall deflections had increased by approximately 2 inches. Had the test not been stopped, it is likely that deflections would have increased beyond this point. After two months of inundation, in the soil above the groundwater table, moisture contents had increased by approximately 5 to 10 percentage points in the active zone above the natural groundwater table (Figure 7.38).

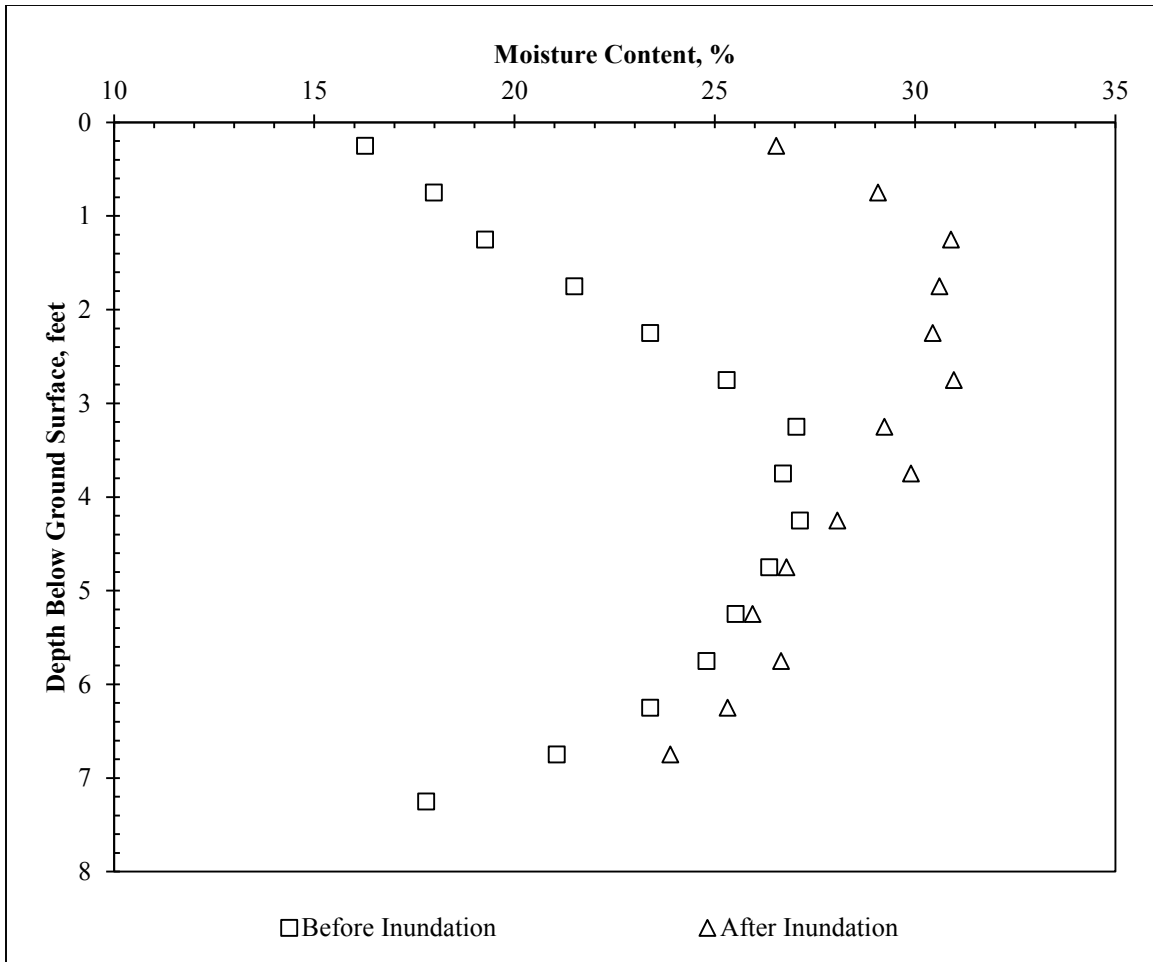


Figure 7.38: Moisture content profiles immediately before and after first inundation cycle. Natural water table is located at a depth of approximately 8 feet.

During the first drying cycle, despite a decrease in soil moisture content, top-of-wall deflections remained relatively stable. During the second inundation cycle, wall deflections began to increase immediately after the re-introduction of water and reached their maximum value as piezometer water levels stabilized near ground surface (Figure 7.9). As the second inundation cycle ended and the second drying cycle began, top-of-wall deflections, TDR electrical conductivity values, and water levels in the stand pipe

piezometers began to decrease (Figure 7.9 to Figure 7.14), suggesting the presence of water plays a key factor in the development of top-of-wall deflections.

#### **7.4.2: DEVELOPMENT AND CHARACTERIZATION OF DRAINED, FULLY SOFTENED STRENGTHS**

After being provided with unlimited access to water, and going through multiple cycles of wetting and drying, it is likely that the retained soil reached drained conditions. In high plasticity clays, this often corresponds to the development of fully softened strengths. To develop potential strength envelopes for the retained soil, the use of fully softened strength correlations were plotted as described in Skempton (1977) and Wright (2005). Additionally, fully softened strength tests were conducted on samples of clay from the test site in accordance with the procedures described in Wright et. al. (2007). Because the fully softened strength is very close to a normally consolidated strength, the native soil is mixed into a slurry at values of moisture content near the liquid limit, then consolidated to the in-situ confining pressure. A drained direct shear test then provides an estimate of the soil's fully softened strength at a given confining pressure. A series of tests at different confining pressures can be used to develop an envelope of fully softened strength. Results from the testing program, along with correlations presented in literature, and data from Ellis (2011) are presented in Figure 7.39. For the Taylor clay on the project site, a nominal fully softened friction angle of 24 degrees was selected as a starting point for analysis (the predicted strength envelope is curved, but average measured values are approximately 24 degrees over the depth of interest).

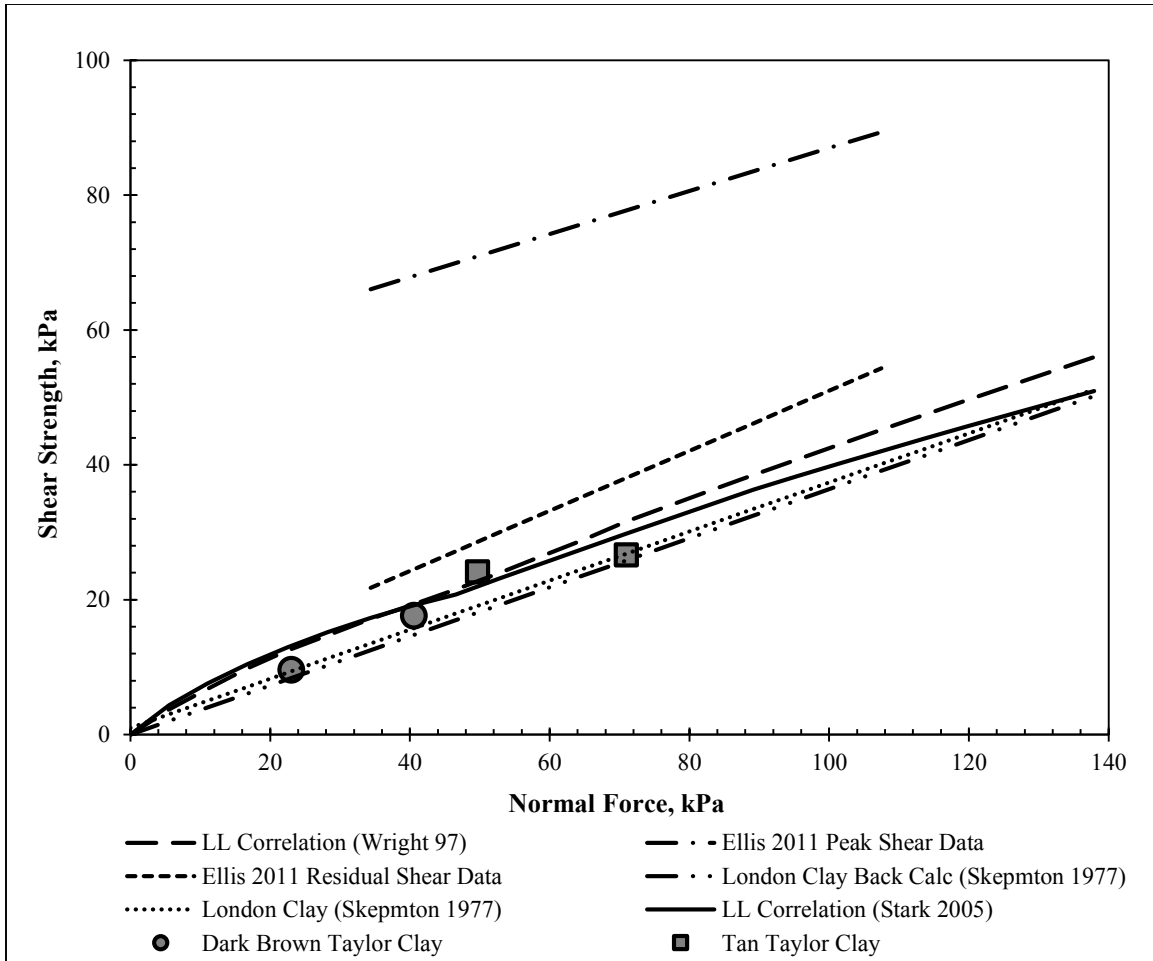


Figure 7.39: Comparison of measured fully softened strength test data from the project site with data from Ellis (2011) and established correlations.

### 7.4.3: LPILE ANALYSIS

To aid in selection of p-y curves for the foundation soil, the calculated p-y curves were compared against the proposed curves from Chapter 2 in Figure 7.40 to Figure 7.44. While the “stiff clay without free water” curves appear to be reasonable at shallow depths, at depths below 22 feet, their predicted response is much stiffer than the observed soil response. To model the behavior of the foundation soil, drained p-y curves based on the fully softened soil strengths with non-default values of initial stiffness were used. For the

conditions imposed on the test wall during the inundation test, the earth pressures were modeled using the combined force of the drained, fully softened strength with  $\phi = 24$  and hydrostatic pressures with the water table at ground surface. The input parameters for the LPILE analysis are provided in Table 7.1, and the earth pressures used to estimate the wall's response using p-y analysis are shown in Figure 7.45. For our test wall data, a reference survey date of October 8, 2010 (installation of facing) was considered to be the most consistent with the assumptions used in p-y analysis, which does not account for immediate global deformations in response to excavation. A p-y analysis using the conditions presented in Table 7.1 predicted a final top-of-wall deflection of approximately 5.4 inches at equilibrium. A summary of the results of the long-term LPILE analysis is provided in Figure 7.45. The selection of p-y curves and input earth pressures for long-term analysis is discussed at length in the following chapter.



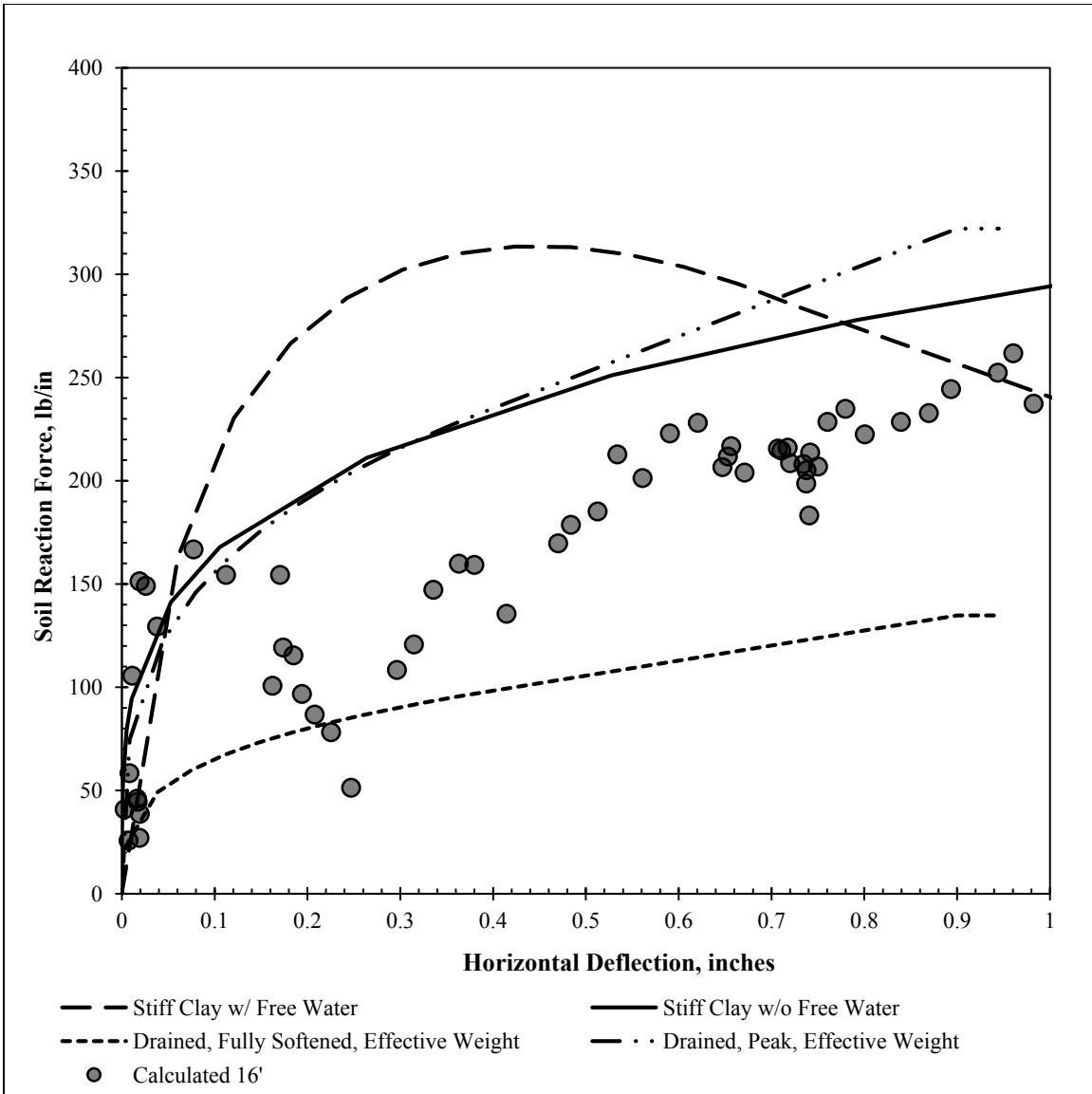


Figure 7.40: Comparison of calculated long-term p-y curves during inundation testing with proposed p-y curves at a depth of 16 feet below original ground surface.

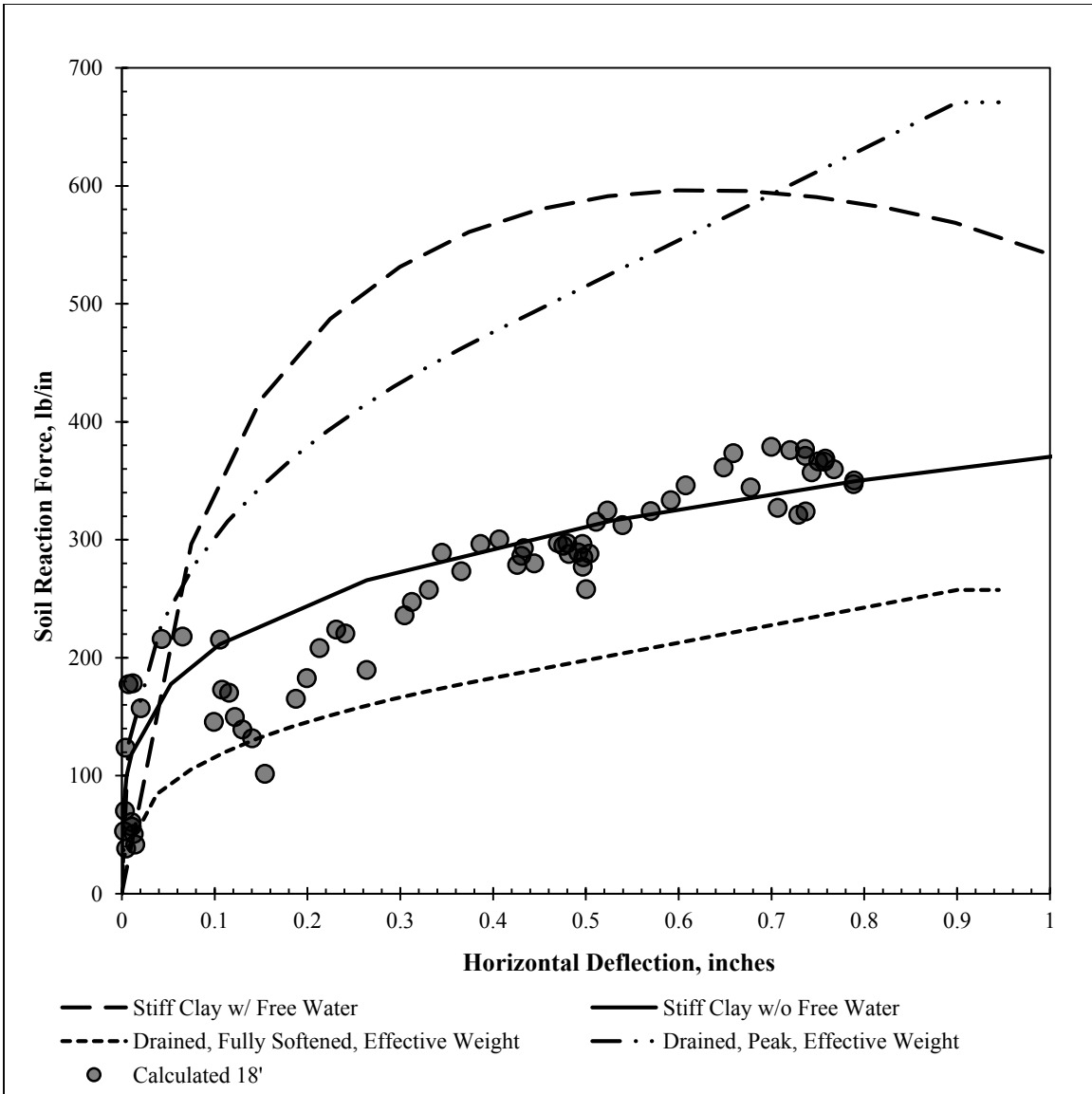


Figure 7.41: Comparison of calculated long-term p-y curves during inundation testing with proposed p-y curves at a depth of 18 feet below original ground surface.

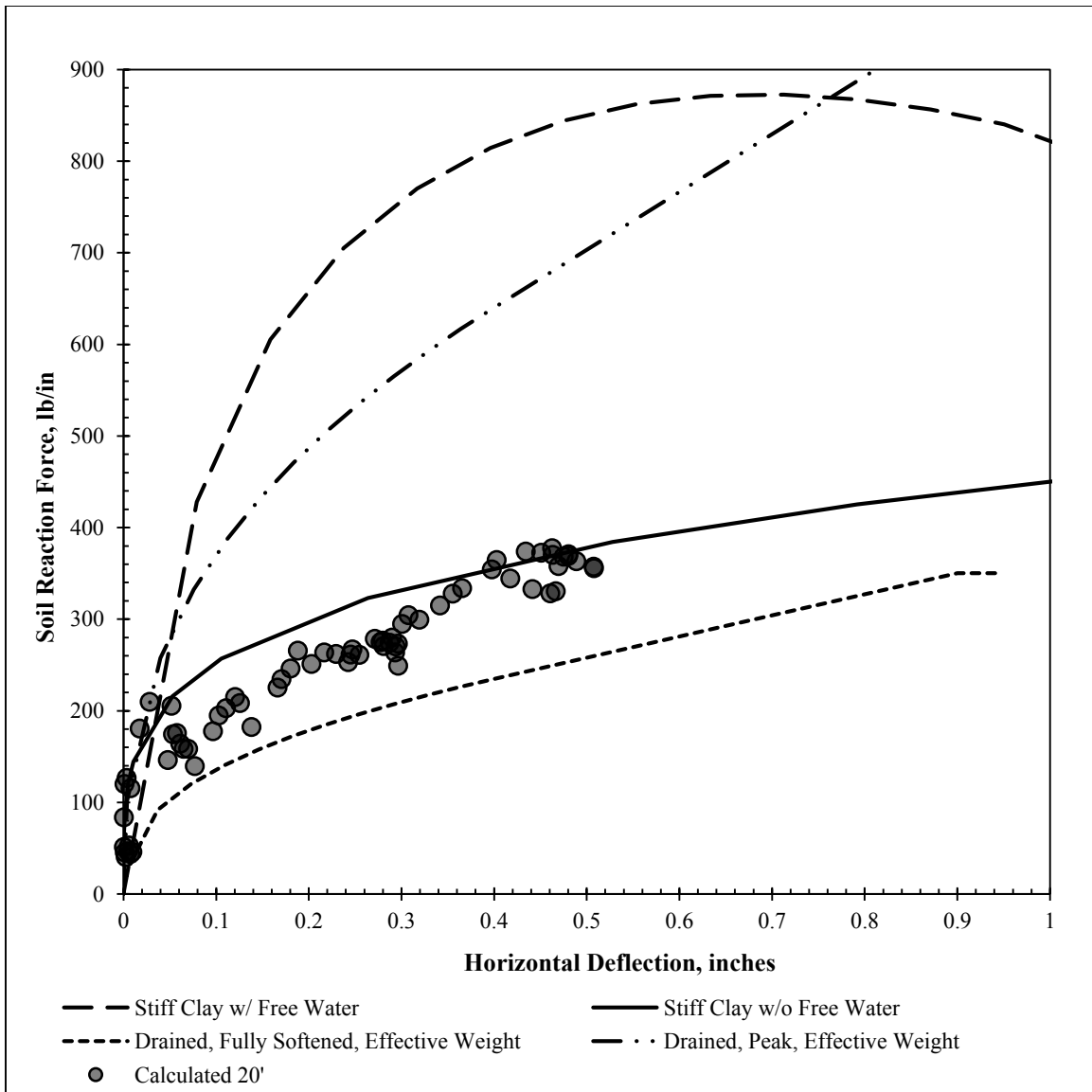


Figure 7.42: Comparison of calculated long-term p-y curves during inundation testing with proposed p-y curves at a depth of 20 feet below original ground surface.

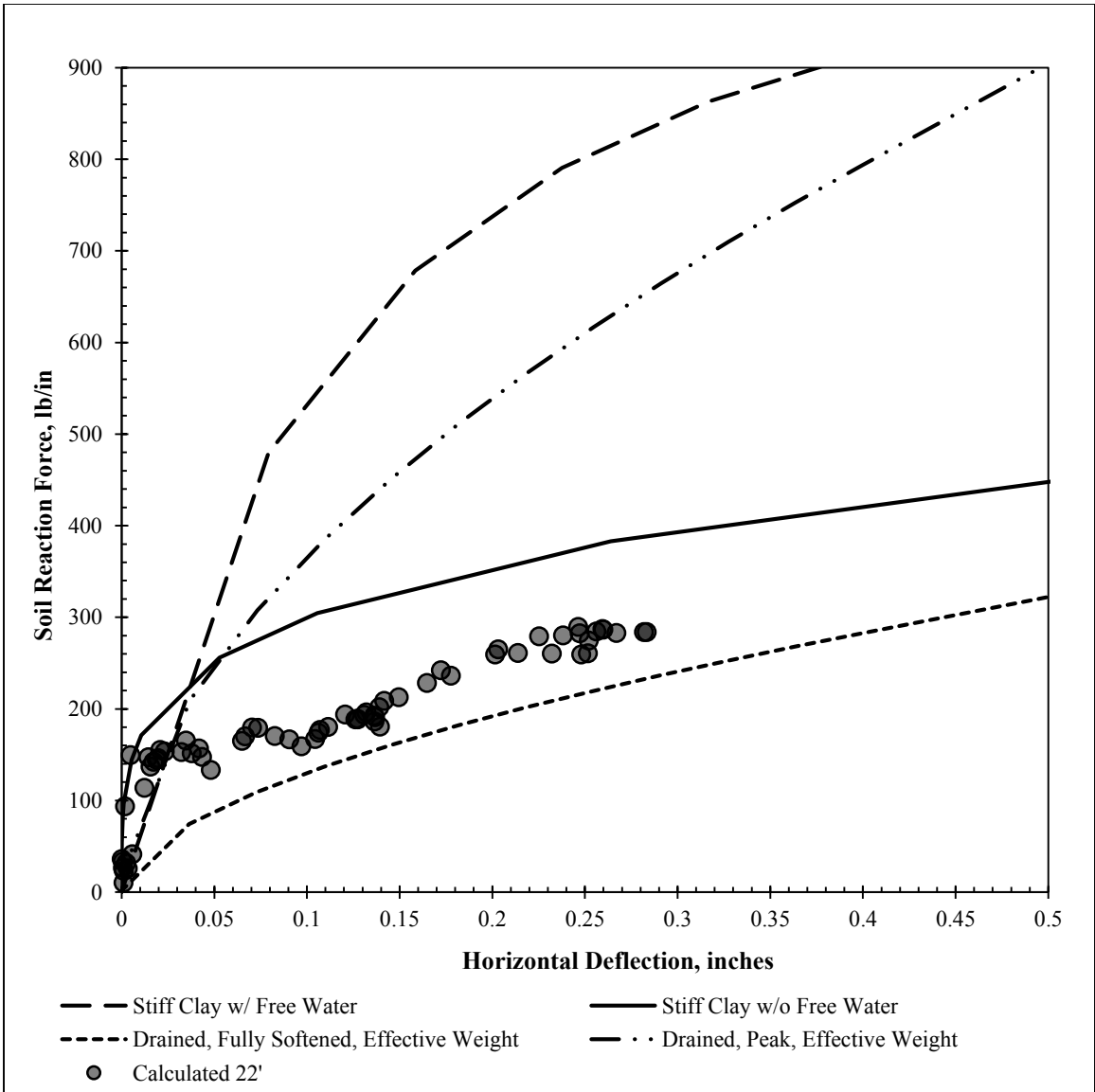


Figure 7.43: Comparison of calculated long-term p-y curves during inundation testing with proposed p-y curves at a depth of 22 feet below original ground surface.

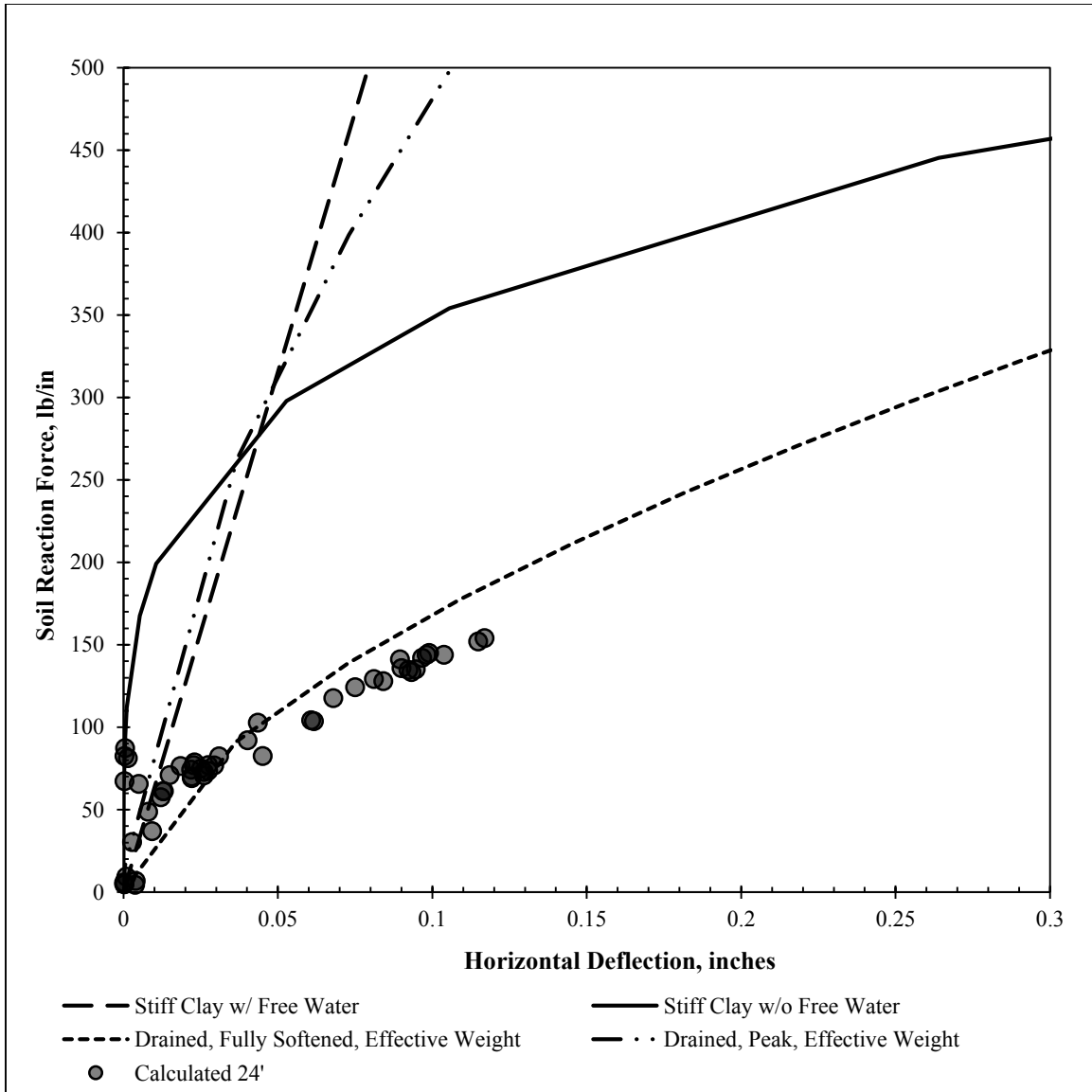


Figure 7.44: Comparison of calculated long-term p-y curves during inundation testing with proposed p-y curves at a depth of 24 feet below original ground surface.

Table 7.1: Baseline assumptions and design parameters for long-term LPILE analysis of inundation conditions.

Parameter	Value
Effective Unit Weight of Soil, $\gamma'$	62.6 pcf
Earth Pressure Loading	Fully Softened ( $\phi = 24$ ) + Hydrostatic (approx.. 90 psf/ft)
Friction Angle of Foundation Soil	24 degrees
Foundation Soil p-y Curves	Sand (Reese)
Non-Default Initial Stiffness, $k_{py}$	375 lb/in <sup>3</sup>
Cracking Moment, $M_{Cr}$	680 k-in.
Yielding Moment, $M_y$	3,200 k-in.
Uncracked Bending Stiffness, $EI_{uc}$	67 x 10 <sup>6</sup> k-in.
Cracked Bending Stiffness, $EI_{cr}$	18 x 10 <sup>6</sup> k-in.
Shaft Diameter	24 in.
Height of Retained Soil, H	162 in.
Reinforcement	12 #7 bars (1.6% of gross area)

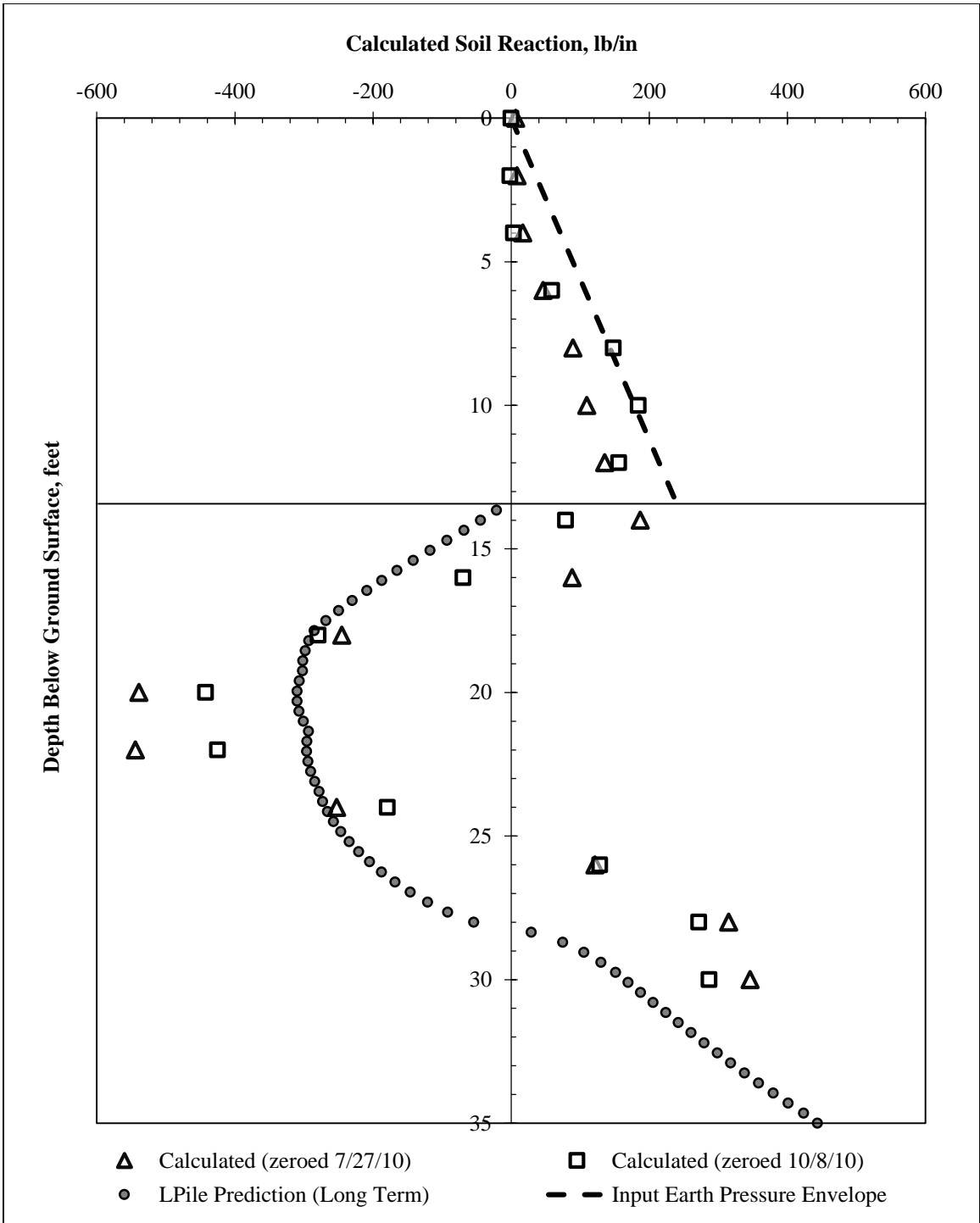


Figure 7.45: Comparison of long-term LPILE Prediction and calculated soil reaction forces.

## 7.5: Summary and Conclusions

The data recorded at the Lymon C. Reese research wall during cycles of controlled inundation testing has provided insights into the behavior of drilled shaft walls in expansive clay. Some of these insights include:

- Fissures in the clay provide preferential pathways for drainage and moisture flow. Drainage through these fissures occurs very quickly, within minutes, when surface water is present. This is supported by first-hand observations and data from TDR moisture probes and stand pipe piezometers.
- In the six total months of controlled inundation, and eight total months of drying cycles, top-of-wall deflections stabilized at 5.2 inches since shaft installation, and 4.2 inches since the installation of facing. Maximum bending moments in the shaft since installation were approximately 2,100 in-kip, approximately two-thirds of the yield moment.
- Wall deflections stabilized at the same time the water levels in stand pipe piezometers stabilized. As water levels decreased after the conclusion of inundation, top-of-wall deflections decreased accordingly. This result suggests the presence of water behind the wall contributes to the development of deflections.
- Based on the author's field observations, the presence of water in the excavation tends to increase wall deflections to a greater degree than the presence of water in the retained soil. Because of the fissured secondary structure of the soil, water behind the wall invariably results in water in the base of the excavation. Deflections tend to increase as water in the retained soil increases.
- The behavior of the foundation soil can be approximated using p-y curves developed for fully softened, drained strengths, with initial stiffness  $k_{py}$  defined by



the original profile of undrained shear strength. Assuming the eventual development of hydrostatic conditions behind the wall during inundation, the upper bound earth pressure envelope for the retained soil can be defined using the drained, fully softened properties of the soil, then adding hydrostatic pressures.

- Even with continued access to water, there is limited evidence to suggest that large earth pressures due to soil expansion are sustained at the test wall. No evidence of earth pressures exceeding the pressure envelope defined by drained, fully softened strengths with additional hydrostatic pressures was observed.

## **CHAPTER 8: DEVELOPMENT OF DESIGN GUIDELINES**

The following chapter presents a summary of the proposed design guidelines for drilled shaft retaining walls in high plasticity clays. The principal source of data for these recommendations is the Lymon C. Reese research wall, a full-scale test wall constructed through high plasticity clay in Manor, Texas. Both long-term and short-term design guidelines are presented, along with comparison data from the test wall.

### **8.1: Long-Term Design Guidelines**

#### **8.1.1: SUMMARY OF LONG-TERM GUIDELINES**

Long-term conditions often govern design in high plasticity clays. To check the long-term response of the wall after cycles of wetting and drying, a drained analysis using fully softened shear strengths is recommended. A summary of the proposed long-term design guidelines is provided in Figure 8.1.

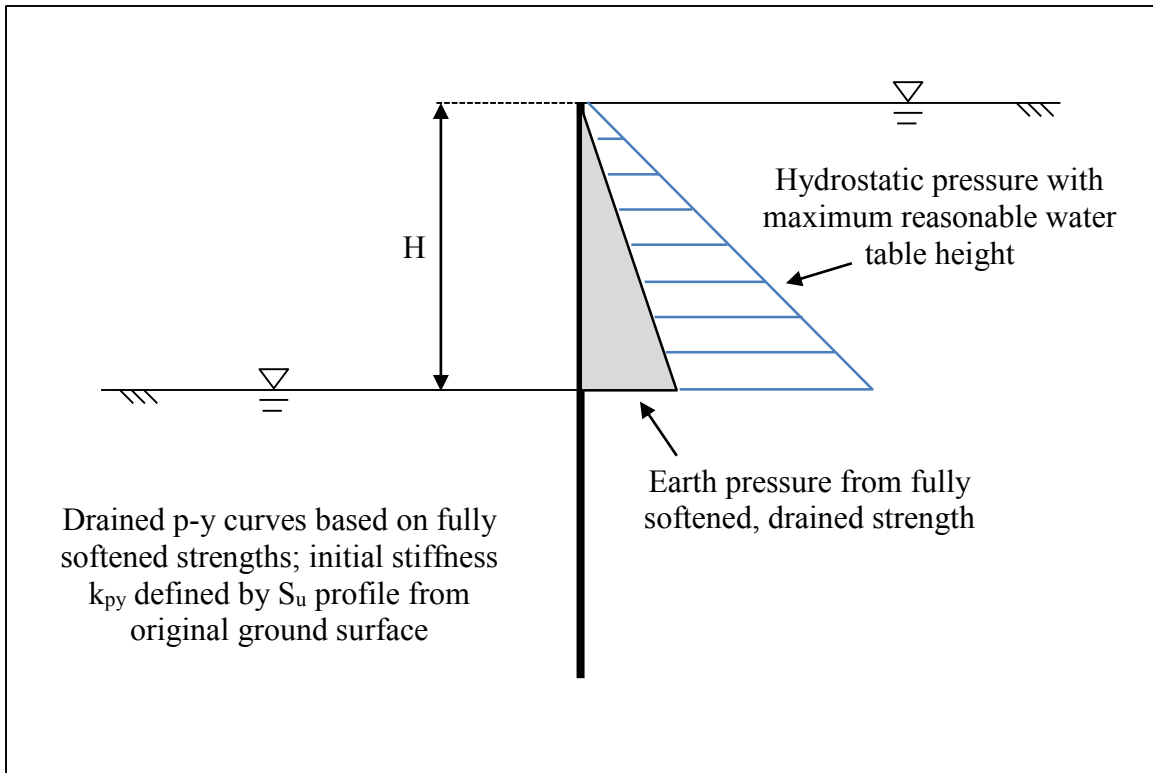


Figure 8.1: Summary of long-term design guidelines.

In the proposed long-term guidelines, the active earth pressure envelope is calculated using the fully softened, drained shear strength of the retained soil (e.g. Wright 2005, Stark et. al. 2005, Wright et. al. 2007). Hydrostatic pressures are calculated with the water table at a reasonable “maximum” level in the retained soil (e.g. during controlled inundation testing, the water table reached the original ground surface), and at the ground level on the excavation side. The long-term presence of hydrostatic pressures acting on a field wall is an unlikely scenario; however, it represents a reasonable “upper bound” value to check allowable deflections and bending moments.

To model the behavior of the foundation soil, drained p-y curves are recommended, based on a friction angle equal to the fully-softened drained shear strength of the soil. The use of non-default initial stiffness values ( $k_{py}$ ) is recommended, with  $k_{py}$  defined by the

original profile of undrained shear strength with depth (Figure 8.2). Because the default initial stiffness for p-y curves in cohesionless soils is defined by friction angle (Figure 8.3), and drained, fully softened friction angles for high plasticity clays are relatively low, the default values of initial stiffness tend to be lower than those observed in the field. To account for the transition from stiff, undrained behavior to soft, drained behavior, an initial stiffness profile defined by the original  $S_u$  profile from the original ground surface is recommended (the relationship between  $S_u$  and  $k_{py}$  for clays is shown in Figure 8.2). While soil strength reductions to account for close pile spacing are recommended for short-term loading in both sand and clay, the test wall data indicates that the use of a friction angle corresponding to the fully softened shear strength of the soil with no reduction factor works reasonably well to model the foundation soil behavior. Further investigation into the long-term loading behavior in expansive clays may be warranted to more clearly define the relationship between ultimate load reductions due to close pile spacing and ultimate load reductions due to the development of fully softened conditions under sustained loading.

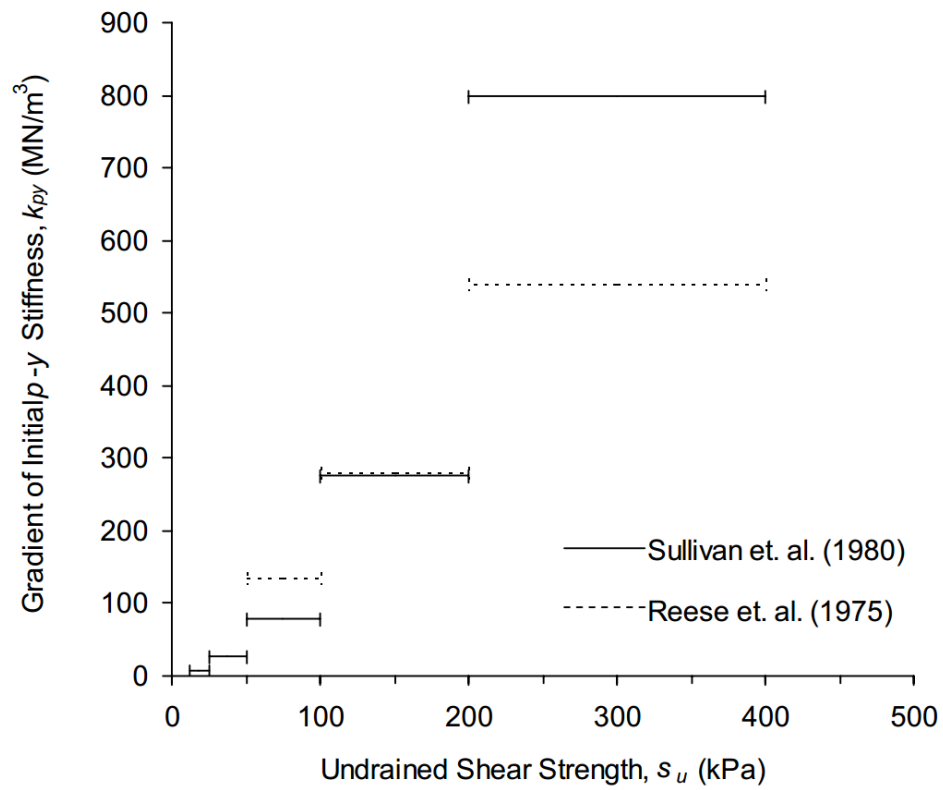


Figure 8.2: Typical  $k_{py}$  values for clays (after Dodds and Martin 2007).

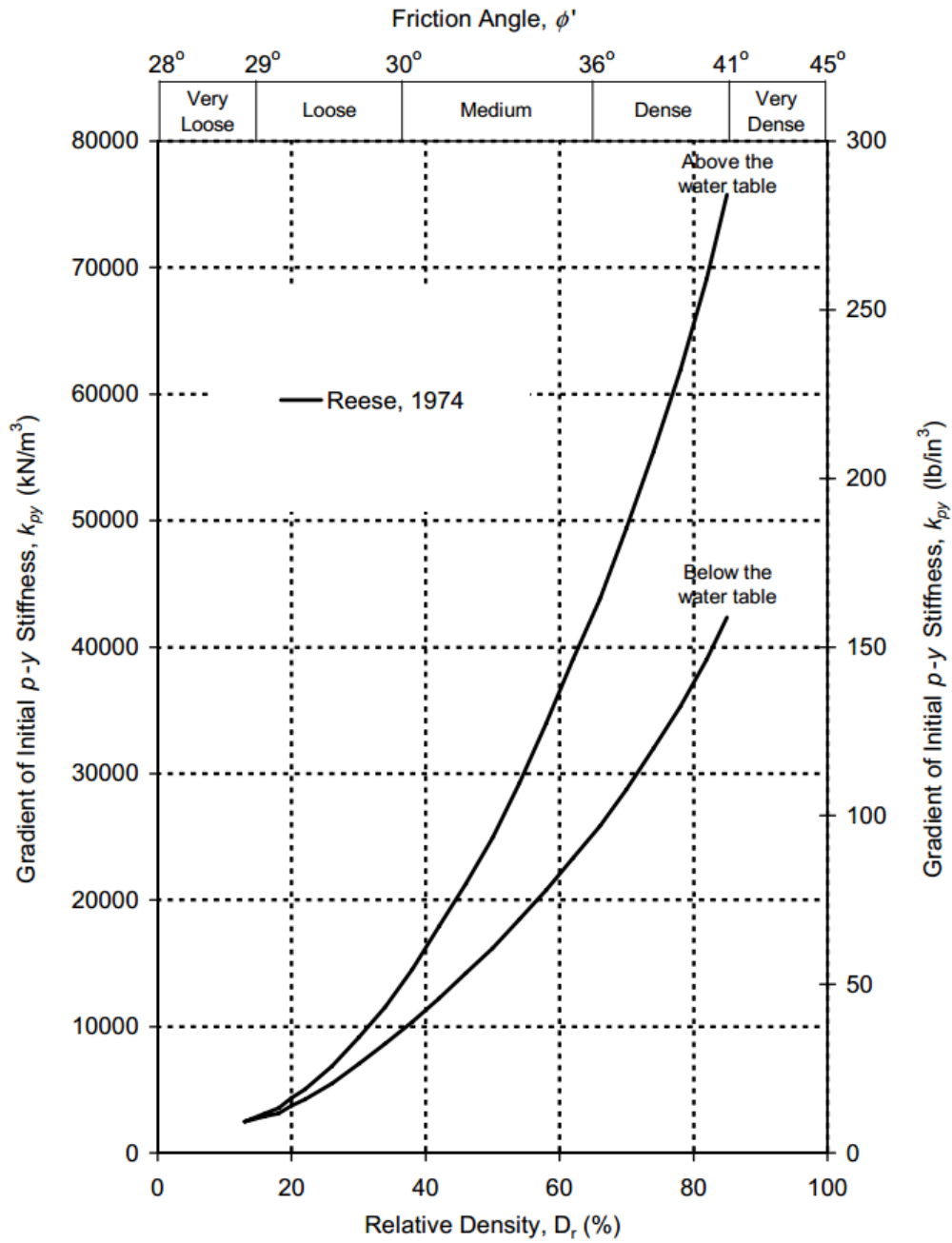


Figure 8.3: Typical  $k_{py}$  values for sands (after Dodds and Martin 2007).

### 8.1.2: DESIGN PREDICTIONS VS. OBSERVED BEHAVIOR

An LPILE analysis was conducted using the proposed long-term guidelines for the Lymon C. Reese research wall in Manor, Texas. Although the test wall had a design height of 15 feet, and an as-built height of 14 feet at the end of excavation, soil erosion into the base of the excavation during large storm events resulted in a final excavation depth of approximately 13.5 feet below ground surface. The small reduction in excavation depth corresponds to a reduction in earth pressure (lower cantilever height) and slightly stiffer response in the foundation soil (additional overburden pressure). Input parameters for the design LPILE analysis are provided in Table 8.1.

Table 8.1: Baseline assumptions and design parameters for LPILE analysis using proposed long-term design guidelines.

Parameter	Value
Effective Unit Weight of Soil, $\gamma$	62.6 pcf
Earth Pressure Loading Above Excavation	Fully Softened ( $\phi = 24$ ) + Hydrostatic
Friction Angle of Foundation Soil	24 degrees
Foundation Soil p-y Curves	Sand (Reese)
Non-Default Initial Stiffness, $k_{py}$	375 lb/in <sup>3</sup>
Cracking Moment, $M_{Cr}$	680 k-in.
Yielding Moment, $M_y$	3,200 k-in.
Uncracked Bending Stiffness, $EI_{uc}$	67 x 10 <sup>6</sup> k-in.
Cracked Bending Stiffness, $EI_{cr}$	18 x 10 <sup>6</sup> k-in.
Shaft Diameter	24 in.
Height of Retained Soil, H	162 in.
Reinforcement	12 #7 bars (1.6% of gross area)

Using the proposed guidelines, the predicted maximum top-of-wall deflection is approximately 5.5 inches, and the predicted maximum bending moment is approximately 2,200 in-kips (Figure 8.5). After a total of two controlled inundation cycles over a period of approximately 1.5 years, the test wall reached equilibrium at a top-of-wall deflection of approximately 4.2 inches since the installation of shotcrete facing (5.2 inches total since shaft installation). The measured maximum bending moment was approximately 1,800 in-kips since facing installation (2,100 in-kips total). Comparisons of measured and predicted values of deflection and bending moment are provided in Figure 8.4 and Figure 8.5. Comparisons of measured and predicted soil reaction forces and p-y curves using the proposed long-term design guidelines are presented in Figure 8.6 and Figure 8.7.



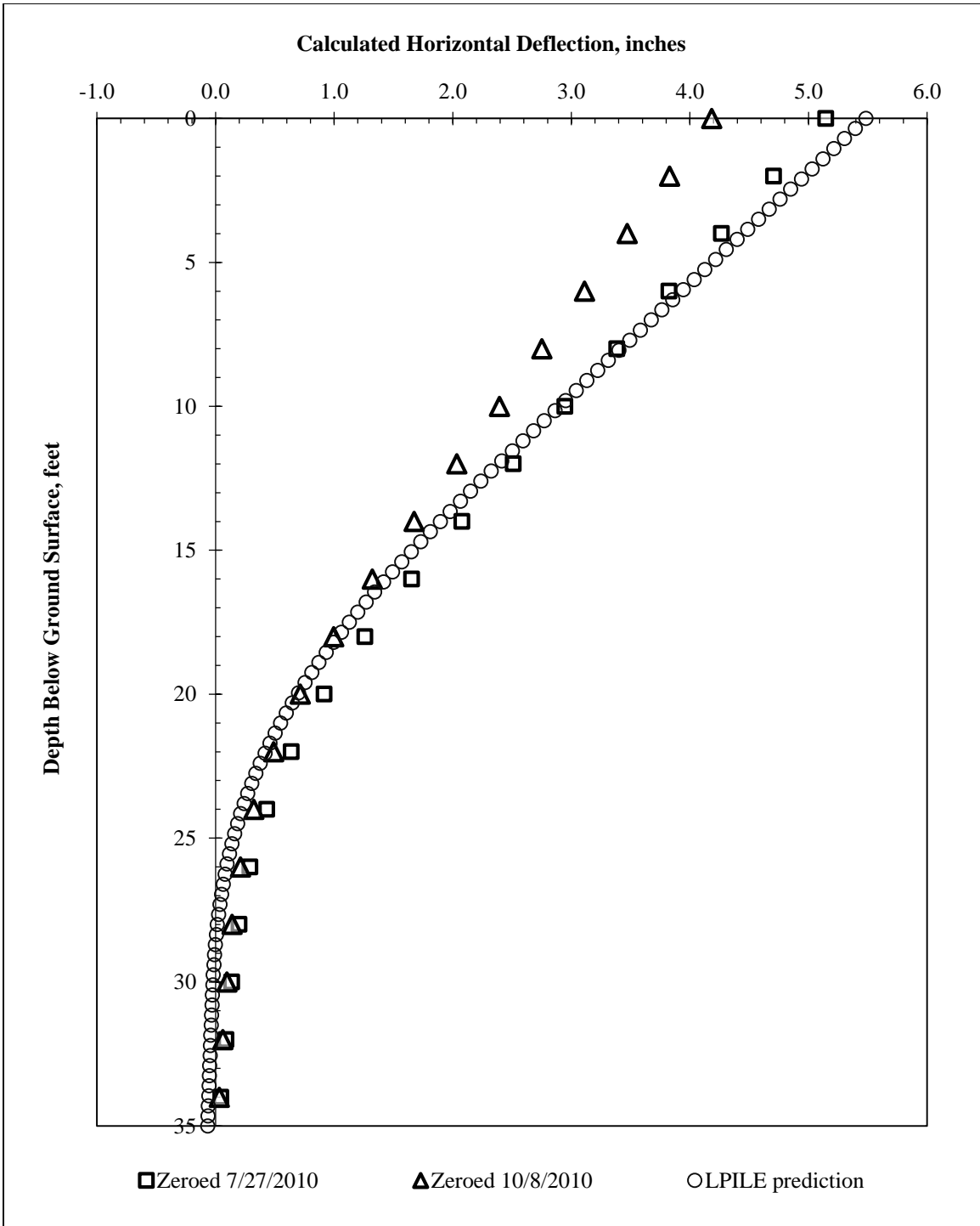


Figure 8.4: Summary of measured and predicted values of deflected shapes using long-term design guidelines.

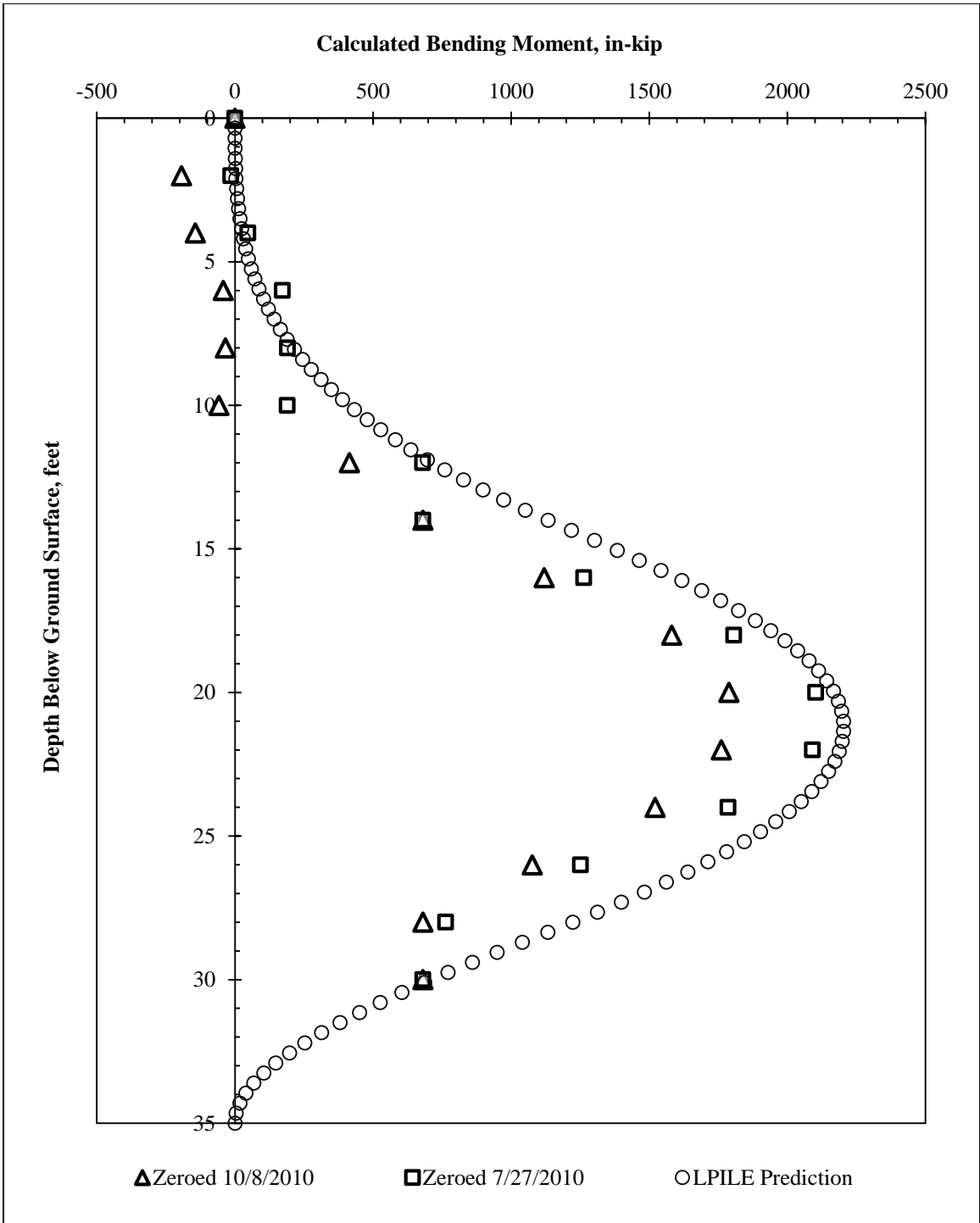


Figure 8.5: Summary of measured and predicted bending moments using long-term design guidelines.

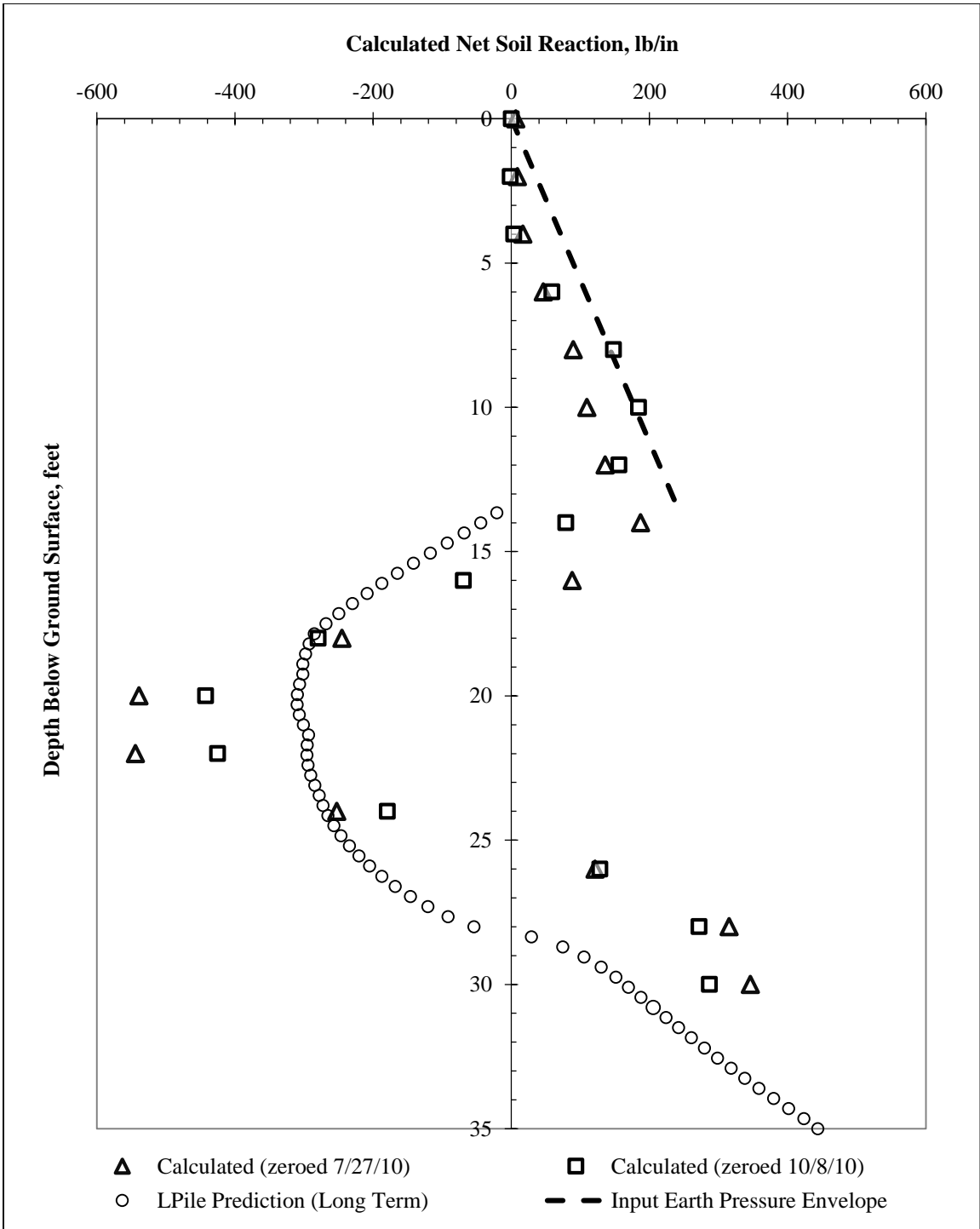


Figure 8.6: Comparison of Long-Term Modified LPILE Prediction and Calculated Soil Reaction Forces.

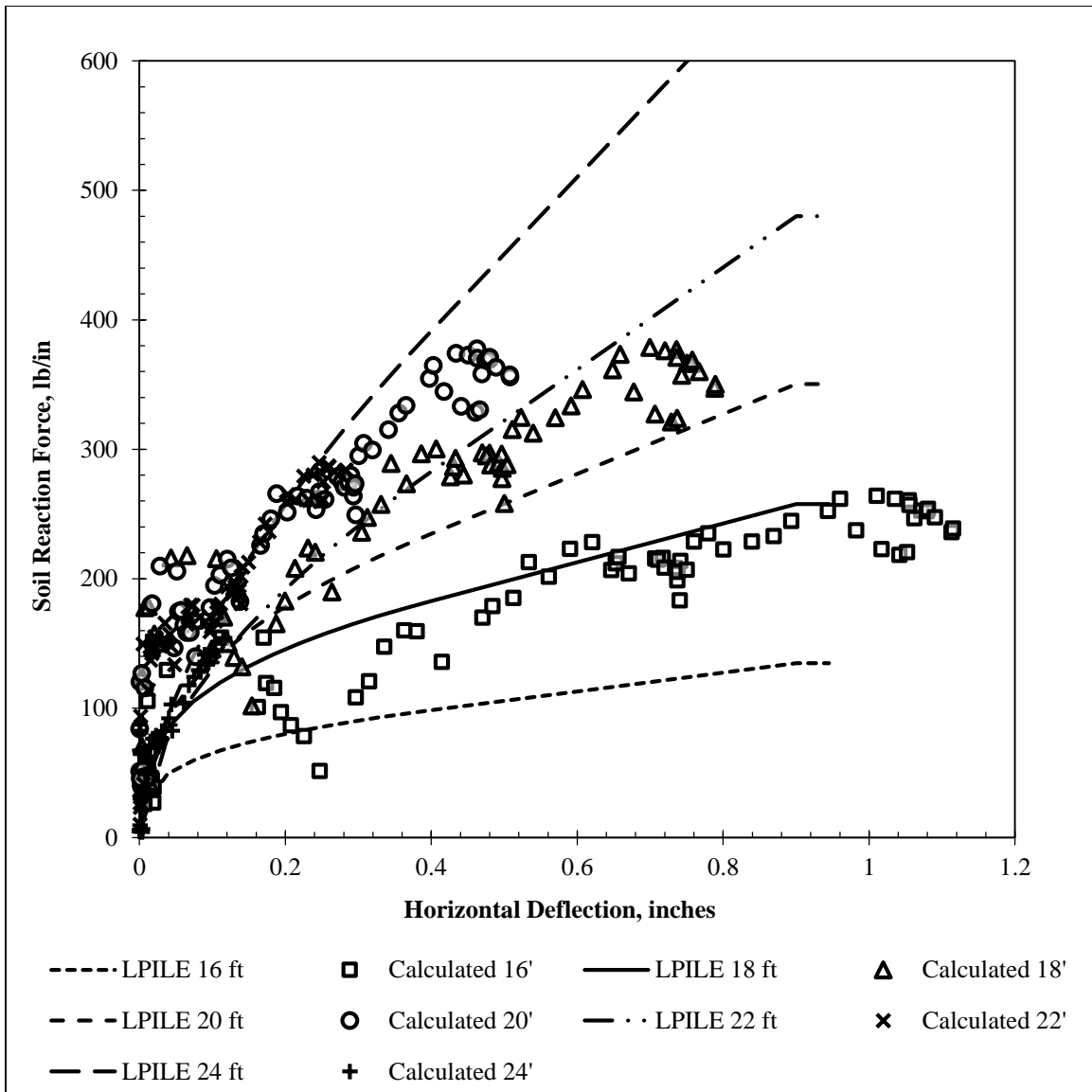


Figure 8.7: Comparison of long-term p-y curves predicted by modified LPILE analysis with p-y curves estimated from field data (reference survey is after installation of shotcrete facing on October 8, 2010).

### 8.1.3: HYPOTHETICAL TEST WALL REDESIGN USING FULLY SOFTENED STRENGTHS AND HYDROSTATIC PRESSURES FROM NATURAL WATER TABLE

To illustrate the impact of the proposed design guidelines on potential wall design, a simple LPILE design analysis was constructed for the test wall in its wettest state prior

to inundation, with the excavation height at the design value of 15 feet. The input earth pressure envelope was defined by the development of fully softened strengths above and below the water table, with hydrostatic pressures acting on the wall below the natural water table location of 8 feet below ground surface. The purpose of this analysis was to illustrate what design changes would need to be made to ensure the test wall met TxDOT's base fixity and top-of-wall deflection requirements. The input earth pressures for this analysis are summarized in Figure 8.8. Under these conditions, the as-built test wall design deflected approximately 4.2 inches (Figure 8.9). In order to achieve TxDOT's fixity and deflection requirements, the shaft embedment had to be increased from 20 feet to 30 feet, the shaft diameter increased from 24 inches to 30 inches, and the reinforcement upgraded from 12 #7 rebar to 12 #8 rebar to maintain an appropriate steel percentage in the shaft (center-to-center spacing remained 30"). The increase in shaft dimensions led to a reduction in top-of-wall deflections from approximately 4.2 inches using the test wall design to approximately 1.6 inches using the hypothetical increased shaft dimensions, which is within allowable values for TxDOT. Despite the significantly different values of top-of-wall deflection, maximum bending moments were similar between the two shafts. This brief example illustrates one potential implication of the proposed design guidelines. Because the proposed p-y relationships for the foundation soil are softer than the commonly accepted relationships used in design, shaft diameter and/or embedment depths may need to increase to ensure that base fixity is achieved and top-of-wall deflections remain within allowable values.

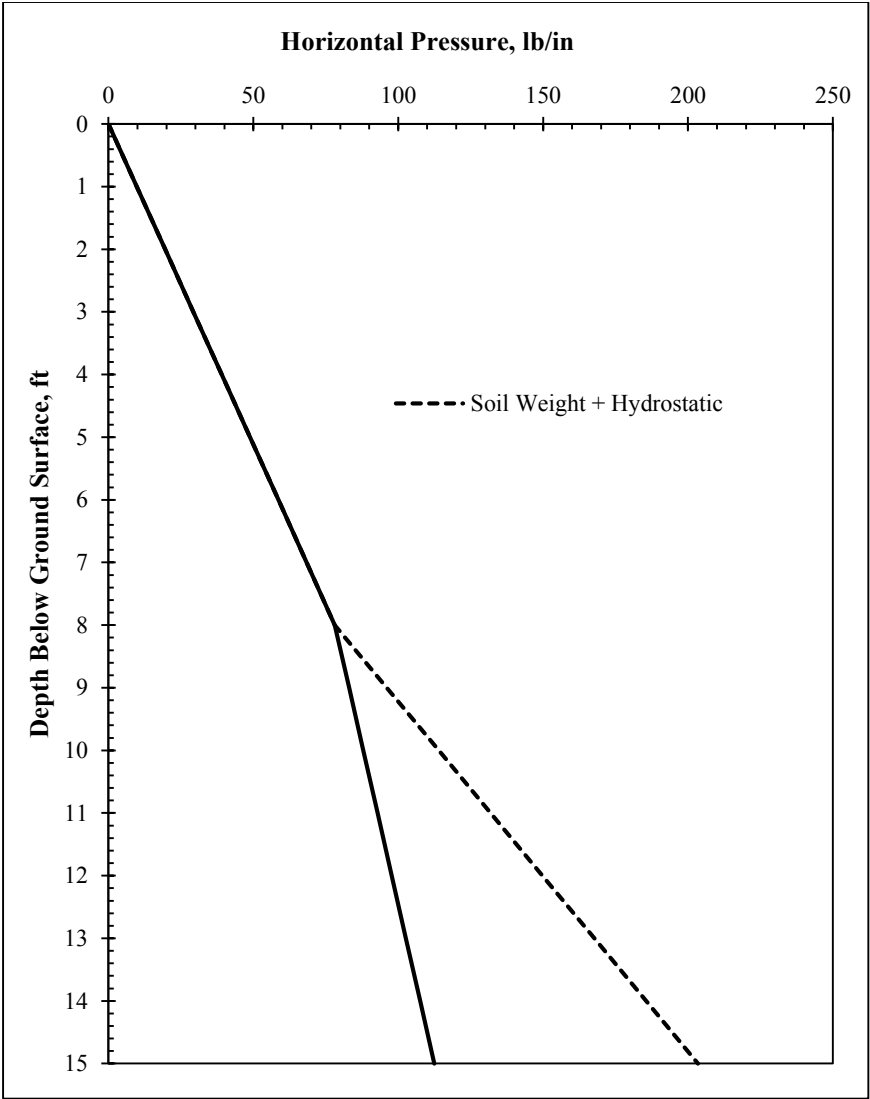


Figure 8.8: Input earth pressure envelope for wettest test wall conditions prior to inundation testing (natural groundwater table at 8 feet below ground surface).

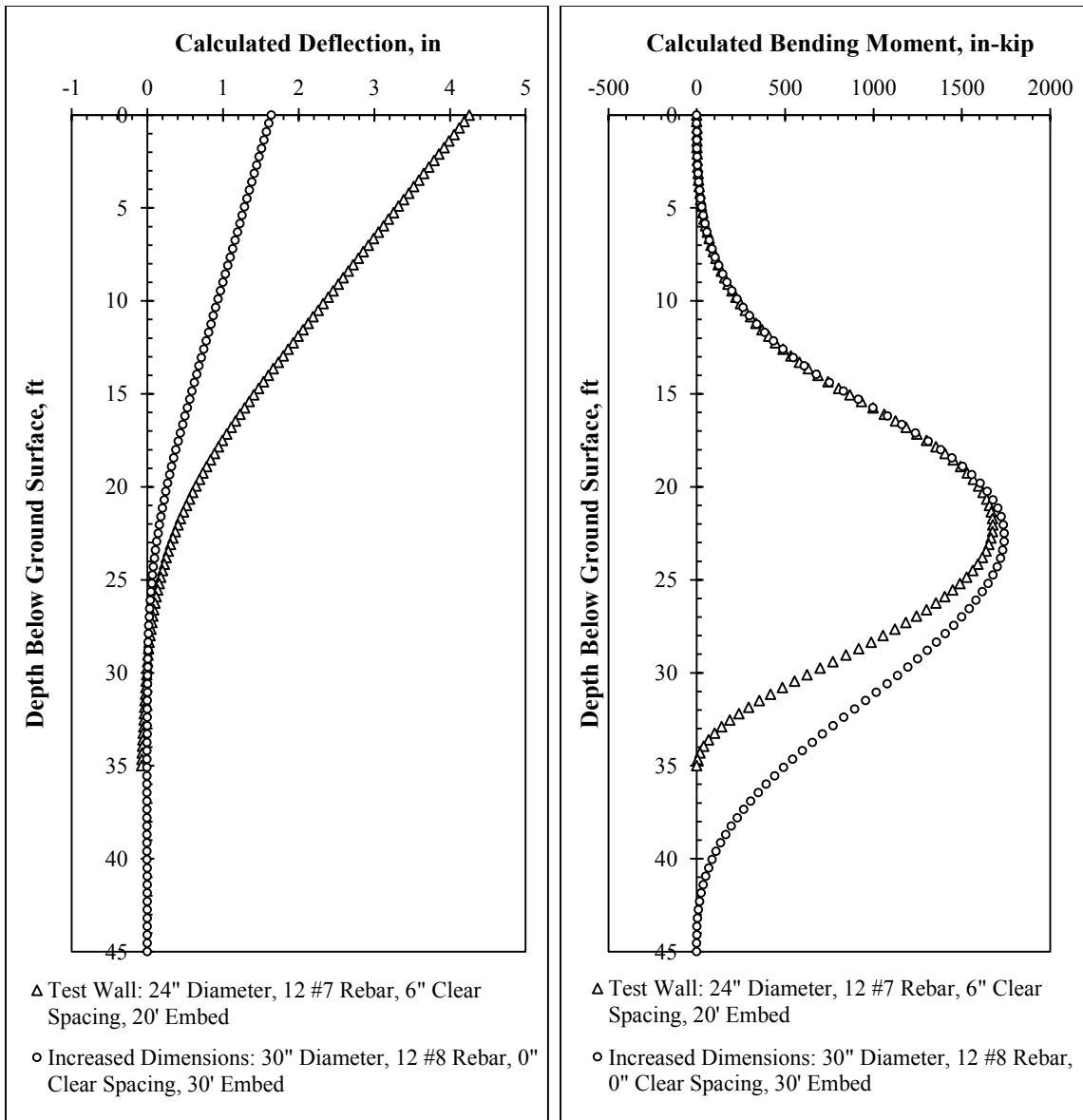


Figure 8.9: Comparison of deflected shapes and bending moments for hypothetical test wall redesign using proposed long-term conditions.

## 8.2: Short-Term Design Guidelines

The short-term behavior of the wall in response to excavation is dominated by global deformations of the soil-shaft system in response to stress relief. These global deformations cannot be easily represented with a p-y analysis. To check short-term

response when the soil is excavated, the use of two-dimensional finite element modeling is recommended. At small strains, the use of simple linear elastic constitutive models is sufficient to gain an understanding of the nature of the expected global deformations.

The choice of finite element model parameters is highly dependent on local soil conditions and experience, but it is recommended that anisotropy due to high in-situ lateral stresses and stiffness reductions due to unloading are incorporated. In highly overconsolidated, stiff-fissured clays, values of  $K_o$  between 2 and 3 are commonly reported (e.g. Cripps and Taylor 1981, Smith et. al. 2009). To account for the high ratio of horizontal to vertical stress, it is recommended that finite element models incorporate anisotropic conditions consistent with the expected field values of  $K_o$ . During excavation, significant stiffness reductions due to unloading were observed. While in-situ values of Young's Modulus ( $E$ ) are commonly estimated to be 1000 times the measured undrained shear strength, stiffness reductions of 60 to 90 percent, corresponding to  $E/S_u$  ratios of between 100 and 400, were required to approximate the behavior of the test wall. The reduced values of Young's modulus for the test wall are consistent with the general observation that stiff-fissured clays experience significant stiffness reductions during and after unloading (e.g. Cripps and Taylor 1981). Results of finite element model for the Lymon C. Reese research wall are presented in Figure 8.10.



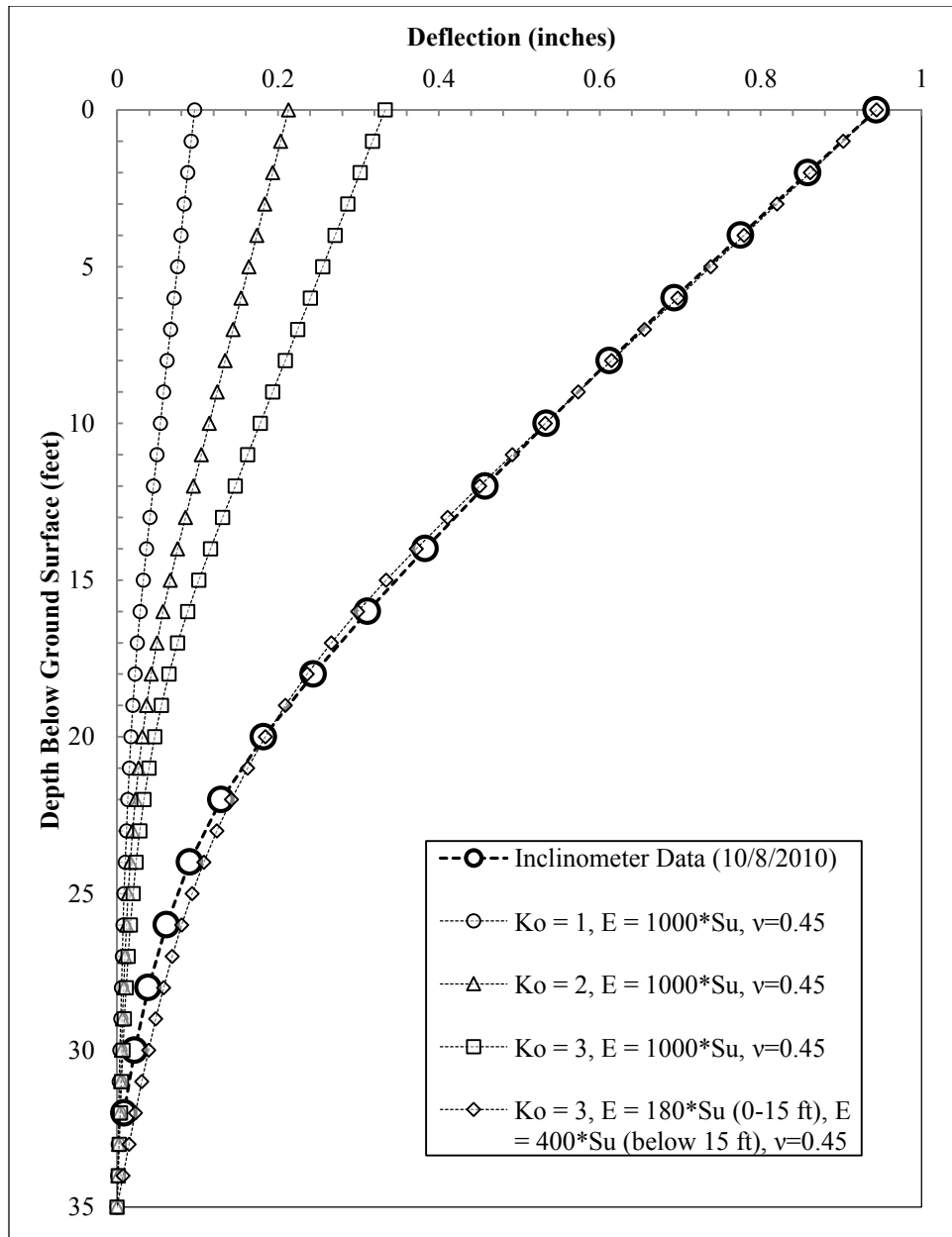


Figure 8.10: Comparison of measured data with predictions from linear elastic finite element model including anisotropy and stiffness reductions.

### 8.3: Summary and Conclusions

Based on design analysis of the proposed guidelines, some conclusions can be drawn:

- Wall behavior is dominated by the long-term development of fully softened, drained conditions in both the retained soil and the foundation soil, which can be modeled with a p-y analysis.
- Short-term deformations during excavation are primarily due to global deformations of the soil-shaft system in response to stress relief. Prediction of short-term deformations is difficult, but the use of two-dimensional finite element modeling with anisotropic in-situ stresses and stiffness reductions can provide some insight.
- The use of drained p-y curves based on the fully softened, drained friction angle of the clay are recommended for long-term p-y analysis. Non-default values of initial stiffness ( $k_{py}$ ), based on the original measured profile of undrained shear strength, are recommended to account for the initial transition from undrained to drained behavior.
- The proposed design guidelines slightly over-predict both bending moment and top-of-wall deflections induced by excavation and controlled inundation of our full-scale test wall. Based on the results of our monitoring program, walls designed for structural stability using the proposed guidelines will be adequate for use in expansive clay soils.
- Because of the influence of pavement and drainage systems, the proposed long-term design guidelines represent a worst-case scenario that is unlikely to exist for an extended time in the field. As a result, it may not be necessary for all walls to design for hydrostatic pressures. Should such a condition develop and remain for a long period of time, wall deflections could potentially exceed tolerable values as the soil approaches fully softened conditions with hydrostatic pressures, but structural loads would remain within acceptable limits.

- Beyond the typical formulation of lateral earth pressures, global movements of the soil-shaft system have been recorded in our test wall (e.g. global elastic response to stress relief during excavation, expansive soil volume change). Because the wall is not as severely stressed by these global movements (the soil and wall move together), top-of-wall deflections can fluctuate without a corresponding increase in bending moment or calculated earth pressures.
- Because the fully softened response of the foundation soil is relatively weak, the top-of-wall deflections predicted by the proposed design guidelines are sensitive to small changes in unit weight, wall geometry, and input earth pressure loading. The predicted values of bending moment are much less sensitive to changes in input values. For this reason, it is recommended that moment capacity, rather than top-of-wall deflection, be emphasized in design.

## **CHAPTER 9: CONCLUSIONS AND RECOMMENDATIONS**

### **9.1: Overview**

This chapter presents brief summaries of the key findings from each chapter of this research study. The original objectives of the research study are revisited, along with summaries of the research findings for each item. Finally, brief recommendations for future research and similar projects are provided.

### **9.2: Summary of Research Study**

#### **9.2.1: INSTRUMENTATION PROGRAM**

##### **9.2.1.a: Structural Performance of Drilled Shafts**

In general, for monitoring the long-term effects of soil moisture on the test wall, inclinometer data was a more consistent indicator of wall behavior than strain gauge data. The direct use of strain gauge data for the determination of bending curvature generally requires more advanced data interpretation than simply taking the first derivative of rotation profiles measured from inclinometer data. Although the precision and resolution of strain gauges is vastly superior to that of an inclinometer, the strain gauges represent the behavior of individual, discrete locations in the shaft. While extrapolating the behavior of individual strain gauges to the entire pile is relatively simple for a short-term lateral load test, for long-term monitoring, inclinometer data provides a more consistent and reliable picture of what is going on in the shaft without the need for subjective data interpretation. After combining rotation profiles from the three instrumented shafts, piecewise polynomial differentiation was used with numerical smoothing methods to approximate p-y curves from inclinometer data at the test wall.

For future studies, or larger scale studies involving several walls, inclinometer data provides a relatively inexpensive, effective, and robust method of performance monitoring. In the test wall, strain gauge data was affected by a number of factors beyond simple lateral loading of the structure, making data interpretation a complex and subjective task. While strain gauges are useful for short-term monitoring, they may not have the long-term stability and consistency of inclinometer data.

#### **9.2.1.b: Soil Moisture Monitoring**

For the Lymon C. Reese research wall, the most reliable moisture data came from physical measurements of samples obtained with a hand auger. The use of Time Domain Reflectometry (TDR) probes to measure moisture content in expansive clay is problematic because of the soil's high electrical conductivity and tendency to pull back from the probe rods during drying cycles. However, electrical conductivity measurements from one TDR probe appear to correlate with moisture contents and top-of-wall deflections. While the electrical conductivity data cannot be directly related to moisture content, it can provide a qualitative indicator of the moisture conditions on the project site. If accurate measurements of moisture content in expansive clay are of high importance, laboratory measurement of soil moisture content is recommended.

#### **9.2.2: BEHAVIOR BEFORE EXCAVATION**

Between shaft construction and excavation, a combination of concrete curing and expansive soil movement led to the development of residual stresses and strains, and evidence of tension cracks developed throughout the shafts. While there are no lateral loads placed on the shafts prior to excavation, the residual stresses and strains developed during this time affect strain gauge data interpretation and the shafts' response to excavation.

### **9.2.3: BEHAVIOR DURING EXCAVATION**

During excavation of the Lymon C. Reese research wall, the soil and wall responded immediately to the relief of stress, leading to wall deformations without the development of large earth pressures. This immediate response is a global movement of the soil-shaft system that extends beyond the shaft base. In the test wall, these global movements resulted in a top-of-wall deflection of approximately 0.5 percent of the cantilever height. Because these movements represent large-scale strains in response to stress relief, they cannot be easily modeled with a traditional lateral earth pressure envelope. The use of more advanced prediction methods, such as finite element modeling, can provide estimates of the quality of these deformations.

### **9.2.4: BEHAVIOR DURING NATURAL MOISTURE CYCLES**

#### **9.2.4.a: Response to Moisture Fluctuations**

Deformations and structural loads in the test wall were affected by moisture conditions on the project site. The test wall's deflection and structural loads were clearly affected by moisture conditions on the project site. During wetting, water infiltrated quickly through the clay fissures; as the retained soil and excavation base had access to moisture, top-of-wall deflections increased. Similarly, during prolonged periods of drying, top-of-wall deflections decreased. While this suggests volume change in expansive soil does play a part in wall deformations, no evidence of extremely high earth pressures or excessive structural loads on the shaft was observed. More importantly, access to moisture allowed negative pore pressures in the soil to dissipate, and volume change allowed the soil to approach a fully softened condition. At the conclusion of approximately 22 months of natural moisture cycles, total top-of-wall deflections since shaft construction had

increased to approximately 0.09 percent of the wall height (approximately 0.04 percent since the installation of shotcrete facing in October 2010).

#### **9.2.4.b: Thermal Strains and Bending Curvatures**

Daily and seasonal cycles of temperature fluctuation lead to the development of thermal strains which can influence data interpretation. If the climatic conditions on survey dates are substantially different, bending curvatures induced by daily temperature differences can be mistaken for bending moments caused by changes in earth pressure. The test wall experiences an average daily temperature fluctuation of approximately 22 degrees Fahrenheit, which corresponds to a daily variation in top-of-wall deflection of approximately 0.05 to 0.1 inches (0.03% to 0.06% of the cantilever height). Daily temperature fluctuations as high as 48 degrees have been recorded at the test site.

Because thermal deformations in the wall are generally consistent from day to day, difficult to model without detailed weather data, and their effect on wall behavior is relatively small, large-scale corrections to the data set for temperature effects are generally not practical. However, if isolated surveys with unusual deflection, rotation, or bending curvatures are observed in the data, an investigation into thermal effects is recommended.

#### **9.2.5: BEHAVIOR DURING CONTROLLED INUNDATION TESTING**

During controlled inundation testing of the test wall, wall behavior was governed by the development of fully softened, drained conditions in both the retained soil and foundation soil. As inundation testing began, water infiltrated quickly into the soil fissures, first appearing in the excavation 30 minutes after the test began. As inundation testing continued over a period of approximately 14 months (6 months with water impounded, 8 months without), total top-of-wall deflections increased to a maximum of approximately 2.9 percent of the wall height. As wall deflections reached their maximum value, water

levels in stand pipe piezometers throughout the inundation zone had stabilized near the ground surface. Moisture contents had increased by an average of 5 to 10 percentage points in the active zone above the groundwater table. Despite continued access to moisture, no evidence of expansive soil damage or earth pressures greater than the envelope defined by the soil's fully softened strength with hydrostatic pressures were observed.

The soil conditions at the conclusion of the inundation test can be approximated with a simple p-y analysis. The earth pressure envelope is defined using fully softened, drained strength parameters for the retained soil, and hydrostatic conditions with the water table at ground surface. For the foundation soil, p-y curves are defined using drained, fully softened strength parameters, with initial stiffness defined by the original measured profile of undrained strength (this implicitly accounts for the transition from undrained to drained behavior with time and moisture cycles). The long-term behavior of the Manor test wall can be reasonably approximated in LPILE using these parameters with the final as-built dimensions of the wall and excavation. Predicted values of deflections, bending moments, and p-y curves are consistent with those measured in the field.

#### **9.2.6: DEVELOPMENT OF DESIGN GUIDELINES**

The behavior of the Manor, Texas test wall can be defined by two distinct stages of wall movement: short-term deformations during excavation and long-term deformations after cycles of wetting and drying. Short- and long-term effects should be combined to check final design deflections and bending moments.

##### **9.2.6.a: Long Term Behavior After Cycles of Wetting and Drying**

Long term behavior can be represented in p-y analysis programs such as LPILE using drained, fully softened strength parameters for the retained and foundation soil. Hydrostatic pressures with the water table at a reasonable maximum level is added to the



input earth pressure envelope. In the foundation soil, the initial stiffness of the p-y curves is defined using the original profile of undrained shear strength and established relationships between  $S_u$  and  $k_{py}$  (e.g. Reese et. al. 1975, Sullivan et. al. 1980). This implicitly accounts for the transition from undrained to drained behavior in the foundation soils.

#### **9.2.6.b: Short-Term Behavior During Excavation**

During excavation, the motion of the wall is governed by global response to stress relief. For the Manor test wall, a linear elastic finite element analysis using  $K_o$  values between 2 and 3, and  $E/S_u$  ratios between 100 and 400, provides a reasonable approximation of the observed behavior during excavation. Values of  $E/S_u$  are significantly lower than those measured during SASW testing on the project site, which may be attributable to the presence of fissures and the effects of stress relief. While further study is required to generalize design guidelines, for highly overconsolidated, expansive soils, an analysis using a two-dimensional linear elastic finite element model with anisotropic in situ stresses and stiffness reductions due to unloading is recommended.

### **9.3: Conclusions of Research Study**

The goal of this research study is to advance our understanding of the long-term behavior of retaining structures in expansive clays. The observed performance and instrumentation data from our test wall are used to address the following objectives:

1. Identify and analyze the processes responsible for wall loading and deformation.
2. Evaluate how these processes change with time and moisture cycles.
3. Provide guidance for design practice to account for these processes and ensure adequate wall performance.

Based on the test wall monitoring and analysis program, conclusions of this research study include:

1. During excavation, wall behavior is governed by global deformations in response to stress relief. During seasonal cycles of wetting and drying, wall behavior was governed by volume change of the retained soil (during wetting and drying) and softening of both the retained soil and the foundation soil (during wetting). During controlled inundation testing, wall behavior is primarily influenced by the development of fully softened, drained conditions in both the retained soil and foundation soil.
2. During excavation, short-term deformations occur almost immediately in response to stress relief. During seasonal moisture cycles, lateral earth pressure and wall deflections decrease slowly in response to drying, and relatively quickly during wetting. During controlled inundation testing, fissures in the retained soil provide preferential pathways for moisture flow, and surface water moves through the soil within minutes. Wall deflections, bending moments, and water levels in stand pipe piezometers stabilized after surface water was present for a total of approximately six months.
3. The behavior of retaining walls in expansive clay can be represented by a combination of short- and long-term deformations in design. The long-term development of drained, fully softened conditions leads to the majority of deformations and structural loads.
  - a. To estimate long-term response, a p-y analysis using drained, fully softened strength parameters for both the retained soil and foundation soil is recommended. Above the excavation line, hydrostatic pressures with the water table at a maximum reasonable level behind the wall are included.

The use of non-default values of initial stiffness ( $k_{py}$ ) defined by the original measured profile of undrained shear strength is recommended to account for the transition from stiff, undrained conditions to fully softened, drained conditions.

- b. To estimate short-term response, a simple two-dimensional finite element analysis to model the effects of stress relief during excavation is recommended. Selection of finite element model parameters is highly dependent on experience and the soil conditions on the project site, but incorporating anisotropy due to high in-situ lateral stresses and stiffness reductions due to unloading is recommended.

#### **9.4: Recommendations for Future Work**

The Lymon C. Reese research wall has provided insight on the behavior of a single drilled shaft retaining wall constructed through expansive clay. While some generalizations can be made, more thorough study of real-world walls is necessary to develop a complete understanding and framework for design. Inclinator casings installed in future walls, with deflection profiles recorded at key dates or automated readings from an in-place unit, would provide an inexpensive and effective way to both verify the performance of existing walls and enhance the theoretical understanding of wall behavior. Additionally, a study of the behavior of a wall constructed during an extremely dry period would be of interest, to assess if initial soil moisture content at construction has any impact on wall behavior.

To minimize the local effects of concrete heterogeneity and tension cracking, future instrumented walls using strain gauges could consider further isolating the gauges from direct contact with the concrete. An early suggestion for the Manor test wall, which

ultimately proved too expensive to implement, was attaching all the strain gauges to the interior of a steel pipe running the length of a drilled shaft. The pipe would then be surrounded by concrete to cast it into place, creating a system with similar moment-curvature behavior to a typical drilled shaft, but without the micro-scale effects of concrete behavior causing difficulty in strain data interpretation. This method would completely isolate the gauges from contacting the concrete, which was a major source of error in the test wall's strain data. While this method may provide some improvement in strain data quality, it could substantially increase expense over the sister bars used for the Manor test wall.

## References

- Adil Haque, M. and Bryant, J. T. (2011). Failure of VERT Wall System: Forensic Evaluation and Lesson Learned. *Geo-Frontiers 2011: Advances in Geotechnical Engineering* , 3487-3496.
- Brown, A. C., Ellis, T., Dellinger, G., El-Mohtar, C., Zornberg, J., & Gilbert, R. B. (2011). "Long-term monitoring of a drilled shaft retaining wall in expansive clay: Behavior before and during excavation". *Geo-Frontiers 2011*, ASCE.
- Brown, A. C., Dellinger, G. F., & Gilbert, R. B. (2011). Long-Term Performance of Drilled Shaft Retaining Walls: Assessment of Existing Walls. Research Report FHWA/TX-11/0-6603-1. Center for Transportation Research. University of Texas at Austin.
- Cripps, J. C., and Taylor, R K. (1981). The Engineering Properties of Mudrocks. *Quarterly Journal of Engineering Geology*, Vol. 14, 325–346.
- Dellinger, G. (2011). The Use of Time Domain Reflectometry Probes for Moisture Monitoring of a Drilled Shaft Retaining Wall in Expansive Clay. M.S. Thesis, The University of Texas at Austin.
- Dodds, Andrew M. and Martin, Geoffrey R. (2007). Modeling Pile Behavior in Large Pile Groups under Lateral Loading. Technical Report MCEER-07-0004. Multidisciplinary Center for Earthquake Engineering Research
- Ellis, Trent. (2011). A Subsurface Investigation in Taylor Clay. Master's Thesis, The University of Texas at Austin.
- Fellenius, Bengt H., Sung-Ryul Kim, Sung-Gyo Chung (2009). "Long-Term Monitoring of Strain in Instrumented Piles." *Journal of Geotechnical and Geoenvironmental Engineering*, Vol. 135, No. 11, November 2009, pp. 1583-1595.
- Fuhr, Peter L., Dryver R. Huston, Timothy P. Ambrose, and Darrell M. Snyder. (1993). "Stress Monitoring of Concrete Using Embedded Optical Fiber Sensors." *J. Struct. Engrg.* 119, 2263.
- Google Inc. (2011). Google Earth (Version 6.0.3.2197) [Software]. Available from <http://www.google.com/earth/download/ge/agree.html>.
- Hong, Gyeong Taek. (2008). Earth Pressures and Deformations in Civil Infrastructure in Expansive Soils. Ph.D. dissertation, Texas A&M University.
- Kim, Myung Hak and Michael W. O'Neill. (1998). Side Shear Induced in Drilled Shaft by Suction Change." *J. Geotech. and Geoenvir. Engrg.* 124, 771.
- Koutrouvelis, Iraklis. (2012). Earth Pressures Applied on Drilled Shaft Retaining Walls in Expansive Clay during Cycles of Moisture Fluctuation. Master's Thesis, The University of Texas at Austin.

- Lytton, R. (2007, December 12). Design of Structures to Resist the Pressures and Movements of Expansive Soils. Texas A&M University.
- P. K. Ooi and T. L. Ramsey. (2003). "Curvature and Bending Moments from Inclinator Data". International Journal of Geomechanics, ASCE.
- Pufahl, D., Fredlund, D., and Rahardjo, H. (1983). Lateral earth pressures in expansive clay soils. Canadian Geotechnical Journal, 20, 228-241.
- Puppala, A. J., Wejrungsikul, T., Willammee, R. S., Witherspoon, T. and Hoyos, L. (2011). Design of Inclined Loaded Drilled Shaft in High-Plasticity Clay Environment. Technical Report 0-6146-1. Department of Civing Engineering. University of Texas at Arlington.
- Quantdec (2004). "Smoothing." Quantitative Decisions, Inc. Online resource, available from <http://www.quantdec.com/Excel/smoothing.htm>.
- Reese, L. C., Cox, W. R., and Koop, F. D. (1974). Analysis of laterally loaded piles in sand. Sixth Annual Offshore Technology Conference, Paper No. 2080, OTC, Houston, Texas, 473-483.
- Reese, L. C., Cox, W. R., and Koop, F. D. (1975). Field testing and analysis of laterally loaded piles in stiff clay. Seventh Annual Offshore Technology Conference, Paper No. 2312, OTC, Houston, Texas, 671-690.
- Reese, L. C., Isenhower, W. M. & Wang, S.-T. (2006). Analysis and design of shallow and deep foundations. John Wiley & Sons, Inc.
- Reese, L. C. & Van Impe, W. F. (2001). Single piles and pile groups under lateral loadings. A. A. Balkema, Rotterdam.
- Skempton, A. W. (1977). "Slope stability of cuttings in brown London clay." Proceedings, Ninth International Conference on Soil Mechanics and Foundation Engineering, Tokyo, Vol. 3, pp. 261-270.
- Smith, R. E., Smith, D. L., Griffin, J. A. (2009). Top-Down Construction of a Bridge in Clay Shale. American Society of Civil Engineers Conference Proceedings. 337, 76, 598-605.
- Snethen, D. R., Townsend, F. C., Johnson, L. D., Patrick, D. M., Vedros, P. J. (1975). A review of Engineering Experiences with Expansive Soils in Highway Subgrades. Soil Mechanics Division, Soils and Pavements Laboratory. U.S. Engineering Waterways Experiment Station.
- Sullivan, W. R., Reese, L. C., and Fenske, C. W. (1980). "Unified method for analysis of laterally loaded piles in clay." Numerical Methods in Offshore Piling Conference, May 1979. Institution of Civil Engineers, London, 135-146.

- Stark, T. D., Choi, H., and McCone, S. (2005). "Drained shear strength parameters for Analysis of landslides." *Journal of Geotechnical and Geoenvironmental Engineering*, ASCE, Vol. 131, No. 5, May, 2005, pp. 575–588.
- Thomas, M. G., Puppala, A. J., Hoyos, L. R. (2009). Influence of Swell Pressure From Expansive Fill on Retaining Wall Stability. *American Society of Civil Engineers Conference Proceedings*. 337, 75, 590-597.
- Tukey, J. W. (1977). *Exploratory Data Analysis*. Addison-Wesley, Reading, MA.
- TxDOT (2009). *Cantilver Drilled Shaft Wall Design*.
- TxDOT Geotechnical Manual. (2012). Texas Department of Transportation, Bridge Division, Austin, Texas.
- Vipulanandan, C., Jospheh, D. (2011). Seasonal Moisture Fluctuation in the Active Zone in a Humid-Subtropical Climate. *Geo-Frontiers 2011: Advances in Geotechnical Engineering*, 2759-2767.
- Wang, Shintower and Reese, Lymon C. (1986). Study of design method for vertical drilled shaft retaining walls. Research Report 415-2F. Center for Transportation Research, Bureau of Engineering Research. University of Texas at Austin.
- Weather Underground (2013). <http://www.wunderground.com/>.
- Welch, R. C., and Reese, L. C. (1972). Laterally loaded behavior of drilled shafts. Research Report 3-5-65-89. Center for Highway Research, University of Texas at Austin.
- Wise, J. R. and Hudson, W. R.. (1971). An Examination of Expansive Clay Problems in Texas. Research Report 118-5. Center for Highway Research, University of Texas at Austin.
- Wright, S. G.. (2005). "Evaluation of Soil Shear Strengths for Slope and Retaining Wall Stability Analyses with Emphasis on High Plasticity Clays." Project No. 5-1874-01. Center for Transportation Research, The University of Texas at Austin.
- Wright, S. G., Zornberg, J. G., and Aguetant, J. E.. (2007). "The Fully Softened Shear Strength of High Plasticity Clays." Report No. FHWA/TX-07/0-5202-3. Center for Transportation Research, The University of Texas at Austin.

## **Vita**

Andrew Charles Brown graduated from Dripping Springs High School in Dripping Springs, Texas in May, 2004. He received his Bachelor of Science in Civil Engineering with Honors from the University of Texas at Austin in May, 2008. In August, 2008, he began his graduate studies at the University of California, Berkeley, and received his Master of Science in Civil and Environmental Engineering in May, 2009. He began his doctoral studies at the University of Texas at Austin in August, 2009.

Permanent address: 19301 FM 150 W  
Driftwood, TX 78619

This dissertation was typed by the author.